U.S. Department of Transportation
Federal Highway Administration

Manual for Heat Straightening, Heat Curving and Cold Bending of Bridge Components

FOREWORD

Heat straightening and heat curving have been effectively and routinely used for decades to fabricate steel bridge components and to repair damage caused during construction due to mishandling, or during service due to uncommon events including overload, vehicle impact, earthquake, or fire. Cold bending has also been widely used to create a variety of structural shapes and connection elements from steel plate in fabrication shops. These methods can be used independently or together to produce a desired outcome with a good understanding of the impact made to the properties and performance of steel once it has yielded.

This new manual provides the background knowledge and information to use heat straightening, heat curving and cold bending for the fabrication or repair of steel bridge components. This manual was adapted from previous FHWA publications addressing similar topics. The updated material includes new findings from recent National Cooperative Highway Research Program (NCHRP) research, new field and shop experiences on heat straightening/heat curving, and a completely new section on cold bending fabrication practices. This document will be a good technical resource for bridge engineers, fabricators, contractors, managers and owners.

Joseph L. Hartmann, PhD, PE
Director, Office of Bridge and Structures
Office of Infrastructure
Federal Highway Administration

TECHNICAL REPORT DOCUMENTATION PAGE

1. Report No. FHWA-HIF-23-003	2. Government Accession No.	3. Recipient's Catalog No.
4. Title and Subtitle Manual for Heat Straightening, Heat Curving and Cold Bending of Bridge Components		5. Report Date
		6. Performing Organization Code:
7. Author(s) Fenton Geoghegan, Ronnie Medlock, Brittany Packard		8. Performing Organization Report No.
9. Performing Organization Name and Address WSP USA		10. Work Unit No.
1 Pennsylvania Plaza New York, NY 10119		11. Contract or Grant No. DTFH61-14-D-00048
12. Sponsoring Agency Name and Address Office of Bridges and Structures Federal Highway Administration 1200 New Jersey Ave SE Washington, DC 20590		13. Type of Report and Period Covered
		14. Sponsoring Agency Code

15. Supplementary Notes
The Contracting Officer's Representative for the IDIQ contract was Tuonglinh Warren (HIBS-10). The Task Order Contracting Officer's Representative was Dayi Wang (HIBS-10)

16. Abstract
The objective of this manual is to provide a comprehensive reference on aspects of heat straightening, heat curving and cold bending as they pertain to steel bridge components. This manual is targeted towards both engineers and steelwork practitioners. This manual is an updated version of FHWA Report, FHWA-IF-99-004, "Heat Straightening Repairs of Damaged Steel Bridges: A manual of Practice and Technical Guide" and FHWA Report, FHWA-IF-09-999, "Guide for Heat-Straightening of Damaged Steel Bridge Members" and includes various updates and suggestions developed from recent studies and investigations.

17. Key Words Bridge, Steel, Heat Straightening, Damage Repair, Curving, Cambering, Cold Bending	18. Distribution Statement No restrictions. This document is available to the public through the National Technical Information Service, Springfield, VA 22161. http://www.ntis.gov		
19. Security Classif. (of this report) Unclassified	20. Security Classif. (of this page) Unclassified	21. No. of Pages	22. Price N/A

Form DOT F 1700.7 (8-72)   Reproduction of completed page authorized.

SI* (MODERN METRIC) CONVERSION FACTORS

APPROXIMATE CONVERSIONS TO SI UNITS

Symbol	When You Know	Multiply By	To Find	Symbol
LENGTH				
in	inches	25.4	millimeters	mm
ft	feet	0.305	meters	m
yd	yards	0.914	meters	m
mi	miles	1.61	kilometers	km
AREA				
in^2	square inches	645.2	square millimeters	mm^2
ft^2	square feet	0.093	square meters	m^2
yd^2	square yard	0.836	square meters	m^2
ac	acres	0.405	hectares	ha
mi^2	square miles	2.59	square kilometers	km^2
VOLUME				
fl oz	fluid ounces	29.57	milliliters	mL
gal	gallons	3.785	liters	L
ft^3	cubic feet	0.028	cubic meters	m^3
yd^3	cubic yards	0.765	cubic meters	m^3
NOTE: volumes greater than 1000 L shall be shown in m^3				
MASS				
oz	ounces	28.35	grams	g
lb	pounds	0.454	kilograms	kg
T	short tons (2000 lb)	0.907	megagrams (or "metric ton")	Mg (or "t")
TEMPERATURE (exact degrees)				
°F	Fahrenheit	5 (F-32)/9 or (F-32)/1.8	Celsius	°C
ILLUMINATION				
fc	foot-candles	10.76	lux	lx
fl	foot-Lamberts	3.426	candela/m^2	cd/m^2
FORCE and PRESSURE or STRESS				
lbf	poundforce	4.45	newtons	N
lbf/in^2	poundforce per square inch	6.89	kilopascals	kPa

APPROXIMATE CONVERSIONS FROM SI UNITS

Symbol	When You Know	Multiply By	To Find	Symbol
LENGTH				
mm	millimeters	0.039	inches	in
m	meters	3.28	feet	ft
m	meters	1.09	yards	yd
km	kilometers	0.621	miles	mi
AREA				
mm^2	square millimeters	0.0016	square inches	in^2
m^2	square meters	10.764	square feet	ft^2
m^2	square meters	1.195	square yards	yd^2
ha	hectares	2.47	acres	ac
km^2	square kilometers	0.386	square miles	mi^2
VOLUME				
mL	milliliters	0.034	fluid ounces	fl oz
L	liters	0.264	gallons	gal
m^3	cubic meters	35.314	cubic feet	ft^3
m^3	cubic meters	1.307	cubic yards	yd^3
MASS				
g	grams	0.035	ounces	oz
kg	kilograms	2.202	pounds	lb
Mg (or "t")	megagrams (or "metric ton")	1.103	short tons (2000 lb)	T
TEMPERATURE (exact degrees)				
°C	Celsius	1.8C+32	Fahrenheit	°F
ILLUMINATION				
lx	lux	0.0929	foot-candles	fc
cd/m^2	candela/m^2	0.2919	foot-Lamberts	fl
FORCE and PRESSURE or STRESS				
N	newtons	0.225	poundforce	lbf
kPa	kilopascals	0.145	poundforce per square inch	lbf/in^2

*SI is the symbol for the International System of Units. Appropriate rounding should be made to comply with Section 4 of ASTM E380.
(Revised March 2003)

TABLE OF CONTENTS

LIST OF FIGURES

vii

LIST OF TABLES

LIST OF ABBREVIATIONS

AASHTO	American Association of State Highway Transportation Officials
AISC	American Institute of Steel Construction
AREMA	American Railway Engineering and Maintenance-of-Way Association
ASTM	ASTM International
AWS	American Welding Society
BCS	Bridge Construction Specifications
CVN	Charpy V-Notch
D1.5	AASHTO/AWS D1.5 Bridge Welding Code
FEA	finite element analysis
FHWA	Federal Highway Administration
HPS	high-performance steel
HSLA	high-strength low-alloy
HSS	hollow steel section
ksi	kilopounds per square inch
LRFD	Load and Resistance Factor Design
NCHRP	National Cooperative Highway Research Program
NDT	nondestructive testing
PBFS	press-brake formed steel
PT	dye penetrant testing
MT	magnetic particle testing
Q&T	quenched and tempered
TxDOT	Texas Department of Transportation
UT	ultrasonic testing

LIST OF SYMBOLS

A.F.	amplification factor
b_f	flange width
b_s	channel flange width for strong axis bending; channel web depth for weak axis bending
c_d	length of damage
d	channel web depth for strong axis bending; channel flange width for weak axis bending; vee depth/flange width as used in section 4.1.3
d_s	web depth
d_v	vee depth
E	modulus of elasticity
E_0	modulus of elasticity at ambient temperature
F_a	stress factor
F_ℓ	external jacking force factor
F_s	shape factor
F_y	yield stress
F_{yo}	nominal yield stress at 70°F
H	height of residual damage
L, L_i, L_r	length of residual damage, see equations 3, 5, and 6, see figure 40
M_j	jacking moment
M_p	plastic moment
M_r	residual moment
n	number of heats
P	axial load
P_{euler}	Euler buckling load
P_u	impact load
R	radius of curvature
R_d	depth ratio
R_y	radius of curvature to the yield curvature
S	shortening (inches); elastic section modulus
S_x	elastic section modulus about the major axis

S_y	elastic section modulus about the minor axis
S'	elastic section modulus for the angle about the axis of bending
SAF	stress amplification factor
T	temperature in degrees Fahrenheit
T_{50}	the temperature at which 50 percent of the upper shelf is absorbed
t_f	flange thickness
V	width of open end of vee
W	plate width
x_1	see figure 73
x_2	see figure 73
x_3	see figure 73
Z	plastic section modulus
Y_0	midpoint deflection
Z_x	plastic section modulus about the major axis
Z_y	plastic section modulus about the major axis
Z'	plastic section modulus for the angle about the axis of bending
φ_b	basic plastic rotation factor
φ_d	angle of damage
φ_p	predicted plastic rotation
μ	strain ratio
y_i	measured offset of beam from reference line
y_{max}	distance from the centroid to the extreme fiber of the element
ε_{max}	maximum strain
ε_y	yield strain
ϑ	vee angle
δ_{max}	deflection that produces a maximum stress equal to 50 percent of yield on a center point loaded member
ℓ	clear span length

CHAPTER 1. INTRODUCTION

1.1. PURPOSE OF THIS MANUAL

This manual is intended to provide the user with information and suggestions for performing heat straightening, heat curving and cambering, and cold bending of structural steel members. The processes of heat straightening and curving, both for the repair of structural steel members and in fabrication, are discussed, as are details on the process of cold bending, its use in industry, and technical considerations. Although this document focuses on repairing damage to members of steel bridge structures, the principles are applicable to any type of steel structure.

Damage caused by overload, vehicle impact, handling, earthquake, or fire is a perennial problem associated with steel bridge structures. For almost half a century, heat straightening techniques have been applied to bends and distortions to restore the original shape of damaged steel elements. The ability to repair damaged structural steel members in place, often without the need for temporary shoring, has generated interest in heat straightening from the engineering profession.

In addition to using heat for in-field repairs of structural members, heat has also been used in fabrication to produce curved and cambered structural members and repair distortions produced due to welding prior to service. The application of heat differs between in-field applications and fabrication in that fabrication heating occurs in a controlled environment and typically results in less severe distortion of the original shape than in-field processes. Further, the process of heat curving is typically performed on undamaged steel to produce gradual curves with large radii. Both fabrication and in-field heating results in similar fundamental behavior of the material, therefore both processes follow a similar methodology and have similar challenges.

Finally, heat curving and cambering are not the only methods for shaping structural steel in fabrication shops. Cold bending is also widely used to create a variety of structural shapes, including members with camber and sweep, as well as connection elements from steel plate. While the process of cold bending differs substantially from heated techniques, both present various challenges which should be considered when determining which application is more beneficial.

The objectives of this manual are:

- Heat Straightening:
  - Describe and quantify the fundamentals of the heat straightening process.
  - Address specific methods for repairing the basic damage categories.
  - Provide information for repairing more complex combinations of the basic damage categories.
  - Provide detailed technical research data for engineers and scientists.
  - Provide information for conducting and supervising heat straightening repairs.
- Heat in Fabrication:
  - Describe and quantify the fundamentals of the use of heat in fabrication.

- o Provide methods for heat curving, heat cambering, and repairing distortions in structural sections.
- o Provide information for conducting and supervising heat curving and cambering processes.
- Cold Bending:
  - o Describe and quantify the fundamentals of cold bending steel.
  - o Describe the use of cold formed steel sections in industry and the variety of sections shaped using cold bending.
  - o Provide insight on the general methodology and various cold bending processes.

1.2. THE BASICS OF HEAT STRAIGHTENING AND HEAT CURVING

Heat straightening is a repair procedure using controlled heat application. Heat patterns are used to plastically deformed regions of damaged steel to straighten the material gradually through repetitive heating and cooling cycles. The process of heat curving is similar, where heat is applied in specific patterns to undamaged steel in repetitive heating/cooling cycles to gradually curve the material. Both processes rely on internal and external restraints that produce upsetting (or thickening) during the heating phase and in-plane contraction during the cooling phase. Heat straightening and curving are distinguished from other methods in that force is not used as the primary instrument to deform the steel. Rather, the thermal expansion/contraction process during each heating/cooling cycle leads to a gradual straightening or curving trend. The process is characterized by the following conditions: (1) the temperature of the steel does not exceed either (a) the lower critical temperature (the lowest temperature at which austenite begins to form; see section 2.1.1), or (b) the tempering temperature for quenched and tempered steels; (2) the stresses produced by applied external forces do not exceed the yield stress of the steel in its heated condition; and (3) only the regions in the vicinity of the plastically deformed zones are heated when performing heat straightening.

The basic concept of heat straightening and heat curving is relatively simple and relies on two distinct properties of steel. First, if steel is stretched or compressed past a certain limit (yield), it does not assume its original shape when released. Rather, it remains partially elongated or shortened, depending on the direction of the originally applied force. Second, if steel is heated to relatively modest temperatures (between 700 and 1,300°F), it expands at a predictable rate and its yield value becomes significantly lower while at the elevated temperature.

To illustrate how steel can be permanently deformed using these two properties, consider the short steel bar in figure 1 images A through D. First, an undeformed bar ((figure 1-A) is placed in a fixture, much stronger and stiffer than the bar itself, and clamped tight (figure 1-B)). The bar is then heated in the region indicated (labeled as "Zone to be Heated") and tries to expand during heating, but is restrained longitudinally by the clamp (i.e., the fixture exerts a restraining force on the bar). Because the bar is prevented from longitudinal expansion, it is forced to expand at a greater amount laterally and transversely through its thickness than an identical unrestrained bar. Consequently, a bulge will occur in the heated zone, as shown in figure 1-C. Because the bulge has been heated, its yield strength has been lowered, resulting in some yielding in the heated zone. When the heating source is removed, the material will cool and contract in three dimensions. Because the clamp cannot prevent the bar from contracting longitudinally, as cooling progresses, the bar shortens, and the bulge shrinks. However, a portion of the bulge

remains even after the bar has completely cooled and the bar is shorter than its original length. Essentially, a permanent redistribution of material has occurred in the heated zone, leaving the bar slightly shorter with a small bulge, as shown in figure 1-D. This permanent bulge, or thickening, in the heated zone is called "upsetting." The redistribution of material is referred to as "plastic deformation" or "plastic flow." The clamping force is often referred to as a "restraining force" that can be applied though the use of an external load, such as a jacking force, or through the unheated portion of the steel element. This topic is discussed further in section 2.2.4. Through several cycles of clamping, heating, and cooling, the bar could be shortened significantly.

(A)   Undeformed steel bar

(B)   Undeformed steel bar

(C)   Upsetting during heating while restrained

(D)   Final configuration of heated bar
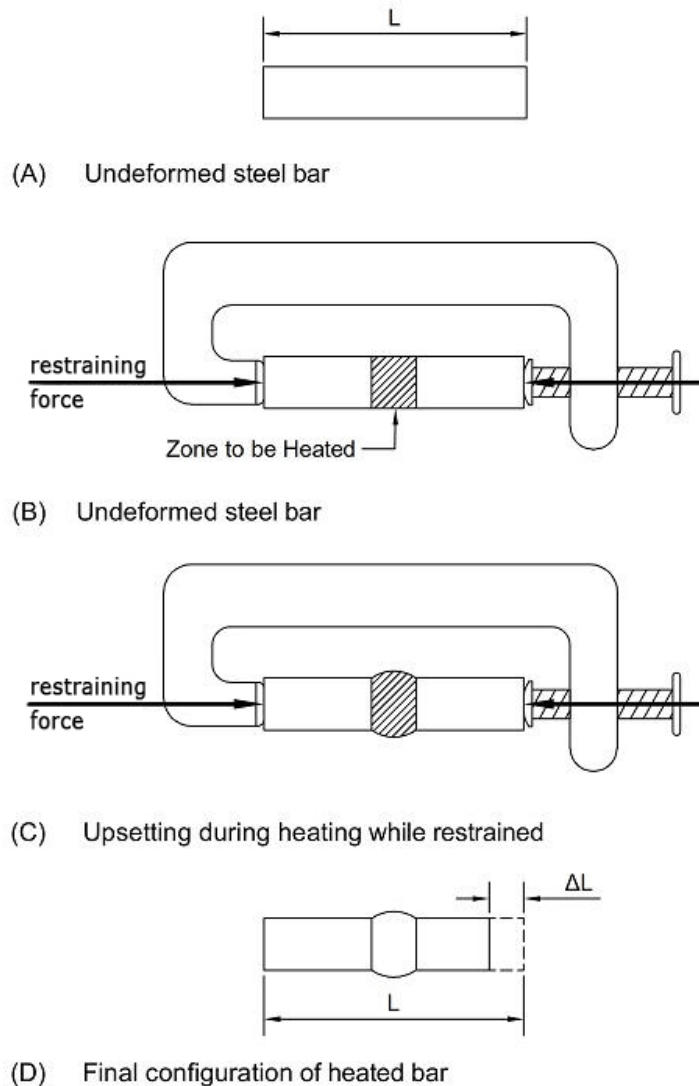
Source: FHWA

Figure 1. Illustration. Conceptual example of shortening a steel bar.

This example illustrates the fundamental principles of heat straightening and heat curving. However, steel section shapes are much more complex than a bar, and different damage

conditions require their own heating and restraining patterns. Damage conditions are categorized into strong axis damage (category S), weak axis damage (category W), torsional damage (category T), local damage (category L), or any combination of these four. These damage types are shown in figure 2 and discussed in more detail in section 2.2.

(A) Category S damage (strong axis)

(B) Category W damage (weak axis)

(C) Category T damage (torsional)

(D) Category L damage (local, flange)

(E) Category L damage (local, web)
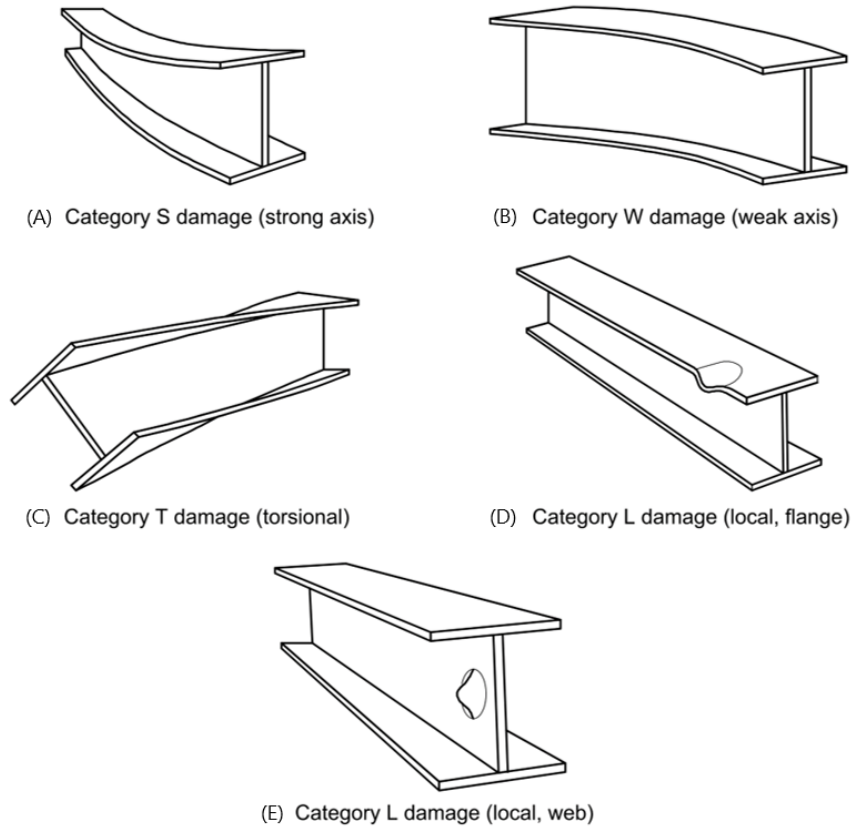
Source: FHWA

Figure 2. Illustration. Damage categories.

Similarly, unique heating and restraining patterns are needed for different structural shapes, depending on the desired curve direction. In general, three elements are key to the heat straightening and heat curving process. The first is to select proper heating patterns and sequencing to fit the damage or desired curvature. Heating patterns consist of some combination of vee heats, line heats, edge heats, spot heats, and strip heats (see figure 3 and section 2.2.2). The second is to properly control the heating temperature and rates of heating and cooling. The third is to provide appropriate restraints during the heating cycle that can be relaxed or modified during the cooling cycle. These basic elements are discussed further in chapter 2.

(A) Vee heat

(B) Strip heat

(C) Edge heat

(D) Line heat

(E) Spot heat
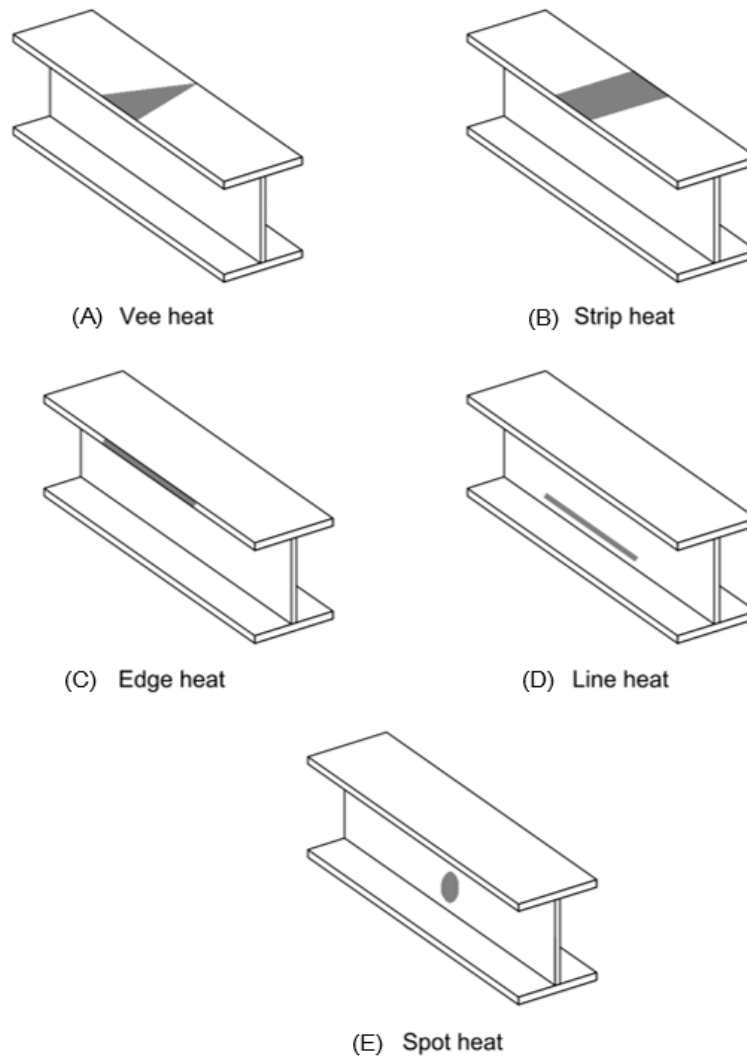
Source: FHWA

Figure 3. Illustration. Basic heating patterns.

Finally, although the fundamentals of heat straightening and curving have been studied and quantified through decades of research, the process is a skill that involves extensive practice and experience. These fundamentals are described in detail in this publication; however, the application of these concepts and the quality of the results depend on the skill and experience of the practitioner.

1.3. THE BASICS OF COLD BENDING

Cold bending is a process in which steel plates and shapes are bent into a desired final configuration at ambient temperature using force. The main difference between cold bending and heat straightening/curving is the lack of applied heat and use of applied force to shape the section. Cold bending is widely used to create a variety of structural shapes and connection elements, including folded or bent plates and curved or cambered structural shapes. Additionally,

cold bending can be used to bend plates to create custom built-up sections and to straighten rolled shapes after they have cooled.

The process of cold bending or bending is characterized by the partial yielding of the section being bent from the application of a bending force. This partial yielding produces permanent deformations that result in the final configuration of the section. Steel is particularly well suited for cold bending because of its ductility, or ability to deform when loaded beyond yield. Because cold formed sections are plastically deformed to create their final configuration, some amount of residual stress is retained. However, when practical strain limits are observed, the residual stresses are typically low, and the deformation resulting from cold bending does not typically affect the performance of the steel. This is particularly important for structural members where the properties of the cross section are important to the performance of the member in service.

A wide variety of cold bending methods are used to form structural shapes and plates. These methods are typically selected based on the type of section being bent and the desired final shape. Practical limits to the bend radius used are also suggested based on the properties of the section being bent. The various shapes, forming methods, and suggested bending limits are discussed in chapter 4.

1.4. HEAT STRAIGHTENING AND OTHER HEAT FORMING METHODS

References to heat straightening in this manual should not be confused with two other methods used in steel fabrication: hot mechanical straightening (also known as hot mechanical bending) and forging. Hot mechanical straightening differs from heat straightening in that external force is applied after heating to straighten the damage. These applied forces produce stresses well above yield, resulting in large movements during a single heat cycle. Often the member is completely straightened by the continued application of a large force during a single cycle. Specific concerns about hot mechanical straightening include fracture during straightening; adverse changes in material properties; and buckling, wrinkling, or crimping developing in the section.

Forging differs from heat straightening in that both large external forces and high heat are used. This method is similar to hot mechanical straightening in that external forces are used. However, for this method, the steel is heated well above the lower critical temperature, often to temperatures above the upper critical temperature where the steel glows "cherry red." At temperatures above the upper critical temperature, the substrate is completely austenite (see section 2.1.1). Specific concerns about hot working include fracture during straightening; severe and irreversible changes in the molecular structure of steel; adverse changes to mechanical properties resulting in increased brittleness; and buckling, wrinkling, or crimping of the section during hot working. It is important to note the differences between heat straightening and these two other methods. The discussion in this manual does not cover hot mechanical straightening or hot working of steel which may require additional engineer approvals or may not be allowed for use on bridges.

1.5. HOW TO USE THIS MANUAL

This manual is a reference for conducting heat straightening, heat curving, and cold bending of steel sections. Chapter 2 provides a general overview of the basic principles and effects that heat

has on steel during heat straightening and heat curving. Chapter 3 provides a detailed review of available analytical research, and a discussion of the heat straightening and heat curving processes for a variety of structural steel sections. Chapter 4 discusses the process of cold bending and the use of cold formed sections in industry and provides general suggestions for cold bending structural steel sections. Summaries and Key Points are provided at the end of each major section.

CHAPTER 2. HEAT STRAIGHTENING AND HEAT CURVING BASICS

2.1. EFFECTS OF HEATING ON THE MATERIAL PROPERTIES OF STEEL

2.1.1. Introduction

The potential detrimental effects from heating a damaged steel member have somewhat limited the implementation of heat straightening in practice. However, with an understanding of the properties of steel, and the effect of heat on those properties, heat straightening can be useful and conducted effectively.

When steel is subjected to elevated temperatures, the yield stress decreases, the modulus of elasticity decreases, and the coefficient of thermal expansion increases. The behavior and interaction of these parameters during heating add complexity to the response of steel during the heat straightening or heat curving process, while also enabling the desired permanent deformation to occur. In addition to these short-term effects, heating steel can also result in long-term changes to the ductility and toughness properties of the material if the steel reaches certain temperatures. Some of the long-term effects can be detrimental to steel's performance in service and can vary depending on steel type, grade, and heating temperature. Understanding of steel properties and care during straightening can help avoid negative long-term effects.

Steel alloys can have various crystalline structures of iron and carbon. Different phases occur because the arrangement of iron atoms affects how carbon can be absorbed into the crystalline structure. The iron-carbon equilibrium diagram shown in figure 4 illustrates the relationship of these phases to carbon content and temperature. Most structural steels used for bridge construction in the United States are low-carbon steel, high-strength low-alloy (HSLA) steel, or quenched and tempered (Q&T) steel. At ambient temperature, these steels have three major constituents (or phases): ferrite, cementite, and pearlite. Ferrite consists of iron with no carbon attached, cementite is an iron-carbon molecule, and pearlite is a mixture of cementite (12 percent) and ferrite (88 percent). Typical bridge steel has less than about 0.1 to 0.3 percent carbon, which is too little to develop 100 percent pearlite. This results in pearlite plus free ferrite molecules at room temperature. As such, low-carbon steels tend to be softer and more ductile, which are recognized characteristics of ferrite. For bridge construction, ductility is an important characteristic, hence, the use of low-carbon or low-alloy steels in steel structures.
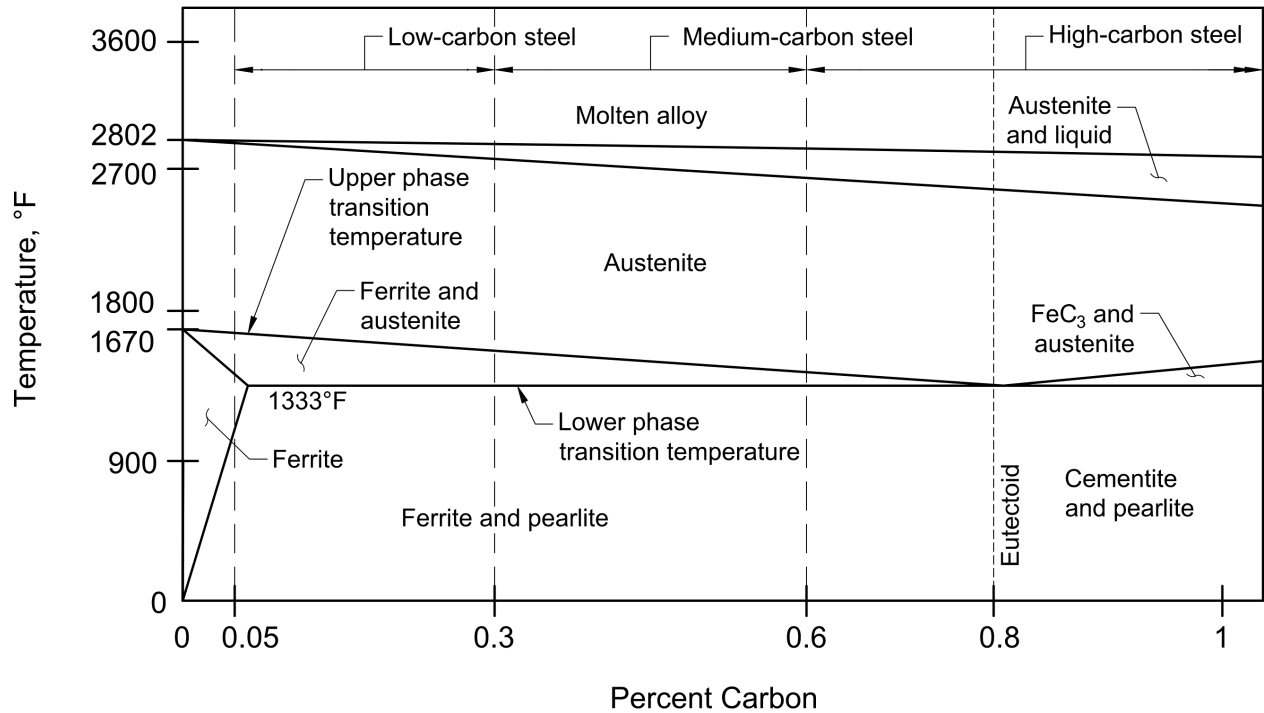
Source: FHWA

Figure 4. Graph. Iron-carbon equilibrium diagram.

The phases of steel are not only a function of carbon content, but are also a function of temperature. Low carbon steels typical in bridge construction have a carbon concentration of 0.3 percent and lower. In these steels, temperatures greater than 1,333°F (approximately) begin to produce a phase change in the steel (figure 4). The phase change refers to a change in the packing of the crystal structure between body-centered cubic (ferrite) to face-centered cubic (austenite). The temperature at which this begins is called the lower critical (or lower phase transition) temperature. At temperatures greater than about 1,500-1,700°F the change in the crystalline structure of the steel is complete, and the steel assumes the form of a uniform solid solution of austenite. The temperature at which this occurs is called the upper critical (or upper phase transition) temperature.

When steel cools slowly from the upper critical temperature, it attempts to return to its original phase, maintaining its original properties. This retransformation occurs over time since it involves the migration of the carbon atoms from the austenite to the carbide structure, reducing carbon in the ferrite. However, if a rapid cooling of the material occurs, the retransformation is halted, and a hard, brittle phase called martensite occurs. This process of rapid cooling following the heating of the steel to its critical temperature is known as quenching and is often done intentionally to improve the hardness and strength of steel. Though quenched steel exhibits improved hardness and strength, it also has reduced ductility and is therefore more sensitive to brittle fracture. Following quenching, steel is usually treated through a process called tempering to improve its ductility and toughness (known as quenching and tempering, Q&T). Tempering is the process of heating steel to a temperature below the lower critical temperature and subsequently allowing the steel to cool in still air or in an oven at a controlled rate. This cooling allows the martensite to form tempered martensite, a tough and strong phase, reducing the

9

brittleness of the steel and improving its ductility and toughness. A higher tempering temperature results in more ductility and toughness, but lower hardness and strength. A lower tempering temperature results in less ductility and toughness, and increased hardness and strength.

For steels whose properties are produced through some form of controlled heat treatment, including Q&T steel, thermo-mechanically controlled processed (TMCP) steels, and some high performance steels (HPS), the maximum heat straightening temperature is of utmost concern. To prevent changes to material properties developed through the Q&T process, the maximum temperature used in heat straightening should be lower than the tempering temperature of the steel. Because tempering temperatures vary for different grades of steel, suggested heat straightening temperatures also vary and depend on steel type. Further discussion is included in section 2.2.7, including suggested maximum heat straightening temperatures for several common Q&T steels. For non-Q&T steels, maximum heat straightening temperature is still a concern. In the case of these steels, the maximum heat straightening temperature should be less than the lower phase transition temperature to prevent changes to the microstructure of the steel.

In addition to changing material properties, heating and cooling steel also alters the residual stresses within a section. When hot steel cools, the surfaces cool more quickly than the interior because they are directly exposed to the cooling environment. As a result, the surfaces of the cooling steel contract more rapidly than the interior. Because this contraction is unequal within the section, residual stresses are produced. This phenomenon commonly occurs in the production of steel plates and shapes and during heat straightening. Thus, it is useful to understand how heat straightening can affect existing residual stresses and create different residual stress patterns. This concept is discussed in detail in section 2.1.2.

Finally, an important issue to consider is how many times a girder can be damaged and heat-straightened safely. Changes in material properties from damage and subsequent heat straightening become more evident with an increasing number of damage/repair cycles. This amplification of material property changes and suggestions regarding the number of damage/repair cycles are discussed in sections 2.1.4 and 2.1.5.

2.1.2. Residual Stress in Heat-Straightened Steel

Residual stresses are present in all structural steel members. These stresses typically result from differential shrinkage during the cooling of hot rolled and welded built-up sections. However, the cutting and punching processes used in steel fabrication can also produce residual stresses. The magnitude of the residual stresses in fabricated steel can be high for rolled shapes and particularly for welded members near the location of the weld.

Residual stress effects on the total stress distribution are considered in design specifications, so engineers do not need to explicitly include them in calculations. For example, research on steel columns has resulted in column design formulas that include the effects of residual stress. In U.S. column design codes, residual stresses in compression members are accounted for by assuming an average residual stress value of 50 percent of the yield stress. This assumption may lead to conservative designs for rolled shapes, which have smaller residual stresses, and less-conservative designs for welded built-up shapes, which have larger residual stresses. These American codes use a more generalized approach when compared to European codes, which

have adopted the multiple column curve approach in which different member capacity equations are used depending on the magnitude of the residual stresses. For European codes, the level of residual stress directly affects the design capacity, while for U.S. codes it does not. As a result, American codes simplify the design approach by not explicitly showing residual stresses in design equations, like codes from American Institute of Steel Construction (AISC 2017), American Railway Engineering and Maintenance-of-Way Association (AREMA 2022), and the American Association of State Highway Transportation Officials (AASHTO 2017a (23 CRF 625.4(d)(1)(iv)), AASHTO 2017b (23 CFR 625.4(d)(1)(v))).

Two other factors should be considered. First, when properly detailed, the ductility of steel allows for residual stresses to be redistributed when a member is subjected to large stresses. Second, residual stresses are self-equilibrating (e.g., large compressive stresses at one location on a cross section are balanced by tensile stresses at another location).

Because residual stresses are present in all structural steel sections, it is important to consider the effect of heat straightening on these stresses. Research conducted by Avent et al. (1992) assessed the effect of heat straightening on residual stresses for plates and various rolled shapes. The distribution of residual stresses for vee-heated ASTM A36 plates with two levels of damage is shown in figure 5. The distribution of residual stresses for various heat straightened A36 rolled shapes are shown in figures 6 through 10.
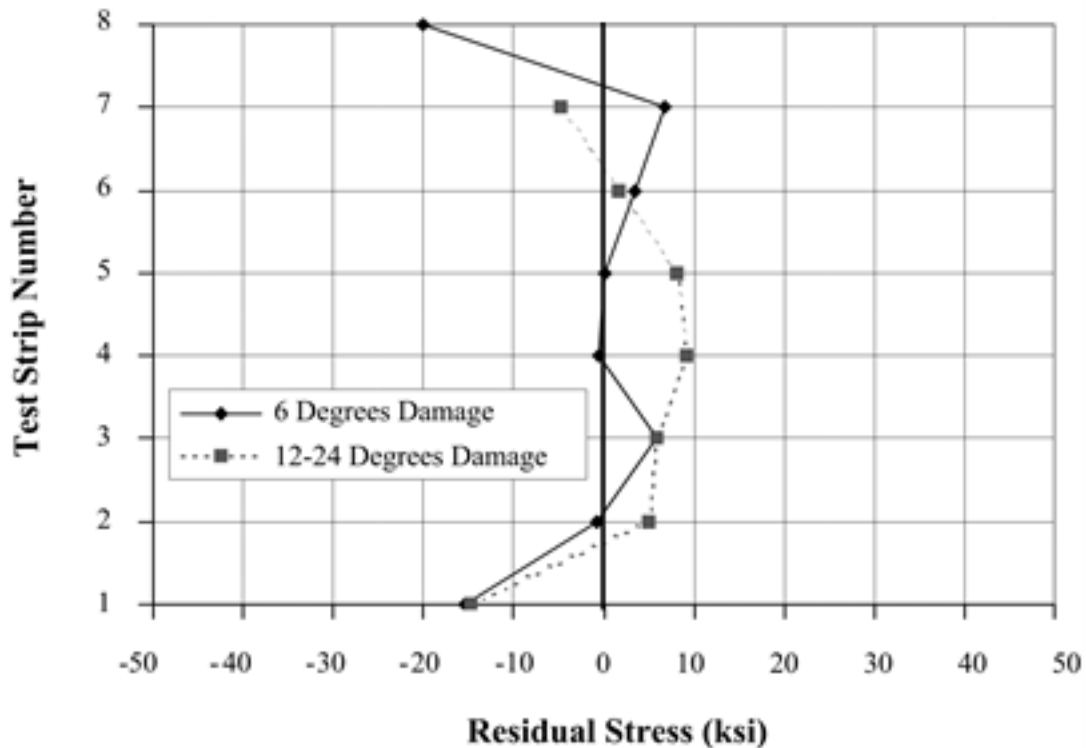
Note: Positive stress indicates tension. Negative stress indicates compression.
Source: Avent et al. (1992)

Figure 5. Graph. Residual stress distribution for plates damaged and then vee-heated.
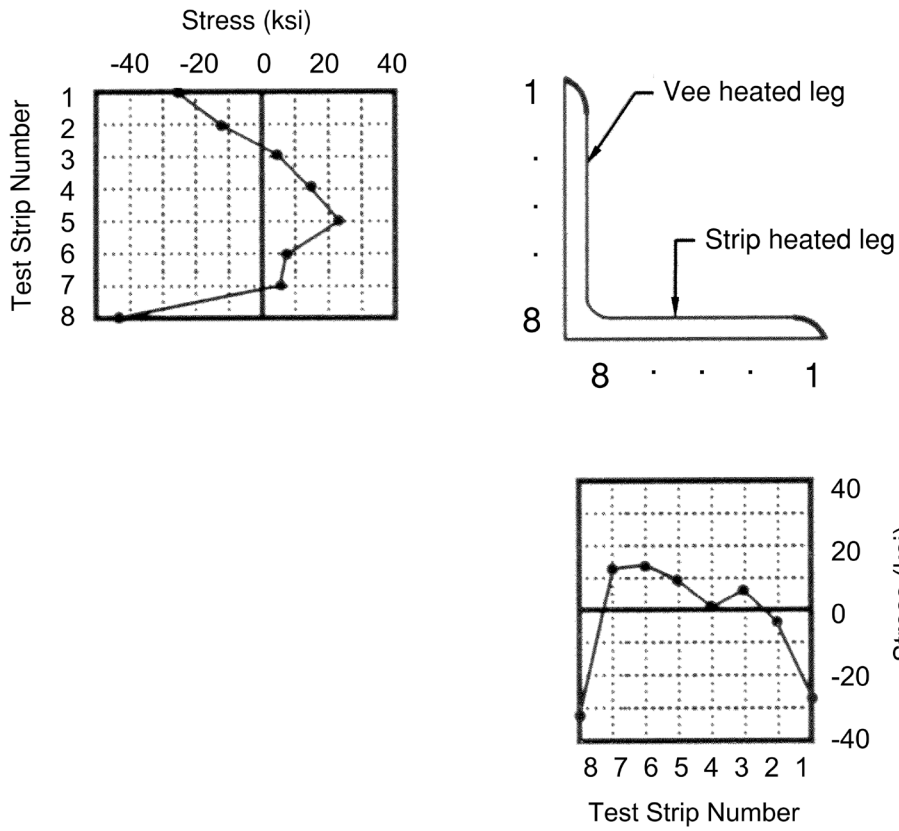
11

Note: Positive stress indicates tension. Negative stress indicates compression.
Source: Avent et al. (1992)

Figure 6. Illustration. Typical residual stress distribution for a heat-straightened angle (vee and strip heat).
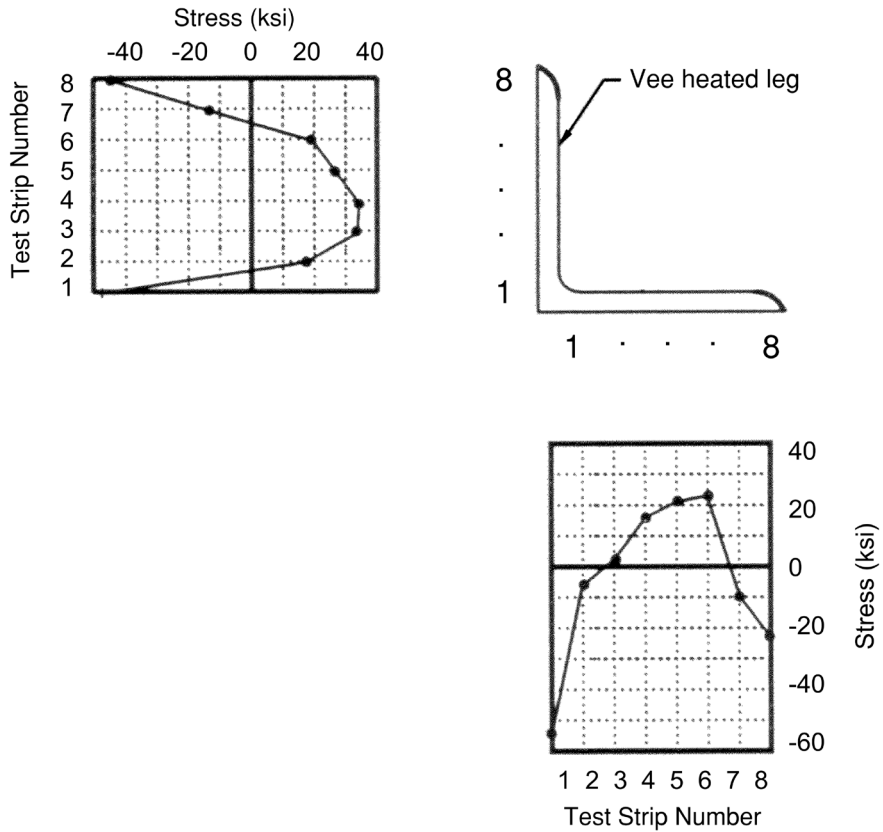
Note: Positive stress indicates tension. Negative stress indicates compression.
Source: Avent et al. (1992)

Figure 7. Illustration. Typical residual stress distribution for a heat-straightened angle (vee heat only).
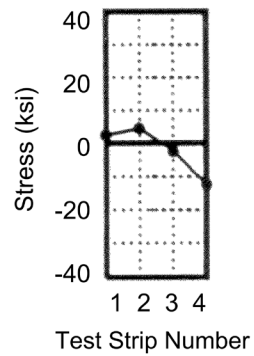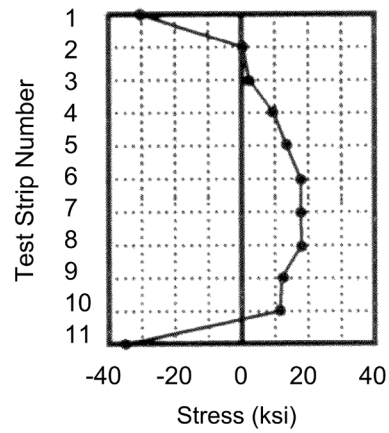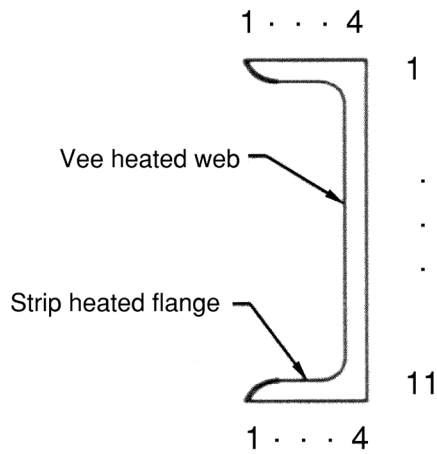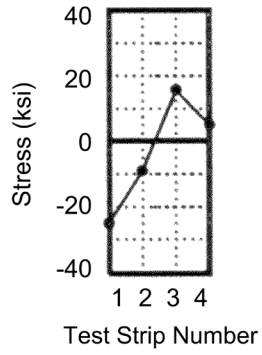
Note: Positive stress indicates tension. Negative stress indicates compression.
Source: Avent et al. (1992)

Figure 8. Illustration. Typical residual stress distribution for a heat-straightened channel.
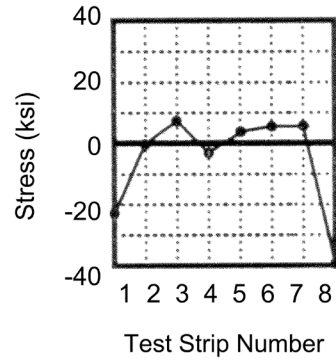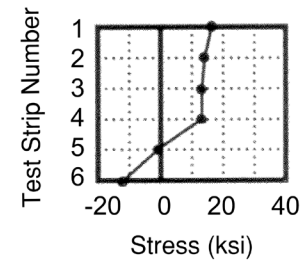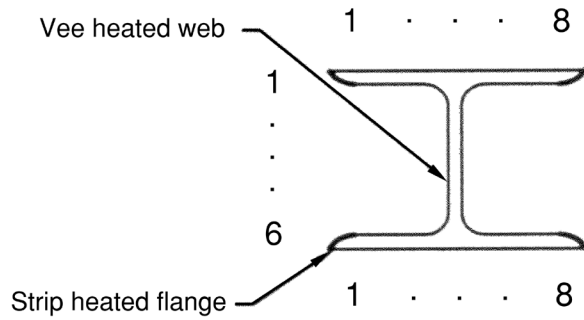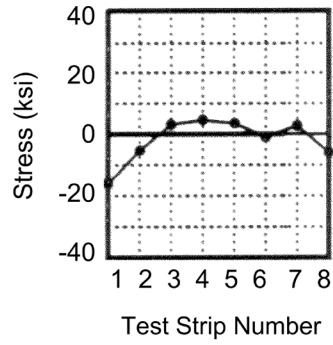
Note: Positive stress indicates tension. Negative stress indicates compression.
Source: Avent and Mukai (1998)

Figure 9. Illustration. Typical residual stress distribution for a Category S heat-straightened wide flange beam.
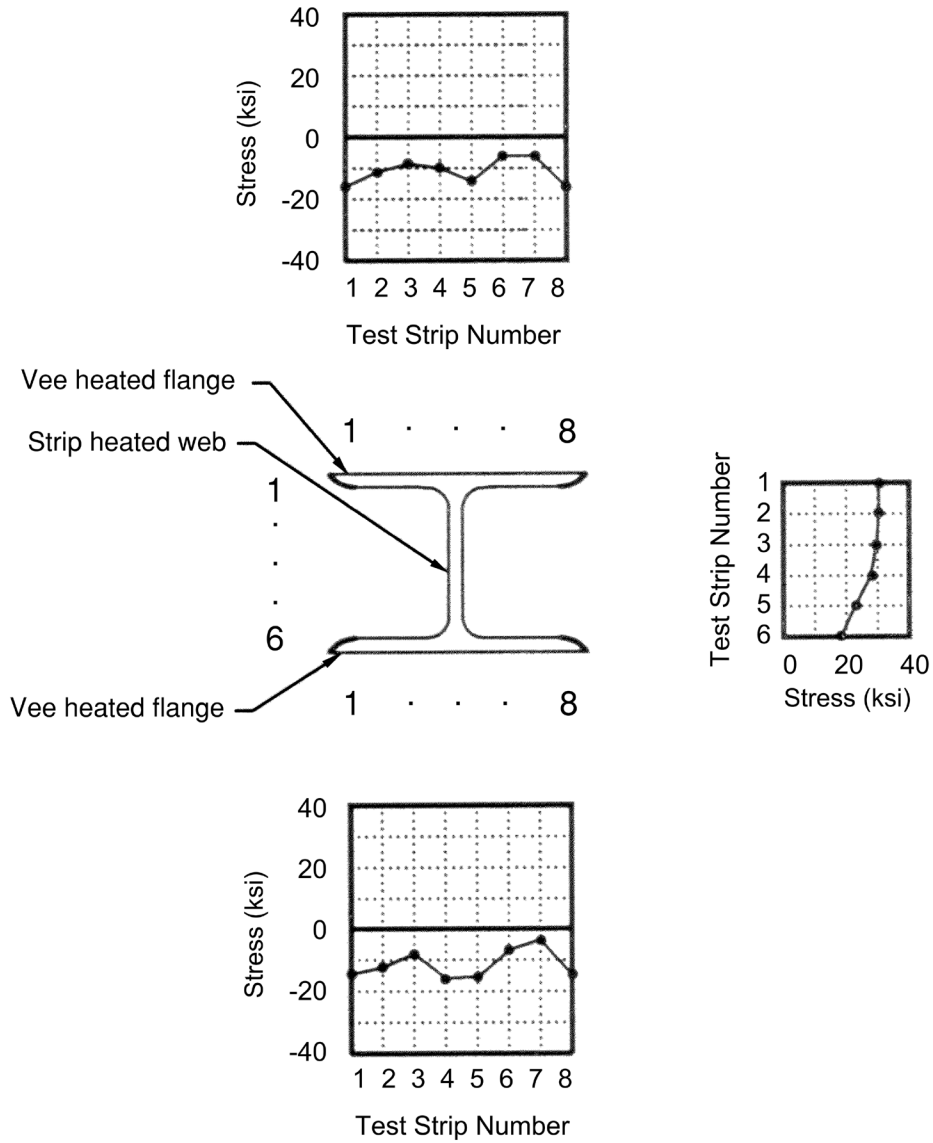
Note: Positive stress indicates tension. Negative stress indicates compression.
Source: Avent and Mukai (1998)

Figure 10. Illustration. Typical residual stress distribution for a Category W heat-straightened wide flange beam.

16

In summary, the residual stresses in the heat-straightened plates were consistent, having maximum compressive stresses of about 20 ksi at the edges and tensile stresses of about one-half that value at the center of the plate. For the heat-straightened angles and channels, compressive residual stresses approaching yield were measured at the toes and heels of the sections. Additionally, relatively high tensile stresses were found near the middle of each leg. For both wide flange beam specimens, compressive residual stresses were the maximum at the flange edges.

The residual stresses created during heat straightening have several implications. First, if the member is a compression element, the residual stresses produced during heat straightening are similar in magnitude to that of welded built-up members. Because many U.S. design specifications use a single column curve concept, these members typically are all treated the same, and no capacity reduction should be assumed. Second, movement during straightening can be reduced, or even reversed, if residual stresses are not accounted for when calculating jacking force (e.g., high tensile residual stresses can cancel out compressive stresses produced by the applied jacking force, and vice versa). Finally, large compressive residual stresses can produce bulges in the compression regions of a cross section during heat straightening. Special heating patterns and sequences may prevent this.

2.1.3. The Effects of Heat on Basic Material Properties

The application of heat can affect the material properties of steel during the heat straightening process and after the material has cooled. The following sections discuss the basic material properties of steel that are integral to bridge performance. Also addressed are changes to properties during the application of heat, as well as following the application. It should be noted that the primary focus of the discussion below is the effect of heat on material properties.

2.1.3.1 Thermal Expansion

One of heat straightening's fundamental aspects is the thermal expansion of steel. The coefficient of thermal expansion is a measure of the rate of strain per degree temperature. The relationship between the coefficient of thermal expansion and temperature for low-carbon steels is shown in figure 11.
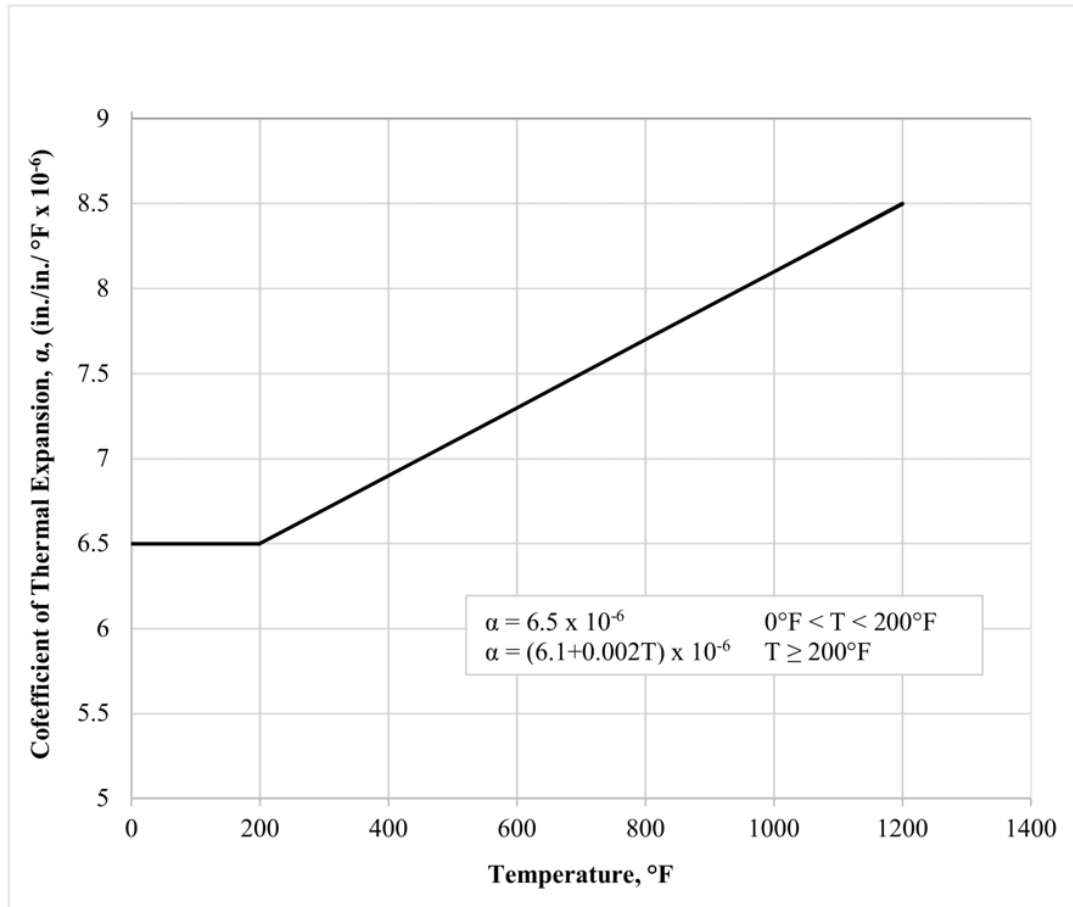
Source: Roeder (1985)

Figure 11. Graph. Variation of coefficient of thermal expansion versus temperature.

Between approximately 200 and 1,200°F, the coefficient of thermal expansion varies linearly with temperature (Blodgett, 1972; Ditman, 1961; Nicholls and Weerth 1972; Roeder 1985, 1986). However, most curves of this type do not exceed temperatures of 1,200–1,400°F because the relationship between coefficient of thermal expansion and temperature becomes irregular beyond this range. The irregularity is likely due to the phase changes that occur in steel at temperatures between 1,300 and 1,600°F.

Although Roeder (1985, 1986) has shown that for vee heats, the coefficient of thermal expansion continues to increase in a predictable manner up to 1,600°F for carbon steels and HSLA steels, surface damage occurs more readily at higher temperatures. As a result, suggested maximum heat straightening temperatures are typically well below 1,600°F. This is discussed in further detail in section 2.2.3.

2.1.3.2 Modulus of Elasticity

The modulus of elasticity of steel varies as a function of temperature. Between 100 and 1,200°F, the modulus of elasticity decreases with increasing temperature, and at 1,200°F is approximately half the value at ambient temperature (70°F). This relationship is shown in figure 12 where E_0 is the modulus of elasticity at ambient temperature (29,000 ksi at 70°F) and T is temperature in

18

degrees Fahrenheit (Roeder, 1985, 1986). Researchers have investigated the changes in modulus of elasticity after heat straightening (Nicholls and Weerth, 1972; Horton, 1973). Tests from this work have shown that for undamaged steel, the modulus of elasticity does not change appreciably after heat straightening and cooling.
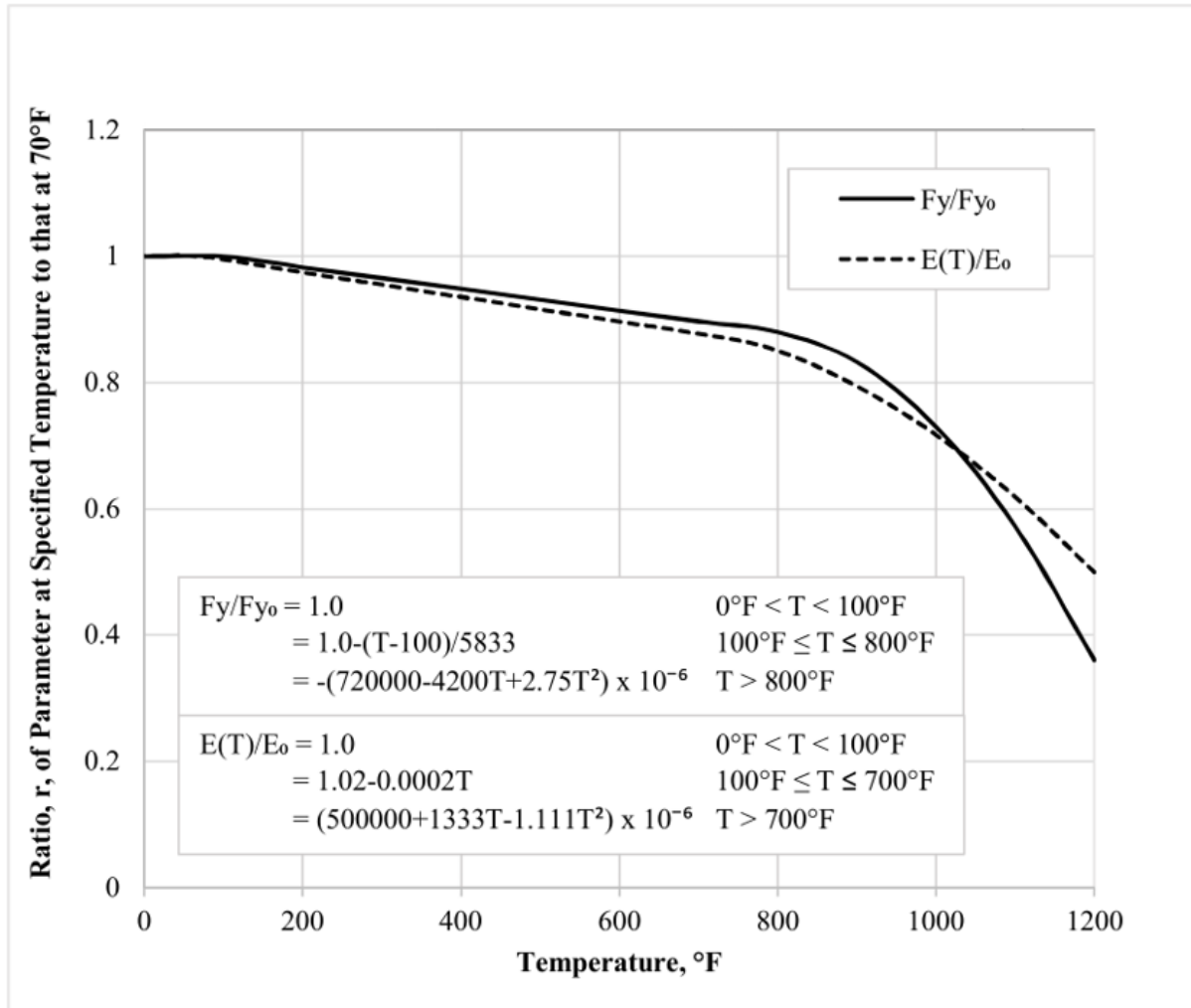
Source: Roeder (1985)

Figure 12. Graph. Normalized yield stress and modulus of elasticity versus temperature.

2.1.3.3 Yield Stress

The process of heat straightening affects the yield stress of steel in two distinct ways. The first is the variation of yield stress during the heating process. The second is the permanent effect heat straightening can have on yield stress after the steel has cooled. Figure 12 shows the relationship between yield stress and temperature for carbon steel where T is the temperature in degrees Fahrenheit and F_{yo} is the nominal yield stress at 70°F. The figure shows that when the temperature of the steel reaches 1,200°F, the yield stress is about 40 percent of its original value. This is an important consideration in the heat straightening process, specifically when calculating and applying external restraining forces. This concept and the associated suggestions are discussed further in section 2.2.3.

Several researchers have studied the effect of heat straightening on the yield stress of steel after cooling. The researchers measured yield stress after heating/cooling cycles to determine the effect of heat straightening on the parameter. Avent and Mukai (1998) compiled the results of such research and state that for carbon steel, the yield stress increased an average of 10 percent after heat straightening. For HSLA steel, they state that a 2 percent increase in yield stress was observed while A537 steel was noted as showing an average 7 percent increase in yield stress. Finally, for Q&T steel, yield stress decreased about 6 percent. Further, the tested specimens were heated for various lengths of time, cooled both by air and by quenching with a mist, and were subjected to various superimposed loads and residual stresses. None of these variables had significant effect on the yield stress except for Q&T steel, but that was not fully evaluated due to the limits of the study. These data indicate that the heat straightening process has a small but generally positive effect on yield stress for steels that are not Q&T steels.

2.1.3.4 Ductility

Ductility, or the ability of a material to deform plastically prior to rupture, is an important characteristic of steel, especially for bridge construction. Maintaining ductility in steel is crucial; therefore, it is important to understand the long-term effects of heat straightening on this property. Many researchers have investigated this by measuring ductility (measuring percent elongation) before and after heat straightening for various types of steel. Research summarized by Avent and Mukai (1998) stated that, in general, there is a "10-20 percent decrease in ductility after the steel has experienced a cycle of heat straightening. This range is the percent reduction and should not be construed as the actual reduction. The average decreases are: carbon steels 8 percent; high strength, low alloy steels, 18 percent; quenched and tempered steels, 14 percent." While these changes in ductility are not trivial and should be considered when using heat straightening, the magnitude of the reductions was within an acceptable range, as stated by Avent and Mukai (1998).

2.1.3.5 Rockwell Hardness

A change in surface hardness before and after heat straightening can indicate changes to the general mechanical properties of steel. Investigators have conducted Rockwell hardness tests on heat-straightened specimens to determine the effect that the heat straightening process has on hardness. Pattee et al. (1970) and Harrison (1952) conducted Rockwell hardness tests following heat straightening for several specimens and found that in general the hardness values did not change appreciably after heat straightening, regardless of steel type. Changes in hardness were limited to approximately 3 to 6 percent. More recently, Varma and Sohn (2013) conducted Rockwell hardness tests on damaged and heat-straightened wide flange sections. Compared to the undamaged and unheated specimens, the hardness of most damaged/repaired specimens was between 8 and 15 percent higher. However, specimens that underwent repair using low temperature and high jacking force, compared to typically used values to replicate deviations from the typical repair procedure, exhibited an average 21 percent increase in hardness compared to the undamaged specimens.

2.1.3.6 Toughness

The Charpy V-Notch (CVN) test is used to infer steel toughness. The test specimen is typically a small rectangular bar with a specified V-shaped notch at its mid-length. The bar is simply supported near its ends, acting as a beam, and is struck by a swinging pendulum. The amount of energy absorbed by the specimen is calculated from the height the pendulum rises after impacting the specimen. The test is done over a range of temperatures, and a plot of the absorbed energy versus temperature is generated. The resulting curve is often S-shaped with an upper limit asymptote of constant energy absorption as the temperature increases and a lower limit asymptote as the temperature decreases. These asymptotes are referred to as the upper and lower shelves, respectively. Like other material properties of steel, the effect of heat straightening on impact energy has been investigated by several researchers. This work, summarized by Avent and Mukai (1998), indicates that, in general, the upper shelf energy absorption does not change significantly before and after the heat straightening process for any grade of steel.

A second measure, the temperature at which 50 percent of the upper shelf energy is absorbed, or T_{50}, can also be obtained from the CVN test described above. The T_{50} can be measured prior to and following heat straightening, and the difference between the original T_{50} and the T_{50} after heat straightening can be calculated. In this case, a positive value indicates a decrease in impact energy after heat straightening and a negative value indicates an increase. Several researchers found impact energy to vary considerably among specimens of the same steel grade. However, Avent and Mukai (1998) note that only the Q&T, low alloy steels exhibited a positive shift, or decrease, in impact energy after heat straightening.

A third measure that can be obtained from the CVN test is the fracture transition temperature. For temperatures below this fracture transition temperature, the material fractures in a brittle manner. For temperatures above this value, the material fractures in a ductile manner. This parameter is typically obtained from the plot of energy absorption versus temperature and is usually described as the vertical line between the upper and lower shelves of the S-curve. A variation of this parameter can be determined based on shear fracture area rather than energy absorption. The 50 percent shear area transition temperature is the temperature at which 50 percent of the cross-section fractures in shear (brittle fracture) and 50 percent fractures via fibrous fracture (ductile fracture). Pattee et al. (1970) used this criterion in evaluating the change in toughness for several grades of heat-straightened steel. The Drop Weight Tear test, similar to the CVN test described above, was used for this experimental program. From this testing, which included specimens tested prior to and following application of heat, the fracture transition temperature changes were modest for all steel types except ASTM A517 grade A steel. In this case, a significant positive shift in 50 percent shear area transition temperature was observed, indicating a sensitivity to brittle fracture following heat straightening.

2.1.3.7 Fatigue

Fatigue resistance is a parameter related to steel bridge component toughness. Fatigue testing of materials subjected to heat straightening alone is limited; most research in this area focuses on the effect of damage and heat straightening on fatigue resistance of full-size specimens. The extent of past research on the fatigue resistance of heated bridge material is limited to work completed by Wilson (1946) and Connor et al. (2008). In the research done by Wilson, eye bars

of ASTM A7 steel were heat-shortened and then fatigue cycled. When compared to similar specimens that had not been heated, the fatigue resistance at both 500,000 and 1,000,000 cycles were similar. The research presented by Connor et al. found that in general, fatigue life is not reduced by damage and repair cycles alone. However, if microcracking, which may be difficult to detect, is present after repetitive damage repair cycles where cracking occurs during the cold bending of impact, a decrease in fatigue life may be observed. On the other hand, in the work by Connor et al., high levels of localized strain were introduced to the large-scale specimens at the exact same location and repaired multiple times. It is unlikely that such repeated damage would occur in actual field conditions where the precision and control achieved in a laboratory cannot occur. Nevertheless, the study suggests that fatigue-sensitive details be limited to two repairs if the damage is confined to the same area. The effect of repeated heat straightening is discussed further in section 2.1.9.2.

2.1.4. Mechanical Properties of Heat-Straightened Plates

In the past, a large portion of testing for the basic mechanical properties of heat-straightened steel has been conducted on undamaged or minimally damaged specimens that underwent a limited number of heating cycles. Avent and Mukai (1998) summarize that, following the heat straightening process, the following changes to mechanical properties were observed:

- Little change in modulus of elasticity
- Slight increase in yield stress
- 10 to 20 percent reduction in ductility.

The mechanical properties of damaged plates (or rolled shapes) after large numbers of heating cycles are of more practical significance, since damage typically requires more cycles to repair.

Avent et al. (1992) investigated this behavior by conducting material property tests on a series of ¼ × 4 × 24 inch ASTM A36 plates (P-9 through P-14) that were damaged and repaired using numerous cycles of heating (25-100 cycles, vee heat). Tensile tests were conducted on coupons taken from various test strips located in the heated region including at the apex (test strip 1 or 2), middle (test strip 4 or 5), and open end of vee (test strip 7 or 8). A strip taken from an unheated region of the same plate (test strip UH) was tested for comparison purposes. Yield strength, tensile strength, percent elongation, percent reduction area, and modulus of elasticity were measured for plates P-9 through P-14 and are shown in table 1.

Table 1. Material properties of damaged and heat-straightened plates[1,2] (Avent and Mukai, 1998).

Specimen/Test Strip		Yield Strength (ksi)	Maximum Tensile Strength (ksi)	Percent Elongation	Percent Reduction in Area	Modulus of Elasticity (ksi × 10³)
P-9	UH	46.8	68.7	45	58	28.9
	1	51.7	70.5	33	46	—
	5	49.8	70.6	38	60	31.7
	7	50.0	70.3	39	60	32.2
P-10	UH	48.7	71.7	41	56	32.2
	2	52.3	71.2	30	62	30.3
	5	51.9	71.9	31	60	24.9
	7	51.7	69.7	34	64	18.2
P-11	UH	45.1	72.4	42	57	31.2
	1	55.4	73.6	30	60	31.7
	4	51.1	72.6	41	58	25.6
	8	48.3	71.2	36	57	22.9
P-12	UH	43.9	66.5	46	60	24.2
	2	52.0	68.4	34	63	22.3
	5	48.3	68.8	36	60	22.9
	7	47.0	69.0	36	60	17.0
P-13	UH	46.9	69.6	43	59	28.6
	2	50.0	70.7	32	57	36.3
	5	46.0	67.9	—	—	21.7
	7	43.7	67.6	35	65	18.3
P-14	UH	42.3	69.0	41	58	27.8
	2	60.1	75.6	28	51	43.6
	4	48.6	71.7	35	59	35.5
	8	50.9	70.7	34	56	28.9

[1] Rate of strain = 0.4545 in/in per minute up to yield, 1.0714 in/in per minute up to failure.
[2] Percent Elongation on 1-inch gauge length.
Note: (—) indicates data not collected or calculated. Vee angle is 45 degrees for all specimens. Vee heats are full depth for all specimens except P-14, which was heated with 0.75 vee depth.

2.1.4.1 Yield Stress and Tensile Strength

The data from table 1 shows that a portion of the heated specimens exhibit increases in yield stress over that of the unheated material (specifically at the apex of the vee, test strips 1 or 2). The average increase for the six specimens taken from the apex of the vee heat was about 17 percent. This value is nearly twice the increase found for the undamaged specimens discussed in section 2.1.3.3. It is likely that the large number of repetitive heat cycles provided some amount of heat treatment resulting in a more significant increase in yield strength (Avent et al., 1992).

The maximum tensile strength values were more consistent. Variations in tensile strength between the heated and unheated strips differed by less than 4 percent, except for plate P-14, where a 10 percent increase was observed. As a result, Avent et al. (1992) concluded that the

application of numerous heat straightening cycles generally reduces the difference between yield stress and tensile stress for damaged plates.

2.1.4.2 Modulus of Elasticity

The research discussed in section 2.1.3.2 concluded that a small number of heating cycles generally do not affect the modulus of elasticity of undamaged steel. However, the work completed by Avent et al. (1992) indicates that the modulus of elasticity of a damaged and heat-straightened plate (considering both heated and unheated test strips) varies more substantially. This variation ranges from 11 to 77 percent across specimens from the same plate. For plates P-9 and P-14, the modulus of elasticity of the heated regions increased an average of 11 and 30 percent, respectively, compared to that of the unheated steel. However, for the other four plates, the modulus of elasticity of the heated regions decreased an average of 13 to 31 percent compared to that of the unheated steel. From this data, Avent et al. (1992) concluded that heat straightening tends to reduce the modulus of elasticity in the heated regions compared to that of unheated and undamaged steel.

2.1.4.3 Ductility

Like previous work discussed in section 2.1.3.4, the ductility of the specimens tested by Avent et al. (1992) was quantified by measuring percent elongation. As shown in table 1, the percent elongation decreased for all test strips tested, consistent with previous tests summarized in section 2.1.3.4. The elongation of the unheated test strips ranged from 41 to 46 percent, while the average for each of the heated plates ranged from 32 to 37 percent. Thus, the ductility of the plates decreased by about one-third after heat straightening. It should be noted that the decrease in ductility was similar for all plates despite differences in the degree of damage, jacking ratio, depth of vee heat, and number of heating cycles applied. From this, Avent and Mukai (1998) concluded that the magnitude of these parameters (degree of damage, number of heating cycles) do not significantly affect the material properties of the steel.

To investigate this further, Avent and Mukai (1998) used the experimental data from Avent et al. (1992) to conduct an independent sample statistical t-test for each property, assigning a statistical significance to the effects of one damage/straightening cycle on material properties. These results are summarized in table 2, which presents the confidence level of one damage/repair cycle causing an increase or decrease (as noted) in each material property. As shown in the table, there is a high level of confidence that yield stress will increase and percent elongation will decrease in all test strips within the test specimen. However, the confidence level of increased tensile stress and decreased reduction of area was low (below 95 percent) for all test strips within the test specimen.

Table 2. T-test confidence levels for changes to material properties of heat-straightened plates (Avent and Mukai, 1998).

Test Strip No.	Yield Strength[1]	Tensile Strength[1]	Percent Elongation[2]	Percent Reduction In Area[2]
1 and 2	99.9	92.0	99.9	69.8
4 and 5	99.2	78.0	99.6	3.7
7 and 8	96.2	53.9	99.9	8.9

[1] Confidence level that heat straightening a deformed plate will cause an increase in the property shown over that of the same specimen before the damage/straightening cycle.

[2] Confidence level that heat straightening a deformed plate will cause a decrease in the property shown over that of the same specimen before the damage/straightening cycle.

Avent and Mukai (1998) compared the heat-straightened specimens to the unheated specimens from Avent et al.'s (1992) testing and ASTM material specifications and noted only the material properties yield strength and percent elongation. These are the properties affected by damage/repair cycles with a high level of confidence. This comparison is shown in table 3, where the material properties of the heated specimens are compared to the unheated specimen and ASTM specifications via percent of unheated (UH) specimen property and percent of ASTM minimum standard property. For ASTM A36 steel, the ASTM minimum yield stress is 36 ksi, and the ASTM standard minimum percent elongation is 23 percent for a 2-inch gauge length. Use of ASTM specifications is not a Federal requirement.

Table 3. Comparison of material properties of heat-straightened steel plates with unheated specimens and ASTM values (Avent and Mukai, 1998).

Plate/Test Strip		Yield Strength		Percent Elongation	
		Heated to Unheated Ratio	Heated to ASTM Ratio	Heated to Unheated Ratio	Heated to ASTM Ratio
P-9	1	1.10	1.14	0.74	0.97
	5	1.06	1.38	0.84	1.12
	7	1.97	1.39	0.87	1.15
P-10	2	1.07	1.45	0.73	0.88
	5	1.07	1.44	0.76	0.91
	7	1.06	1.44	0.83	1.00
P-11	1	1.23	1.54	0.71	0.88
	4	1.13	1.34	0.98	1.21
	8	1.07	1.31	0.86	1.06
P-12	2	1.18	1.44	0.74	1.00
	5	1.10	1.34	0.78	1.06
	7	107	1.31	0.78	1.06
P-13	2	1.07	1.39	0.74	0.94
	5	1.10	1.28	—	—
	7	1.07	1.21	0.81	1.03
P-14[1]	2	1.42	1.67	0.68	0.82
	4	1.15	1.35	0.85	1.03
	8	1.20	1.41	0.83	1.00

[1] A three-quarter depth vee heat was used on this plate.
Note: (—) indicates data not collected or calculated.

Based on table 3, it should be noted that the material properties of the heated specimens, in most cases, remained above the ASTM minimum values for both yield stress and percent elongation. As such, although material property changes were noted following heat straightening of the damaged specimens, in general the final material properties of the specimens still satisfied the ASTM material property limits for A36 steel.

In addition to the above conclusion by Avent and Mukai (1998), Avent et al. (1992) noted that the highest value for yield stress after heat straightening (60.1 ksi) was obtained in test strip 2 of plate P-14. This was the only plate in the testing program where a vee heat depth ratio of 0.75 was used instead of 1. Because test strip 2 was in a region that had undergone compressive deformation but had not been directly heated, due to the three-quarter depth vee heat, Avent et al. concluded that it was likely to retain more strain hardening effects than if it were contained within the vee-heated area. Further, Avent et al. (1992) proposed that the minor re-stretching effect in the upper portion of this plate (addressed by Roeder, 1985 and 1986) may have caused cyclic hardening that would not have been present had the material been directly heated. This is exhibited in the fact that test strip 2 alone among the plates experienced a significant increase in tensile strength over the unheated specimen for that plate (10 percent). A similar behavior was noted near the apex of the three-quarter depth vee heat during further testing conducted by Avent

et al. (1992) on damaged and heat-straightened wide flange beams. The results of this testing and similar, more recent testing programs are discussed in section 2.1.5.

2.1.5. Mechanical Properties of Heat-Straightened Wide Flange Beams

While the testing of damaged and heat-straightened plate specimens, discussed in section 2.1.4, provides valuable insight into the material properties of damaged and heat-straightened steel, the performance of damaged and heat-straightened wide flange beams provides further practical insight with similar results in a more detailed investigation.

Avent et al. (1992) also conducted laboratory-scale testing on a series of wide flange beams subjected to several cycles of damage and heat straightening. Tensile tests were conducted on test strips taken from four W6×9 beams damaged by bending about their minor/weak axis (category W, as discussed in section 2.2). In each case, 45-degree, 3/4 depth vees, as described in section 2.2.2, and a 50 percent jacking ratio, described in section 2.2.3, were used. Vee heats were applied on both flanges, and a strip heat was applied on the web. In addition to evaluating material properties, the purpose of these tests was to determine the effects of repetitive cycles of damage and repair. Beam B-1 was damaged and repaired once, while Beams B-2, B-3, and B-4 were damaged and repaired twice, four times, and eight times, respectively. In each case, the degree of damage (angle) was in the range of 6 to 8 degrees, and about 20 heat cycles were needed to complete the repair. After the last damage/repair cycle for each beam, one of the flanges was sectioned, and tensile tests were conducted on test strips near the apex (test strips 1 or 2), center (test strips 4 or 5), and open end (test strips 7 or 8) of the vee. An unheated test strip (labeled UH) was also tested. Figure 13 illustrates the test strip numbering and locations.
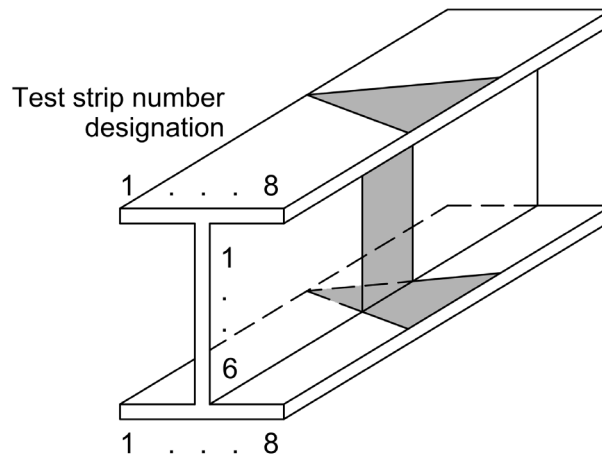
Source: FHWA

Figure 13. Illustration. Residual stress strip locations (Category W heat).

More recent testing programs, of similar scope and approach to that of Avent et al. (1992), capture different steel types, section sizes, and section types. Research completed by Connor et al. (2008) included large-scale testing of wide flange sections made from ASTM A992 Grade 50, A572 Grade 50, ASTM A709 Grade 50, and ASTM A709 Grade 36 steel fabricated with a variety of fatigue-sensitive details, including transverse stiffeners and cover plate terminations. The test specimens underwent one, two, and three damage (weak axis bending) and repair cycles.

Following damage and heat straightening, full-scale fatigue testing was completed to investigate the post-repair behavior of the sections at the fatigue-sensitive details. In addition, specimens were taken from various locations within the heated regions to complete tensile and CVN testing of the damaged and heated steel.

Similarly, research by Kowalkowski and Varma (2007) included testing of wide flange sections made from ASTM A7 (legacy steel type obtained from a decommissioned bridge girder), ASTM A588 and ASTM A36 steel that each underwent three damage (weak axis bending) and repair cycles. The severity of damage, magnitude of restraining force and heating temperature were varied between the specimens to capture the effect of these variables on the material properties of the steel. Specimens were taken from various locations within the heated regions for tensile testing of the damaged and heated steel. In addition, CVN testing was performed to investigate the impact energy of the specimens following damage and repair.

Similar testing was completed by Varma and Sohn (2013) in a comprehensive research program where both small- and large-scale testing was completed. The small-scale testing comprised a series of non-composite wide flange sections fabricated using ASTM A36 steel. Six beam specimens were subjected to cycles of damage and repair. Following these cycles, specimens from these beam sections were tested to investigate the effect of the following on material properties: the number of damage/repair cycles (up to three cycles were tested), excessive damage, overheating, and underheating with overstraining during repair. All specimens were damaged about their weak axis. The large-scale testing was similar, except a large-scale two-span "test bridge" was used. The test bridge was composed of four A36 W30×90 rolled beams (two per span) with an 8-inch, 4000 psi reinforced concrete composite deck. The steel was also damaged about the weak axis. Like the small-scale tests, specimens taken from the four test girders were tested following cycles of damage and repair to investigate the effect of number of damage cycles (up to three cycles), overheating, and underheating with overstraining on material properties. The results of the small- and large-scale tests were comparable, and similar conclusions were drawn from both. Results from both experiments are discussed in following sections.

In the case of the work completed by Connor et al. (2008), Kowalkowski and Varma (2007), and Varma and Sohn (2013), test results for the damaged and heated steel were compared to those of undamaged and unheated steel to quantify the changes to material properties following cycles of damage and repair. The results of these more recent investigations are discussed below and compared to the work by Avent et al. (1992) to corroborate similar findings and provide further, more recent data on the effect of damage and heat straightening on the performance of steel sections.

2.1.5.1 Yield Stress and Tensile Strength

Based on the testing completed by Avent et al. (1992), the change in yield stress of the damaged and repaired steel compared to that of undamaged steel was investigated (see table 4 and figure 14). The most significant increase in yield stress was noted in specimens near the apex of the vee heat, with yield stress increasing further with additional damage and repair cycles. The yield stresses at other locations within the vee heat increased in the range of 9 to 21 percent, with an average increase of 13 percent (similar to that of damaged and heat-straightened plates, section

2.1.4). Avent et al. (1992) concluded that these data confirm the sensitivity of the apex region of the vee heat, and that repetitive damage and repair cycles increase yield stress (especially beyond two cycles).

Table 4. Material properties of damaged and heat-straightened W6×9 wide flange beams[1,2] (Avent and Mukai, 1998).

Specimen/ Test Strip	Number of Damage/ Repair Cycles	Vee Angle (degree)	Yield Strength (ksi)	Tensile Strength (ksi)	Percent Elongation	Percent Reduction in Area	Modulus of Elasticity (ksi x 10³)
B-1 (UH)			45.4	67.4	43	63	32.3
1	1	20	57.7	73.6	30	62	33.9
5			53.9	73.4	36	64	24.1
7			49.4	70.2	29	64	31.6
B-2 (UH)			47.6	68.3	42	66	29.4
2	2	30	63.5	78.0	31	60	24.7
4			51.3	75.4	32	61	17.9
8			52.2	71.0	31	65	29.4
B-3 (UH)			45.1	68.0	43	65	26.9
2	4	45	70.9	82.5	22	59	33.7
4			56.6	75.3	26	57	28.8
8			52.7	75.9	27	42	38.7
B-4 (UH)			46.8	68.1	45	66	38.7
2	8	45	88.1	99.1	15	41	39.2
4			51.3	76.3	24	52	—
8			49.8	71.5	23	61	—

[1] Rates of Strain = 0.2206 in/in per minute up to yield, 0.8824 in/in per minute up to failure.
[2] All values have been converted to represent an ASTM sized specimen, as noted in Avent et al., 1992, and a 1-inch gauge length was used.
Note: (—) indicates data not collected or calculated. Full depth vee heats used for all specimens. Jacking ratio of 0.25 used for specimen B-4, while all other jacking ratios were 0.00.
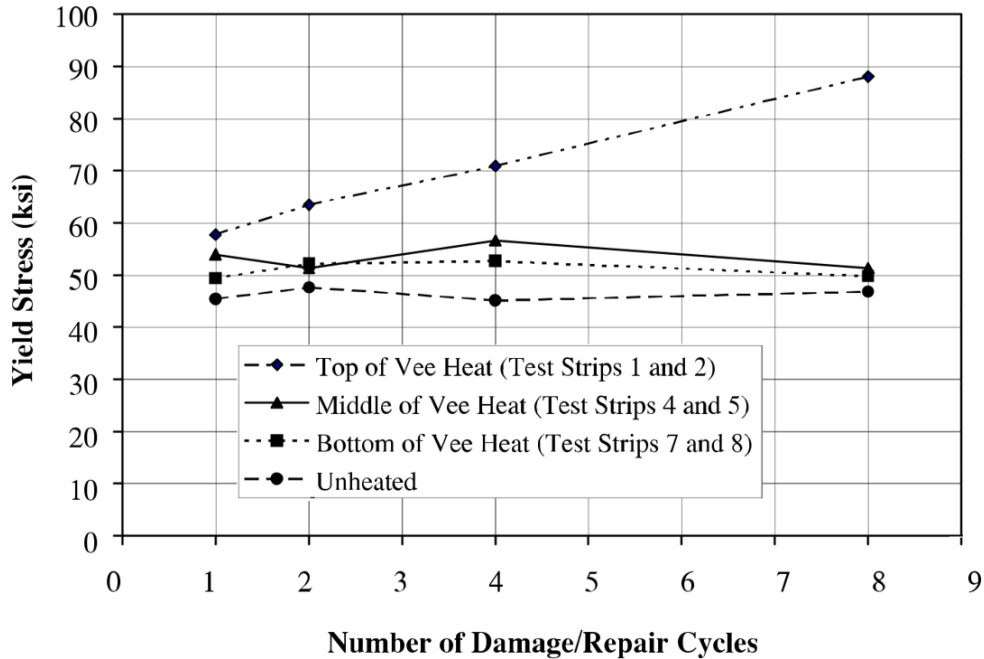
Figure 14. Graph. Yield stress versus number of damage/repair cycles.

Testing conclusions presented by Varma and Sohn (2013) provide further evidence of an increase in yield stress as a result of heat straightening. Results from their experiments, shown in table 5 and table 6, support the conclusions stated by Avent et al. (1992). The yield and tensile stress for repairs performed at 1,200°F of heat-straightened materials increased with the number of repairs performed. However, for members that were overheated and straightened at 1,400°F, the increase in yield and tensile stress was reduced with additional damage-repair cycles. Varma and Sohn noted that the results from overheating would require replication before reliable conclusions can be made.

Table 5. Uniaxial tension test results on varying heat straightening repairs in small scale testing (Varma and Sohn, 2013).

Specimen	Repair Temp. (°F)	Number of Repair Cycles	Restraining Moment (M_r)	Yield Strength (ksi)	Tensile Strength (ksi)	Elongation (%)	Reduction In Area (%)
#1	1,200	1	0.4 M_p	47.51	69.61	36.76	58.12
#2	1,200	3	0.4 M_p	54.78	73.75	29.24	56.25
#3	1,400	3	0.4 M_p	53.10	71.61	36.79	58.02
#4	1,400	1	0.4 M_p	54.92	71.50	34.69	56.89
#5	1,400	1	0.4 M_p	45.48	70.47	31.88	57.19
#6	800	1	0.6 M_p	47.24	71.80	33.80	57.37
Undamaged	-	-	-	44.46	64.75	39.20	56.23

Note: M_p is the plastic moment capacity of the member.

Table 6. Uniaxial tension test results on varying heat straightening repairs in large scale testing (Varma and Sohn, 2013).

Specimen	Repair Temp. (°F)	Number of Repair Cycles	Restraining Moment (M_r)	Yield Strength (ksi)	Tensile Strength (ksi)	Elongation (%)	Reduction In Area (%)
S1	1,400	3	0.4 M_p	46.05	66.75	33.50	64.50
S2	1,400	1	0.4 M_p	48.80	65.25	35.50	65.50
N1	1,200	3	0.4 M_p	57.75	71.25	29.50	64.00
N2	800	1	0.6 M_p	54.00	68.00	33.00	63.00
Undamaged	-	-	-	40.90	59.75	42.50	67.50

Note: M_p is the plastic moment capacity of the member.

In similar tests completed by Connor et al. (2008), yield stress of the damaged and repaired specimens increased between 7 and 20 percent for one damage/repair cycle, 8 to 15 percent for two damage/repair cycles, and 8 to 30 percent for three damage/repair cycles. These increases are generally in agreement with that observed by Avent et al. (1992), which generally agree with results on 1,200°F specimens from Varma and Sohn (2013). The scatter in the data obtained by Connor et al. (2008) is attributed to the limited test specimens from each section tested. In addition to testing damaged and repaired specimens, the researchers tested several specimens that underwent damage only to investigate the effect of damage on yield stress. Yield stress from damage alone increased by a wider margin than in beams subjected to damage and repair. Connor et al. (2008) concluded that damage alone primarily contributes to the increase in yield stress, while the application of heat during straightening tends to reduce or restore yield stress in damaged specimens. This is in general agreement with the findings discussed in section 2.1.4 regarding the unheated, damaged portion of the plate specimens exhibiting increased yield stress compared to that of the heated/repaired portions (Avent et al., 1992).

In similar work completed by Kowalkowski and Varma (2007), the yield stress of the damaged and repaired specimens generally increased compared to that of the undamaged and unheated specimen. The magnitude of the increase was in general agreement with that observed by Avent et al. (1992) and Connor et al. (2008) except for the ASTM A588 specimens. For both the ASTM A7 and A36 specimens, an approximate 7 to 25 percent increase in yield stress was observed. For ASTM A588 steel, the increase was much smaller, within 10 percent of the undamaged and unheated specimens. This work was limited, however, in number of damage and repair cycles tested. All specimens were subjected to three damage and repair cycles.

Based on the work completed by Avent et al. (1992), tensile strength of the damaged and repaired steel increased compared to that of undamaged and unheated steel, but only by a small margin, about 10 percent, for most specimens. The specimen near the apex of the vee heat exhibited a more substantial increase in tensile strength than other specimens, as shown in figure 15. However, the tensile strength increase at the apex was smaller than the yield strength increase, narrowing the gap between yield and ultimate stress for the material. From this, Avent et al. (1992) suggest that heat straightening should be limited to no more than two damage and repair cycles to prevent a further decrease between ultimate strength and yield stress. However, their conclusions are based on observations of material property changes in small, localized

areas, and the effect of repetitive damage and repair on the element as a whole are not expected to be significant.
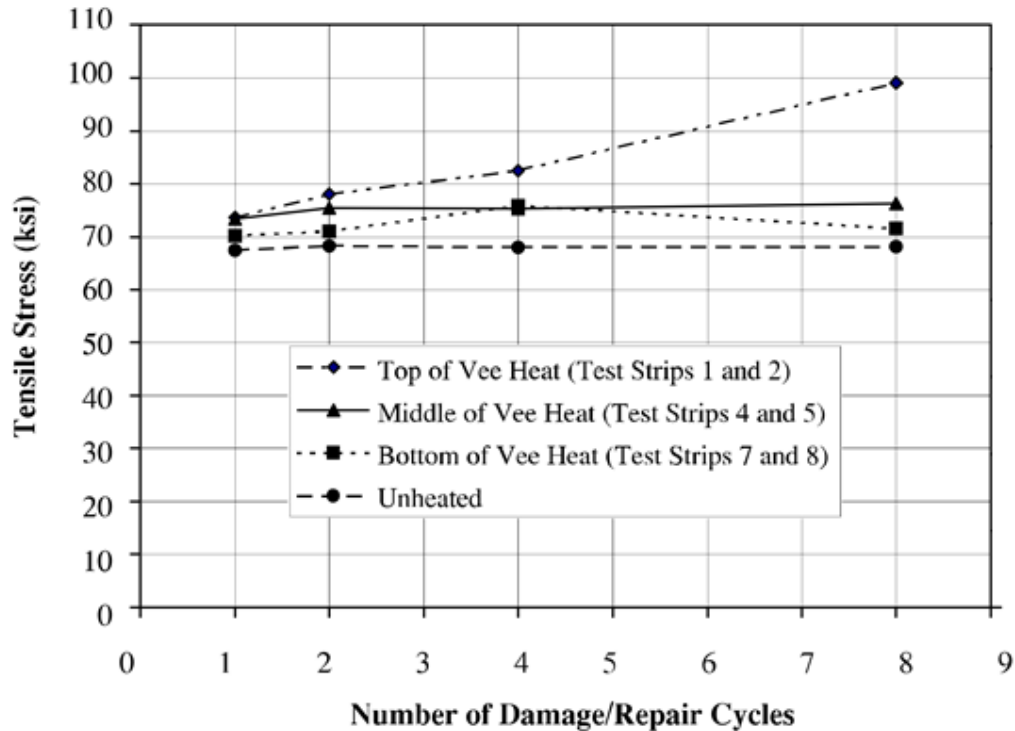
Source: Avent et al. (1992)

Figure 15. Graph. Tensile stress versus number of damage/repair cycles.

Similarly, Connor et al. (2008) found that although tensile strength increased for damaged and repaired specimens, it increased by a smaller margin compared to yield stress. The margin by which tensile strength increased was about 10 percent, regardless of the number of damage and repair cycles. This finding is in general agreement with Avent et al. (1992).

Finally, Kowalkowski and Varma (2007) found that damage and repair cycles did not generally affect the tensile strength of the specimens, and that the tensile strength of the specimens following cycles of damage and repair were within 10 percent of the undamaged and unheated specimen with no distinct trend observed. However, the specimens tested by Kowalkowski and Varma (2007) did not include specimens located in the apex of the vee heat region, which Avent et al. (1992) found to be the most sensitive to damage and repair cycles. As such, the behavior of specimens tested by Kowalkowski and Varma (2007) is expected to differ compared to the behavior of the specimens near the apex of the vee heat region tested by Avent et al. (1992). Excluding those apex-region specimens, the findings from both investigations are in general agreement.

2.1.5.2 Modulus of Elasticity

Avent et al. (1992) found that modulus of elasticity, on average, decreased between 8 and 23 percent for specimens with one and two damage/repair cycles. However, on average, an increase in modulus of elasticity was observed for specimens with four damage/repair cycles. In general,

comparing specimen results, the modulus of elasticity varied regardless of the number of damage/repair cycles, with no distinct trend observed by the researchers.

Kowalkowski and Varma (2007) found that, although modulus of elasticity varies between specimens, it is generally unaffected by damage/repair cycles. The modulus of elasticity for most specimens, following damage and heat straightening, was within 10 percent of the undamaged and unheated specimens. Connor et al. (2008) and Varma and Sohn (2013) did not directly measure or discuss change in modulus of elasticity due to damage/repair cycles.

2.1.5.3 Ductility

Avent et al. (1992) found that, in general, ductility decreased substantially, approximately 30 percent, following one damage/repair cycle. Ductility decreased further with additional damage/repair cycles; the largest reductions occurred in the specimens near the apex of the vee heat region that underwent four and eight damage/repair cycles. Figure 16 summarizes these results.
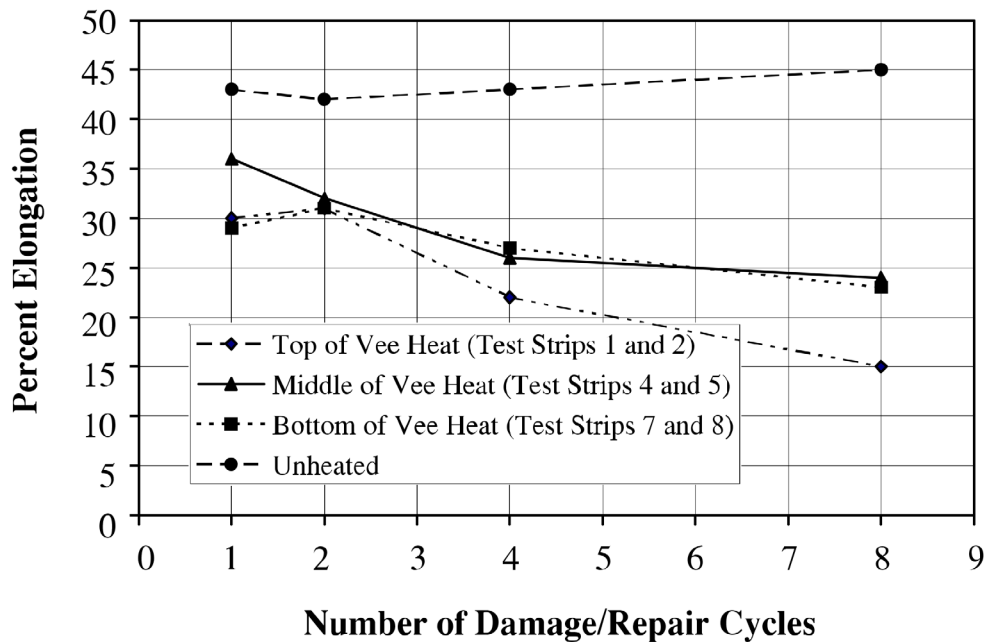
Source: Avent et al. (1992)

Figure 16. Graph. Percent elongation versus number of damage/repair cycles.

The results presented by Connor et al. (2008), Kowalkowski and Varma (2007), and Varma and Sohn (2013) agree with the conclusions of Avent et al. (1992). In all cases, ductility decreased substantially following several cycles of heat straightening. Of particular interest is the dramatic effect that underheating and overstraining had on ductility, as Varma and Sohn (2013) observed. For example, table 6 shows where one heat straightening cycle resulted in elongation that was only 78 percent of that from an undamaged specimen.

As a result of these observations, Avent et al. (1992) concludes that the number of damage/repair cycles should be limited to two cycles to prevent undesirable changes to material properties as

after two cycles of damage/repair, changes to material properties generally become unacceptable. However, the research presented by Connor et al. (2008), Kowalkowski and Varma (2007), and Varma and Sohn (2013) suggest that a decrease in ductility alone does not substantiate a two-cycle limit on damage/repair cycles for girders.

2.1.5.4 Rockwell Hardness

Kowalkowski and Varma (2007) conducted Rockwell B hardness tests to measure the effect of damage/repair cycles on the surface hardness of steel. For all steel types considered—ASTM A7, ASTM A588, and ASTM A36—independent of the number of damage/repair cycles, there was no significant change in Rockwell B hardness for damaged/repaired specimens compared to undamaged specimens. In all cases, the Rockwell B hardness values for the damaged/repaired specimens were within 10 percent of that of the undamaged specimens.

Similarly, Varma and Sohn (2013) conducted Rockwell B hardness tests on damaged and heat-straightened wide flange sections. For most damaged/repaired specimens from both the small-scale and large-scale testing, an 8 to 15 percent increase in Rockwell B hardness was observed compared to that of undamaged specimens. However, small-scale specimens that underwent repair using low temperature and high jacking force (compared to typically used values) exhibited an average 21 percent increase in hardness compared to undamaged specimens. The average results of the Rockwell B hardness tests for both small-scale and large-scale test specimens are shown in tables 7 and 8, respectively.

Table 7. Rockwell hardness tests results on varying heat straightening repairs in small scale testing (Varma and Sohn, 2013).

Specimen	Repair Temperature (°F)	Number of Repair Cycles	Restraining Moment (M_r)	Average Rockwell B Hardness
#1	1,200	1	$0.4\,M_p$	82.6
#2	1,200	3	$0.4\,M_p$	82.8
#3	1,400	3	$0.4\,M_p$	80.9
#4	1,400	1	$0.4\,M_p$	84.6
#5	1,400	1	$0.4\,M_p$	84.6
#6	800	1	$0.6\,M_p$	89.2
Undamaged	-	-	-	73.8

Note: M_p is the plastic moment capacity of the member.

Table 8. Rockwell hardness tests results on varying heat straightening repairs in large scale testing (Varma and Sohn, 2013).

Specimen	Repair Temperature (°F)	Number of Repair Cycles	Restraining Moment (M_r)	Average Rockwell B Hardness
S1	1,400	3	0.4 M_p	79.0
S2	1,400	1	0.4 M_p	75.8
N1	1,200	3	0.4 M_p	78.1
N2	800	1	0.6 M_p	76.8
Undamaged	-	-	-	69.9

Note: M_p is the plastic moment capacity of the member.

Avent et al. (1992), and Connor et al. (2008) did not consider Rockwell hardness.

2.1.5.5 Fracture Toughness

CVN tests were conducted by Connor et al. (2008) to capture the change in fracture (or notch) toughness due to damage/repair cycles. Specimens were tested at 40°F, and absorbed energy was measured. Compared to that of undamaged steel, for one damage/repair cycle, fracture toughness decreased an average 64 percent; for two damage/repair cycles fracture toughness decreased a total of 37 percent; and for three damage repair cycles fracture toughness decreased a total of 50 percent. However, considerable variability was observed in data and, as such, no specific relationship between heat straightening and percent reduction in fracture toughness per damage cycle could be established. Connor et al. (2008) concluded that, in general, a decrease in toughness was typical as the number of damage/repair cycles at the same location increased. From this, the researchers conclude that the number of damage/repair cycles should be limited to two when "subsequent damage falls within the limits of the first impact repair." See section 2.1.5.6 for further discussion of this limit.

Kowalkowski and Varma (2007) also conducted CVN tests on their specimens to capture the change in fracture toughness due to damage/repair cycles for several types of steel. These researchers also observed significant variability in their data. For some damaged/repaired specimens, fracture toughness decreased significantly and for others toughness increased. These results depended on the severity of damage, grade of steel, and repair methodology. For damage levels and repair methodologies similar to those used by other researchers (Connor et al., 2008; Avent et al., 1992; Varma and Sohn, 2013), a general decrease in fracture toughness was observed.

Finally, Varma and Sohn (2013) conducted CVN tests for both large- and small-scale test specimens. For the specimens taken from the small-scale test beams, CVN testing was conducted at 40°F and absorbed energy was measured. These measured values, however, were abnormally low; well below the minimum values as per Federal regulation (23 CFR 625.4(d)(1)(v)) even for the undamaged specimens. Through further testing of the undamaged specimens over a variety of temperatures, this was found to be due to the initial testing temperature of 40°F being in the transition region of the temperature versus impact energy graph. To rectify this issue, the researchers selected a new CVN test temperature of 70°F from this graph. These results were in

better agreement with the expected values for the undamaged steel, and thus allowed for comparison between the damaged/repaired and undamaged specimens. These results—average values for each tested beam specimen—are shown in table 9. CVN testing was also conducted on the specimens from the large-scale tests. A test temperature of 40°F was used similar to the initial testing on the small-scale specimens and tests conducted by other researchers. The results of this testing, average values for each tested beam specimen, are shown in table 10.

Table 9. Charpy V-Notch test results on varying heat straightening repairs in small scale testing (Varma and Sohn, 2013).

Specimen	Repair Temp. (˚F)	Number of Repair Cycles	Restraining Moment (M$_r$)	Mean CVN Result @ 40˚F (lb-ft)	Standard Deviation (lb-ft)	Mean CVN Result @ 70˚F (lb-ft)	Standard Deviation (lb-ft)
#1	1200	1	0.4 M$_p$	11.8	1.5	27.7	11.3
#2	1200	3	0.4 M$_p$	8.9	2.0	21.4	11.8
#3	1400	3	0.4 M$_p$	12.3	7.3	28.0	16.6
#4	1400	1	0.4 M$_p$	9.3	2.1	21.0	12.9
#5	1400	1	0.4 M$_p$	11.3	3.0	40.1	10.2
#6	800	1	0.6 M$_p$	5.7	0.5	9.6	1.7
Undamaged	-	-	-	19.9	4.3	47.9	8.5

Note: M_p is the plastic moment capacity of the member.

Table 10. Charpy V-Notch test results on varying heat straightening repairs in large scale testing (Varma and Sohn, 2013).

Specimen	Repair Temp. (˚F)	Number of Repair Cycles	Restraining Moment (M$_r$)	Mean CVN Result @ 40˚F (lb-ft)	Standard Deviation (lb-ft)
S1	1400	3	0.4 M$_p$	66.1	63.8
S2	1400	1	0.4 M$_p$	78.4	24.1
N1	1200	3	0.4 M$_p$	49.7	28.3
N2	800	1	0.6 M$_p$	77.9	43.3
Undamaged	-	-	-	243.9	6.3

Note: M_p is the plastic moment capacity of the member.

2.1.5.6 Fatigue

Connor et al. (2008) used several fatigue details on their girder specimens to capture the fatigue resistance of the steel following damage and subsequent heat straightening. The fatigue details considered are consistent with those in AASHTO 2017b and required by 23 CFR 625.4(d)(1)(v) and included: base metal (Category A), longitudinal web-to-flange welds (Category B), transverse stiffeners welded/not welded to the flanges (Category C'), cover plate terminations (Category E'), and flange attachments (Category E). The fatigue testing itself was conducted following one, two, and three cycles of damage and repair.

Nondestructive testing (NDT) was conducted by Connor et al. (2008) following damage and repair to confirm that no surface cracks were present at any of the fatigue details due to damage and repair. Any cracks, nicks, and gouges were treated by grinding and sanding both the base metal and weld toes as needed. Additionally, any cracks observed at the welds of the fatigue details were repaired by removing and re-welding prior to testing. This allowed researchers to capture the fatigue resistance independent of localized damage due to impact. Following this, the girder specimens were loaded under four-point bending with hydraulic actuators, inducing a constant amplitude loading at a frequency of 64 cycles per minute. Category C' details were located in the constant moment region of the girder and Category E and E' details were located in the moment gradient regions of the girders. This allowed researchers to test all fatigue details on a girder specimen using different amplitudes of loading simultaneously. Stress-cycle curves were produced from testing results. These curves were used to illustrate the fatigue life of the specimen being tested. Fatigue life is the total number of cycles (load fluctuations) at a certain stress level needed to cause the initiation and propagation of cracks to a critical size.

In general, Connor et al. (2008) found that after up to two cycles of damage/repair, no appreciable effect on the fatigue life of the girders was noted when post-damage/repair treatments, including grinding, sanding and re-welding of weld toes, were conducted. This "treatment" of the fatigue details following damage and repair removed any cracks or surface defects from which cracks could propagate during fatigue testing. However, in two instances, girders subjected to three cycles of damage/repair had fatigue cracks prematurely appear in the base metal. Since no cracks or defects were noted during NDT prior to fatigue testing, further examination was required. Upon further investigation of the fracture surface, Connor et al. (2008) concluded that a flaw (micro-crack) within the thickness of the flange (undetectable by traditional surface NDT techniques) may have propagated and led to the premature failure. Based on these observations, Connor et al. suggests that the maximum number of damage/repair cycles be limited to two. However, Connor et al. presented this recommendation with the caveat that it applies only to cases where subsequent instances of damage/repair are separated by less than 12 inches. For cases where subsequent instances of damage/repair are greater than 12 inches apart, the suggested limit of two damage/repair cycles is conservative. Similarly, the researchers note that this suggestion would also be conservative for girders without such fatigue details.

2.1.6. Material Properties of Field Heat-Straightened Wide Flange Beams

Although studies of the material properties of field heat-straightened girders are limited, one such study was conducted by Putherickal (1992) using specimens provided by the Iowa DOT. The Iowa DOT had allowed heat straightening of bridge girders for several years prior to the time of the study. One such girder (W30×108) was removed from service several years after repair for reasons unrelated to the original heat straightening repair. Tensile tests were conducted on specimens taken from both the heat-straightened zone and unheated zone of the girder. Similar to the investigations by Avent et al. (1992), Connor et al. (2008), Kowalkowski and Varma (2007), and Varma and Sohn (2013), material properties of the damaged and repaired specimens were compared by Putherickal (1992) to that of the undamaged and unheated specimens. In addition to tensile testing, microstructure comparisons between the heated and unheated specimens were completed to investigate the differences between the specimens on a microscopic level.

Table 11 summarizes the material properties measured. Both yield and tensile strength increased significantly after damage and repair, but the increases were not proportional. Elongation decreased significantly and hardness (Brinell Hardness) increased, indicating that the material was overheated. The CVN values in the unheated regions were below modern acceptable limits. However, the values in the heated regions were even lower. All data from the material testing suggest that the material in the overheated zone became more brittle. Further, the microstructure comparison between the heated and unheated specimens showed clear signs of recrystallization in the heat-straightened area. The heated piece was partly austenitized and recrystallized into finer grains, providing further evidence that steel was heated above the lower critical temperature. The results of this testing illustrate the effects of overheating steel during the heat straightening process and exemplify the need for careful control of material temperature during heating.

Table 11. Material properties from an improperly heat-straightened girder taken from Iowa bridge, removed from service (Putherickal, 1992).

	FLANGE		WEB	
	Unheated Section	**Heated Section**	**Unheated Section**	**Heated Section**
Yield Strength (ksi)	37.4	59.0	45.3	57.4
Tensile Strength (ksi)	64.1	69.2	63.7	72.2
Ratio of Yield and Tensile (Percent)	58	85	71	80
Elongation[1] (Percent)	36	26	34	22.5
Reduction in Area (Percent)	62	61	60.4	51.8
Charpy V-Notch[2] (Ft. Lb.)	19, 22, 16	6, 7, 9	16, 11, 10	--, 4, 6
Brinell (500 Kg) Hardness	119, 114, 107	139, 143, 143	119, 114, 109	150, 158, 143

[1] Percent Elongation on a 2-inch gauge length
[2] Charpy V-Notch values taken at 40°F
Note: Chemical analysis percent by weight: Carbon-0.289; Manganese-0.647; Silicon-0.032; Sulfur-0.031; Phosphorus-0.009

The results from Putherickal (1992) illustrate that, although it is not advisable to overheat steel during heat straightening, the member should not necessarily be removed from service if accidentally overheated. Engineering judgment and data presented in this manual should be used to determine the safety of the member. This concept is further corroborated by the findings of Varma and Sohn (2013), where researchers found that, although overheating the steel during heat straightening is not advised, slight overheating, at least up to 1,400°F, may be an acceptable deviation from the suggested procedures. Test data showed that the increase in yield and ultimate stress and decrease in ductility in the overheated specimens were similar to that of the normally heated specimens (1,200°F). Varma and Sohn (2013) suggest that, since research on this topic is still limited, further investigations should be conducted to validate this conclusion.

2.1.7. Member Shortening

Little direct research has been conducted on member shortening due to heat straightening. The amount of shortening in a member following heat straightening can be quite significant, regardless of heating pattern, depending on the scale of the member size. For minor damage to

large bridge elements, member shortening is typically not an issue. Figure 17 illustrates the basic concept of member shortening during the heat straightening process. If the plate shown in the figure is damaged about its strong axis with a midpoint loading (as shown), the top edge of the plate experiences compressive yielding (shortening) and the bottom edge of the plate experiences tensile yielding (stretching). As the plate is subjected to the heat straightening process, the top edge experiences some "re-stretching." However, these positive strains are small in comparison to the simultaneous shortening that occurs in the bottom edge of the plate.
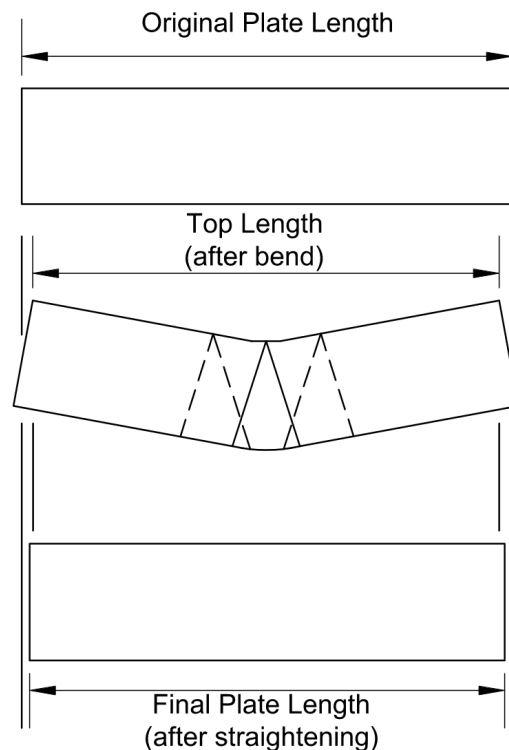
Source: FHWA

Figure 17. Illustration. Shortening of a beam or plate after heat straightening.

Avent et al. (1992) sought to quantify the amount of shortening experienced for a given amount of damage. To investigate this, researchers measured the series of damaged and heat-straightened plates discussed in section 2.1.4. The plates, ¼ × 4 × 24 inch, were damaged via bending about their strong axis.

When studying the effect of heat straightening on damaged steel plates, the researchers damaged the steel plate specimens by cold bending them to a desired radius. Cold bending usually increases the centerline length of a member. Thus, to eliminate this factor from the investigation, the researchers measured initial length of the plate prior to damage and final length after heat straightening was completed. Note that, regardless of initial and final lengths, shortening occurs only within the damaged and repaired region, meaning shortening should not be expressed as a percentage of total length, but rather as a length itself.

Figure 18 shows a plot of member shortening versus degree of damage, obtained from the study completed by Avent et al. (1992). As shown in the figure, shortening varied directly with degree of damage, up to about 18 to 24 degrees for the specimens studied. Additionally, the researchers found that shortening appeared to be a function of plate width and was affected by the degree of damage itself. It was observed that shortening did not vary with vee depth ratio, at least when considering vee depth ratios of 0.75 to 1.00. The amount of shortening in the full-depth vees (plate P-14) was about the same as that for three-quarter depth vees (plates P-9 and P-11). All specimens with three-quarter depth vees followed the same trend of shortening exhibited by those heated with full-depth vees. From this work, Avent et al. (1992) developed the following formula for estimating shortening:

$$S = 0.005 W \varphi_d \quad 0 < \varphi_d < 24° \tag{1}$$

where S = shortening in inches, φ_d = angle of damage in degrees, and W = plate width.
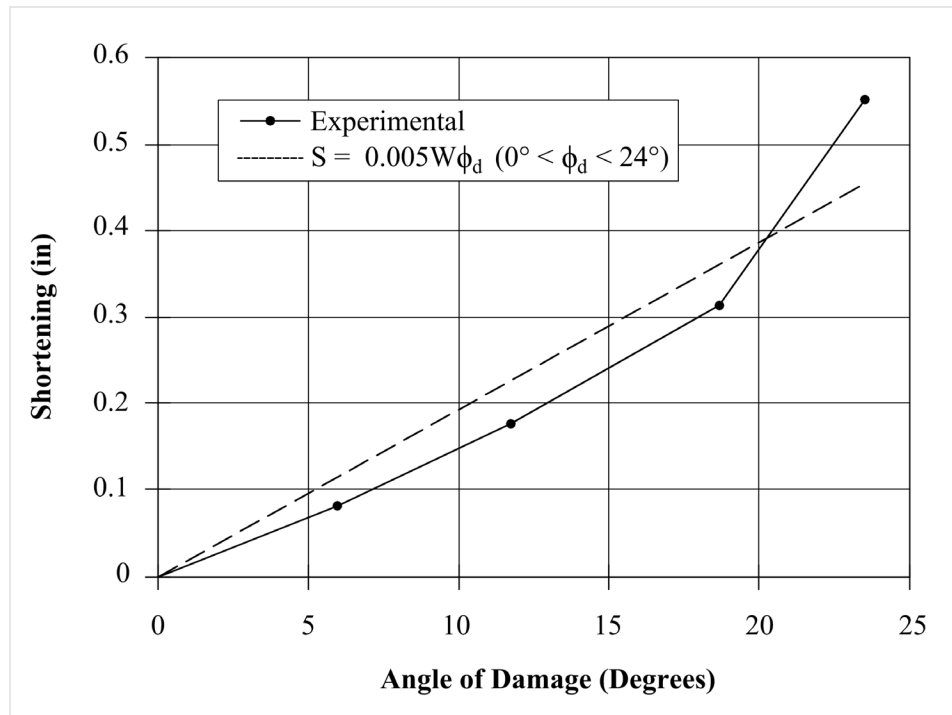
Source: Avent et al. (1992)

Figure 18. Graph. Shortening versus degree of damage for plate elements.

In addition to the plates discussed previously, Avent et al. (1992) also tested four damaged and heat-straightened W6×9 beams for shortening. These beams, discussed further in section 2.1.5, were damaged repeatedly about their weak axes to an angle of about seven degrees, approximately the same as the least damaged of the deformed plates discussed above. Each incident of damage was repaired using 45-degree vees with a depth ratio of 0.75 and a jacking ratio of 0.5. The number of damage/repair cycles varied for each of the beams, but each repair cycle consisted of approximately 20 heat cycles. Each time a beam was damaged and straightened, researchers measured a net shortening of about 0.10 inch in the heated region. These values were in general agreement with the plate shortening equation, equation 1. As a

result, Avent et al. (1992) concluded that the shortening equation developed for plates could also be applied to estimate shortening in wide flange beams.

2.1.8. Redistribution of Materials

In addition to measuring shortening in damaged and heat-straightened plates, Avent et al. (1992) investigated the redistribution of materials through upsetting because of the damage/repair process. Consider, again, the damaged and heat-straightened plates discussed in sections 2.1.4 and 2.1.7.

As a result of the heat straightening process and the concept of member shortening, the heated portions of the deformed plate elements studied by Avent et al. (1992) thickened, or upset, during straightening. To quantify this thickening, researchers, milled test strips from each plate specimen and measured thickness at various locations along each test strip. Five locations were measured along each test strip, with a thickness measured to 0.001-inch accuracy. The researchers found that thickening was greatest for the plates damaged to the largest degrees. For example, in plate P-10, the specimen with the greatest amount of damage (an angle of 23.62 degrees), the thicknesses along the center of damage averaged 0.655 inch. When compared to the average thickness of the plate before damage (0.485 inch), the thickening resulted in a 32 percent increase in cross-sectional area. At points farther away from the center of damage, thickening was less pronounced. Regardless, some amount of thickening occurred across the entire yield zone. Although a thicker cross-section does result in a stronger member at that location, researchers suggest that this thickening is not structurally significant.

Similarly, Avent et al. (1992) also measured the redistribution of materials in the damaged wide flange beams discussed in sections 2.1.5 and 2.1.7. Their work also showed thickening in the heated region of the wide flange beam specimens. After the first damage/repair cycle, researchers found that the thickening that occurred in the cross section resulted in a spreading of the yield zone in each subsequent re-damage. Due to the larger yield zone after subsequent damage cycles, the heating locations were spread over a greater length to ensure heat was applied to the entire yield zone. Researchers found that the number of heating cycles needed to straighten each bend remained consistent but was more widely distributed due to the larger yield zones.

2.1.9. Impact on Material Properties of Heat-Straightened Steel and Practical Considerations

As discussed in previous sections, research data indicate that heat straightening does affect the material properties of steel. Early researchers used undamaged steel and a small number of heating cycles to conclude that property changes were minimal. More recent research (Avent et al., 1992; Connor et al., 2008; Kowalkowski and Varma, 2007; Varma and Sohn, 2013) included testing on damaged and heat-straightened steel specimens (plates and wide flange beams) subjected to numerous damage and repair cycles. As a result of this work, researchers have concluded that changes to the material properties due to both damage and heat application can be significant enough to potentially affect the damaged/repaired member in service. However, the changes may not be detrimental or significant enough to prevent the material from meeting current specification-required minimums. As discussed in sections 2.1.4 and 2.1.7, after damage and repair, yield stress increased, especially in the vicinity of the apex of vee heats. Tensile strength also increased but by a much smaller margin than yield stress. Ductility, as measured by

percent elongation, decreased after cycles of damage and repair, and the modulus of elasticity, on average, decreased (Avent et al., 1992), though the values were highly variable across the specimens. Additionally, impact energy (toughness), although highly variable in the damaged/repaired specimens, generally decreased with increased number of damage and repair cycles (Kowalkowski and Varma, 2007; Connor et al., 2008; Varma and Sohn, 2013). Similarly, the base metal fatigue life, for the base metal specifically located near fatigue-sensitive details (e.g., stiffeners, cover plates), was found to be reduced by 50 percent or more after three cycles of damage/repair at the same exact location compared to the first two damage/repair cycles (Connor et al., 2008).

2.1.9.1 Material Properties and Fatigue Resistance

The decreased ductility in the damaged and repaired specimens relates to stress concentrations and fatigue resistance. Stress concentrations occur around discontinuities in structural members such as holes, welded stiffeners, and notches (Barsom and Rolfe, 1987). Structural designers rely on the ductility of the material to redistribute the load around a mild stress concentration, such as a drilled hole, within specification-imposed limits for fatigue. However, a decrease in ductility may reduce inelastic stress redistribution, thus leaving a higher stress concentration.

Regarding yield and tensile strength of a material and fatigue resistance, studies have confirmed that the fatigue strength of welded and bolted structures and connections is independent of the strength of steel. The small benefit associated with higher strength steels is outweighed by the negative effects on fatigue life introduced by welding and bolting. For example, the defects and residual stresses present in every welded detail will dominate the fatigue strength far more than the influence of yield strength. As such, the minor changes to yield and tensile strength resulting from multiple heat straightening repairs are not expected to have a substantial effect on fatigue resistance.

A decrease in fracture toughness, a value proportional to the energy consumed during plastic deformation, after several damage/repair cycles was observed in several investigations (Connor et al., 2008; Kowalkowski and Varma, 2007; Varma and Sohn, 2013). Captured via the CVN test, fracture toughness contributes to the prevention of sudden unstable cracks and crack growth. Fracture toughness was found to decrease with increased damage/repair cycles; however, the measured data were highly variable.

Investigations performed by Connor et al. (2008) on the fatigue resistance of damaged and heat-straightened girders found that base metal fatigue life at the point of impact or damage decreased substantially in two specimens after three or more high strain damage/repair cycles at the exact same location. This scenario is unlikely to occur outside of a laboratory setting. This decrease in fatigue life was found to likely be the result of micro-cracks that developed within the thickness of the section due to the repetitive severe impacts at the exact same location. These micro-cracks, undetectable by traditional NDT techniques, likely propagated in fatigue and lead to the observed fracture. As such, spacing between impact locations and severity of damage strains produced should be considered when evaluating an acceptable limit on the number of repairs for in-service members versus observations from laboratory test specimens.

The subject of stress concentrations, brittle fracture and fatigue resistance discussed above is dependent on the specific geometry or configuration; thus, it is difficult to make general suggestions without detailed analyses of a particular situation. In general, heat straightening areas that will sustain high stress concentrations in service should be avoided when possible and only done after a sufficient analysis by a qualified engineer. The impact of damage and heat straightening of beams with various typical fatigue-sensitive details (stiffeners, cover plates, etc.) were studied by Connor et al., (2008). Although the behavior of the beams following damage and repair cycles was in general agreement with that observed for beams without stiffeners (Avent et al., 1992), a number of considerations related to the welded stiffeners (including localized damage from the impact, bunching and surface cracking near welds due to damage, etc.) needed to be addressed prior to heat straightening. Section 2.3 discusses repair techniques, suggested by Connor et al. (2008), used to address these considerations prior to heat straightening. These techniques include grinding smooth any cracks, gouges, or nicks prior to heat straightening repair to reduce the creation or propagation of fatigue stressors. Although these considerations are almost entirely related to the local damage imparted on the specimen due to impact and not heat straightening itself, these observations demonstrate the complexity introduced to the heat straightening repair process when stress concentration and fatigue-sensitive areas are involved.

2.1.9.2 Suggested Maximum Number of Repairs

As a result of the investigations discussed in this section, researchers developed suggested limits for the number of damage and repair cycles at the same location. A limit of two heat straightening repairs was suggested by Avent et al. (1992) and Avent and Mukai (1998) for beams re-damaged at the same location. For damage occurring within 12 inches of previous damage, Connor et al. (2008) suggested limiting the number of heat straightening repairs of damaged beams to two repairs at the same location. However, researchers note that this suggestion is conservative for base metal without fatigue-sensitive details and conservative for instances of subsequent damage and repair located more than 12 inches apart. As such, for these scenarios, a maximum of three damage and repair cycles may be acceptable. Similarly, Kowalkowski and Varma (2007) found that, for up to three damage and repair cycles, heat straightening had only a modest effect on the material properties of all three steel grades tested (ASTM A588, A7, and A36). Based on their findings, Kowalkowski and Varma (2007) suggest a three damage and repair cycle limit. A similar conclusion was drawn by Varma and Sohn (2013), which found three damage and repair cycles acceptable. However, they suggested conducting further research to validate such a suggestion.

Based on the findings from the body of research discussed in this section, engineers should consider the following conditions, in addition to engineering judgment, when determining the number of acceptable subsequent heat straightening repairs:

- A maximum of three damage and repair cycles may be acceptable when damage to a section is located more than 12 inches from a previous damage location; and damage strain, as discussed in section 2.3.3, is less than 150 times the yield strain.
- A maximum of two damage and repair cycles may be acceptable when damage to a section is located less than or equal to 12 inches from a previous damage location; and damage strain, as discussed in section 2.3.3, is less than 150 times the yield strain.

Caution and engineering judgment are needed in using the data presented in this section to use heat straightening in sensitive or otherwise complex scenarios.

2.1.10. Important Considerations

- While at elevated temperatures, nearing the lower critical temperature, the yield strength and tensile strength of steel is reduced.
- The coefficient of thermal expansion increases with temperature above 200°F and becomes irregular with temperatures beyond the 1,200-1,600°F range.
- The maximum heating temperature should not exceed the lower critical temperature (approximately 1,333°F) for non-quenched and tempered steels, or the tempering temperature for quenched and tempered steels, to prevent phase changes in the steel.
- Residual stresses are altered in heat-straightened members with maximum values reaching yield at some locations. This characteristic is similar to that of typical welded built-up members.
- The most sensitive area for material property changes is the region of the vee heat apex.
- Engineers should consider the data presented in this publication and utilize engineering judgment when determining the number of damage and repair cycles that are acceptable for each specific damage scenario.
- Records of damaged and heated zones should be kept for future reference in case the member is re-damaged.
- Member shortening will occur and should be anticipated. Full and ¾ -depth vee heats produce similar levels of member shortening.
- The heated zone will thicken as a result of heat straightening.

2.2. BASICS OF FABRICATION AND STRAIGHTENING WITH HEAT

This section provides a basic introduction to the categorization of damage types, the principal heating techniques used to introduce curves or repair curvature to various steel sections, as well as an outline of the overall heat straightening process.

2.2.1. Typical Types of Damage

Damage to steel bridge members may result from a variety of causes. While the damage to a structure may appear random, certain patterns and characteristics are distinguishable.

One way to classify damage is to consider the four fundamental damage patterns or categories. The importance of this classification system is that well-defined heating patterns can be established for each damage category. Once these patterns are understood, they can be used in combination for damage that includes multiple categories. The fundamental damage categories are described in the following sections.

2.2.1.1 Category S

This damage type refers to damage as a result of bending about the "strong" or major axis of the section. For rolled or built-up shapes, the web element is bent about its strong axis with one flange element in compression and one in tension. In addition to plastic deformation, the

compression flange and web may sometimes exhibit local buckling due to the high compressive stresses. A typical example of category S damage is shown in figure 19.
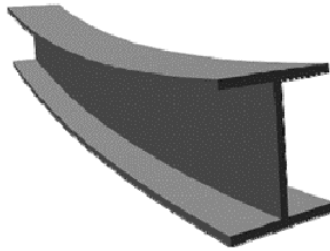
(A)   ISOMETRIC VIEW
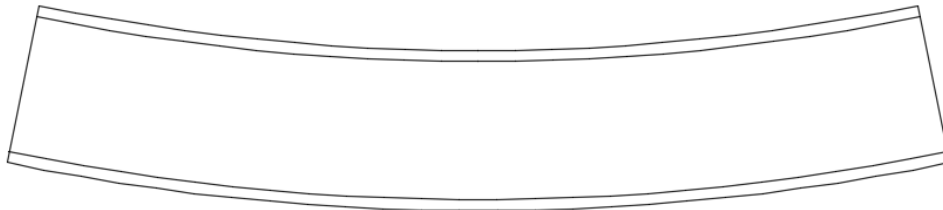
(B)   ELEVATION

Source: FHWA

Figure 19. Illustration. Category S damage.

2.2.1.2 Category W

This damage category refers to damage as a result of bending about the "weak" or minor axis of the section. For rolled or built-up I-shapes, the neutral axis is usually within or near the web. Consequently, the web may not yield or deform into the inelastic range. If neither is laterally restrained, the flange elements are bent about their strong axes and usually exhibit classical flexural yield patterns. An example of category W damage is shown in figure 20.
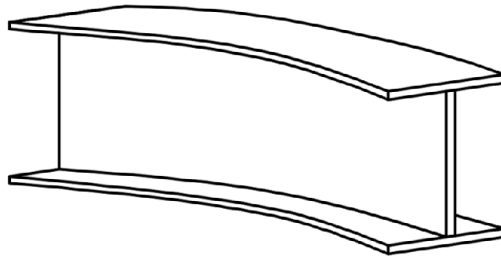
(A) ISOMETRIC VIEW
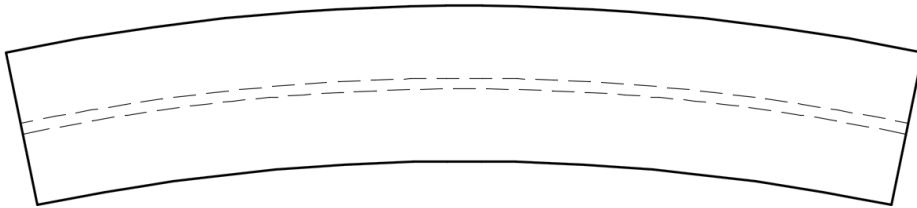
(B) PLAN VIEW

Source: FHWA

Figure 20. Illustration. Category W damage.

2.2.1.3 Category T

This type refers to damage from torsion or twisting about the longitudinal axis of a member. For rolled or built-up shapes, if neither is laterally braced, the flange elements tend to exhibit flexural plastic deformation in opposite directions. The web is often stressed at levels below yield. However, if one flange is constrained (such as the case of a composite bridge girder), then the unconstrained flange element is subjected to plastic deformation and yielding may also occur in the web. An example of this behavior is shown in figure 21.

Source: George Watson, 2021

Figure 21. Photo. Category T damage on a bridge girder in Indiana.

2.2.1.4 Category L

This category includes damage that is localized in nature (e.g., local flange or web buckling, web crippling, web damage at bracing locations, and bends or crimps in plate elements). An example of category L damage is shown in figure 22.
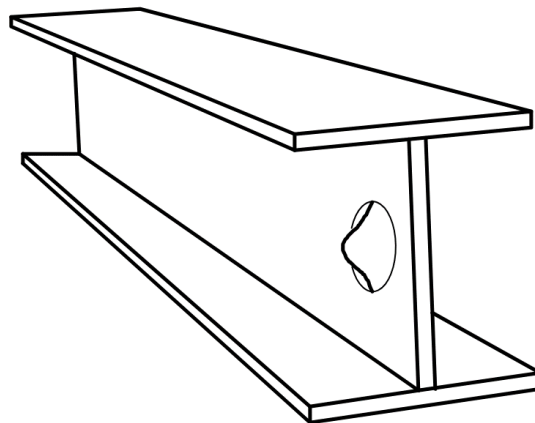
Source: FHWA

Figure 22. Illustration. Category L damage on the web of a wide flange section.

2.2.2. Basic Heating Patterns

2.2.2.1 Vee Heats

The vee heat is the most fundamental pattern used to straighten strong axis (category S) bends in steel plate elements. As shown in figure 23, a typical vee heat starts with a very small spot heat

applied at the apex of the vee-shaped area. When the desired heating temperature is reached, the torch is advanced progressively in a serpentine motion toward the base of the vee. This motion is efficient for progressively heating the vee from top to bottom. The plate initially moves upward (figure 23-A) as a result of longitudinal expansion of material above the neutral axis producing negative bending. The cool material adjacent to the heated area resists the normal thermal expansion of the steel in the longitudinal direction. As a result, the heated material tends to expand, or upset, to a greater extent through the thickness of the plate, resulting in plastic flow.

(A)   Plate movement during early heating phase (deflection decreases)

(B)   Plate movement near the completion of heating (deflection increases)

(C)   Plate position after cooling (deflection decreases)
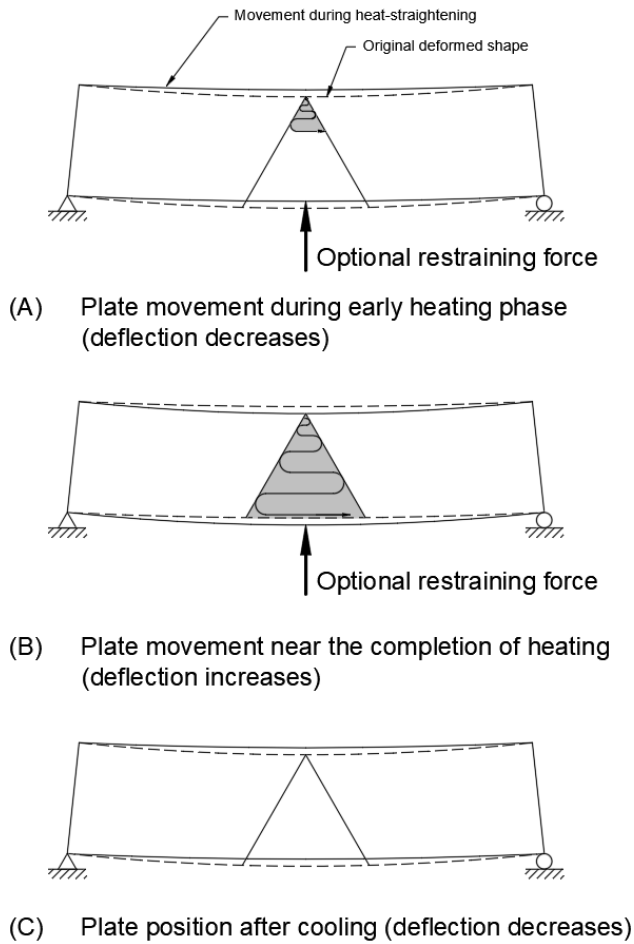
Source: FHWA

Figure 23. Illustration. Stages of movement during vee heat.

At the completion of the heat, the entire heated area is at a high and relatively uniform temperature. At this point the plate has moved downward (figure 23-B) due to longitudinal expansion of material below the neutral axis, producing positive bending. As the steel cools, the material contracts longitudinally to a greater degree than the expansion during heating because it is less restrained after the full vee is heated. Thus, a net contraction occurs. The net upsetting is proportional to the width across the vee, so the amount of upsetting increases from top to bottom of the vee.

This variation in upsetting produces a closure of the vee. As a result, bending is produced in an initially straight member, or straightening occurs (if the plate is bent in the opposite direction to that of the straightening movement, figure 23-C).

2.2.2.1.1. Vee Depth

For many applications, it may be most efficient to use a vee that extends over the full depth of the plate element; however, partial depth vees may be applicable in certain situations. When using partial depth vees, the open end should extend to the edge of the element. In the case of partial depth vees used on the web of girders, the flange at the base of the vee should also be heated so that it does not prevent contraction of the steel as it cools. The vee depth is varied by placing the apex at a partial depth location. The most typical partial depth vees are three-quarter and half depth. In general, the vee depth should be equal to the width of the plate being straightened. Partial depth vees do not reduce member-shortening. The primary application for half depth vees is the repair of local damage.

2.2.2.1.2. Vee Angle

The angle of the vee is usually limited by practical considerations. It should be as large as practical for the specific application. If the open end of the vee is too wide, out-of-plane distortion often occurs. Likewise, the vee area should be small enough to heat quickly to limit differential cooling. A good rule of thumb is to limit the open end of the vee to approximately one-third to one-half the plate width but not greater than 10 inches. These limits translate roughly to 20-to-30-degree vee angles. For a given width of the open end of the vee, V, is selected, the vee angle is:

$$\theta = 2tan^{-1}\frac{V}{2W} \tag{2}$$

where W is the plate width.

2.2.2.1.3. Number of Simultaneous Vee Heats

Simultaneous vee heats may be performed with proper spacing. It is suggested that the vees be spaced at least one plate width, W, apart. Also, if multiple plastic hinges occur, each hinge may be heated simultaneously.

2.2.2.2 Edge Heats

If a smooth gentle bend is desired, a line near the edge of the member is heated. The line may be continuous or intermittent, depending on the angle of curvature desired. This pattern is often used to heat curve rolled shapes and plate girders in the fabrication shop. A schematic is shown in figure 24. Line heats are generally applied about 2 inches from the edge for inelastically stretched edges and thermal cut flanges with small notches but may also be applied directly to the edge. In both instances, with thermal cut flanges, it is suggested to clean up and smooth rough edges before performing heat curving is performed to limit the potential for brittle fractures and crack propagation.
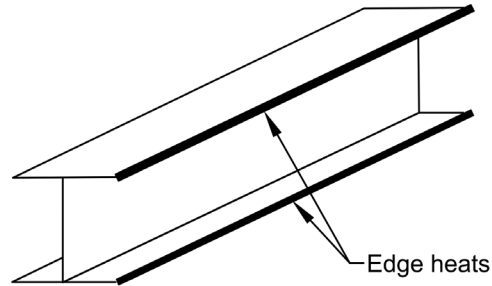
Source: FHWA

Figure 24. Illustration. Schematic diagram of edge heats used to heat curve a beam.

2.2.2.3 Line Heats

A line heat consists of a single straight pass of the torch but may consist of using a pair of torches to heat each face for thicker materials. Line heats are often employed to repair a bend in a plate about its weak axis. Such bends, if severe enough to produce yielding of the material, often result in long narrow zones of yielding referred to as yield lines.

The restraint in this case is often provided by an external force, although some movement can occur without external constraints. This behavior is illustrated in figure 25. A line heat is applied to the underside of a plate element subjected to bending moments produced by external forces (figure 25-A). As the torch is applied and moved across the plate, the temperature distribution decreases through the thickness (figure 25-B). The cool material ahead of the torch constrains thermal expansion, even if external constraints are not present. Because of the thermal gradient, more upsetting occurs on the torch (or hotter) side of the plate. During cooling, this side consequently contracts more, creating a concave movement on the torch side of the plate similar to that shown in figure 25-D. Thus, to straighten a plate bent about its weak axis, the heat should be applied to the convex side of the damaged plate.
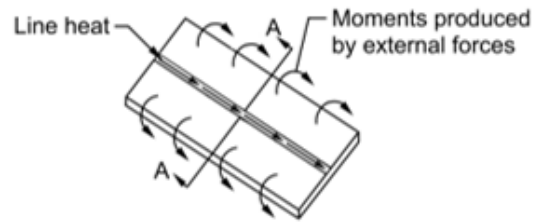
(A) Plate with line heat applied to underside
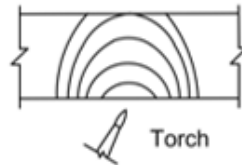
(B) Transverse section AA showing a schematic of decreasing steel temperature contours proportional to distance from torch tip
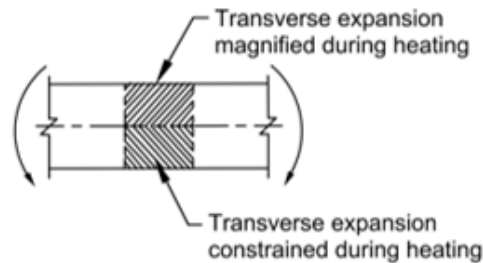
(C) Transverse section AA during heating showing effect of bending moment constraints
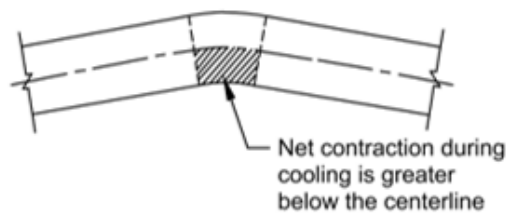
(D) Transverse section AA during cooling

Source: FHWA

Figure 25. Illustration. Schematic of line heat mechanism.

The movement can be magnified by the use of applied forces that produce bending moments about the yield line. Referring to a section through the plate transverse to the line heat (figure 25-C), the restraining moments tend to prevent transverse expansion below the plate centerline. In a manner similar to the vee heat mechanism, the material tends to expand through the thickness, or "upset." Upon cooling, the restraining moments tend to magnify transverse contraction (figure

51

25-D). The speed of the travel of the torch is critical as it determines the temperature attained. With proper restraints and a uniform speed of the torch, a rotation will occur about the heated line.

2.2.2.4 Spot Heats

For a spot heat, a small round area of the metal is heated by moving the torch in a slow circular motion, increasing the diameter until the entire area of the metal is heated. A spot heat causes upsetting of the metal through the thickness, due to the restraint provided by the cool surrounding material. On cooling, a spot heat leaves tensile stresses in all the radial directions across the heated area. During a spot heat, the torch should not be held at a particular point for too long, as the spot may get too hot and buckling may occur due to excessive thermal expansion on the heated side of the member. Spot heats are used to repair localized damage such as bulges, dents, bellies, or dishes in a plate element.

2.2.2.5 Strip Heats

Strip heats, also called rectangular heats, are used to remove a bulge in a plate element or to complement a vee heat. Strip heats are similar to vee heats and are accomplished in a similar manner. Beginning at the initiation point, the torch is moved back and forth in a serpentine fashion across a strip for a desired length as illustrated in figure 26. This pattern sequentially brings the entire strip to the desired temperature.
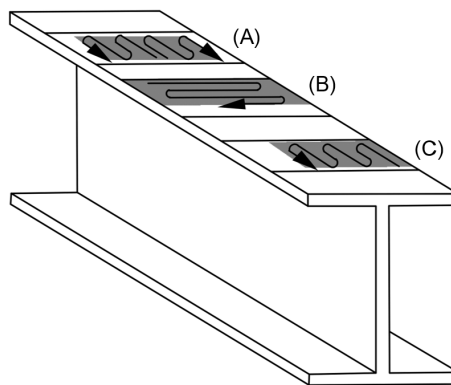
Source: FHWA

Figure 26. Illustration. Schematic of strip heat on the flange of a rolled beam.

The orientation of the torch path can be an important consideration. The strip heat may be initiated at the midpoint of the plate and moved toward both edges simultaneously using two torches. This approach, shown in figure 26-A, would minimize weak axis bending of the beam. A second alternative, with similar effect, is shown in figure 26-B where a single torch starts the heat from one side and moves to the other. Depending on the structural configuration, the strip may also be started at a free edge as shown in figure 26-C. However, without restraints, this orientation may produce some weak axis bending in the member. By alternating the initiation point to opposite edges in successive heating cycles, the weak axis bending can be minimized.

2.2.3. Restraining Forces

Earlier, a distinction was made between hot mechanical straightening and heat straightening. The technique of hot mechanical straightening consists of lowering the yield strength of the steel by heating and then applying sufficient jacking loads, in a single application, to straighten the damage or bend the member by inelastically deforming the section. For heat straightening, on the other hand, restraining forces should not result in stresses exceeding yield at the elevated temperature. Movement (straightening) occurs as a result of plastic deformations during contraction, not by mechanical overload. Therefore, calibrating initial restraining forces is an integral part of heat straightening.

First, one should know how much external force is being applied to the system. Thus, all jacks used should be gauged and calibrated. Second, the maximum jacking force should be calculated to ensure that overstress at elevated temperatures does not occur. Often, these computations involve a structural engineering analysis, but for frequently encountered cases, some rules of thumb may be established. Finally, the practitioner should be aware that over-jacking may cause over-correction, buckling or a sudden fracture during the process. It might also result in difficulties in detecting micro-cracks that could severely reduce fatigue resistance.

The term "restraining forces" in heat straightening refers to either externally applied forces such as jacking forces and self-weight, or internal forces such as those provided by the steel surrounding the heated segment acting to restrain the member during straightening. These forces, when properly utilized, can expedite the straightening process. However, if improperly applied, restraining forces can hinder and prevent straightening or create an overload condition and instability.

Figure 23 illustrates a simplified explanation of the effect of restraining forces. The basic mechanism of heat straightening is to create plastic flow, causing expansion through the material thickness (upsetting) during the heating phase, followed by elastic longitudinal contraction during the cooling phase. This upsetting can be accomplished in two ways, as the figure shows. First, as the heat progresses toward the base of the vee, the cool material ahead of the torch prevents complete longitudinal expansion of the heated material, thus forcing an upset through the material thickness. However, because the surrounding cool material does not offer perfect confinement, some longitudinal expansion does occur. After cooling, the damage-induced distortion in the section is reduced in proportion to the confinement level provided by the internal restraints. A second method of producing the desired upset through the material thickness (used in conjunction with internal restraint) is to provide an external restraining force. Like the internal restraining forces, the role of the external restraining force is to reduce or prevent longitudinal movements associated with expansion during the heating phase. This, again, creates an upset through the thickness of the material. The severity of the upset and consequently the amount of straightening achieved during cooling is proportional to the level of restraint. Figure 23 illustrates an example of an externally applied restraining force. In this case, the restraining force is applied such that longitudinal expansion at the open end of the vee is constricted.

The external restraining force shown in figure 23 acts in in conjunction with the internal restraining forces. Figure 27 illustrates the material behavior and interaction between internal and external restraining forces. A small element from a plate, when constrained in the x-direction

and heated, expands and flows plastically primarily through the thickness or z-direction (Figure 27-C). Secondary plastic flow occurs in the y-direction. However, this movement is small compared with that of the z-direction, because the plate's z-dimension (thickness) is much smaller than its y-dimension and offers less restraint to plastic flow. Upon cooling with unrestrained contraction, the final configuration of the element is smaller in the x-direction and thicker in the z-direction compared to its original size (Figure 27-D). Plastic flow occurs with internal and external restraint. The material itself cannot distinguish between constraints caused by internal forces or an externally applied force.
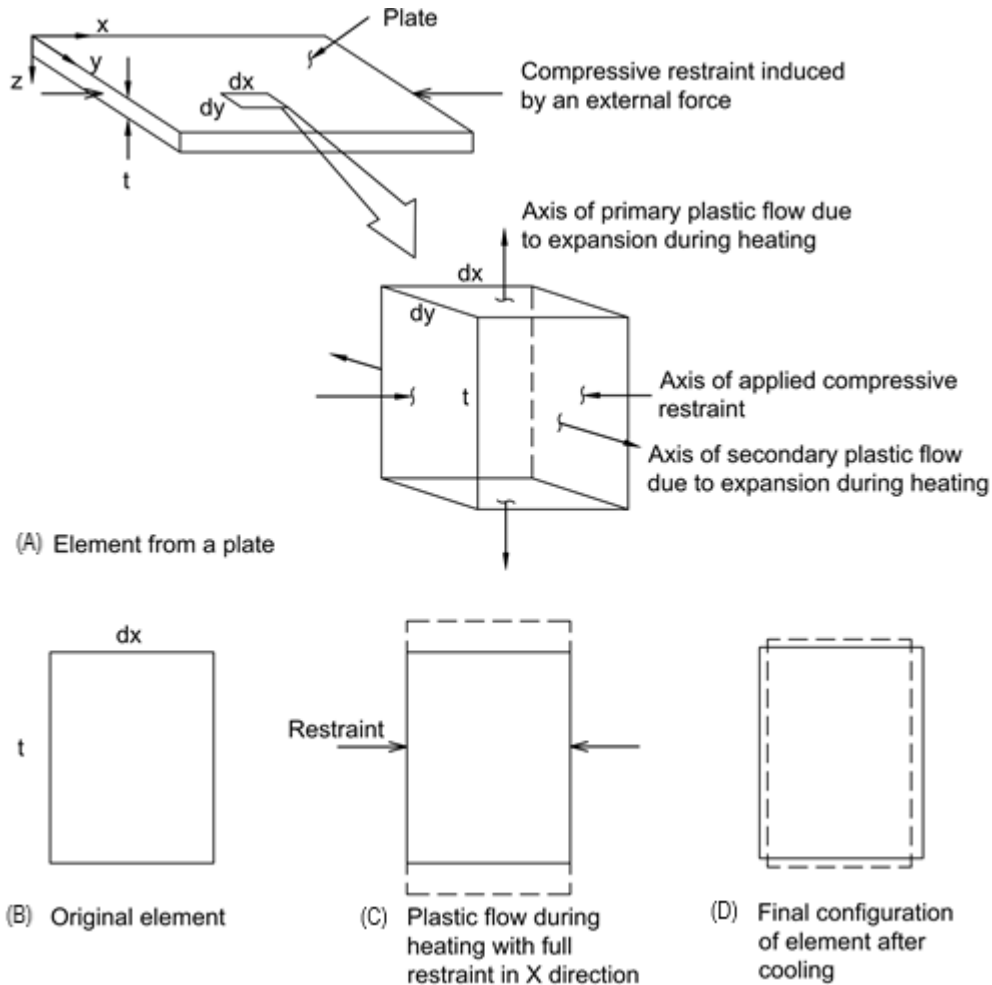
Source: FHWA

Figure 27. Illustration. Characteristics of plastic flow and restraint during heat straightening.

Sometimes the structure itself provides additional internal restraint through redundancy. For example, if the simply supported beam depicted in figure 23 were fixed at the supports, the member stiffness would increase by 33 percent. This increased stiffness would provide additional internal restraint over the simply supported case. In general, structural redundancy increases internal restraint, and thus increases the magnitude of movement per heat cycle in a member.

While increased restraint generally leads to increased movement per heat cycle, for external restraint, the magnitude of the applied force is restricted for two reasons. The first is that higher jacking forces increase the risk of fracture during the heating cycle. This concept is discussed later in this section. The second reason is, to stay within the criteria for heat straightening, the restraining forces should not produce stresses greater than yield in the heated zone. In that case, the process would be more accurately described as hot bending.

At a temperature of 1,200°F, the yield stress of steel is reduced by approximately 50 percent. Therefore, at this temperature, a restraining force producing stresses equal to 50 percent of yield stress at ambient temperature would result in stresses near initial yield in the heated section. The use of forces producing stresses greater than yield in a heated section falls under hot mechanical straightening rather than heat straightening. Therefore, limiting the combined load from the external restraint due to self-weight and externally applied force to 50 percent member capacity in the heated area is suggested. Some owner specifications restrict the maximum jacking force. The main goal is to keep the stresses due to the applied jacking force below the yield stress at the elevated temperature. When considering local damage (category L) or composite girders, however, the calculation of member capacity is not well-defined. For local damage, one way to determine the capacity is experimentally, such as applying a jacking force in an undamaged low stress area until initial yielding is reached. For composite girders, refer to section 3.3.4 for suggested computation methods.

The suggestion to limit the combined load from the external restraint to 50 percent member capacity in the heated area is somewhat conservative because the entire cross section is never simultaneously at 1,200°F during heat straightening. Rather, just the immediate area around the torch reaches 1,200°F, and the remainder of the cross section has either already begun to cool (behind the torch) or is not yet heated (ahead of the torch). Regardless, limiting the applied force to 50 percent of member capacity keeps the procedure within the realm of heat straightening and allows for some variation in temperature.

Research on the effects of using higher jacking forces during heat straightening is somewhat limited. The effect that jacking force has on heat straightening, however, is captured in the work completed by Avent and Mukai (1998). The researchers utilized experimental data from two large-scale testing programs (Avent and Fadous, 1989; Avent et al., 1993) where damaged composite steel girders were repaired using heat straightening. The authors used the data to quantify the behavior of composite girders during heat straightening and study the interaction between internal and external restraining forces. This work is discussed in more detail in section 3.3. One specific test from this series of experiments included the use of jacking forces producing moments greater than 50 percent of M_p in the test specimen. In this case, the movements observed during heat straightening were excessive and indicated that some hot mechanical straightening had taken place. During the 8th heating cycle for this specimen, the lower flange of the composite beam fractured as shown in figure 28. The fracture occurred on the edge of the lower flange, which was compressed when damaged. Similar fractures have also been observed in actual field repairs. In each case, the fracture occurred on the flange edge that was compressed during the damage. During the heat straightening repair, the jacking force induced tension in the area that fractured. The results of this testing, corroborated by field observations, indicate that excessive jacking forces increase the risk of sudden fractures, specifically in areas compressed during damage (Avent et al., 1993; Avent and Mukai, 1998).
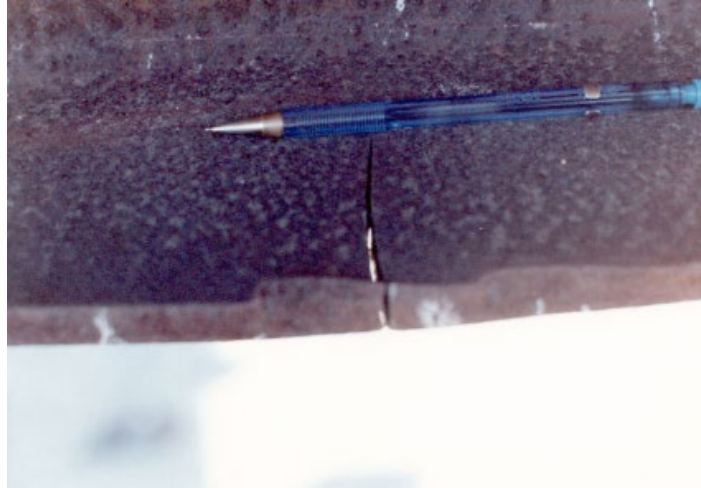
Source: FHWA

Figure 28. Photo. Brittle fracture during heat straightening.

More recent research by Sharma (2005) has provided insight into such fractures. A series of plates were damaged by bending about their weak axes and heat-straightened using line heats. Jacking forces producing plastic moments of 50, 70, and 90 percent of member capacity were used. As expected, the plate movement during heat straightening was directly proportional to the magnitude of jacking force. Material property tests showed that, in general, the level of jacking force had little effect on yield stress, tensile strength, modulus of elasticity, and ductility. However, there were significant differences in local material properties on the side of the specimen compressed during the damage. Comparing material properties from the areas placed in tension and compression by the damage, the compression side had significantly: (1) higher yield stress, (2) lower ductility, and (3) lower CVN impact energy.

These results indicate that the compressed side is more brittle and thus more likely to fracture during repair with large jacking forces. Additional research by Connor et al. (2008) found that the impact itself can be the cause of brittle fractures such as those described later in section 2.3.2. The steel at the point of impact is cold-worked, resulting in localized regions that are considerably more brittle than the areas surrounding them. As such, the area of impact is much more prone to cracking upon subsequent damage at a different or nearby location, or while heat straightening. This research and suggested techniques to mitigate such effects are discussed further in section 2.3.

Higher restraining forces on repairs conducted with lower heat straightening temperatures was researched by Varma and Sohn (2013). In their experiments, restraining forces of approximately 60 percent of member capacity were used in combination with heat straightening temperatures of 800°F. Because the yield stress of steel is higher at lower temperatures, higher restraining forces are used to compensate. The results of this work showed that the combination of underheating and overstraining resulted in a significant increase in heating cycles needed to perform the repair. For the large-scale testing, the increase in heating cycles was more than 900 percent. Additionally, increases in yield stress and ultimate stress were noted in addition to a decrease in fracture toughness compared to repairs completed with smaller restraining forces. While these findings have not yet been verified by additional studies, it is suggested that the use of excessive

restraining forces over 50 percent of member capacity be avoided, even when using lower temperatures.

Based on the above discussion, the following set of suggestions for restraining forces is presented. These suggestions apply for internal as well as external constraints and are as follows:

- Constraints should be passive during the heating phase, i.e., they should be applied before heating and not increased by external means during heating or cooling.
- Constraints should not impede contraction during the cooling phase.
- Constraints should not cause local buckling of the compression element during the heating phase.
- Constraints should not produce an unstable structure by either the formation of plastic hinges or member instability during the heating phase.
- Constraints should be limited such that the maximum moment in the heated zone does not cause stresses that exceed 50 percent of yield at ambient temperature.

From a practical viewpoint, in the case of the vee heat shown in figure 23, these criteria mean that (a) the vee angle should be kept small enough to avoid local buckling, (b) the external restraining forces should be applied before heating and be self-relieving as contraction occurs, and (c) the magnitude of any externally applied forces should be based on a structural analysis of the complete structure that includes the reduced strength and stiffness of the heated member due to the heating effects.

2.2.4. Select Heating Patterns and Parameters

Repair of damaged steel members can involve a combination of the basic heating patterns: vee, strip, line, and spot heats. A series of such heats, applied consecutively, is referred to as a heating pattern. The order in which these individual heats are conducted is referred to as the heating sequence. The process of conducting a complete heating sequence and allowing it to cool is referred to as a heating cycle.

Structural steel shapes for bridges are often an assemblage of flat plates. Almost invariably, damage to these shapes involves the bending of some of these plate elements about their own major axes. Consequently, the heat straightening of steel begins with the application of vee heats on these plate elements. The heating patterns used to repair the four fundamental damage categories are outlined in this section for typical rolled shapes.

Many damage situations do not fit neatly into one of the fundamental damage categories. Rather, the damage is a combination of several of these categories. To repair these more complex cases, the damage should be viewed as a combination of the fundamental cases. The approach is to preplan all sequences, starting with the component of damage that is most severe. As straightening progresses, the process is redirected to other components, minimizing overlaps that counteract or unnecessarily reheat areas. By focusing on the fundamental damage categories in sequence, complex damage can be repaired by using the basic heating patterns described in this section. When severe local damage occurs along with strong and weak axis damage, it may be necessary to address the local damage first. It may also be necessary to reduce the restraining

forces when performing strong and weak axis repairs simultaneously with local damage repairs. This is discussed further in section 2.3.4.4.

2.2.4.1 Flat Plate Bent About Major Axis (Category S)

Figure 29 shows the deformed shape of the typical damaged plate. The heating pattern shown in the figure is the full-depth vee. Because the net change in curvature after one cycle of heats is small, several cycles of heating and cooling are needed to completely straighten a damaged plate. For each cycle, the vee (or vees) should be moved to a different location in the vicinity of the yield zone region, as suggested by the dashed lines in figure 29, so that the exact same spot is not continuously reheated. More heats should be placed in the central part of the yield region and fewer near the extremities, resulting in applying more heat to the regions with more damage. This principle applies for all heating patterns discussed in the following sections.
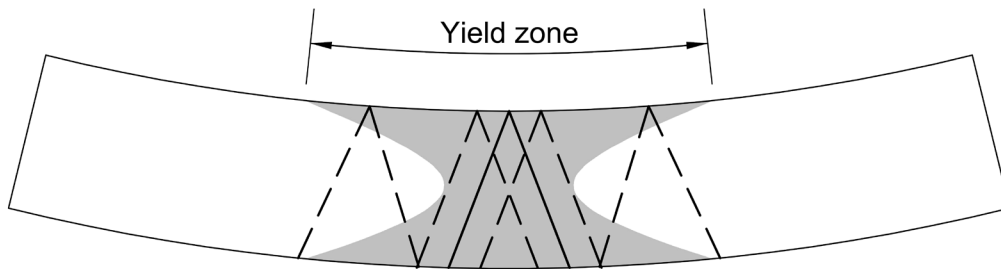
Source: FHWA

Figure 29. Illustration. Plate vee heat pattern over yield zone.

2.2.4.2 Structural Members Bent About Their Strong (Major) Axis (Category S)

As figure 30 shows, the heating patterns used for typical structural sections (wide flange sections and channels) consist of a vee and strip heat combination. To describe the heating patterns used, refer to the elements of a cross section as either primary or stiffening elements. The primary elements are those damaged by bending about their local major axes, such as the webs in figure 30. The stiffening elements are those bent about their local minor axes, such as the flanges in figure 30.
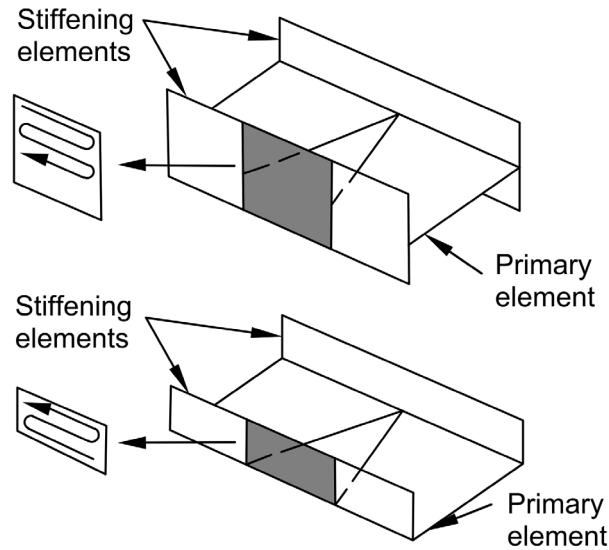
Figure 30. Illustration. Heating patterns for wide flange beams and channels bent about their major axis (category S).

Typically, vee heats are applied to primary elements while strip, line, or no heat at all may be applied to stiffening elements. For this case, a vee heat is first applied to the web. Upon completion, a strip heat is applied to the flange at the open end of the vee. The width of the strip equals the width of the vee at the point of intersection. This procedure allows the vee to close during cooling without restraint from the stiffening element. No heat is applied to the flange at the apex of the vee. This vee and strip heat combination is repeated by shifting laterally over the vicinity of the yield zone until the member is straight.

2.2.4.3 Structural Members Bent About Their Weak (Minor) Axis (Category W)

The heating pattern for these cases is similar to category S cases, but the primary and stiffening elements are reversed. The vee heat is first applied to both flanges simultaneously or one at a time as shown in figure 31. After heating these primary elements, a strip heat is applied to the web. The exception is that no strip heat is applied to stiffening elements located adjacent to the apex of a vee-heated element since this element offers little restraint to the closing of the vee during cooling. The width of the strip heat is equal to the width of the vee heat at the point of intersection. For all cases, the pattern is repeated by shifting within the vicinity of the yield zone until the member is straight.
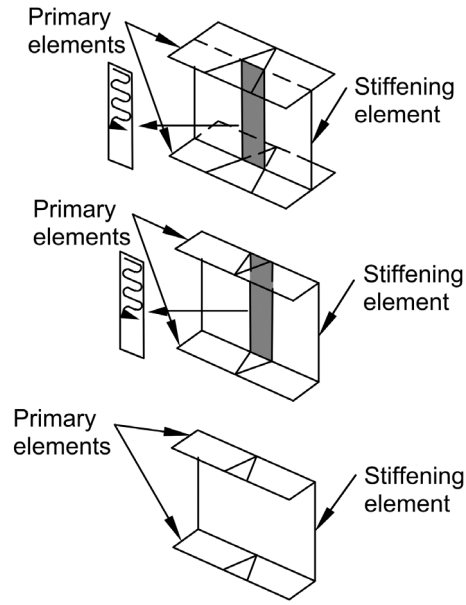
Note: The web heating zones are shaded in the figure. The flange heated zones are not shaded for clarity.
Source: FHWA

Figure 31. Illustration. Heating patterns for wide flange beams and channels bent about their minor axis (category W).

2.2.4.4 Structural Members Subject to Twisting Damage (Category T)

Figure 32 shows the heating pattern for this damage case. The vees on the top and bottom flange are reversed to reflect the different directions of curvature of the opposite flanges. The vee heats are applied first and then the strip heat is applied. For the channel, the strip heat should only be applied to half depth, which allows the lower flange vee to close with minimal restraint from the web.
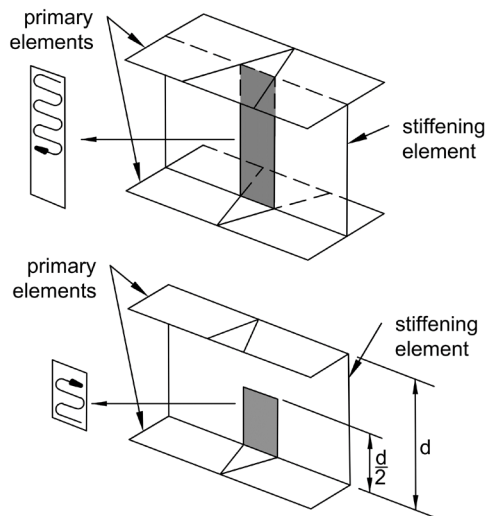
Note: The web heating zones are shaded in the figure. The flange vee heated zones are not shaded for clarity.
Source: FHWA

Figure 32. Illustration. Wide flange and channels with twisting damage (category T).

2.2.4.5 Flanges and Webs with Local Buckles (category L)

A local buckle or bulge reflects an elongation of material. To rectify this damage, the bulging area must be shortened. A series of vee or line heats can be used for this purpose as shown in figure 33. These vees are heated sequentially across the buckle or around the bulge. For web bulges, either lines or vees may be used. If vees are used, they are spaced so that the open ends of the vees touch. Using too much heat to remedy web bulges can be counterproductive. It is suggested line heating be done in a spoke or wagon wheel pattern. In either case, heat should be applied to the convex side of the web or curve. For the flange buckle pattern (figure 33-B), either lines or a combination of lines and vees may be used. Typically, the line pattern with few or no vees is effective. Since the flange damage tends to be unsymmetrical, more heating cycles are needed on the side with the most damage.
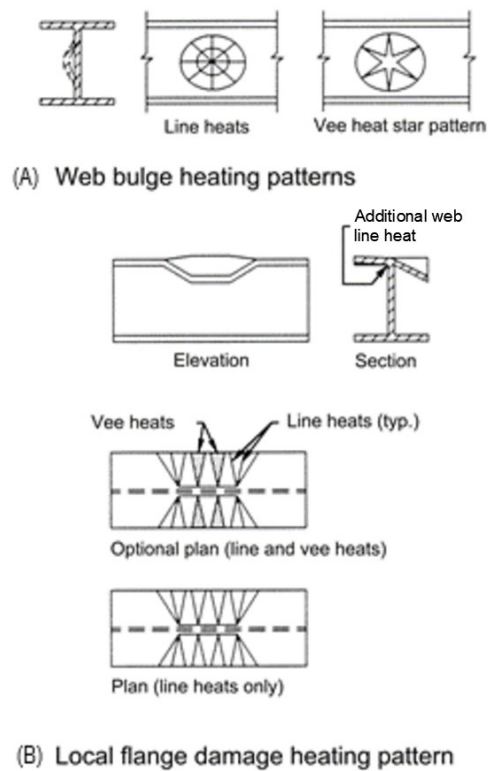
Source: FHWA

Figure 33. Illustration. Typical heating patterns for local damage.

2.2.4.6 Angles

Because angles are single symmetric, their heating pattern warrant special consideration. Typically, the heating pattern is similar to that of a channel. However, the vee heat on one leg of an angle produces components of movement both parallel and perpendicular to the heated leg. Thus, the heating pattern shown in figure 34 may need to be alternated on the adjacent leg. Another method to minimize out-of-plane movement is to use strip heat patterns.

61

(A) Heating pattern for damage primarily in the plane of the top leg

(B) Heating pattern for damage primarily in the plane of the vertical leg
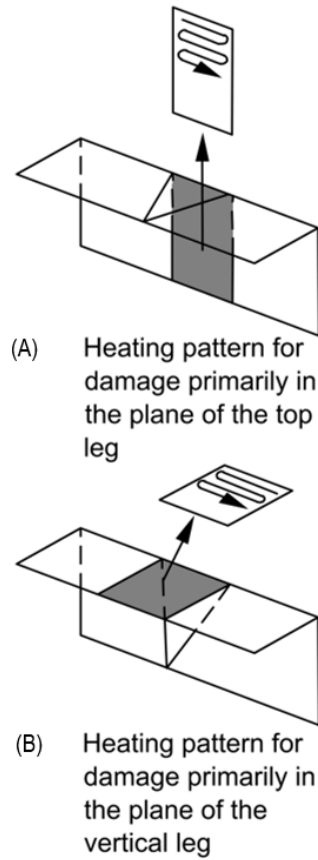
Note: The flange heating zones are shaded in the figure. The web vee heated zones are not shaded for clarity.
Source: FHWA

Figure 34. Illustration. Heating pattern for angles.

2.2.4.7 Repair of Combined Damage Types

Because typical damage can be a combination of several fundamental damage types, a combination of heating patterns may be needed for repair. The key is to select the combination of patterns to fit the damage. When in doubt, it is suggested that fundamental damage categories be addressed one at a time. For example, remove the category W damage prior to addressing the category L damage. Note that, with proper combinations, several types of damage can be removed expeditiously. For example, consider a wide flange section impacted such that bending occurs about both the strong and weak axis of the member. The heating pattern, shown in figure 35, uses a vee heat on the web to restore the strong axis damage and vee heats on the flanges to restore the weak axis damage. The heats should be executed sequentially as numbered in the figure 35. Note that no strip heat is needed on the web because a vee heat is used there. Restraining forces should be used to produce bending moments about both the strong and weak axes, as indicated in figure 35, tending to straighten the damage. Once the damage is corrected about one of the principal axes, the other fundamental patterns should be used until straightening is complete about the other principal axis. In instances where the local damage is severe, it may be necessary to address the category L damage before other damage types. This is discussed further in section 2.3.4.4.
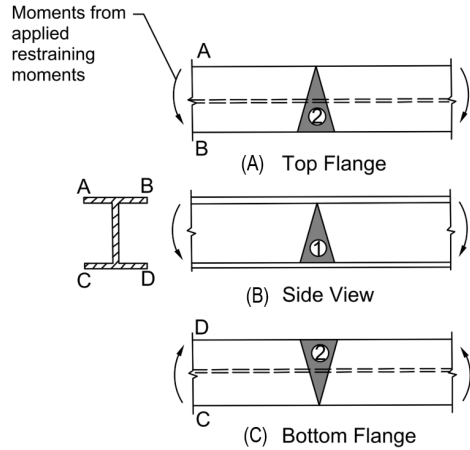
Source: FHWA

Figure 35. Illustration. Heating pattern and sequence for bending about both the strong and weak axes.

As a second example, consider a wide flange beam with weak axis bending damage combined with a local bulge in one flange. The heating pattern is shown in figure 36. Vee heats are used on the top and bottom flanges along with a web strip heat, similar to the standard heating pattern suggested for weak axis damage. However, partial depth vees are used on the flange with the local bulge, along with a series of line heats along the bulge yield lines. Since a yield line is likely to occur at the lower web fillet, a line heat is also needed on the web. Restraining forces are used to create bending moments about the weak axis as shown in figure 36. In addition, a jacking force should be applied on the local bulge as shown on the cross section. The sequence of heats is also indicated in the figure 36.
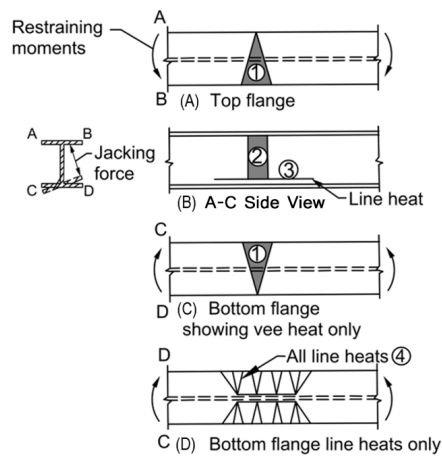
Source: FHWA

Figure 36. Illustration. Heating pattern and sequence for weak axis bending and local flange bulge.

A third example is damage resulting from impact of a composite bridge girder that produces weak axis damage to the bottom flange and twisting due to the restraint of the top flange. The

heating pattern is shown in figure 37, consisting of a bottom flange vee heat, a web strip heat, and a line heat at the top fillet of the web. The heating sequence is shown in figure 37, as well as how the restraining moment should be applied to the bottom flange to induce straightening.
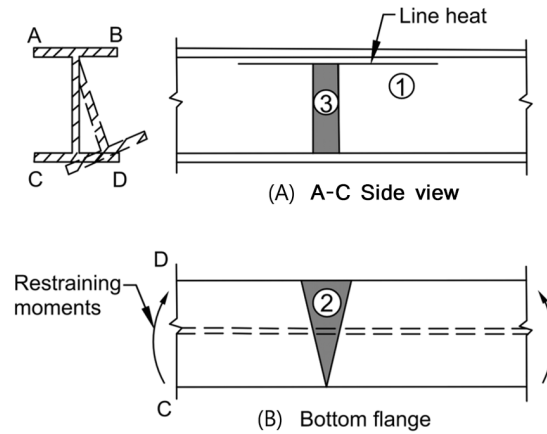
Source: FHWA

Figure 37. Illustration. Heating pattern and sequence for weak axis bending of lower flange and twisting.

A final example is the case of multiple plastic hinges formed about the weak axis, such as what might occur for a beam continuous over interior supports. The heating pattern is shown in figure 38. Note the reversed direction of the vees to reflect the multiple curvature damage. The restraining moments should also reflect the reverse curvature nature of the damage as shown in the figure.
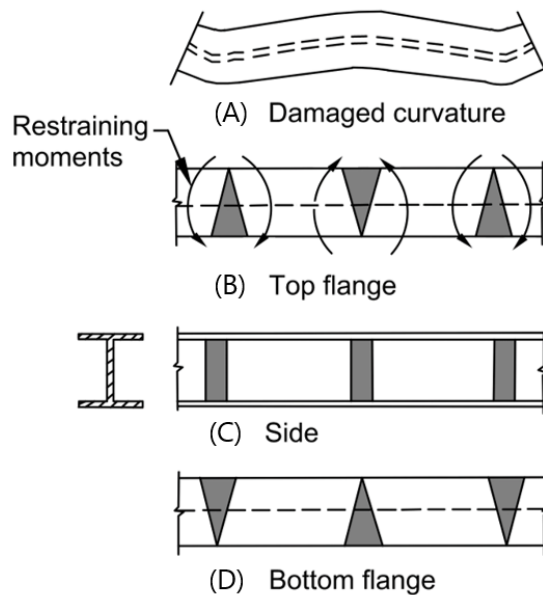
Source: FHWA

Figure 38. Illustration. Heating pattern for reverse curvature bending.

64

2.2.5. Equipment and Its Use

The primary equipment used for heat straightening is a heating torch with an oxygen-fuel mixture as the heat source. Typical fuels include acetylene, propane, and natural gas. The appropriate fuel is mixed with oxygen under pressure at the nozzle to produce a proper heating flame, and a regulator is used to reduce pressures to working levels (15-20 psi). For the torch tip, either a single or multiple orifice tip may be used. The size and type of tip used is based on the fuel selected and thickness of material to be heated. Both fuel type and torch tip selection are based on the ability to quickly heat the material, throughout the entire thickness, to a specified temperature. Note that, regardless of fuel type, orifice type, or orifice size used, the torch itself should be a heating torch and not a cutting torch.

Although many prefer oxyacetylene fuel for this purpose due to its high burning temperature, this fuel is also highly volatile. As such, some prefer a propane fuel, which is safer to handle compared to oxyacetylene. However, because propane does not burn as hot, a larger tip or rosebud orifice may be needed.

The selection of fuel type, orifice type, and orifice size are interdependent. As long as the goal of quickly and thoroughly heating the material is met, selections can be adjusted to meet the needs and experience of each fabrication shop. Fuel delivery may be by tank, or in the case of shops, the shop may be plumbed with fuel and oxygen.

2.2.6. Safety Considerations

The fuel used in heat straightening is volatile. Fuel tanks should always be handled with extreme care. Safety precautions include but are not limited to:

- Placing a protective cap on the head of the tank before handling.
- Securing tanks prior to heat straightening.
- Examining tanks for damage prior to each use.
- Checking lines and fixtures for leaks or damage prior to each use and seeing that proper check valves are installed.

Torch technician safety precautions include, but are not limited to:

- Wearing protective goggles while heating (a no. 3 lens is suggested).
- Being conscious of where the lit torch is pointed.
- Wearing protective gloves and clothing.
- Fixing a stable, secure position prior to opening valves and lighting the torch.
- Following proper procedures when using scaffolding and using safety harnesses when working above the ground.
- Securing tanks and hoses in safe positions prior to heat straightening.

2.2.7. Temperature Control

One important yet difficult to control parameter of heat straightening is the heated metal's temperature. Factors affecting the temperature include the size and type of the torch orifice,

intensity of the flame, speed of the torch movement, material thickness, and configuration of the member. Assuming adequate control of the applied heat is maintained, the question arises as to what temperature produces the best results in heat straightening without altering the material properties. Some previous comprehensive testing programs have shown that the plastic deformation produced as a result of heat straightening is directly proportional to the heating temperature, up to at least 1,600°F.

As discussed in section 2.1.1, Q&T steels cannot be heated above their tempering temperature without altering their material properties. The same also applies for other heat-treated steels including TMCP steels. As a result, some owners may specify a maximum temperature of 1,150°F or even 1,100°F for these types of steels.

For non-Q&T steels, higher temperatures may result in greater rotation, but out-of-plane distortion becomes likely and surface damage such as pitting occurs at approximately 1,400°F to 1,600° F. Additionally, temperatures in excess of the lower phase transition temperature, approximately 1,300°F, may cause changes in molecular structure, which can alter material properties after cooling. The chemical composition of the steel plays a crucial role in the exact temperature the lower phase transition occurs. Limiting temperature to 1,200°F allows for about 100 degrees of temperature variation, a common range among experienced practitioners. This is the maximum temperature suggested by many researchers and industry publications for non-Q&T steels.

Varma and Sohn (2013) investigated the effect of overheating steel through a set of small- and large-scale experiments where cycles of damage and heat straightening repair were performed on wide flange sections. Following damage and repair, specimens from the girders were tested to determine the effect of various imperfections in the heat straightening process on material properties. Varma and Sohn found that overheating the steel may not be as detrimental of an imperfection in the heat straightening process as underheating and overstraining. Their study, discussed in detail in section 2.1.5, showed that overheating the steel during repair to 1,400°F resulted in a smaller increase in yield and tensile stress, as well as a smaller decrease in ductility, compared to heating to 1,200°F. Additionally, results from their experiments on imperfections such as underheating and overstraining showed that, compared to repairs at 1,200°F, yield and tensile stresses increase while fracture toughness values decrease. In addition, substantially more heating cycles were needed to complete the straightening process. However, as they concluded in their report, before this heating limit can be suggested as an acceptable deviation from suggested procedures for heat straightening, additional studies on this topic must be performed. The composition of the steel being heated plays a critical role in the limit of the acceptable heating temperature. With different steel compositions, the lower phase transition temperature can vary and the steel's reaction to temperatures exceeding this point can differ.

The AASHTO/AWS D1.5 Bridge Welding Code (AWS 2015 (23 CFR 625.4(d)(2)(i))) specifies maximum heating temperatures for various types of steel used in bridge construction: 1,200°F for non-Q&T steels (ASTM A709 Grades 36, 50, 50W, 50S and HPS 50W) and 1,100°F for Q&T steels (ASTM A709 Grades HPS 70W and HPS 100W).

In general, steel industry metallurgists may suggest that the heat applied during the straightening process not exceed the published nominal tempering temperature. If the tempering temperature is

less than 1,100°F, use a heat straightening temperature below the steel's tempering temperature. The tempering temperature may be found on the mill certificate for the steel or provided by the mill. For ASTM A913 steel, 1,100°F is typically suggested as the heat straightening temperature for Grades 50, 60, 65, and 70 while the heat straightening temperature for Grade 80 is limited to 1,000°F, based on the maximum tempering temperature used for these steel grades. Additionally, research by Yu (2006) has shown that heating temperatures used near the location of high-strength bolts should be limited to 800°F to prevent any permanent reduction in fastener assembly strength unless the bolts are subsequently replaced. Table 12 provides a summary of these heating temperatures, including values that are and are not Federal requirements.

Table 12. Summary of maximum heat straightening repair temperatures.

Material	Grades	Maximum Heat Straightening Temp. (°F)
ASTM A709	36, 50, 50W, 50S, HPS 50W	1,200*
Q&T ASTM A709	HPS 70W, HPS 100W	1,100*
ASTM 514	-	1,100**
ASTM 913	50, 60, 65, 70	1,100**
ASTM 913	80	1,000**
F3125 and F3148 Bolts	all	800**

Note:
*These temperature are from AASHTO/AWS 2016, which is incorporated by reference in CRF (23 CRF 625.4(d)(2)(i))
**These temperatures are suggestions, not Federal requirements. Owner specifications may have additional limitations.

To control the temperature, the speed of the torch movement and the size of the orifice are adjusted for different material thicknesses. During heating, temperature is monitored using a variety of methods including use of special temperature sensing crayons or pyrometers, infrared electronic temperature sensing devices and visual observation of the color of the steel. Visual observation of steel color can be an extremely unreliable temperature indicator when observed in daylight, and temperature sensing crayons are typically preferred by steel industry metallurgists. More details on the use of these techniques are given in section 2.2.8.3.

2.2.8. Practical Considerations

In the preceding sections, the general discussion of the heat straightening process and variables involved provided basic methodology. However, the proper application of heat and restraining force is a skill that needs practice and experience. The following sections describe some variables involved in the practical application of heat straightening.

2.2.8.1 Torch Tip Size and Intensity

The amount of heat applied to a steel surface is a function of several variables: the type of fuel used, the number and size of the torch orifices, the adjustment of the fuel pressure, and the fuel intensity at the nozzle tip. Selecting the appropriate tip size is primarily a function of the thickness of the material. The goal is to rapidly bring the steel in the vicinity of the torch tip to the specified temperature, not just at the surface, but throughout the thickness. Once this

condition is obtained at the initial heating location, the torch should be moved along the path at a rate that brings successive sections of steel to the specified temperature. A tip that is too small for the thickness results in an inadequate heat input at the surface. As a result, heat does not penetrate adequately through the material thickness. If the tip is too large, heat is inputted into the region too quickly such that it is difficult to control the temperature and distortion of the material. This can also lead to burning and subsequent damage to the surface of the steel.

A no. 8 single orifice tip is generally satisfactory for material thicknesses up to 3/4-inch, or 1 inch if acetylene fuel is used. For thinner material, use a smaller tip. If heavy sections are being heated, a single orifice tip may not be adequate. For such cases, use a rosebud or multiple orifice tips. Table 13 provides general suggestions for selecting torch tip size based on material thickness. Owner requirements may provide additional suggestions or limitations on the type or size of tip, as well as fuel type that can be used. Intensity of the torch, ambient temperature, steel configuration, access, and fabrication details may influence tip choice. Adjustments can also be made to the torch intensity to improve the heating response. A hotter flame is helpful if the configuration of the steel tends to draw heat away from the location of heating. A less intense flame allows for a slower pace as the torch is moved along the path. The intensity may be adjusted to compensate for variables encountered in the field and multiple torches may be necessary for heating thicker materials. The oxygen jet of a cutting torch should not be applied.

Table 13. Suggested torch tips for various material thicknesses (Avent and Mukai, 1998).

Steel Thickness (in)	Orifice Type	Size
<1/4	Single	3
3/8	Single	4
1/2	Single	5
5/8	Single	7
3/4	Single	8
1	Single	8
1	Rosebud	3
2	Single	8
2	Rosebud	4
3	Single	5
>4	Single	5

2.2.8.2 Material Configuration

The pace at which the torch is moved along the heating path is a function of the configuration of the member, location of damage, heating pattern selected, and fabrication details. At the initiation of heating, the torch typically remains on a single spot as the temperature rises. Once the heating temperature is reached, a steady movement along the path of heating can usually be maintained. However, backside attachments such as stiffeners may serve as a heat sink requiring the slowing of the torch movement over certain zones.

One typical scenario of member configuration influencing heat straightening is the heating of the flange of a rolled beam. When heating the flange, the web-flange junction should be heated more slowly because the web draws heat away from the flange. In contrast, sometimes the pace may need to be quickened to maintain a uniform heat. A common example of this is at the conclusion

of a vee heat at a free edge. As the torch approaches the unheated free edge of the section, heat has already been conducted through the steel from the portion of the vee that has been heated. Since the edge of the section has already been pre-heated by conduction, the last pass of the torch is usually relatively quick. In general, practice heats will allow for the development of a feel for how to vary the torch speed over various configurations.

2.2.8.3 Judging the Temperature

The heating temperature can be observed and controlled by using temperature sensing crayons, pyrometers, and/or infrared sensors. However, doing so in practice may not be easy and may meet several challenges.

Observing the color of steel to determine the temperature is highly subjective and dependent on the amount of ambient light. Under ordinary daylight conditions, a halo will form on the steel around the torch tip. At approximately 1,200°F this halo will have a satiny silver color in daylight or bright light. However, as mentioned previously, the color of the glowing hot steel varies depending on quality and amount of ambient light. This method is useful for the technician using the torch to maintain a constant temperature but is especially unreliable for judging the steel temperature in daylight or under bright indoor light. In a well-lit environment, the actual temperature of the steel is often higher than the steel color indicates because bright lighting (daylight or bright indoor light) obscures the color of the hot steel. This makes the coloring appear duller. In addition, the colors observed are subjective and should not be used in place of actual temperature readings.

Temperature measurements should only be made using calibrated high temperature measuring devices (e.g., temperature sensing crayons, pyrometers, and infrared temperature guns). Temperature sensing crayons usually have some degree of error, which should be accounted for in sensitive areas and for temperatures nearing the maximum suggested temperature. Infrared temperature guns must have the proper material emissivity set and be perpendicular to the surface. Otherwise, errors can exceed 10 percent. Emissivity varies with temperature and surface conditions: for carbon steel, it can range from 0.24 to 0.95. Referencing instrument instructions and manufacturer's guidelines is imperative to ensure accurate temperature readings.

One of the most accurate techniques is to use temperature sensing crayons. These crayons melt at a specified temperature and are available in increments as small as 25°F (figure 39). By using two crayons that bracket the desired heating temperature, accurate control can be maintained.

Source: FHWA

Figure 39. Photo. Temperature sensing crayons.

Finally, when taking the surface temperature, the steel directly under the flame will briefly exceed specified limits to convey heat into the metal. Due to this, care should be taken to not burn the surface of the steel. Additionally, steel temperature should only be measured after the flame has left the area for 3 to 5 seconds, allowing the heat to "soak in." This 3 to 5 second range is referred to as "soak time." Although a 3 to 5 second soak time is typical, some owners specify a soak time as long as 10 seconds. This is particularly important when using crayons, as crayons and their marks burn if exposed directly to the flame of the torch. Therefore, the torch should be outside the area being measured or be momentarily removed (one to four seconds) before the crayons are struck on the surface of the steel. An alternative for thinner material is to strike the crayon on the backside at the point being heated.

2.2.8.4 Heating Patterns

One key to heat straightening is selecting the appropriate heat patterns to fit the yield zones of the steel. Yield zones, in the case of heat straightening, are where the steel has been inelastically deformed due to damage and occur in the regions of sharpest curvature. The goal of the heat patterns is to ensure that only the steel in the vicinity of the yield zone is heated. Selection of the appropriate heat pattern to use depends on the type of steel cross section and type of damage experienced. These patterns, organized by cross section and damage type, can be selected based on each heat straightening scenario, to ensure that only the steel in the yield zones is heated. Some practitioners tend to heat in a broader zone, but this is not suggested. The bridge owner requirements may limit the type or size of heating patterns that may be used for fabricating or straightening steel.

2.2.8.5 Sequence of Heats

Heat straightening is a cyclic process, and the movement occurs gradually by contraction during cooling. Sometimes 20 or more heating cycles may be needed to straighten a damaged member. Because a heating pattern usually covers only a portion of the yield zone, the pattern should be shifted on a cycle-by-cycle basis. Heating cycles should be concentrated near the center, where curvature is the sharpest, and fewer near the edges. During a given heating cycle, returning to a previously heated region and reheating the material before it has cooled interrupts the contraction of the material and limits the movement. This should be avoided because doing so reduces both the predictability and effectiveness of the heat straightening process. Instead, performing a heating pattern at a separate location while allowing the first to cool has been found to be beneficial in efficiently heat straightening a member.

When any combination of vee, strip, or line heats are used together in a series, it is referred to as a heating pattern. The order in which the heats are applied is referred to as the heating sequence. The sequencing of heats may be important in some straightening operations as some practitioners feel that proper sequencing accelerates the straightening process and helps keep residual stresses to a minimum. However, little research has been conducted to verify the effect of sequence.

Consider the case of an I-beam with category S damage in need of a vee heat in the web and a strip heat in the flange (discussed in detail in section 2.2.4.2). A common sequence is to heat the web vee first, followed immediately by the flange strip. An alternative used by some practitioners is to heat the web vee first and allow it to cool for a few minutes before heating the

flange strip. The available research data and different sequences used in practice indicates that more than one sequence can be successful in many cases. Because different sequences are successfully used in practice, this indicates that heat straightening is not particularly sensitive to the sequence used, and documentation does not support the use of one sequence over another for a particular heating pattern. The experience of the practitioner is the most reliable source to proper sequencing. The sequencing patterns shown in this manual are based on those often successfully used in practice.

2.2.8.6 Lack of Movement

One of the more perplexing aspects of heat straightening is that sometimes, following several cycles of heating and subsequent cooling, no movement occurs. Although many factors can lead to this, often the source of this issue is residual stress in the section opposing the straightening movement. To rectify this, it is suggested that the heat pattern is repeated for several cycles, ensuring the pattern location is shifted between cycles. The application of several heating cycles tends to redistribute or dissipate these opposing stresses and may lead to the desired movement. If the problem persists, it is probable that the jacking forces are too low. In this case, a reanalysis of the jacking layout is suggested, considering any redundancies that may exist in the system. Finally, the heating patterns should be checked to ensure that they are consistent with the damage being corrected. For example, neglecting to heat all separate yield zones during one heat cycle could prevent movement.

Several factors can lead to lack of movement during heat straightening. Narrowing down these factors for more complex or difficult scenarios may involve seeking advice from a consultant more experienced in heat straightening. In all cases, overheating and over-jacking should be avoided.

2.2.8.7 Cooling the Steel

Typically, a combination of ambient air cooling and rapid cooling is used during the heat straightening process. Ambient air cooling is the safest way to cool steel members from high temperatures. Rapid cooling from high temperatures, particularly near or exceeding the lower phase transition temperature (1,300°F), is detrimental to the steel's material properties and can produce brittle hot spots. As a result, during heat straightening, many practitioners allow the steel to cool in ambient air until a certain temperature is reached and then complete the cooling process using accelerated cooling methods. Typically, the steel is cooled in ambient air until the surface of the steel is below 600°F, although owner specifications may require different temperatures below which other cooling methods are permitted. As differential cooling may occur within the steel, allowing for a reduction in surface temperature ensures that the interior steel temperature has also decreased to a temperature safe for rapid cooling. After this, the steel can be cooled further using accelerated cooling methods. Typically, reheating or re-jacking of steel may be performed after the material has cooled to temperatures below 250°F, although the exact value may vary by specification.

One approach to accelerated cooling is to use compressed air blown on the heated steel surfaces. Another accelerated cooling method is water-mist cooling. The steam generated with this method presents a burn risk to the technician, and the water runoff could lead to clean-up issues. It also

may not be allowed under certain owner specifications. Use of the following cautionary measures is recommended when considering water-mist cooling: (1) a mist applicator that allows the technician to remain at a safe distance, (2) protective clothing and goggles, and (3) a method for safely disposing of the wastewater.

2.2.9. Important Considerations

- Heat straightening is based on the principle of partially constraining the material expansion during heating while allowing unrestrained contraction during cooling.
- Fundamental heating patterns include: vee, line, edge, spot, and strip heat. These heating patterns are discussed in detail in section 2.2.2.
- Fundamental heating patterns may be used separately or in combination depending on the damage type.
- Heating equipment usually consists of oxygen and gas fuel tanks, heating torches, hoses, single- or multiple-orifice heating tips, and temperature sensing crayons or equipment.
- Safety precautions should be exercised at all times.
- Become familiar with the yield zone patterns, detailed in section 2.2.4, associated with various damage conditions:
  - Category S: Strong axis bending
  - Category W: Weak axis bending
  - Category T: Twisting
  - Category L: Localized damage
- Proper heating patterns are associated with each category of damage.
- The maximum heating temperature is dependent on the type and grade of steel. These temperatures are detailed in section 2.2.7.
- Proper restraining forces can expedite the heat straightening process.
- Restraining forces (usually jacks) should be set to restrain the steel during heating but to allow free contraction during cooling.
- Restraining forces should be applied in a direction tending to restore the member.
- Restraining forces should be limited so that the material is not over-stressed during heating.
- It is suggested that heated areas be allowed to cool below 250°F prior to reheating; artificial cooling methods should be used only after the steel has cooled below 600°F. Reheating too soon may prevent the potential movement, impose unnecessary heating cycles and result in additional damage to the steel.

2.3. ASSESSING, PLANNING, AND CONDUCTING REPAIRS

As with any type of repair, a successful heat straightening repair needs assessment, planning, and design. Several procedures should be considered as part of the process, among which the following are considered critical aspects: determination of degree of damage; location of yield zones and regions of maximum strain; repair of any nicks, gouges, or cracks due to damage; limitations for heat straightening repair; selection of heating patterns; and planning a combination of external restraints. Each procedure involves the exercise of engineering judgment. Outlined in this chapter are some key aspects of assessing, planning, and designing a repair.

2.3.1. Role of Engineer, Inspector, and Contractor

The engineer should select the most appropriate repair technique for the specific damage. Alternatives should be evaluated to determine the most effective solution. Key considerations include cost, ease of implementation, adequate restoration of strength, longevity of repair, time to complete repair, aesthetics, and impact on traffic. These aspects are critical to the planning of the repair.

Repairs should be planned in a similar manner to new structures. The typical process includes selecting a trial repair scheme, conducting a structural analysis (which may involve making assumptions for certain geometric or material properties), defining the parameters of the repair (or verifying the capacity after repair), possibly re-analyzing and replanning, evaluating alternate repair or replacement schemes, and finally, providing complete details and specifications for the system selected. The engineer should also establish the acceptable levels of residual damage following repair, that may remain without adversely affecting performance of the member in both strength and fatigue. Further, the engineer should consider the potential of brittle fracture during or after the heat straightening repair process (Connor et al., 2008). Brittle fracture is discussed further in section 2.3.2 and 2.3.3.

Heat straightening repair is not the solution for every damage situation. The engineer's role is to assess its specific applicability. Aspects to consider include:

- the current condition of the rest of the structure and other anticipated repairs
- degree of damage
- presence of fractures
- cause of damage
- likelihood of repetitive damage
- accessibility
- repair method's impact on material properties to safely carry load during and after repair

Once the heat straightening alternative is selected, then the repair parameters such as traffic control, contractor access and work areas, permitted hours of work, heating patterns, maximum restraining forces and locations, and maximum heating temperature should be chosen. Finally, plans and specifications should be developed that generally define the process for the repair.

Because many heat straightening repairs are conducted by contractors, a representative of the bridge owner should be present whose responsibility is to ensure that the repair is being conducted according to plans and specifications. One particularly important responsibility is ensuring that the engineer-specified procedures are followed to prevent damage to the steel.

The third member of the team is the contractor who executes the repair. Although others may design the repair plan, the details of execution typically lie with the contractor.

Despite current knowledge and analytical capabilities, movements during heat straightening cannot always be predicted accurately because (1) damage patterns are often a complex mixture of the idealized cases; and (2) residual stresses and moments which may have been locked into the structure during both original construction and the damage phase are difficult to predict and

may prevent or increase the expected movement. The contractor should be able to assess the reaction of the structure to the planned repair and suggest modifications if the structure is not behaving as expected. These modifications may range from changes in heating patterns and jacking arrangements to decisions on whether to remove secondary or bracing members during the repair. Perhaps most important is that the engineer, the inspector, and the contractor maintain open and clear channels of communication.

2.3.2. Keys to a Successful Repair

The success of a repair depends on the control and selection of specific parameters. The first key is the detailed inspection of the member following damage to identify any nicks, gouges, or cracks that result from the impact. Prior to heat straightening, these defects should be removed to minimize potential brittle fractures or crack propagation during the repair process (Connor et al., 2008). Non-destructive testing, as described in section 2.3.3.2, should be considered, when appropriate, to properly identify the total extents of such defects.

The second key is the selection of the heating patterns and sequences. The combination of vee, line, and strip heats should be chosen to fit the damage patterns. Heat should only be applied in the vicinity of the regions in which yielding of the material has occurred. Typically, vee heats should be relatively narrow. A good rule of thumb is to limit the open end of the vee to 10 inches for 1-inch-thick plates. However, a smaller limit should be considered for thinner plates. This minimizes the distortion that may occur due to local buckling of the plate element. Additional guidance on the size of vee heats is detailed in section 3.1.2. Of additional consideration, as mentioned in section 2.2.8.4, are limitations set by owner guidelines. The size of heating patterns, such as the open edge of vees, may be limited by certain owners.

The third key is to control how the steel is quickly brought to the desired uniform heating temperature using the limits described in section 2.2.7 and table 12. Higher heats may adversely affect the material properties of the steel and lead to a weaker structure. This is discussed further in section 2.2.7, in addition to other temperature limitations.

The fourth key is to control the applied restraining forces during repair. Research has shown that the use of jacks to apply restraint can greatly shorten the number of heating cycles needed to repair a member. However, over-jacking can result in buckling or a brittle fracture during or shortly after heat straightening. To prevent such a sudden fracture, jacking forces, previously discussed in section 2.2.3, should be limited. Suggested procedures for determining acceptable jacking forces are provided later in this manual in sections 3.3.3.3 and 3.3.4. Precautions should also be taken when applying restraining forces for different types of damage at one location. If practitioners do not take these precautions, brittle fractures or excess deformation may occur. Additionally, the jacking forces should always be applied in the direction tending to straighten the beam. The execution of a heat straightening repair that incorporates these keys begins with the assessment of the damaged structure.

2.3.3. Steps in the Assessment Process

The first step in the rehabilitation process is a site investigation to assess the degree of damage and the safety of the existing structure. The following section provides suggestions for damage

assessment in the form of steps to be followed for a complete damage assessment. Not all steps are needed for each case, so judgment should be used when deciding if, and when, to eliminate a part of the assessment process.

2.3.3.1 Initial Inspection and Evaluation for Safety and Stability

The purpose of the initial inspection is to protect the public, employees of the owner, and repair personnel. This inspection is often visual and conducted with special concern for safety. The major aspects of damage are recorded and documented with photographs and measurements. During this inspection, a preliminary list of repair requirements and options should be made. Particular attention should be paid to temporary needs such as shoring, traffic control, access, and other short-term considerations.

If heat straightening is not chosen as the repair method or it is anticipated that the damage will remain for any period, the impact area along with any welded details effected by the impact should be examined and treated. This work should be performed as early as possible. As such, it is suggested that it take place at the time of the initial inspection. In general, treatment consists of grinding the impact area to remove any surface nicks or gouges, removing any cracks revealed through inspection, and smoothing weld toes on nearby welded details to prevent an increase in stress at these locations during the repair process. Microcracks introduced during the impact may result in a severe brittle fracture under a subsequent impact, even if the subsequent impact does not occur at the same location (Connor et al., 2008).

Part of this evaluation may involve a review of the drawings and computations to determine the safety and stability of the damaged bridge. The specific cause of damage may also influence the final decision on repair and should be investigated if possible. Typical damage causes are: (1) over-height or overwide vehicle impact, (2) overweight vehicles or overloads, (3) out-of-control vehicles or moving systems, (4) mishandling during construction, (5) fire, (6) blast, (7) earthquakes, (8) support or substructure movement, and (9) wind- or water-borne debris.

2.3.3.2 Detailed Inspection for Specific Defects

The applicability of a heat straightening repair depends on the type and degree of damage. To evaluate this, three items should be checked: (1) signs of cracks or fractures; (2) angle of damage; and (3) material degradation.

Signs of Fracture

While some cracks and fractures are immediately apparent, others may be too small to visually detect. However, it is important to determine if such cracks exist because they may propagate during the heat straightening process. Attention should be focused on the impact area where severe compressive plastic deformation has likely occurred. Micro-cracks often form during the impact, thus inspection following the smoothing treatment of the impact region, discussed in section 2.1.5.6, should ensure that such defects have been removed by grinding, leaving a smooth surface. Welded details near the impact area or at locations of plastic deformations caused by the impact should also be thoroughly inspected by either magnetic particle testing, ultrasonic methods, or dye penetrant testing, all of which are discussed below. Additionally, any defects at the weld toes of welded details, including cracks and tears, should also be ground

smooth (Connor et al., 2008) or rewelded. Should the presence of cracks or defects be unclear, the following NDT can be used to confirm their presence.

Non-Destructive Testing (NDT)

To avoid the removal of material sections, or when testing for the presence of non-visible defects, non-destructive testing allows for the evaluation of components without damaging or compromising strength. While numerous testing methods are available, the most common for field testing are listed in this section.

The use of a dye penetrant can be effective in detecting cracks that are open to the surface. The process involves first thoroughly cleaning the surface. Then a liquid dye is sprayed on the surface and permitted to stand, during which time the dye is drawn into surface discontinuities. Excess dye is then cleaned from the surface and a developing solution is applied. The developer draws the dye remaining in the cracks back to the surface and also provides a color contrast to the dye.

Another procedure is to use magnetic particle inspection. A magnetic field is introduced by touching the metal with a yoke or prods. A flaw in the steel causes a disruption of the normal lines of magnetic flux. If the flaw is at or near the surface of the steel, lines of magnetic flux leak from the surface. Fine iron particles are attracted to the flux leakage and indicate the crack location.

A third procedure is ultrasonic testing by one of several techniques. These procedures typically involve the analysis of pulses passing through undamaged versus damaged material. Ultrasonic testing should not be used for testing of fillet welds because the geometry of the fillet does not allow a thorough reading. Testing usually results in an error due to discontinuities existing from lack of complete fusion of members.

Finally, radiographic testing may be used to produce a visual image of any subsurface flaws within the material. When testing is conducted in the field, ultrasonic testing should be considered before the use of radiographic testing due to the complexity that this test entails. Generally, the equipment needed for these tests are much larger and expensive. It is also more difficult to interpret the results from 2D testing and requires access to both sides of the member.

Degree of Damage

Degree (or severity) of damage can be evaluated using two different criteria. One is the angle of damage, φ_d, which is a measure of the change in curvature. The other is the strain ratio, μ, which is a measure of the maximum strain occurring in the damaged zone. For either case, an evaluation of the degree of damage involves measuring the damage. Two types of damage are quantified by measurements: (1) overall bending or twisting of a member, and (2) localized bulges or sharp crimps. These measurements can be used to compute μ or φ_d.

For determining angle of damage, the usual procedure is to begin by measuring offsets from a taut line, laser beam, or straight edge. A typical layout is shown in figure 40, which also illustrates the definition of φ_d. This layout may be done by either using the unyielded adjacent

regions on either side of the damage as reference lines, since their curvature is small in comparison to the plastic zones, and determining the angle between them, or by establishing a base line and finding the offsets in the damage zone. For the first case, tangents from the straight portions define the angle of damage between the tangents. If the offsets are taken in the elastic zone on either side of the damage as shown in figure 40-B, the angle of damage, φ_d, can be computed.
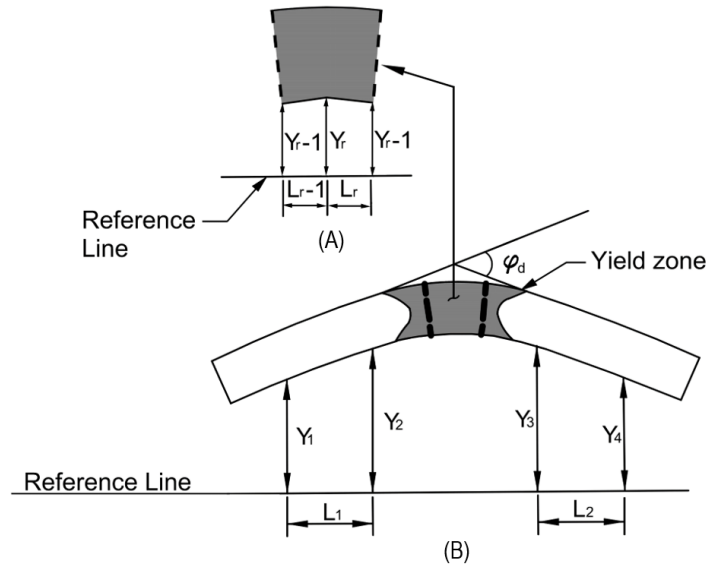
Source: FHWA

Figure 40. Illustration. Offset measurements to calculate angle of damage and radius of curvature.

Based on measurements taken at the site, the angle of damage can be calculated as follows:

$$\varphi_d = \tan^{-1}\left(\frac{Y_2 - Y_1}{L_1}\right) + \tan^{-1}\left(\frac{Y_3 - Y_4}{L_2}\right) \tag{3}$$

where φ_d is the angle of damage or angle of permanent deformation at the plastic hinge, Y_i is a measured offset and L_i are measured lengths along the member as shown in figure 40-B.

The length of damage, C_d, is defined by the chord connecting the tangents to the inelastically damaged region as shown in figure 41. If φ_d and C_d are known, the radius of curvature can be computed as:

$$R = \frac{C_d}{2\sin(\varphi_d/2)} \tag{4}$$
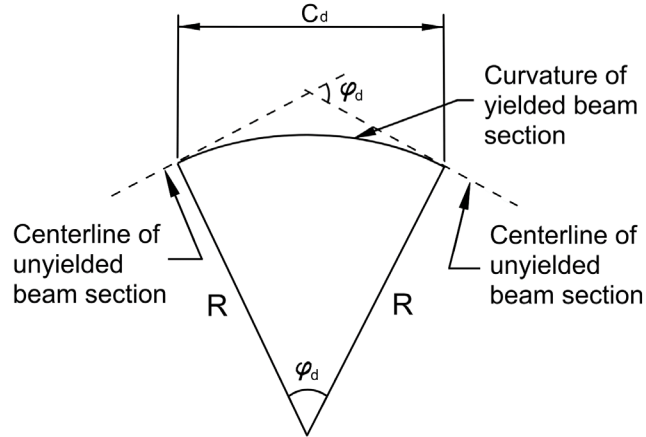
Source: FHWA

Figure 41. Illustration. Relationship of angle of damage to radius of curvature and chord length.

In some cases, direct measurements of φ_d can be made from a photograph. If a photograph can be taken perpendicular to the plane of curvature, tangents can be laid out and measured directly. For small zones of damage, two straight edges can be used to produce the tangent intersections. Again, the angle of damage can be measured with a protractor. While this method may seem simplistic, a reasonable degree of accuracy can be obtained.

For the case where the offsets are taken in the damage zone (see figure 40-A), the radius of curvature, R, can be approximated as:

$$\frac{1}{R} = \frac{Y_{r-1} - 2Y_r + Y_{r+1}}{L^2} \tag{5}$$

The angle of damage can then be calculated from:

$$\sin\frac{\varphi_d}{2} = \frac{L}{R} \tag{6}$$

or

$$\varphi_d = 2\sin^{-1}\left(\frac{L}{R}\right) \tag{7}$$

Where: $L_{r-1} = L_r = L$

Approximations are involved in using these equations. The assumption is made that the radius of curvature is constant over the entire length of the damage although it usually varies. If the damage curve is smooth, this assumption is fairly accurate. If the curve is irregular, the assumption becomes more approximate. For highly irregular curvatures, only the worst portion of the damaged region needs to be measured. This can be done using the three-point offset procedure. Following this, the radius of curvature can be calculated using equation 4. In general, the approaches described here give an adequate estimate of the radius of curvature and angle of damage.

To calculate the maximum strain ratio, the maximum curvature should be measured as previously described. Shown in figure 41 is a damaged beam of uniform curvature. The radius of the bend is defined as radius of curvature, R. Strain is proportional to curvature and curvature can be computed from field measurements, so the radius of curvature to the yield curvature, R_y, may be expressed as:

$$R_y = \frac{E y_{max}}{F_y} \tag{8}$$

where E is modulus of elasticity, F_y is yield stress, and y_{max} is the distance from the centroid to the extreme fiber of the element.

The radius of curvature is related to the strain by:

$$\varepsilon_{max} = \frac{1}{R} y_{max} \tag{9}$$

where R is the actual radius of curvature in the damaged region.

Because damage measurements are taken at discrete locations, the radius of curvature can be approximated from equation 4. Once the smallest radius of curvature is determined in the damaged region, the maximum strain can be computed from equation 8 and compared to the yield strain:

$$\varepsilon_y = \frac{F_y}{E} \tag{10}$$

From equations 8 and 9, the strain ratio is:

$$\mu = \frac{E y_{max}}{R F_y} \tag{11}$$

Research data show that heat straightening can be successful on steel with plastic strains up to 230 times the yield strain, ε_y. However, engineering judgment should be used for strains exceeding $150\varepsilon_y$ (Connor et al., 2008). This is discussed further in section 2.3.4.1.

Material Degradation

Certain aspects of material degradation may influence the decision to heat straighten a damaged section. The first area of concern is nicks, gouges, and other abrupt discontinuities in the damage zone. These discontinuities form stress risers during the repair process when jacking forces and heat are applied. Further, such defects, compounded by reduced material toughness, can lead to brittle fracture if not treated. As such, these discontinuities should be noted and ground to a smooth transition prior to heat straightening. As stated in research completed by Connor et al. (2008), an acceptable transition slope is at least 1 to 10.

A second concern is exposure to high temperature such as a fire when the damage occurred. As long as the steel temperature did not exceed either the tempering temperature or the lower phase transition temperature during that high temperature exposure, no permanent material degradation would be expected. However, if the damaged steel reaches these higher temperatures, especially if fire hoses applied water on the steel when extinguishing the fire, metallurgical tests should be performed to ensure material integrity before heat straightening. Tests that should be considered

include: (1) chemical analysis; (2) grain size and micro-structure analysis; (3) Brinell hardness tests; (4) CVN impact energy tests; and (5) tensile tests to determine yield strength, ultimate strength, and percent elongation. In-place, non-destructive tests (Brinell hardness tests, Rockwell tests, Laser Induced Breakdown Spectroscopy (LIBS), and visual inspection of appearance) avoid removing material. CVN and tensile tests involve significant removal of material in order to machine specimens from damaged and undamaged areas for comparative results.

Visual signs that suggest exposure to high temperatures include melted mill scale, distortion, black discoloration of steel, and cracking and spalling of adjacent concrete. Tests can then be conducted at suspect regions. For example, a significant increase in Brinell hardness, in comparison to undamaged areas of the same member, indicates potential heat damage. Or, for the CVN test at 40°F, a significant reduction in measured values compared to those from an undamaged specimen may indicate damage. The most definitive test, however, is a metallurgical comparison of micro-structure between damaged and undamaged areas. Evidence of partial austenitization, discussed in section 2.1.1, and recrystallization into finer grain size indicates heating above the lower phase transition temperature.

Geometry of the Structure

Often the design drawings are available to confirm the structure's original configuration, design parameters, and type(s) of steel. If the drawings are available, the structural system or configuration in the field should be confirmed with that shown on the drawings. If drawings are not available, then enough measurements should be taken such that a structural analysis can be conducted if needed.

2.3.3.3 Defining Basic Damage Patterns and Zones

The fundamental damage categories are described and discussed in section 2.2.1. A yield pattern or zone is associated with each damage category. The yield zone of a steel section is the area in which inelastic deformation has occurred. It is important to recognize the yield zones of a damaged section because heat should only be applied in the vicinity of these regions. Typical yield zones are shown in figure 42. The sketches shown in figure 42 are schematic and depict the basic yield patterns. The yield zones may vary in length depending on the type of loading and severity of damage. Often, these zones can be determined by visual inspection and are identified by paint peeling or loosened rust and mill scale. Analytical methods are also available when necessary to accurately determine yield zones.
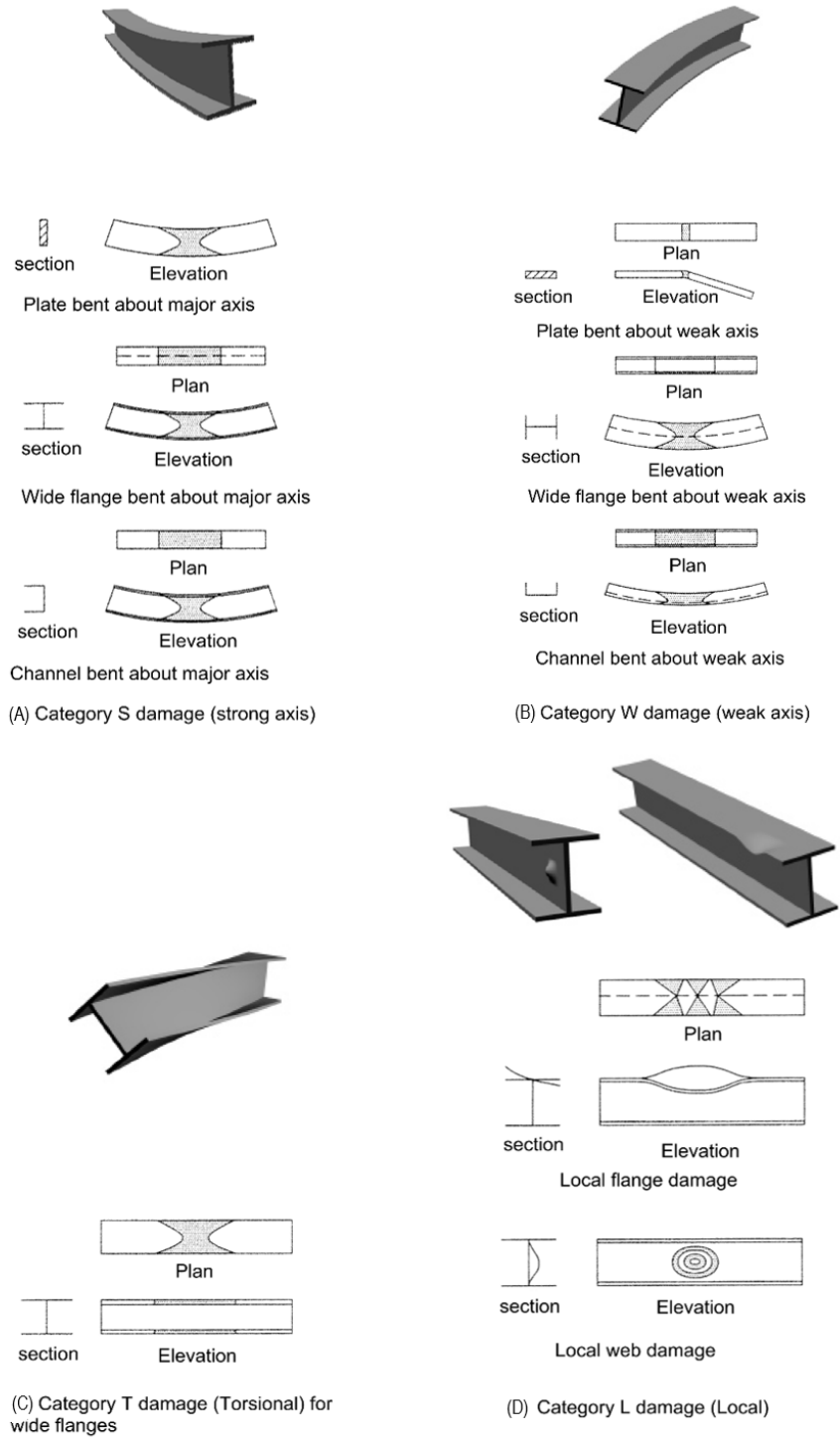
Source: FHWA

Figure 42. Illustration. Yield zones for basic damage patterns.

2.3.4. Steps in the Planning and Design Process

Once the damage assessment is complete, the repair can be designed. Consider the following steps as part of this planning and design process:

- Analyze the angle of damage and maximum strains induced.
- Conduct a structural analysis of the system in its damaged configuration.
- Select applicable regions for heat straightening repair.
- Select heating patterns and parameters.
- Develop a constraint plan and design the jacking restraint configuration.
- Estimate heating cycles needed to straighten members.
- Prepare plans and specifications.

The following sections discuss each of these steps.

2.3.4.1 Analysis of Damage and Determination of the Maximum Strain Due to Damage

Early studies capturing the behavior of steel during heat straightening repair were limited to damage strains of up to 100 times the yield strain, ε_y, or $\mu=100$ (Avent and Mukai, 1998). However, more recent research studies have captured the behavior of steel during and after heat straightening with damage strains exceeding this value. Sharma (2005) conducted research on heat straightening bent plates with strains below and exceeding $100\varepsilon_y$ to quantify the relationship between damage strain and behavior during heat straightening repair. Similarly, Connor et al. (2008) concluded from their work that heat straightening can be successful on damaged steel with plastic strains up to $230\varepsilon_y$ without drastically affecting the material properties of the steel. While research has shown that repairing damage strains far exceeding $100\varepsilon_y$ is possible, researchers suggest using engineering judgment when considering heat straightening for damage strains exceeding $150\varepsilon_y$. Additionally, the owner's guidelines limiting the maximum damage strain ratio for heat straightening repair should be checked prior to repair.

As a general suggestion, for single curvature bends with a plate depth (about the axis of bending) of up to 12 inches, if the angle of damage is less than 12 degrees, it may not be necessary to measure for maximum strain. A category W damaged girder with flanges less than 12 inches would be one example for this condition. An exception would be if the region of damage were concentrated in an extremely short length, resembling a sharp crimp, as opposed to a more uniform bend.

2.3.4.2 Conduct a Structural Analysis of the System

A structural analysis may be necessary to evaluate the damaged structure. This analysis serves two purposes: (1) to determine the capacity of the structure in its damaged configuration for safety purposes; and (2) to compute residual forces induced by the impact damage that may affect safety and influence the level of applied restraining forces during heat straightening. The analysis can be based on the undeformed geometry except when the displaced geometry of the frame or truss system after damage results in changes in internal forces by more than 20 percent. Even if undeformed geometry is used in the analysis, the deformed geometry should be used when computing the member stresses. The allowable stresses should be based on the original

properties of the material. Note that the deformed geometry refers to the global member deformations, not local bending that is sometimes present at the point of impact.

When a member has a significant change in shape due to damage, the section properties should be modified when calculating stresses. While each specific application should be considered on an individual basis, some general strategies can be developed. Assuming no fractures have occurred, bending and compression members are the most critical to evaluate. Forces due to applied loads in tension members tend to straighten out-of-plane damage (and are thus self-correcting), while such forces in bending or compression members tend to magnify the damage.

Change in Cross Section Shape

The primary variable in evaluating the stress level for a damaged bending member is the section modulus. Typically, the most serious strength reduction is due to deformations resulting from twisting or lateral distortion of the cross section. An example is the impact on the bottom flange of a bridge girder by an over-height vehicle. The following cases were originally presented by Avent and Mukai (1998).

Two cases were evaluated for two different wide flange sections. As shown in figures 43 and 44, the damage to both sections due to the over-height vehicle impact is assumed to produce a rotation of the web about the juncture of the web and top flange.
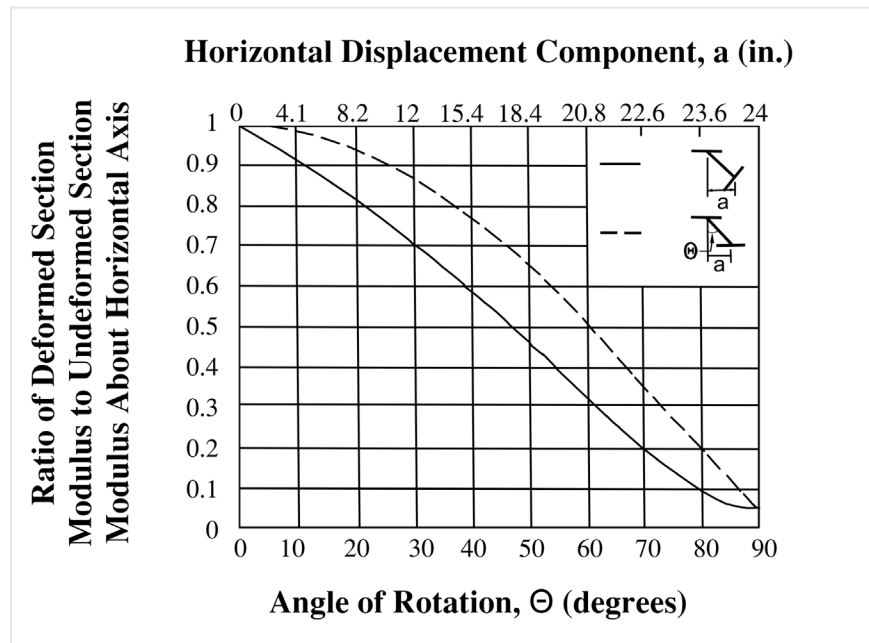
Source: Avent and Mukai (1998)

Figure 43. Graph. Reduction in effective section modulus for a W24×76 beam subjected to varying degrees of idealized damage.
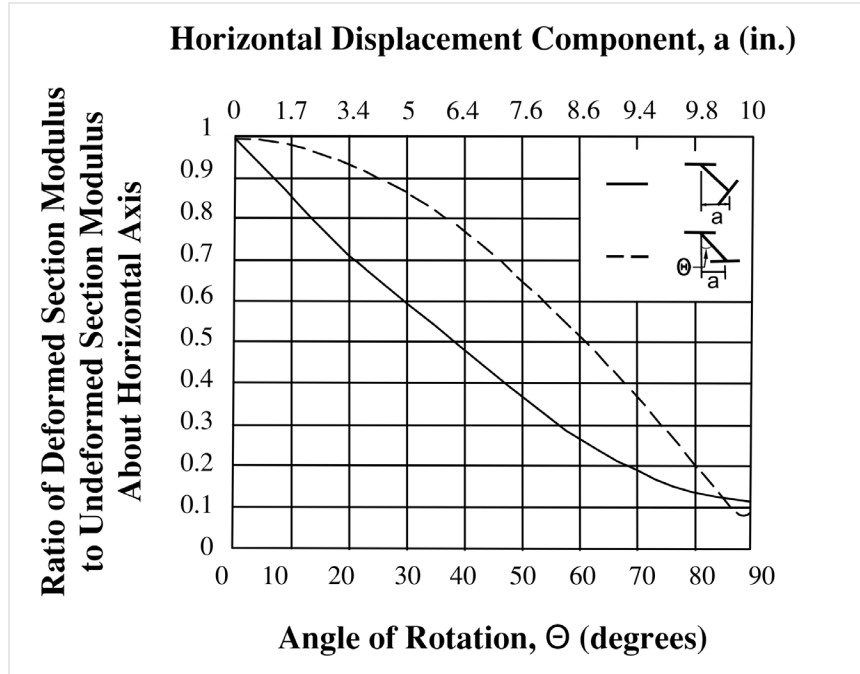
Source: Avent and Mukai (1998)

Figure 44. Graph. Reduction in effective section modulus for a W10×39 beam subjected to varying degrees of idealized damage.

The bottom flange was modeled in two ways: (1) remaining parallel to the top flange, and (2) remaining perpendicular to the web. Actual combinations of damage often fall between these two conditions. Plotted in figures 43 and 44 are the variations in the section modulus (for bending about the strong axis) associated with different levels of damage for two beams: a W24×76 and a W10×39. The case of the bottom flange remaining perpendicular to the web is the more critical case for the comparison of section modulus values. As shown in the figures, the section modulus decreases relatively rapidly with an increase in the cross-section rotation. A 10-degree rotation results in a strength reduction within the range of 8 to 15 percent, depending on the section, while at 20 degrees, strength reduction is between 18 and 29 percent. Although an engineer should evaluate the specific conditions and configuration of each case, one approach is to repair the member if the section modulus is reduced by at least 10 percent. This level of damage typically corresponds to a rotation of approximately 10 degrees (Avent and Mukai, 1998).

Considering the field tests conducted on W10×39 and W24×76 beams (Avent and Mukai, 1998), as described in section 3.3, the damage induced was moderate. For both sections, the flange remained almost perpendicular to the web. The calculated bending strength reduction for the W10×39 beam was calculated in the range of 25 percent. The reduction for the W24×76 beam was on the order of 9 percent. The details of these tests and results are discussed further in section 3.3.

P-Δ Effects

For compression members, the square of the minimum radius of gyration is the section property associated with the strength of the member. Considering the two idealized damaged cases

discussed previously, the effect of damage on the square of minimum radius of gyration is plotted in figure 45 and 46 (Avent and Mukai, 1998). For this section property, the configuration in which the bottom flange remains parallel to the top flange is most critical. The curves are very similar for both wide-flange sections. The reduction in strength, as measured by the square of the radius of gyration, is not quite as large as the corresponding case for section modulus. The reduction is only about 5 percent for the 10-degree rotation and about 14 percent at 20-degree rotation.
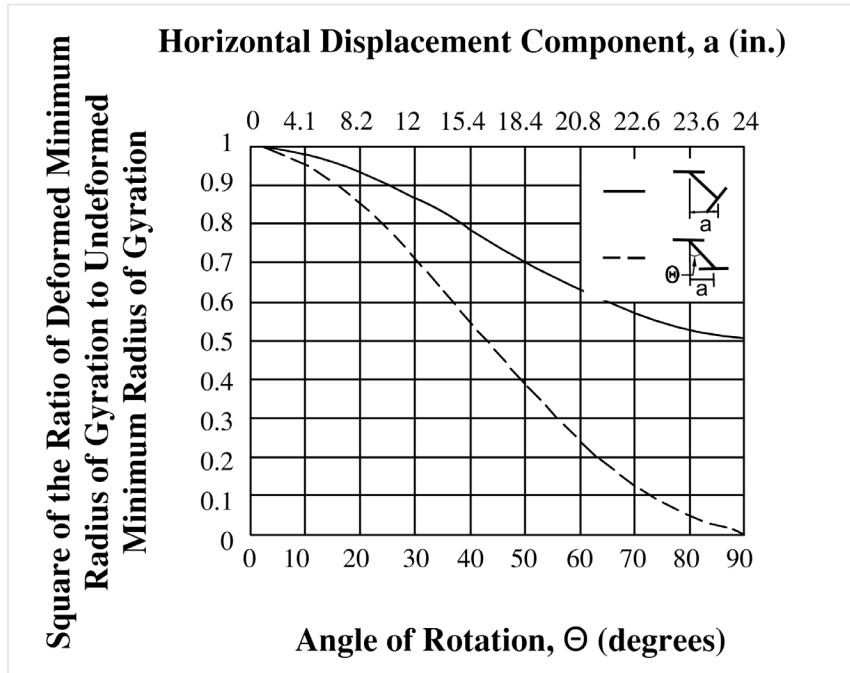
Source: Avent and Mukai (1998)

Figure 45. Graph. Reduction in the square of the effective minimum radius of gyration for a W24×76 beam subjected to varying degrees of idealized damage.
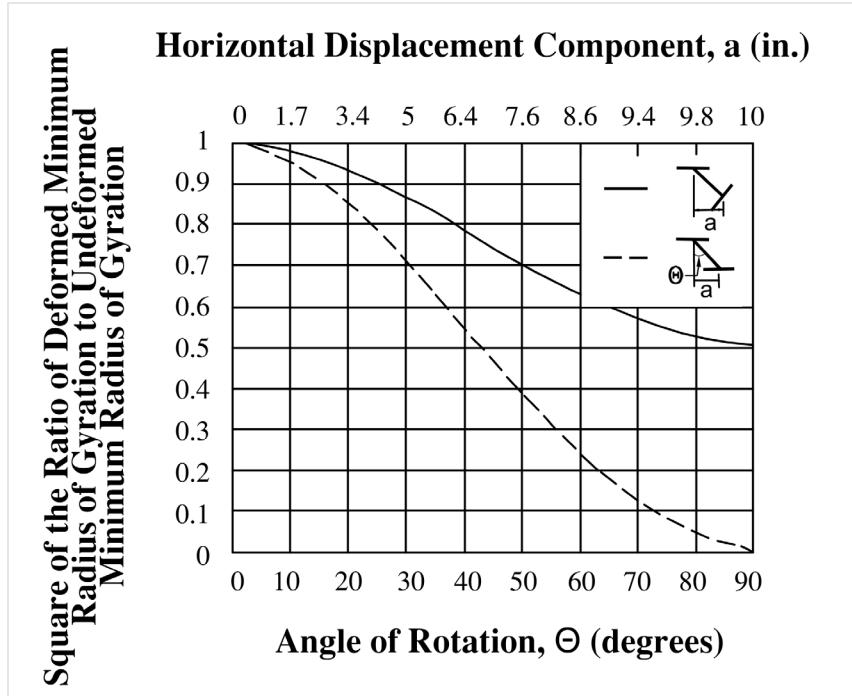
Source: Avent and Mukai (1998)

Figure 46. Graph. Reduction in the square of the effective minimum radius of gyration for a W10×39 beam subjected to varying degrees of idealized damage.

Another aspect that should be considered when evaluating compression members is the strength reduction due to the P-Δ effect. If a simply supported column has an initial midpoint deflection, Y_0, due to impact damage, then the deflection (and bending moment) is amplified according to the amplification factor:

$$A.F. = \frac{Y_o}{1 - P/P_{euler}}$$ (12)

where P is the axial load and P_{euler} is the Euler buckling load.

Figure 47 gives a plot of the amplification factor, originally presented by Avent and Mukai (1998), which is accounted for in design codes by an adjustment in the safety factor for columns. While this graph on the amplification factor was developed with the application of allowable stress design, it is still applicable to damage/repair processes. As the load approaches the critical buckling load, the deflection (and consequently the moment) approaches infinity. Failure was therefore defined as the point where the deflection (and consequently the moment) remains finite but becomes excessively large. The safety factor for column buckling was therefore increased by 0.25 above that used in tension members. As shown in figure 47, this extra safety factor accounts for 0.08 of the total load ratio reduction to allowable values. In using this value, it was assumed that relatively small initial values of lateral deflections would exist due to lateral loads or fabrication imperfections, e.g., within the elastic range. When a compression member has larger permanent deformations well into the plastic or strain-hardening range due to damage, then the effective strength of the member is reduced by a larger factor than expressed by even the column safety factor.
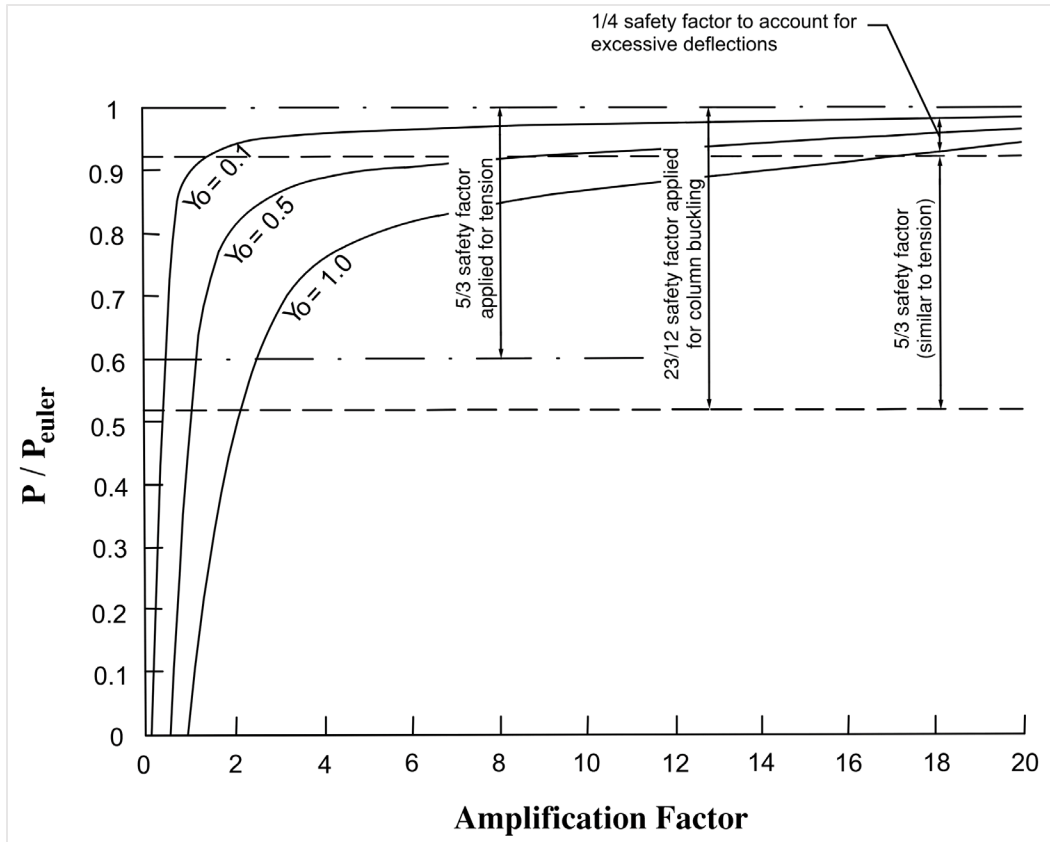
Source: Avent and Mukai (1998)

Figure 47. Graph. Effect of applied axial load and initial midpoint deflection on amplification factor for compression members.

In light of these considerations, even relatively small permanent deformations should be repaired for compression members unless additional bracing is added, or a stability analysis is performed to justify that the strength reduction is small. When investigating the possibility of heat straightening compressions members, the effect of creep, as discussed in section 3.4.3, should also be considered.

Residual Forces

The analysis of residual forces in damaged systems involves a plastic analysis. To illustrate the analysis procedure, consider a bridge girder laterally braced by diaphragms. For lateral impact, similar to that from an over-height vehicle, the girder acts as a continuous beam with the diaphragms as interior supports. If an impact load occurs, the lower flange experiences positive bending at the impact point and negative bending at the adjacent diaphragm supports. A layout modeling this type of girder is shown in figure 48. During impact, it is assumed that plastic hinges form at the impact point and at adjacent supports. These hinges form a mechanism from which the impact load can be computed. Using a plastic analysis, the load, P_u, can be calculated and a moment diagram constructed, as seen in figure 48-B. The impact load is now applied in the reverse direction and an elastic analysis is performed, as seen in figure 48-C. The superposition of these two diagrams (B and C) results in the residual moments due to the impact which

87

produce plastic deformation, as seen in figure 48-D. These resulting moments should be assessed in combination with other loadings such as the live and dead load on the bridge.

The effects of previous impacts, should they exist, should also be considered in the evaluation of residual forces. Instances of brittle fractures propagating from previously damaged areas not directly damaged during the more recent impact were observed by Connor et al., (2008). Additionally, they note instances of this phenomenon occurring during field repairs completed by others. As such, consider previous impacts and their effect on more recent damage prior to repair.
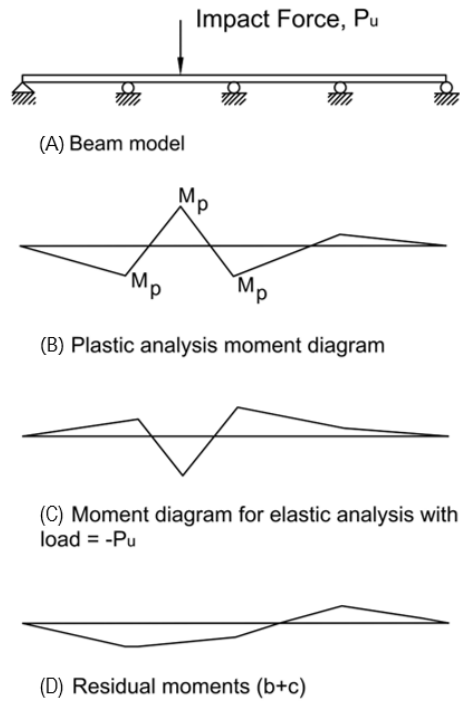
Source: FHWA

Figure 48. Illustration. Plastic analysis for residual moments in a laterally impacted girder.

2.3.4.3 Select Regions Where Heat Straightening is Applicable

While the primary consideration for determining whether heat straightening repair is appropriate is the degree of damage, other criteria may also influence the decision. Particularly important is the presence of fractures or previously heat-straightened members. Although sometimes repairable, a fracture may necessitate the replacement of part, or all, of a structural member. In some cases, it may be feasible to heat straighten the suspect region and then repair it in-place by mechanical connectors. In other cases, a portion of the member may be replaced while the remainder is repaired by heat straightening.

An example of combining heat straightening with replacement is when one or more girders are impacted by an over-height vehicle. This type of accident often displaces the bottom flange. If the impact point is near diaphragms, the diaphragms are often severely damaged. It is usually

much more economical to simply replace a diaphragm rather than taking the time to straighten it. The suggested procedure is to remove the diaphragm, especially if it would restrain desired movement of the girder, then heat straighten the girder, and finally replace the diaphragm with a new one.

In general, heat straightening can be applied to a wide variety of structural members. Some researchers have cautioned against straightening fracture critical members (Shanafelt and Horn, 1984). However, more recently, research has been conducted on the fatigue and fracture performance of steel bridge girders subjected to cycles of damage and heat straightening repair (Connor et al., 2008). This research has shown that, for up to three damage and repair cycles, heat straightening had minimal adverse effects on material properties and fatigue resistance. However, when subsequent damage occurs at the same location as initial damage, the researchers suggested a limit of two damage and repair cycles. If heating temperature is carefully controlled, jacking forces are maintained, and notches and nicks are ground smooth, there is no reason to expect unusual problems. A discussion on the decision to perform heat-straightening on previously repaired members is presented later in section 3.2.5.

2.3.4.4 Develop a Constraint Plan

Because jacking forces and member self-weight can expedite repairs, such forces should be used. Jacks should be located to produce the maximum effect in the zones of plastic deformation. Jacks should be gauged and calibrated prior to use and properly secured so that they do not fall out as pressure subsides during cooling. The loads applied to the structure should be controlled, and the limiting values established.

For cases where residual moments are small, the jacking moment, M_j, should be limited to:

$$M_j \leq \frac{M_p}{2} \tag{13}$$

where M_p is the plastic moment capacity of the member or damaged element (such as the lower flange of a composite girder). For cases where residual moments exist, the jacking moment should be limited to:

$$M_j \leq \frac{1}{2}(M_p \pm M_r) \tag{14}$$

where M_r is the residual moment and is positive when tending to straighten the member. Residual moments are relieved during the first few heats. Thus, rather than computing residual moments, an alternative is to use a jacking moment of only ¼ M_p during the first two cycles. Additional methods of computing jacking forces for various member configurations are discussed in sections 3.2, 3.3, 3.4, and 3.5.

On occasion, a hairline fracture may occur or become visible during heat straightening repair. This behavior was captured by Connor et al. (2008) during testing of a wide flange section subjected to both category L and category W damage. Instrumentation of the category L damage present on the flange showed that horizontal forces used to remove the category W damage caused hairline fractures in the vicinity of the local damage regions. It was concluded that the presence of the category L damage produced secondary bending stresses when the horizontal forces used to remove the category W damage were applied.

Due to this observed behavior, Connor et al. (2008) concluded that, during the analysis of the member, the presence of category L damage should be considered when determining restraining forces. The researchers suggested that to prevent cracking, the category L damage should be removed prior to applying the horizontal forces used to repair the category W damage. If both repairs are to occur simultaneously, the magnitude of the horizontal forces should be reduced. Reducing the horizontal force by 1 percent for every 1 increment of damage past the yield strain for the category L damage was suggested by Connor et al. (2008). For example, if a bulge in the flange of a section, due to an impact to the flange, has a strain ratio of 50, the horizontal forces should be reduced by 50 percent (compared to the force that would be used should no local damage be present). If the bulge had a strain ratio greater than 100, the local damage must be removed (fully, or partially to a strain ratio of less than 100) prior to applying horizontal force. As the category L damage is removed, the horizontal forces can be increased. When the local damage is fully removed, the full horizontal force, as calculated, can be used. This approach produced successful results for Connor et al. (2008) in all instances of use.

In addition to local damage, another cause of cracking is believed to be successive repairs of a re-damaged element and/or the growth of micro-cracks initiated during initial damage. Since the presence of local (category L) damage is the primary cause of these cracks, restraining forces should be specified at safe limits and be monitored during repair. Further discussion of the research conducted by Connor et al. (2008), similar work conducted by other researchers, and subsequent suggestions for number of damage and repair cycles are included in section 2.1.9.2.

One problem associated with the computation of jacking forces is that, for indeterminate members, the bracing, diaphragms, or other attachments may be difficult to model. In addition, it is sometimes necessary to make an estimate in the field as to the magnitude of the jacking forces. The jacking force limit can be approximated by measuring the deflection when the force is applied. Since end support restraint conditions generally fall between the two ideal cases of simple and fixed supports, the deflection can be calculated by estimating the degree of restraint. The deflection that produces a maximum stress equal to 50 percent of yield for 36 ksi yield strength steel on a center point loaded member with simple supports can be expressed as:

$$\delta_{max} = \frac{1}{\gamma_{max}} \left(\frac{\ell}{140}\right)^2 \tag{15}$$

and for fixed supports:

$$\delta_{max} = \frac{1}{\gamma_{max}} \left(\frac{\ell}{200}\right)^2 \tag{16}$$

The deflection that produces a maximum stress equal to 50 percent of yield for 50 ksi yield strength steel on a center point loaded member with simple supports can be expressed as:

$$\delta_{max} = \frac{1}{\gamma_{max}} \left(\frac{\ell}{120}\right)^2 \tag{17}$$

and for fixed supports:

$$\delta_{max} = \frac{1}{\gamma_{max}} \left(\frac{\ell}{170}\right)^2 \tag{18}$$

where ℓ is the clear span length and γ_{max} is the distance from the centroid of the steel section to the extreme fiber. A safe jacking force should produce a midpoint deflection for simple supports

and for fixed supports within the range of these two values, depending on the level of end restraints.

2.3.4.5 Estimate the Heats Required to Straighten or Curve the Members

The estimate of number of heats provides a schedule for the project. Comparing the estimated movement with the actual movement as it progresses is also useful as a rough indicator into whether the heating is being properly done. The number of heats, *n*, can be estimated:

$$n = \frac{\varphi_d}{\varphi_p} \tag{19}$$

where φ_p is the predicted plastic rotation per heat and φ_d is the angle of damage. Formulas for the plastic rotation associated with various structural shapes and damage conditions are provided throughout chapter 3 of this manual.

2.3.4.6 Prepare Repair Plans and Specifications

The final step is to prepare plans and specifications for the project. These plans act as the inspector's guide as well as the contractor's directive. As noted in section 2.3.1, the owner should provide inspectors to verify the contractor complies with contract requirements.

2.3.4.7 Be Aware of Supervisor Responsibilities

During the course of a heat straightening repair, proper supervision and consideration of the following conditions dictates the outcome of the repair. The supervisor should be aware of these considerations and continuously monitor them throughout the duration of the repair.

Preparing the Repair Area

Research by Connor et al. (2008) shows that small nicks and gouges produced during impact can propagate and lead to brittle failure during the heat straightening repair process. Additionally, hairline cracks and small defects can develop at weld toes (at stiffeners and other welded details) as the repair proceeds. As such, prior to beginning the repair process, the supervisor should ensure that all nicks, cracks, gouges, and other small defects are ground smooth prior to repair. Weld toes should also be ground smooth to reduce stress concentrations at the toe before beginning the repair.

Monitoring the Heating Temperature

Excessive temperatures may cause surface damage or lead to increased brittleness. Temperature can be monitored in several ways and are discussed in detail in section 2.2.8.3.

Controlling Restraining Forces

Another concern for the heat straightening supervisor is the control of restraining forces. Typically, hydraulic jacks are used to apply restraining forces, as shown in figure 49, and should be calibrated such that the force being exerted can be determined. Mechanical jacks should only

be permitted if they are calibrated to control applied loads. The maximum allowable force should be computed as part of the design process and specified in contract documents.

Source: George Watson, 2021

Figure 49. Photo. Jacks in place on an Indiana Bridge

Reviewing the Heating Patterns

The supervisor should review the heating patterns and torch paths proposed by the contractor. The general patterns can be set as part of the repair plan. However, as the repair progresses, there may be a need to modify the patterns to ensure a successful repair. Additionally, the supervisor should continuously inspect the member, using appropriate techniques, for the development of cracks at susceptible locations. Further, the supervisor should understand the principles behind the use of various heating patterns and approve modifications to heating patterns on site as needed.

Checking Tolerances

A significant concern is the tolerance for the completed repair. The contract documents should specify the allowable tolerances, and the inspector should verify that these limits either have been met or where and why exceptions were accepted.

Research conducted by Connor et al. (2008) investigated acceptable tolerances of a completed heat straightening repair. From this work, it was determined that the presence of residual, local damage (category L) in the flange of a wide flange section can cause secondary stresses that can increase the in-service stress at that location. This will not likely affect the strength of the girder, as the increase in local stresses will redistribute. However, it can be of particular concern if the

localized damage is near a welded detail (e.g., stiffener, cover plate), in sections that are particularly fatigue sensitive.

An analytical solution was developed by Connor et al. (2008) to capture the amplification of stress at a location due to residual damage. Equation 20 calculates the stress amplification factor, *SAF*, at a location due to residual damage:

$$SAF = \left(\frac{(1.35\ln(H)+4.25)t_f^{-0.06}-1.2}{-\ln(40H^{0.43})}\right)\ln(L) + (1.35\ln(H) + 4.25)t_f^{-0.06} + 0.1H(b_f - 10) \qquad (20)$$

where H is the height of the residual damage (inches), L is the length of the residual damage (inches), t_f is the flange thickness (inches), and b_f is the flange width (inches). This equation can be used to evaluate the effect of residual damage at a location to determine an acceptable tolerance for a repair. Note that the above equation is applicable only to category L damage located on the flange of a wide flange section (Connor et al., 2008).

While tolerance may be similar to those for new construction, often a greater tolerance is specified to avoid an excessive number of heat cycles to complete the repair, especially in restricted areas, and to reduce the cost and time required for the repair. This decision should be made as part of the design process.

2.3.4.8 Avoid Common Mistakes

Because heat straightening has evolved over time, many practitioners have developed their own set of skills that can result in mistakes. The sections below detail common mistakes and how they can be avoided.

Mistake No. 1. Heating the Steel Without Proper Temperature Control

Such an approach is dangerous because the steel may pass through both the lower critical and the upper critical temperatures. Because of this, the heating and cooling cycle may result in an irreversible microstructural change in the steel. The heat-straightened steel may have brittle characteristics and may no longer be suitable for bridge applications. Temperature sensing crayons or other direct temperature monitoring methods, discussed in sections 2.2.7 and 2.2.8.3, should be used to verify the heating temperature.

Mistake No. 2. Jacking the Girder While It Is Hot

While increasing the jacking load during a heat cycle may be tempting, particularly as the steel cools and yield stress increases, it is not something that can be properly controlled in the field and may lead to overstressing. Over-jacking can lead to a sudden brittle fracture during the repair process. It may also result in hard-to-detect micro-cracks that can weaken the structure. All jacks should be gauged, and forces limited to safe levels, well below the material's yield stress at the temperature of repair.

Mistake No. 3. Heating too Large an Area

Some practitioners may believe that the more surface area heated, the better the repair result. However, the principle of heat straightening is to allow differential heating followed by

contraction during cooling to move the steel. Heat straightening is most effective when small regions are heated so that the entire heating pattern can be allowed to cool uniformly. Narrow vee, strip, or line heats, with unheated metal in between, minimize overall expansion yet allow contraction during cooling to take place. Trying to heat a large portion of the member with one pattern may prevent the repair from being successful and should be avoided.

Mistake No. 4. Heating Outside the Yield Zones

The goal of heat straightening is to gradually restore the deformed zones to their original configurations. By limiting heat to only the vicinity of these areas, the damage mechanism is reversed. Heating in non-distorted regions often results in a misaligned structure because new deformations can be introduced in undamaged areas.

Mistake No. 5. Using Insufficient or Improper Heating Patterns

Certain heating patterns have been shown to be particularly effective: vee heats on major axis plate element bending, line heats for minor axis bending, and strip heats on stiffening elements. However, effective repair patterns may not be readily apparent, particularly for local damage. Sometimes a repair pattern may need to be relocated or substituted with an alternative when movements after a heating cycle are not noticed. An understanding of the role of each heating pattern is essential to effective heat straightening.

Mistake No. 6. Not Conducting a Proper Inspection and Surface Preparation

Defects (nicks, cracks, gouges) on the damaged steel have been noted to cause fractures and cracks upon repair (Connor et al., 2008). To limit the chances of unwanted deficiencies, the damaged location should be carefully inspected, and all surface imperfections, such as nicks and gouges, should be ground smooth. Additionally, to reduce the chances of hairline crack propagation at welded details, weld toes should also be ground smooth, or impact treated, and thermal cut plate edges should be ground smooth.

2.3.4.9 Verify Critical Items by Supervisors

The goal of a heat straightening repair is not just to straighten the damage, but to straighten it safely. It is suggested that the supervisors verify several critical items as the repair progresses:

- Ensure heating patterns are submitted, reviewed, and accepted by the engineer prior to initiating the repair.
- Ensure all nicks and gouges are ground smooth, regardless of whether a heat straightening repair will be performed.
- Check the jack gauges periodically to ensure that excessive force is not being applied before heating.
- Monitor the heating patterns, torch motion, and temperature for conformance with the procedure.
- Monitor the temperature of the steel periodically using temperature sensing crayons, contact pyrometer, or other temperature-sensing devices.
- Check periodically to ensure no cracks have appeared.

- Ensure desired movement using established reference points. A taut line can be useful although it may need to be moved aside during heating. In small regions, a straight edge may be used. Sometimes it is convenient to measure from a part of the adjacent structure which will not move during the straightening process.
- Monitor worker and public safety issues continuously since work is usually performed with at least some traffic nearby. Ensure that jacks and other equipment are secured from falling and protected from heat damage.
- Verify repair meets the specified dimensional tolerances without exceeding temperature or restraint limitations.

The above items relate specifically to heat straightening. The contractor's supervisor exercises normal control of the job site, as with any construction project, including monitoring of safety procedures.

2.3.5. Important Considerations

- A successful repair starts with a good design and plan.
- To meet the design plan and the owner specifications, field supervision and monitoring is important.
- The implementation of the repair is equally important.
- Good communication is essential among all parties working on the job.
- Keys to a successful repair include:
  o Select appropriate heating patterns and sequences.
  o Control the heating temperatures.
  o Use suitable restraining forces.
- Damage assessment includes:
  o Determining the cause of damage.
  o Inspecting and evaluating for safety and stability.
  o Detailing specific defects such as signs of fracture, cracks, tears and material degradation that may not be amenable to heat straightening repair.
  o Taking measurements to characterize damage.
  o Grinding and smoothing any surface nicks and gouges.
- Steps in the planning and design process include:
  o Analyzing angle of damage and determination of maximum strain due to damage.
  o Conducting a structural analysis of the system.
  o Selecting regions where heat straightening is applicable.
  o Selecting heating patterns and parameters.
  o Developing a constraint plan.
  o Developing repair plans and specifications.
- The supervisor's responsibilities include:
  o Monitoring the heating temperature.
  o Monitoring restraining forces.
  o Approving heating patterns.
  o Checking tolerances.
  o Ensuring the continued use of NDT to verify the quality of the repair or to verify that no cracks are initiating or propagating throughout the repair process.

- The engineer's responsibility is to provide good engineering judgment. Although some rational limitations exist when considering the heat straightening process, engineering judgment is essential for a successful repair.

2.4. USE OF HEAT IN FABRICATION

The use of heat in steel fabrication follows the same principles and techniques as the use of heat for in-field damage repair. The heating patterns, temperatures, and restraining forces used to induce or correct curvature (vertical and horizontal) in structural sections during the fabrication process are the same as those used for field-repairs of damaged sections previously discussed in chapters 2 and discussed further in chapter 3. The only difference between the two processes is the environment in which the heating occurs, with the fabrication shop offering more control of heat, restraining force, and other key variables. As such, the heating techniques and limitations detailed in previous sections are applicable and should be considered in combination with suggested techniques discussed in the following sections.

2.4.1. Heat Cambering

Heat cambering of plate girders as a means of introducing the design camber is not a common practice. Rather, girder web plates are typically cut to the desired camber profile with the flanges drawn and welded to the girder webs. Shrinkage from web-to-flange welding does occur and can affect camber in fabrication; however, fabricators can often predict and counteract this behavior, particularly with deeper and stiffer girders. Distortion from web-to-flange welding is more common for shallower (i.e., shorter in depth) sections.

Heat cambering is occasionally used for rolled beams, although fabricators generally prefer using cold bending to introduce camber into rolled sections (see chapter 4). When heat cambering is used, the process is usually performed with the beam inverted (resting on the top flange) and supported as necessary to allow for the desired stresses to be induced at the locations to be heated. Additional loads may be applied to provide supplemental restraint. As heat is applied to the section in a concentrated area, the surrounding material at room temperature applies restraint to the heated section and prevents the steel from expanding. The stability of the beam in this position should be ensured throughout this process because the introduction of heat and restraining force can introduce instability.

The location of the applied heat along the length of the section is an important consideration because it affects the magnitude of induced camber. Heats located at midspan of a simply supported beam produce the largest camber, while heats applied along the beam at points between midspan and the end supports will produce camber values proportional to their distance from midspan. As such, the vee heats applied to the web of the beam in combination with the strip heats applied to the bottom flange (discussed in section 2.2 as producing movement about the strong axis of a section) are concentrated in the midspan region of the beam. Because multiple heats may be required to achieve the necessary magnitude of camber, multiple vee heats can be applied at the same time, if enough unheated material is maintained between the vee heats to provide appropriate restraint. Typically, a spacing of two times the beam depth is maintained between the centerline of simultaneous heats. When vee heats are applied non-concurrently (i.e., for separate heat sequences), spacing of heats is of less concern. A typical cambering

configuration is shown in figure 50, where the number of heating sequences can be increased or decreased to achieve the desired camber. Limiting devices, such as catch blocks, can be employed to prevent excess deflection or buckling during heating.
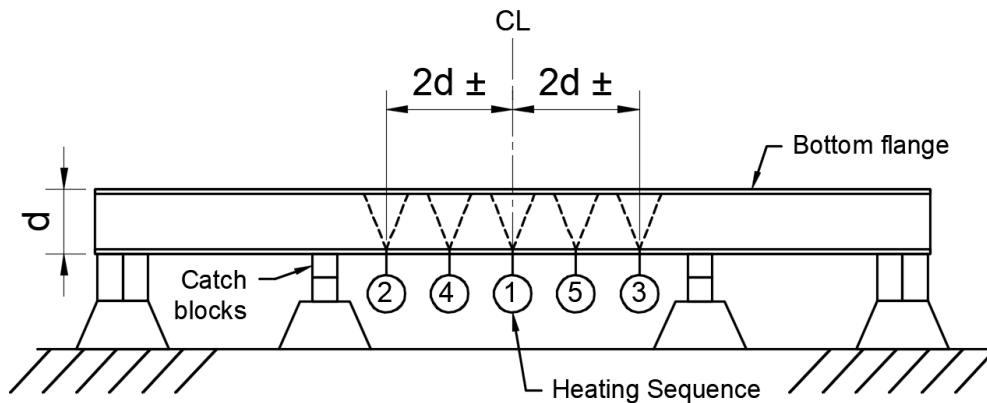
Source: FHWA

Figure 50. Illustration. Typical heat cambering scheme.

The depth of the vee is an important factor to consider while cambering members. Large beams may require vee heats with depths between 2/3 beam depth and full depth (where the apex is located just above the fillet, k region, of the top flange). In contrast, beams with thin webs, where the thickness is less than 3/8 inch, may require a vee depth limited to 1/2 of the beam depth to avoid web buckling. The vee angle, as noted in section 2.2.2.1, should be between 20 and 30 degrees. Additionally, heating temperatures should be limited as described in section 2.2.7. Heating patterns should be limited to areas small enough that the desired temperature can be reached quickly.

2.4.2. Heat Curving

Horizontally curving steel beams can be achieved using the heating patterns and techniques described in section 2.2.4.3. Two methods are used for heat curving beams. The first method is similar to the method described above for heat cambering. The heating patterns used for horizontal curving (weak axis) are similar to those of cambering (strong axis); however, the vee and strip heat locations differ. For horizontal curving, vee heats are applied to the flanges while a strip heat is applied to the edge of the flanges. Like cambering, restraining forces are a combination of self-weight and externally applied loads. Heat is applied at specific locations along the beam's length to obtain the shape and radius of curvature desired. With the second method, the girder is positioned horizontally and supported at points necessary to induce the desired stresses such that the desired curvature is towards, or away from, the floor. Strip heats are applied along the edges of the flanges for the full length of the girder. While the flange edges are hot, the weight of the unheated portion of the girder resists expansion; as the flange edges cool, they shrink, introducing curvature with the assistance of the girder's weight. The fabricator may place supports under the girder to control curving and ensure the desired amount of curvature is achieved. A photo with heating locations marked, illustrating method 2 described above, is presented in figure 51.

Source: Ronnie Medlock, 2022

Figure 51. Photo. Horizontal heat curving with strip heats.

Horizontal curves involve much tighter curvature than cambers do. While tight, small-radius curves can be achieved with either method stated above, there are industry code limitations to the curvatures that can be induced using heat alone. For bridge members, *AASHTO LRFD Bridge Construction Specifications* (AASHTO 2017a (23 CFR 625.4(d)(1)(iv))), limits heat curving based on beam and girder geometry. Geometry, including the thickness and width of the flanges and the thickness and depth of the web, are used in the *AASHTO LRFD Bridge Construction Specifications* (AASHTO 2017a (23 CFR 625.4(d)(1)(iv))) to determine the minimum radius of curvature allowable for heat curving a beam or girder, with a minimum allowable radius of 150 feet.

For members where AASHTO specifications are not applicable, *AISC's Design Guide 33 for Curved Member Design* (AISC 2018) suggests that the minimum radius of curvature be limited to approximately 150 times the depth of the member in the plane of bending. AISC's design code is not regulatory.

2.4.3. Fitting and Distortion Control

Distortions to the web can occur during the fabrication of built-up girders, even when the girders are not curved or cambered. To mitigate the development of distortions, fabricators can use extra preheat and maintain elevated interpass temperature during welding in accordance with AASHTO and AWS (AWS 2015 (23 CFR 625.4(d)(2)(i))) requirements and recommendations. Often, clamping, blocking and restraining are not enough to prevent distortions from occurring and may be discouraged in some applications. Repairing distortions can be accomplished using the various techniques described within this manual, with localized repair methods of particular

importance. Per AWS stress relieving after welding is allowable and maximum temperatures must be adhered to. The AASHTO/AWS D1.5 bridge welding code (AWS 2015 (23 CFR 625.4(d)(2)(i))) should be consulted before any procedures are attempted. A photo illustrating the use of a line heats to repair a web distortion is shown in figure 52.

Source: Tory Lebaron, 2020

Figure 52. Photo. Web distortion repair with line heats.

CHAPTER 3. HEAT STRAIGHTENING REPAIR

3.1. HEAT STRAIGHTENING OR HEAT CURVING OF FLAT PLATES

3.1.1. Introduction

Many primary structural steel shapes can be thought of as being composed of flat plates. Understanding the behavior of heated plates is fundamental to the heat straightening and heat curving processes for all structural shapes. For bridge structures, usually constructed of plates forming an I-shaped section, damage typically involves combinations of these plate flanges and webs being bent about their strong and/or weak axes. As such, the heat straightening repair of these types of elements is based on the heat straightening of the flat plates that compose these sections. The same concept applies for heat curving or cambering structural steel sections, where the principles of heat straightening or curving of flat plates inform the process used for various structural steel shapes.

The purpose of this chapter is to describe experimental and analytical research on heat straightening as it applies to plates and to present related engineering design criteria for its use. While the research discussed in this section focuses primarily on the heat straightening of plate elements, these principles can be applied to heat curving. This work forms the basis for the heat straightening and curving of rolled shapes discussed in chapter 3.

3.1.1.1 Background

Several studies from the late 20th century sought to capture the effect of various parameters on plate movement during heat application (Weerth, 1971; Nicholls and Weerth, 1972). These studies focused on vee heats and attempted to develop predictive models to capture the behavior based on various parameters. These early studies formed the baseline for experiments by Roeder (1985, 1986), later expanded upon by Avent (1987), that focused on the application of vee heats to undamaged plates and sought to fully examine the factors affecting heat straightening of plates. This work was then extended further by Avent et al. (1992) to capture the behavior of damaged plates subjected to heat straightening with varying parameters. Finally, Avent and Mukai (1998) and Avent et al. (2000) completed a comprehensive review of all five experiments to develop an analytical model to predict plate movement as a function of various heat straightening parameters in practice.

The basis of the analytical models developed by Avent and Mukai (1998) and Avent et al. (2000) are the simplistic plate models developed by Holt (1965) and Moberg (1979). Consider figure 53, showing vee heat geometry for a plate element, from which Holt (1965) developed one of the first and simplest methods for predicting plastic rotations, φ_p, in a vee-heated plate.
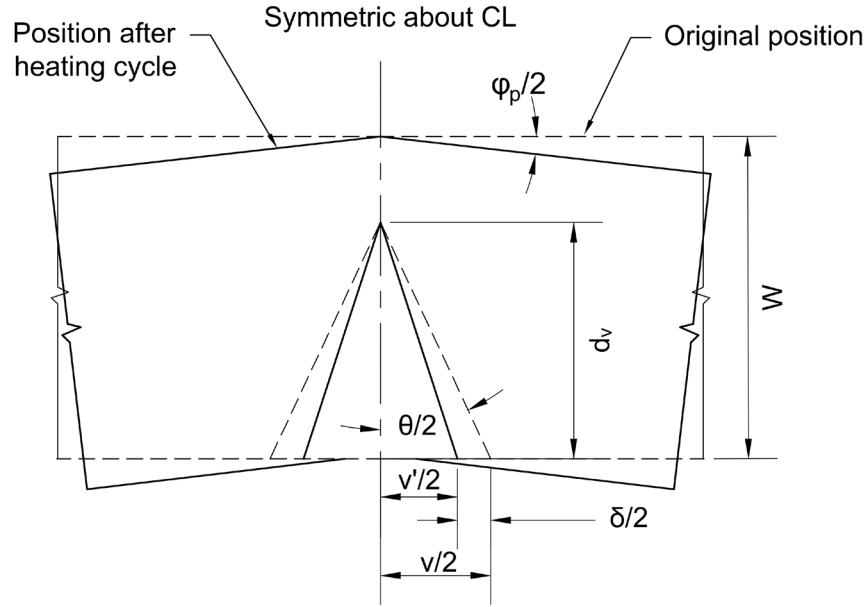
Source: FHWA

Figure 53. Illustration. Vee heat geometry.

Recognizing that heat straightening merely reshapes the volume of material being heated, Holt (1965) assumed that the deformation through the vee was linear over the depth of the plate and that perfect single axis confinement existed longitudinally during heating. The resulting formula in terms of the plastic rotation, φ_p, is:

$$\varphi_p = \frac{S_p V}{W} \tag{21}$$

where S_p is the plastic strain resulting at temperature, T, for the single axis perfect confinement case (a temperature of 1,200°F was used by Holt (1965)), V is the width of the open end of the vee heat, and W is the plate width. Moberg (1979) later modified this equation to account for the depth of vee using the experimental work of Weerth (1971). In addition to the assumptions used by Holt (1965) listed above, Moberg (1979) assumed that the plastic rotation is proportional to the depth ratio d_v/W where d_v is the depth of the vee heat. The resulting equation is:

$$\varphi_p = \frac{S_p V d_v}{W^2} \tag{22}$$

An important consideration excluded from these early formulations is the influence of external and internal restraining forces. As discussed in chapter 2, external restraining forces, producing compression in the vee during heating, increase confinement and therefore increase the rotation produced per heat. The field applications cited by Holt (1965) and Moberg (1979) involved the use of restraining forces. However, the effect of restraining force on movement per heat cycle was not considered in the resulting analytical formulations.

Avent (1987) and Avent et al. (1992, 2000) sought to quantify the effect of various heat straightening parameters on plate movement and develop analytical procedures for using heat straightening repair in practice. This research filled gaps in early analytical models (Holt, 1965; Moberg, 1979) and expand on early experimental work by Weerth (1971), Nicholls and Weerth

(1972), and Roeder (1985, 1986). The details of this work as it relates to the earlier baseline research are discussed below. The experimental results, conclusions, and analytical model from the studies discussed in this section provide a baseline knowledge for heat straightening and curving of plate elements and the foundation for further research and discussion on the topic of heat straightening and curving of rolled shapes captured in later sections.

3.1.2. Experimental Data and Results

The tests conducted in the experimental program by Avent (1987) and Avent et al. (1992) expanded on the experiments conducted by Roeder (1985, 1986). Both Avent (1987) and Roeder (1985, 1986) applied vee heats to straight, undamaged, specimens, measuring the resulting change in geometry. Using straight specimens allowed a larger variety and number of tests to be conducted efficiently. Roeder (1985, 1986) considered 60 heating cycles. Avent (1987) performed 255 heating cycles on similarly sized plate specimens. Avent et al. (1992) also conducted additional experiments in which plates with mechanically induced strong axis damage (bends) were heat straightened. A center point loading on the simply supported plates was used to create various degrees of damage. The degree of damage was measured as the angle of the tangents formed by the edges of the unyielded portions of each plate on either side of the yield zone. This angle ranged from 6 to 25 degrees. Between 20 and 100 vee heats were applied to straighten the 10 plates with differing degrees of damage. A total of 336 vee heat cycles were applied.

For all experiments (Roeder, 1985, 1986; Avent, 1987; Avent et al. 1992), the plate specimens were hot rolled A36 steel with dimensions around $4 \times 24 \times 1/4$ inches. An exception to these dimensions were specimens used to study the impact of plate dimensions and thickness on heat straightening.

Several parameters including temperature, restraining force, and plate geometry were varied throughout these experiments to investigate the effect of various heat straightening configurations on plate movement. Each parameter considered is discussed in the following sections.

3.1.2.1 Vee Angle

One of the most important parameters influencing the plastic rotation of a plate during heating is the vee angle. The impact of this parameter, focusing on plastic rotation, φ_p, as a function of vee angle, has been studied by several researchers, including Nicholls and Weerth (1972), Roeder (1985, 1986), Avent (1987), and Avent et al. (1992).

In the case of the four studies mentioned above, the experimental data show a fairly linear relationship between vee angle and plastic rotation. However, the data show a significant amount of scatter. For the results of Avent (1987) and Avent et al. (1992), involving approximately 600 plate tests, and Roeder (1985, 1986), involving 59 plate tests, a similar level of scatter was observed. In both cases, heating temperature was controlled using two methods to limit temperature variation: (1) temperature sensing crayons, and (2) thermocouples or calibrated contact pyrometers. Despite such efforts, a significant amount of variation in plastic rotation occurred in almost identical repetitive tests. In contrast, the smaller scale study by Nicholls and

Weerth (1972), which included 21 specimens, showed no evidence of this large scatter. The consistency of data points was such that smooth curves were produced with no curve fitting necessary. Temperature sensing crayons were the only temperature control used for this study. The results from Nicholls and Weerth's (1972) are omitted from the comparative discussion in this section since their experimental results do not agree with the more comprehensive studies by Roeder (1985, 1986), Avent (1987), and Avent et al. (1992).

To determine the source of the large scatter in the experimental data, Avent and Mukai (1998) evaluated the methodology and results from all three experiments. From this, the source of the scatter was narrowed down to one of several parameters. The first was the control of both the restraining force and heating temperature. The percent error in measured value for the equipment used by Roeder (1985, 1986), Avent (1987), and Avent et al. (1992) to measure restraining force was 10 to 15 percent. Similarly, percent error for temperature measurements was also in the range of 10 to 15 percent. The second parameter suggested by Avent and Mukai (1998) was the development of residual stresses during heating. Although Holt (1971) and Roeder (1985, 1986) suggested that residual stress does not have a significant impact on the heat straightening process, results from research presented by Avent and Mukai (1998), discussed in section 2.1, indicate that large residual stresses are possible because of the heating process. As such, Avent and Mukai (1998) concluded that the large scatter in the experimental data was likely due to a combination of challenges associated with the control of the restraining forces and heating temperatures, and the possible development of large residual stresses in the test specimens during heating.

3.1.2.2 Depth of Vee

Early researchers (Nicholls and Weerth, 1972; Roeder, 1985 and 1986) concluded that plastic rotation was proportional to the depth ratio, R_d, which is the ratio of vee depth, d_v, to plate width, W. To further evaluate this behavior and expand on Roeder's (1985, 1986) work, Avent (1987) conducted a series of tests for depth ratios of 0.5, 0.75, and 1.0, and vee angles ranging from 20 to 60 degrees. At least three heats were conducted on initially straight plates for each case, and the results were averaged. The results, compiled and evaluated by Avent et al. (2000), are shown in figure 54 for a combination of three depth ratios, three vee angles, and two jacking ratios. The jacking ratios reflect that a jacking force was used to create a moment at the vee heat equal to either 25 or 50 percent of the ultimate bending capacity of the plate. As shown in figure 54, the values for plastic rotation achieved for depth ratios of 0.75 and 1.0 percent were similar for almost all vee angle and jacking ratio combinations. The depth ratio of 0.75 resulted in slightly larger plastic rotations in all but one of the six cases presented. The plastic rotations measured for cases where a depth ratio of 0.5 was used were erratic; no distinct trend was observed. In three of the six cases, the depth ratio of 0.5 produced much smaller plastic rotations. In the other three cases, the plastic rotations were similar to those of the other depth ratios considered.
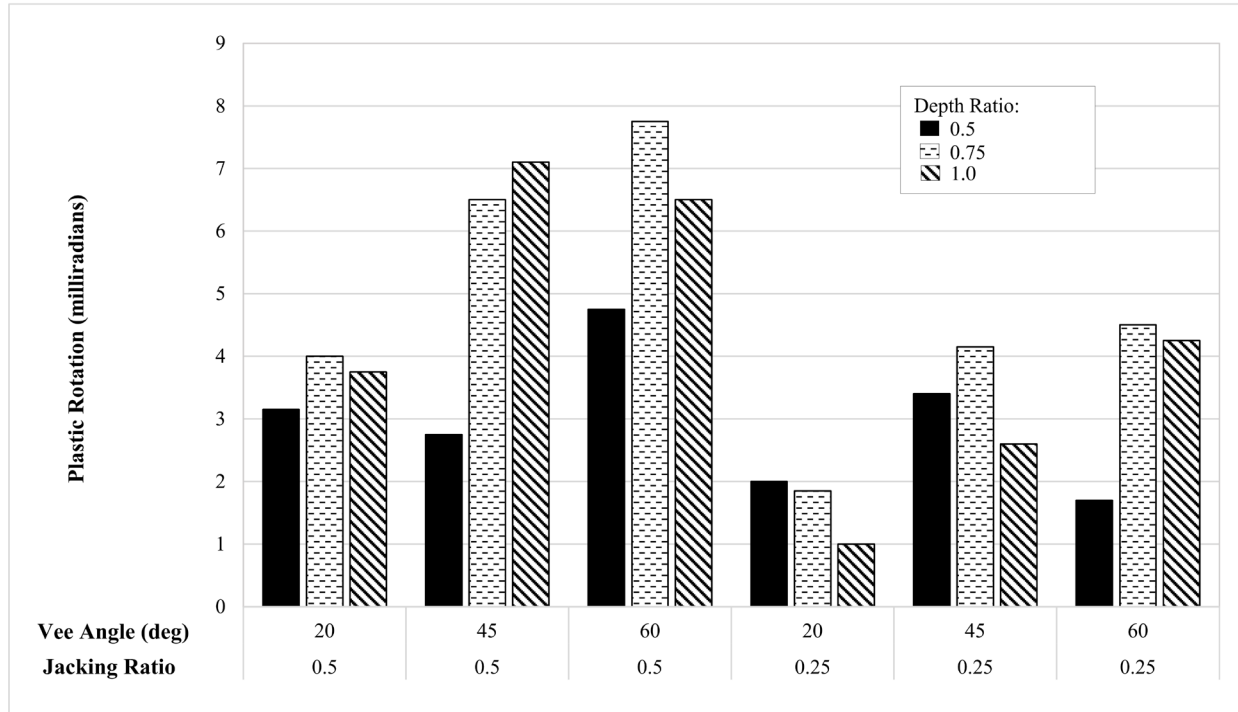
Source: Avent and Mukai (1998)

Figure 54. Graph. Influence of vee depth ratio on plastic rotations of originally straight plates for various vee angles and jacking ratios, heating temperature of 1,200°F.

To further verify this behavior, Avent et al (1992) damaged and straightened a series of plates. The degree (severity) of damage induced was large enough that at least 20 heats were used for the repair of most of the plate specimens. Therefore, more statistically significant average plastic rotations were obtained from these tests compared to the undamaged specimens (an average of 20 values compared to an average of 3). The results from these tests are shown in figure 55 for a jacking ratio of 0.5 and two vee depth ratios: 0.75 and 1.0. The findings from these experiments were the same as those for the undamaged specimens: the magnitude of plastic rotation achieved during heating does not have a direct correlation to vee depth. The variation of vee depth ratios between 0.75 and 1.0 had little influence on plastic rotation. Additionally, a vee depth ratio of 0.5 may result in reduced plastic rotations. However, the experimental data discussed in this section are inadequate justifications for a generalized suggestion or conclusion regarding vee depth ratio and plastic rotation during heating.
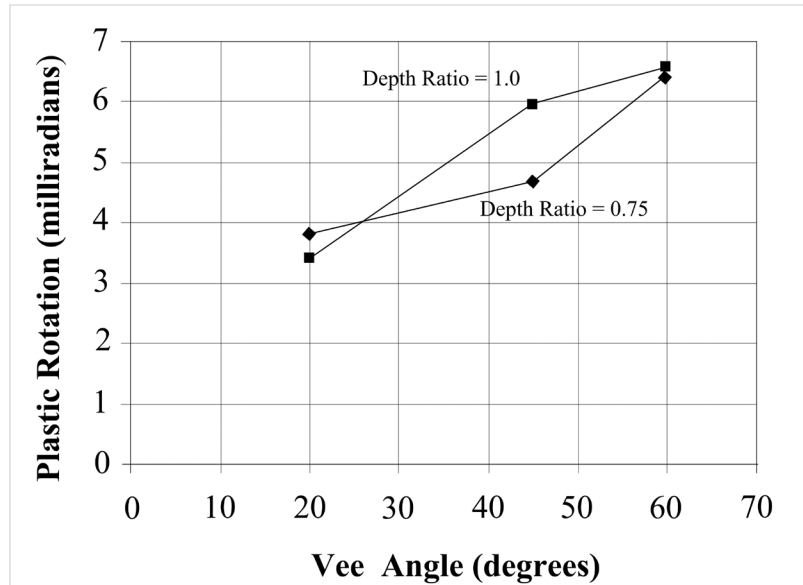
Source: Avent and Mukai (1998)

Figure 55. Graph. Vee angle versus average plastic rotation for damaged plates with different vee depth ratios, jacking ratio=0.5, heating temperature=1,200°F.

3.1.2.3 Plate Thickness and Geometry

Early researchers studying heat straightening generally considered plate thickness to have a negligible effect on plastic rotation. The only reservation expressed, as noted by Avent and Mukai (1998), was related to plate thickness and heat application: the plate being heated should be thin enough to allow a relatively uniform penetration of the heat through the thickness.

Later researchers, Roeder (1985, 1986), Avent (1987), and Bourdeaux (1987) sought to quantify the effect of plate thickness and width on plastic rotation. Avent (1987) considered plates of four different thicknesses: 0.25, 0.375, 0.5 and 0.625 inch. Full depth vee heats were applied to each specimen using a variety of vee angles and no jacking force was used. The results from tests involving different plate thicknesses are shown in figure 56 where each bar represents the average of at least three heats. The results illustrate the level of variability in plastic rotation that may occur among groups of heats. However, there is no discernable pattern for plastic rotation as a function of plate thickness for the three different vee angles used.
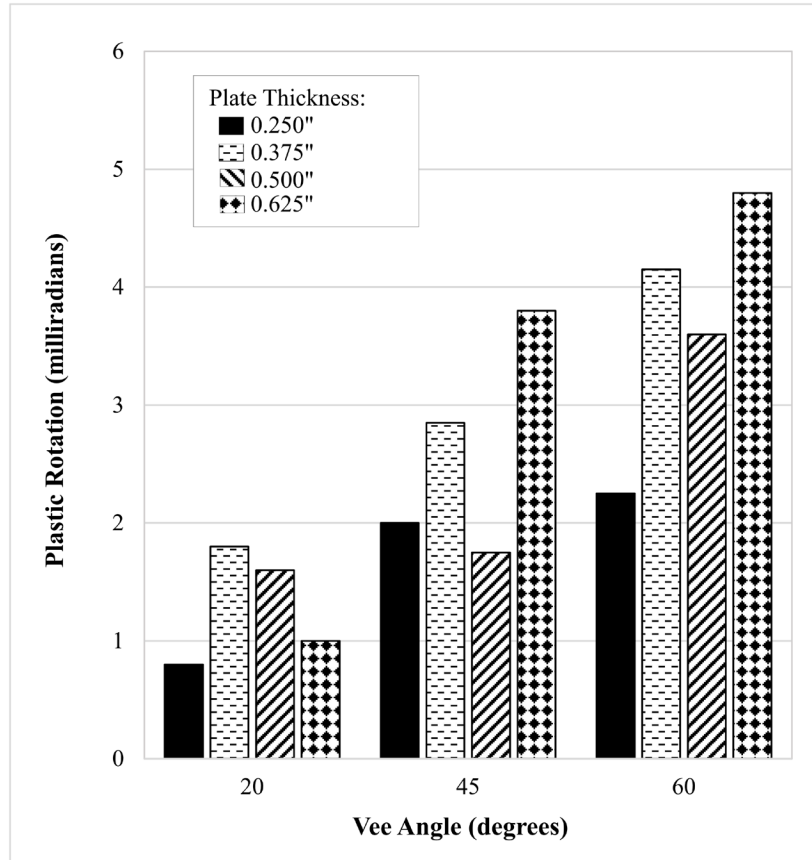
Source: Avent and Mukai (1998)

Figure 56. Graph. Comparison of average plastic rotations for plates of four thicknesses, vee depth ratio=1, jacking ratio=0, heating temperature=1,200°F.

A similar result was observed by Roeder (1985, 1986), shown in figure 57. In these tests only one vee angle was used ($\theta = 60$ degrees) along with several different jacking forces. Plate thicknesses of 0.25, 0.375, and 0.75 inch were considered. Again, no discernable pattern of plastic rotation was observed among the plate thicknesses.
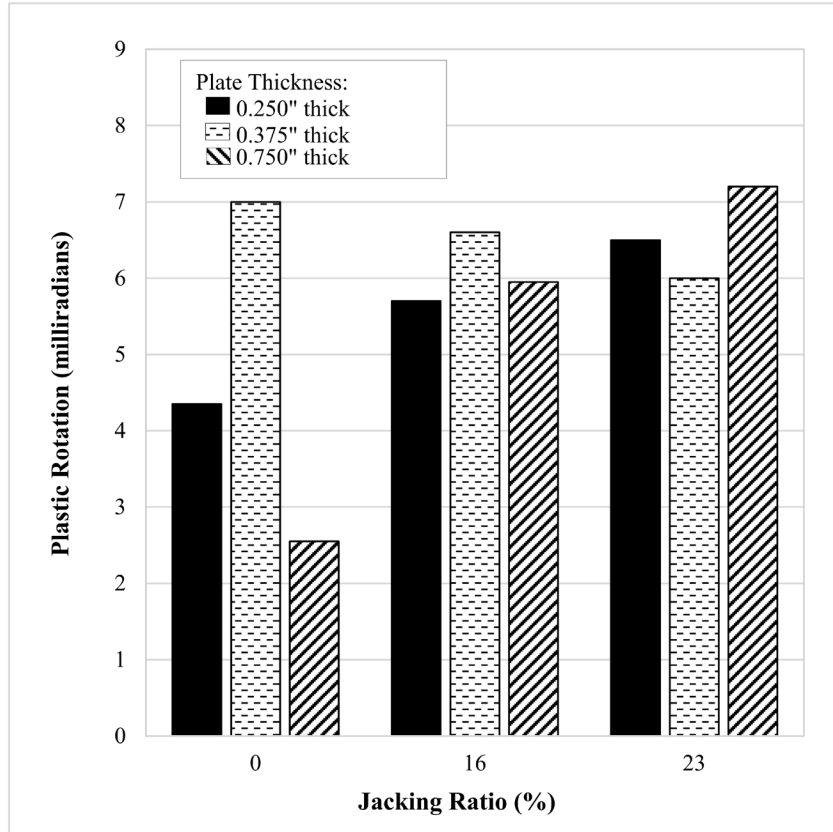
Source: Avent and Mukai (1998)

Figure 57. Graph. Comparison of plastic rotations for plates of three thicknesses, θ=60 degrees, vee depth ratio=0.67, heating temperature=1,025-1,260°F.

The effect of plate width on plastic rotation was also investigated by Roeder (1985, 1986). Figure 58 shows the results of these tests, comparing plastic rotations for two plate widths (5.9 inches and 7.9 inches) and a variety of jacking ratios. One to two heats were applied per case. Only a small difference in plastic rotation was observed between the two plate widths tested.
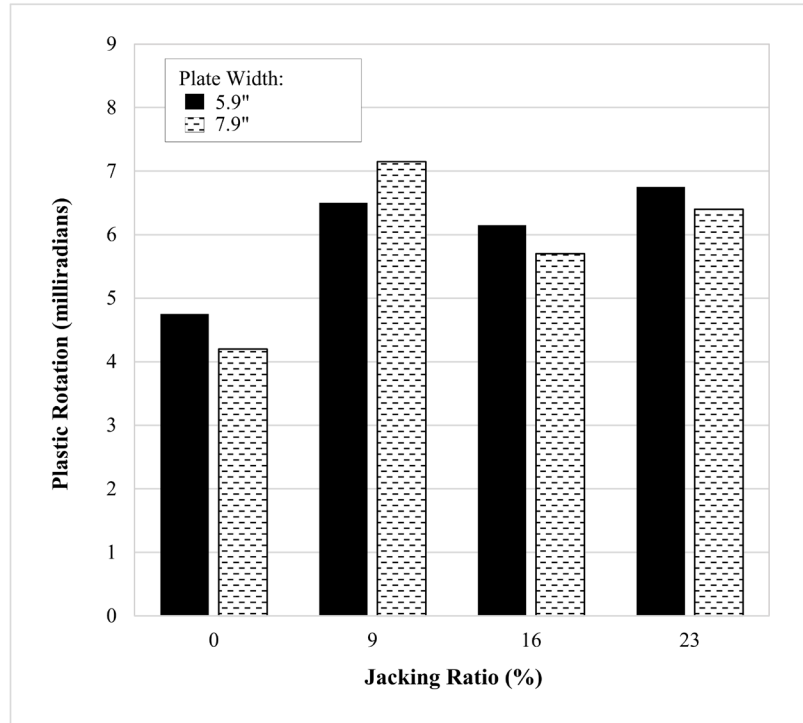
Source: Avent and Mukai (1998)

Figure 58. Graph. Comparison of average plastic rotations for plates of two widths, θ=60 degrees, vee depth ratio=0.67, heating temperature=1,200°F.

In a test series conducted by Boudreaux (1987), three plate widths were studied as shown in figure 59. The plastic rotations shown in the figure are the average of three heats. An unusually low average was observed for the 4-inch width. However, little difference was found between the 8-inch and 12-inch widths. The results of these tests show no clear relationship between plastic rotation and plate width.
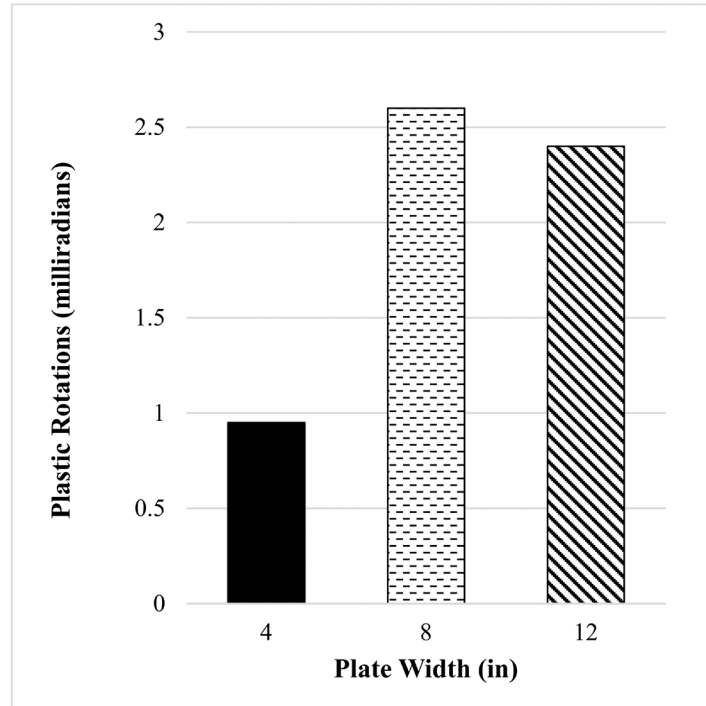
Source: Avent and Mukai (1998)

Figure 59. Graph. Comparison of average plastic rotation for plates of three widths, jacking ratio=0, θ=20 degrees, vee depth ratio=0.75, heating temperature=1,200°F .

In summary, the test results from Roeder (1985, 1986), Avent (1987), and Boudreaux (1987) illustrate that plate thickness and width have only a minor influence on plastic rotation. The results from all three experiments illustrate the variability of response that is typical of heat straightening (discussed briefly in section 3.1.2.1). However, no distinct relationship between plastic rotation and plate geometry was observed. Thus, plate geometry is considered only a minor influence on plastic rotation.

3.1.2.4 Temperature

One of the most important and yet difficult to control parameters of heat straightening is the temperature of the heated steel. Factors affecting temperature include number and size of torch orifices, temperature of the flame, speed of torch movement, and thickness of the plate being heated. As a result, there can be considerable variability if heat application is not appropriately monitored. This is discussed in detail in section 2.2.

Assuming adequate temperature control is maintained, the question arises as to what temperature produces the best heat straightening results without negatively affecting the material properties. Researchers have disagreed on this topic. Shanafelt and Horn (1984) stated that heats above 1,200°F on carbon and low alloy steels will not increase plastic rotation. Rothman and Monroe (1973) concluded that reheating areas where previous spot heats were performed did not improve plastic rotation. Roeder (1985, 1986), however, concluded that the resulting plastic rotation was generally proportional to the heating temperature up to at least 1,600°F.

Avent (1987) sought to more clearly define the behavior suggested by Roeder's (1985, 1986) study. To do so, a series of heats were applied to plates in which the heating temperature was varied from 700° to 1,500°F in increments of 100°F. The results of this testing, compiled by Avent et al. (2000) and shown in figure 60, establish a clear relationship of increased plastic rotation with increasing temperature.
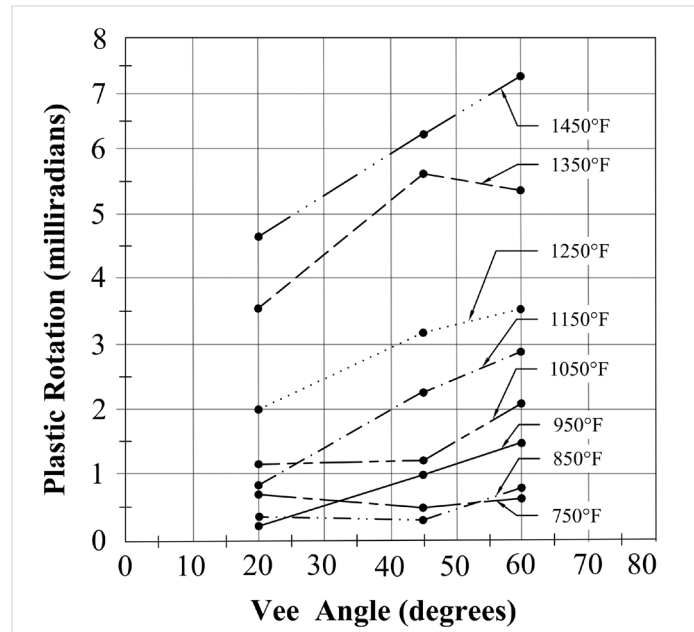
Source: Avent and Mukai (1998)

Figure 60. Graph. Influence of heating temperature on plastic rotation, vee depth ratio=0.75, jacking ratio=0.16.

Although the results from Roeder (1985, 1986) and Avent (1987) indicated higher temperatures result in greater plastic rotations, the maximum temperature used for heat straightening and curving should be limited. These suggested temperature limits, categorized by steel type, are discussed in detail in section 2.2.7. To control the temperature throughout the heating process, the speed of the torch movement and the size and type of torch orifice should be adjusted for different material thicknesses as discussed in section 2.2.8.

3.1.2.5 Restraining Forces

The use of restraining forces during heat straightening was introduced in section 2.2.3. The proper procedure for applying a restraining force is to create a moment tending to compress the stretched area of the cross section. The ratio of the moment due to the jacking force, M_j, to the plastic moment of the cross section, M_p, is referred to as the jacking ratio. Roeder (1985, 1986) and Avent (1987) studied the effect of jacking ratio on plastic rotation during heat straightening. Like the experiments discussed in earlier sections, the work by Avent (1987) sought to expand on the testing program conducted by Roeder (1985, 1986).

Jacking ratios between 0 and 50 percent with four different vee angles were considered by Avent (1987) . The results of this testing are shown in figures 61 and 62 for 3/4 and full depth vee

heats, respectively. The data points shown in the figures are the average of three to four values (three to four heats per specimen), and the lines represent a least squares curve fit of the data. The results indicate that higher jacking ratios resulted in greater plastic rotation during heating. A smaller set of test specimens and variables were observed by Roeder (1985, 1986) to have a similar pattern of behavior. The results of this testing are shown in figure 63.
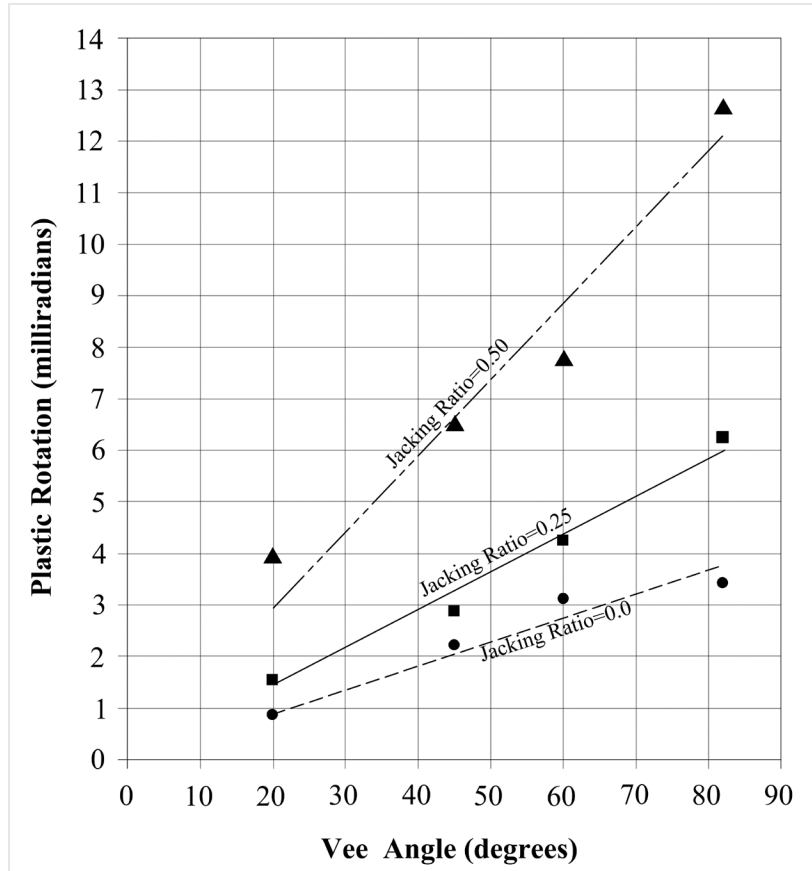
Source: Avent and Mukai (1998)

Figure 61. Graph. Influence of jacking ratio on average plastic rotation, vee depth ratio=3/4, heating temperature=1,200°F.
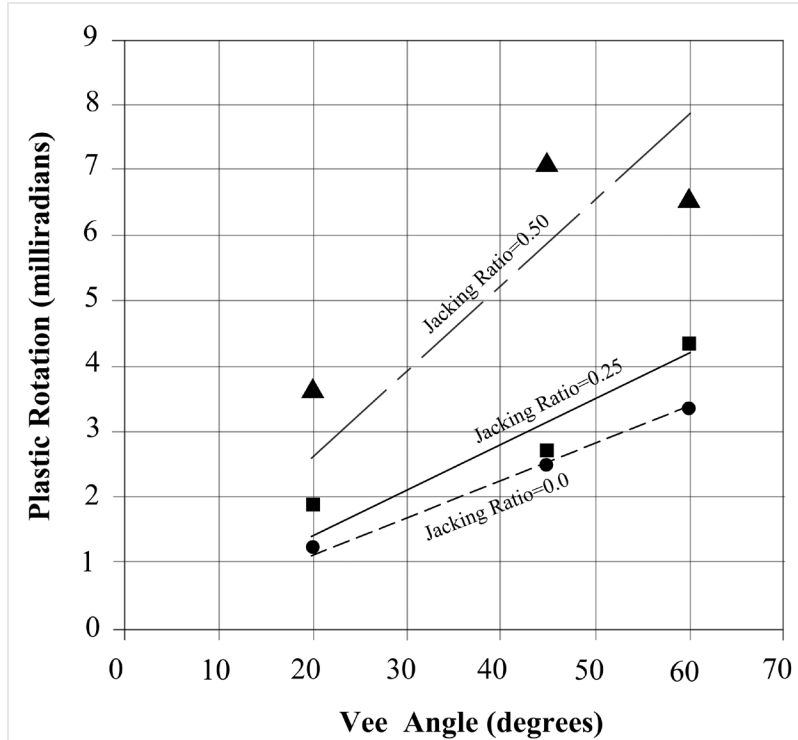
Source: Avent and Mukai (1998)

Figure 62. Graph. Influence of jacking ratio on average plastic, vee depth ratio=1, heating temperature=1,200°F.
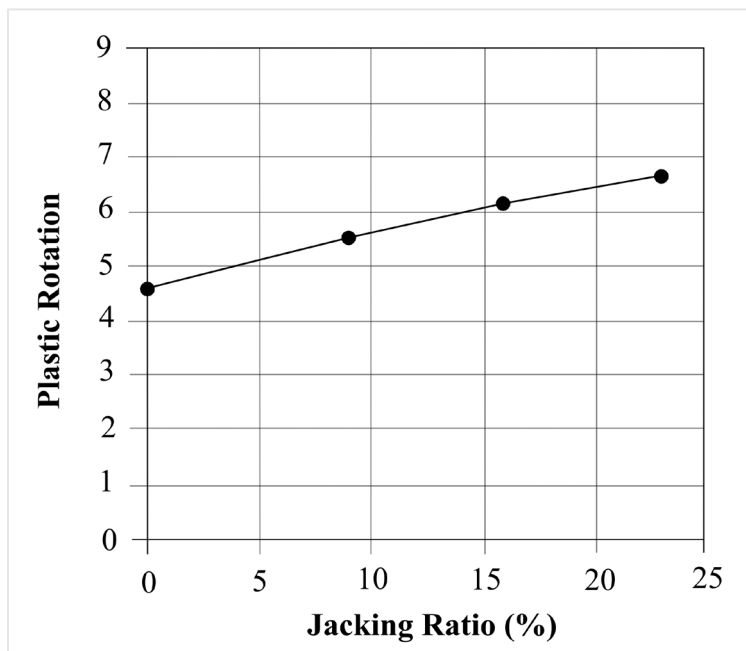
Source: Avent and Mukai (1998)

Figure 63. Graph. Average plastic rotation versus jacking ratio, θ=60 degrees, vee depth ratio=0.67, heating temperature=1,200°F.

112

To expand on the testing programs of Roeder (1985, 1986) and Avent (1987) that focused on undeformed plate specimens, Avent et al. (1992) conducted a series of tests on similarly sized, 0.25-inch-thick plates, subjected to damage prior to heat straightening. Between 20 and 100 heats were applied to heat straighten the specimens (see section 2.1 for a discussion on residual stresses in some of these plate specimens). A summary of the test parameters and resulting plastic rotations is given in table 14. The heating temperature for all specimens was 1,200°F. An excerpt of the results is plotted in figure 64. Again, plastic rotation was found to vary linearly with jacking ratio.

Table 14. Heating conditions and degree of damage for damaged plate specimens (Avent and Mukai, 1998).

Specimen/Strip	Angle of Damage (deg./mrad)	Maximum Strain (Multiple of Yield Strain)	Vee Angle (deg.)	Jacking Ratio (M_j/M_p)	Vee Depth (-)	Avg. Plastic Rotation per Vee (mrad)
P-9	6.40/111.8	30	45	0.25	1.00	4.63
P-10	23.62/412.2	100	45	0.25	1.00	3.82
P-11	5.58/79.4	30	45	0.50	1.00	5.94
P-12	11.80/205.9	80	45	0.50	1.00	5.60
P-13	18.7/327.6	90	45	0.33	1.00	5.56
P-14	5.99/104.5	30	45	0.50	0.75	4.69
P-15[1]	21.12/368.6	80	20	0.50	0.75	3.81
P-16[1]	25.06/437.4	90	20	0.50	1.00	3.41
P-17[1]	18.21/317.8	100	60	0.50	0.75	6.43
P-18[1]	25.02/436.7	100	60	0.50	1.00	6.56

[1] The last four specimens were used just for plastic rotation data and were not straightened completely (20 heats were applied to each).
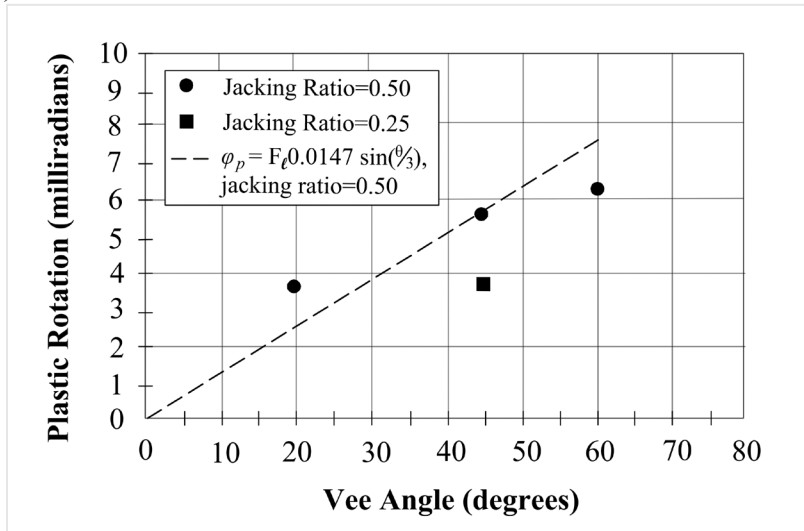
Source: Avent and Mukai (1998)

Figure 64. Graph. Jacking ratio versus vee angle, damaged plates, vee depth ratio=1, heating temperature=1,200°F.

In addition to flexural restraining forces producing a moment that restrains the heated region, axial restraint can also be used during heat straightening. A series of tests, conducted by Avent (1987), using a superimposed axial load on undamaged plates for various vee angles. The applied load created a 20 ksi compressive axial stress (an actual stress to nominal yield stress ratio of 56 percent). Avent et al. (2000) compiled the results of similar tests with various vee angles and vee depths of ¾ the member depth or greater. The results from these tests are shown in figure 65. As shown in the figure, the application of axial load resulted in slightly greater plastic rotations compared to cases with no restraining force, however, the effect was limited.
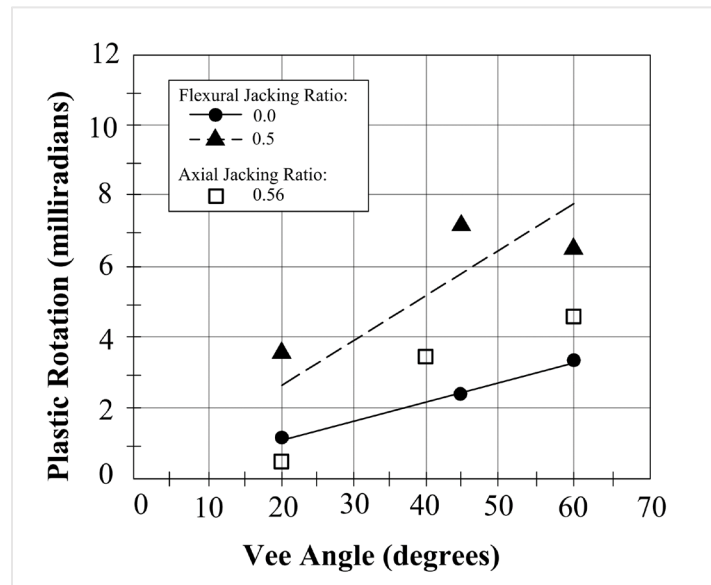
Source: Avent et al. (2000)

Figure 65. Graph. Influence of axial jacking force on plastic rotation of vee-heated plates, vee depth ratio=1, heating temperature=1,200°F.

Testing by Roeder (1985, 1986), Avent (1987), and Avent et al. (1992) suggests that plastic rotation is generally proportional to the flexural jacking ratio (referred to throughout this document as the jacking ratio) and the proper use of external force greatly expedites the heat straightening and heat curving processes. However, restraining (jacking) forces should be limited in practice to avoid fracturing or hot bending the steel during the heat straightening or heat curving process. The suggested limits for external restraining forces are discussed in detail in section 2.2.3.

In summary, based on the research presented above, the parameters that have a substantial influence on the plastic rotations produced by vee heats are: (1) vee angle, (2) steel temperature, and (3) external restraining force. The depth of the vee (between 3/4 and full depth) has little effect on plastic rotation. Likewise, the plate dimensions are of minor significance assuming the steel within the heated region is heated thoroughly and properly.

3.1.3. Analytical Development

Two general approaches have been used in the past to develop an analytical procedure for predicting member response during a heat straightening repair. The first approach involves finite

114

element/finite strip thermal and stress analyses that include inelastic behavior. In this method, the stress-strain equilibrium is evaluated over small time steps, capturing the effect of non-uniform temperature distribution. This approach, while valid, is computationally expensive and time consuming; even when analyzing a single vee heat. In contrast, the second approach considers the global behavior of the vee during straightening. The goal of this approach is to develop an analytical model and equation that can be used to predict the plastic rotation produced by a vee heat. The focus of this section is this second method. An analytical model to predict plastic rotation was developed by Avent et al. (2000) using the experimental data and the early analytical models from Roeder (1985, 1986), Avent (1987), and Avent et al. (1992).

The model developed by Avent et al. (2000) was based on the following baseline assumptions: (1) longitudinal plastic strain occurs only in the vee-heated zone and in a reflected vee about the apex for partial depth vees (see figure 66); (2) at any specified distance from the neutral axis of the plate, the strains in the longitudinal direction are constant over the vee-heated zone; (3) the planes defined by the sides of the vee remain planes after heating and rotate about the apex of the vee; and (4) the heating temperature is 1,200°F. The development of additional assumptions by Avent et al. (2000) based on the observations and experimental results from Roeder (1985, 1986), Avent (1987), and Avent et al. (1992) are discussed below.
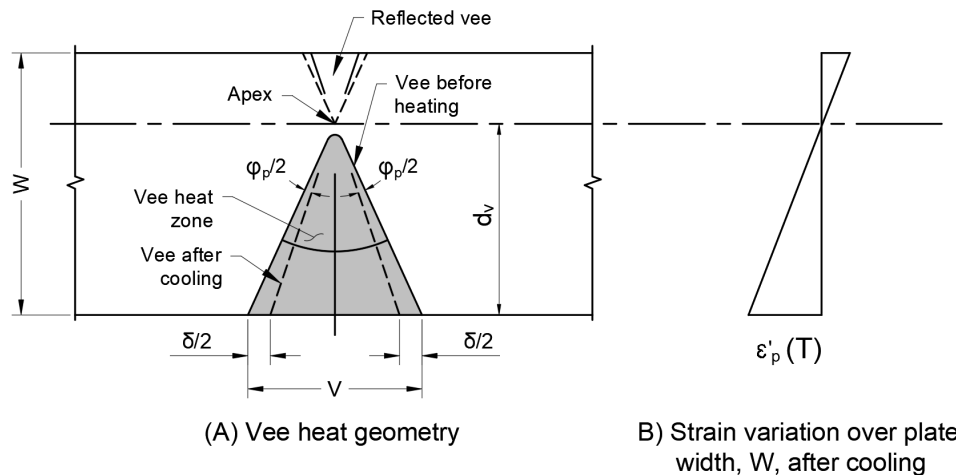
Source: FHWA

Figure 66. Illustration. Geometric changes resulting from a vee heat on a plate.

Using experimental data from Roeder (1985, 1986) and Avent (1987), the geometry of a vee-heated plate, before and after heating, was evaluated analytically using the four baseline assumptions listed above (Avent et al., 2000). The geometry of the vee-heated plate is shown in figure 66, with vee geometry before and after heating illustrated in the figure. The change in the width of the open end of the vee, δ, can be written as:

$$\delta = 2d_v\left[\tan\frac{\theta}{2} - \tan\left(\frac{\theta}{2} - \frac{\varphi_p}{2}\right)\right] \tag{23}$$

Defining $\varepsilon_p{}'(T)$ as the final plastic longitudinal strain at the open end of the vee for a specified maximum heating temperature, T, after a heating and cooling cycle, and is calculated as:

$$\varepsilon_p'(T) = \frac{\delta}{V} \tag{24}$$

Using trigonometric relations from figure 66 to eliminate V:

$$\delta = 2d_v\varepsilon_p'(T)\tan\frac{\theta}{2} \tag{25}$$

Equating equations 23   and 25 and using the trigonometric identity for the tangent function:

$$\varepsilon_p'(T)\tan\frac{\theta}{2} = \left[\tan\frac{\theta}{2} - \frac{\tan\frac{\theta}{2}-\tan\frac{\varphi_p}{2}}{1+\tan\frac{\theta}{2}\tan\frac{\varphi_p}{2}}\right] \tag{26}$$

Since experimental data from Roeder (1985, 1986) and Avent (1987) showed that both φ_p and $\varepsilon_p'(T)$ are small, Avent et al. (2000) assumed that $tan(\varphi_p/2)$ is approximately equal to $\varphi_p/2$ and that $\varepsilon_p'(T)$ is significantly smaller than 1, and solved equation 26 for φ_p in radians:

$$\varphi_p = 2\varepsilon_p'(T)\sin\frac{\theta}{2} \tag{27}$$

Based on measurements of strain distribution over the vee-heated regions of the plate specimens, Roeder (1985, 1986) found that most of the permanent strains occurred within the inner two-thirds of the vee heat. Avent et al. (2000) incorporated this observation into the analytical model as an additional assumption: (5) permanent strains occur within the inner two-thirds of the vee (with an effective vee angle of two-thirds the full vee angle). Incorporating assumption (5) into the equation for plastic rotation below:

$$\varphi_p = 2\varepsilon_p'(T)\sin\frac{\theta}{3} \tag{28}$$

To determine the actual plastic strain in the vee, $\varepsilon_p'(T)$, Avent et al. (2000) used the preliminary analytical model from Roeder (1985, 1986). Roeder (1985, 1986) developed an analytical model that approximated the actual plastic strain in the vee, $\varepsilon_p'(T)$ based on heating temperature and level of confinement for the plate. During heat straightening, the heating temperature is usually known; however, the exact level of confinement is unknown. To develop the analytical model, Roeder (1985, 1986) assumed that the restraining forces provide perfect single axis confinement with the strain designated as $\varepsilon_p(T)$. With this, $\varepsilon_p'=\varepsilon_p$.

Writing $\varepsilon_p(T)$ in terms of the total unconfined thermal strain, $\varepsilon_t(T)$, and the elastic strain, $\varepsilon_e(T)$:

$$\varepsilon_p(T) = \varepsilon_t(T) - \varepsilon_e(T) \tag{29}$$

where:

$$\varepsilon_t(T) = \int \alpha(T)dT \tag{30}$$

$$\varepsilon_t(T) = \frac{F_y(T)}{E(T)} \tag{31}$$

$F_y(T)$ is the yield stress at temperature T, $E(T)$ is the modulus of elasticity at temperature T, and $\alpha(T)$ is the coefficient of thermal expansion at temperature T.

To obtain values for ε_t and ε_e, equations are needed for F_y, E, and α as a function of temperature. Roeder (1985, 1986) used the equations shown in figures 11 and 12 to approximate $\alpha(T)$, $F_y(T)$, and $E(T)$, where T is in degrees Fahrenheit and E is in ksi. Substituting $\alpha(T)$ from figure 11 into equation 30, assuming the ambient temperature of the steel is 70°F and carrying out the integration:

$$\varepsilon_t = (0.001T^2 + 6.1T - 415)10^{-6} \tag{32}$$

By substituting $F_y(T)$ and $E(T)$ from figure 12 into equation 31, the unconfined elastic strain for T greater than 800°F was calculated as:

$$\varepsilon_e = \frac{F_y(-720,000+4,200T-2.75T^2)}{29,000(500,000+1,333T-1.111T^2)} \tag{33}$$

Substituting equations 32 and 33 into equation 29 and assuming T equals 1,200°F and F_y equals 45 ksi (for the steel plates tested by Roeder (1985, 1986)), ε_p is calculated as 0.00735. For the case of perfect confinement, where the actual strain, ε_p' equals ε_p, plastic rotation can be calculated from the following equation:

$$\varphi_b = 0.015\sin\frac{\theta}{3} \tag{34}$$

To evaluate the model developed by Roeder (1985, 1986), Avent et al. (2000) compared the equation for plastic rotation, equation 34 to the experimental data from Avent (1987) and Avent et al. (1992). This comparison is shown in figure 67. The plot includes the experimental data for both damaged and initially straight plates with jacking ratios of zero and 50 percent. A linear least squares curve fit is shown for the 0 percent and 50 percent jacking ratios.
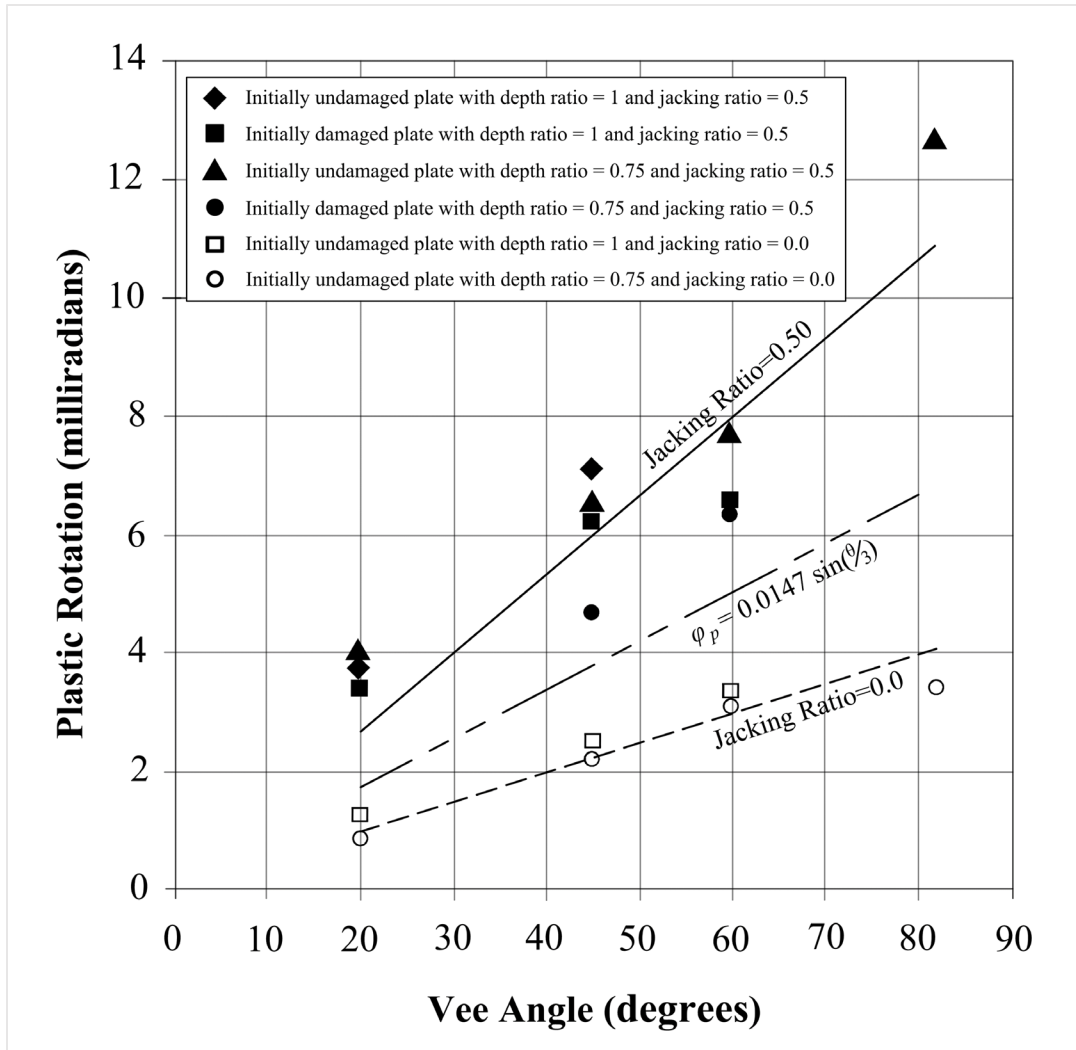
Source: Avent and Mukai (1998)

Figure 67. Graph. Plastic rotation versus vee angle for vee-heated plates having a heating temperature of 1,200°F.

Avent et al. (2000) noted that the theoretical equation for the perfect confinement case, equation 34, is nearly linear and falls between the experimental data for the zero percent and 50 percent jacking ratio (for external restraint). Assuming plastic rotation varies linearly with the jacking ratio, the theoretical perfect confinement case corresponds to an external jacking ratio of 20 percent, and the case of zero jacking force corresponds to 60 percent of the perfect confinement case (based on the data shown in figure 67). Incorporating the additional contribution of internal restraint and the reduction in yield stress at 1,200°F, as shown in figure 12, the uniaxial perfect confinement case corresponds to a total jacking ratio of 36 percent. Thus, the theoretical equation for perfect confinement is consistent with the experimental data.

Using the findings above, Avent et al. (2000) developed a theoretical model to predict plastic rotation for various levels of jacking force and heating temperature. This model is based on the equation developed by Roeder (1985, 1986), but corrects for the observations made based on the

data presented in figure 67. The model also uses a jacking load factor, F_ℓ, and a temperature factor, $F_t(T)$. These factors are developed below using four additional assumptions proposed by Avent et al. (2000): (1) confinement during heating is not perfect single axis confinement in the longitudinal direction (i.e., some longitudinal movement during heating is assumed, which is an important distinction from assumptions made by previous researchers (Holt, 1965) discussed in section 3.1.1); (2) plastic rotation varies linearly with jacking ratio, (3) perfect confinement corresponds with a jacking ratio of 20 percent, and (4) a jacking ratio of zero is equivalent to 60 percent of the perfect confinement case.

Using the above assumptions and the data shown in figure 67 above, the jacking load factor, F_ℓ, can be expressed as:

$$F_\ell = 0.6 + 2\frac{M_j}{M_p} \tag{35}$$

and the plastic rotation is:

$$\varphi_p = 2F_\ell\varepsilon_p(T)\sin\frac{\theta}{3} \tag{36}$$

Equation 36 can be used to predict plastic rotation for heating temperatures between 750°F and 1,150°F. While Avent et al. (2000) found little discrepancy between the plastic rotations predicted by equation 36 and experimental values at higher temperatures, at lower temperatures, the plastic rotations calculated with equation 36 were much larger than the experimental values. This discrepancy was attributed the computation of $\varepsilon_p(T)$ that uses the assumption that the entire vee has been instantaneously heated to a uniform temperature. The actual heating process is sequential and results in a non-uniform temperature distribution across the vee. To account for this temperature variation in the equation for plastic rotation, Avent et al. (2000) added an additional modification factor, assuming a linear variation in $\varepsilon_p(T)$ from 800°F to 1,200°F with ε_p at $T = 800$°F reduced by 50 percent. The resulting equation for the temperature factor, $F_t(T)$, is:

$$F_t = [0.5 + 0.00125(T - 800)] \tag{37}$$

where T is the heating temperature in degrees Fahrenheit. The modified equation for plastic rotation is then:

$$\varphi_p = 2F_tF_\ell\varepsilon_p(T)\sin\frac{\theta}{3} \tag{38}$$

Comparing equation 38 with experimental data, Avent et al. (2000) found that the theoretical equation for plastic rotation correlates reasonably well over the temperature range of 750 to 1,200°F. However, the equation is not applicable for temperatures above 1,200°F because the equation for F_y as a function of temperature, from which equation 38 is derived, is not valid beyond that point.

For carbon steel with a yield strength ranging from 33-50 ksi and a 1,200°F heating temperature, ε_p varies by only 3 percent. Therefore, ε_p is approximately equal to 0.00735. For this case $F_t(T)$ equals 1.0 and the equation for plastic rotation of a plate element can be simplified to:

$$\varphi_p = F_\ell\varphi \tag{39}$$

where φ is the plastic rotation factor, defined as:

$$\varphi = 0.015\sin\frac{\theta}{3} \tag{40}$$

and F_ℓ is defined by equation 35.

Equations 39 and 40 compare well to the experimental data and capture the effect of both heating temperature and magnitude of jacking force on plastic rotation (Avent et al., 2000).

Because the plate is the basic element of any rolled or built-up shape, understanding its response to heat straightening and curving is fundamental to understanding the behavior of more complex sections. As such, this basic analytical model for the behavior of plates has been used to develop similar analytical models for rolled shapes, axially loaded members, and composite girders. The development of these models based on the plate equations is discussed in detail in chapter 3 of this manual.

3.1.4. Important Considerations

- During heating, plastic strain occurs primarily within the vee-heated region.
- Due to the difficulty in controlling the many variables associated with heat straightening and heat curving, the magnitude of movements for individual heats may vary.
- Plastic rotation is defined as the change in angle of tangents located on either side of the damaged zone of a plate after the completion of a vee heat as shown in figure 53.
- Based on research by Roeder (1985, 1986), Avent (1987), Avent et al. (1992), and Avent et al. (2000):
  - o Variation in vee depth between 75 and 100 percent of the plate depth has little influence on the plastic rotation.
  - o Plate width and thickness do not significantly influence plastic rotation (provided heat is applied to generate a consistent temperature within the vee).
  - o Plastic rotations are proportional to the heating temperature used.
  - o Plastic rotations are proportional to the angle of the vee heat.
  - o Plastic rotations are proportional to the magnitude of external restraining force. External restraining forces, however, should be limited as discussed in section 2.2.3.
  - o Axial forces can be used as external restraining forces but are less efficient than flexural restraining forces with similar jacking (or stress) ratios.
  - o For damaged plates, plastic rotations during the initial heating cycles are often larger than subsequent heats. This is discussed further in section 3.2.
  - o A simple analytical formula for predicting the plastic rotation in a vee-heated plate was developed as a function of vee angle, heating temperature of the steel, and restraining force.

3.2. HEAT STRAIGHTENING ROLLED SHAPES

3.2.1. Introduction

The process of heat straightening damaged rolled shapes is based on a logical extension of straightening the plates. Rolled shapes can be viewed as an assemblage of flat plate elements. When damaged, some elements are bent about their strong axis, some about their weak axis, and some about both axes. The overall effect on the member results in damage in one or more of the fundamental damage categories described in section 2.2.1.

To develop a methodology for heat straightening complex damage on rolled shapes, it is important to understand the behavior of such shapes when subjected to a single fundamental type of damage. Focusing on category S and category W damage, a distinction can be made between a cross section's primary elements and stiffening elements. The primary elements are defined as plate elements subjected to bending about their local strong axes. The stiffening elements are defined as elements perpendicular to the primary elements and bent about their own local weak axes. Torsional distortions (category T) and local distortions (category L) are addressed in sections 3.3 and 3.5, respectively.

The channel shown in figure 68 has been plastically deformed about its major axis, resulting in category S damage. The web of this channel, a plate element bent about its major axis, is therefore a primary element. The two flanges, bent about their minor axes, are stiffening elements.

(A)   ISOMETRIC VIEW

(B)   ELEVATION
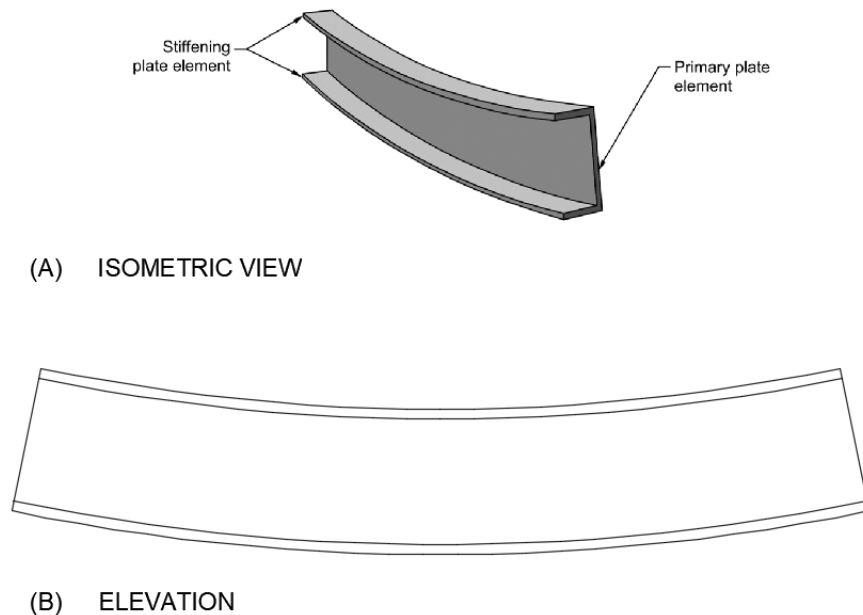
Source: FHWA

Figure 68. Illustration. Primary and stiffening plate elements for a channel bent about its major axis (category S damage).

For rolled shapes with flexural damage, the pattern of yielding usually differs for the primary and stiffening plate elements. The primary plate elements usually develop plastic hinges, a state of stress in which the entire cross section has reached yield (F_y); tensile yield in one region and compressive yield in the other as shown in figure 69-A.

(A) Web element

(B) Bottom Flange element
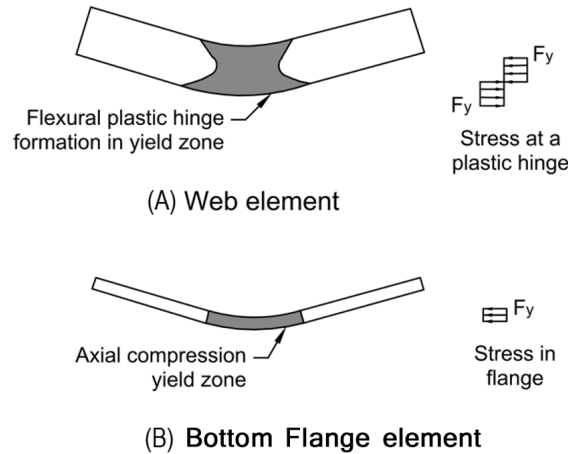
Source: FHWA

Figure 69. Illustration. Typical yield zone patterns in the plate elements of the channel shown in figure 68.

The stiffening elements of a damaged rolled shape may exhibit one of several conditions. In the first condition, yielding does not occur because the stiffening element is located near the neutral axis of the cross section. An example of this is when a wide flange beam is bent about its minor axis. In this case, the web may not reach yield because it is located at or near the neutral axis of the section. In the second condition, the stiffening element is located near the extreme fibers of the section and exhibits flexural yielding (such as the flanges of the channel in figure 68). In this situation, the flanges yield because of axial stress (either tension or compression) as illustrated in figure 69-B. In the third condition, the stiffening element is yielded in weak axis bending through which a region of yield is formed as shown in figure 70. The stress distribution is similar to that shown in figure 69-A. However, the result of the weak axis bending is a narrow strip of flexural yielding often referred to as a yield line.

Top view

Edge view
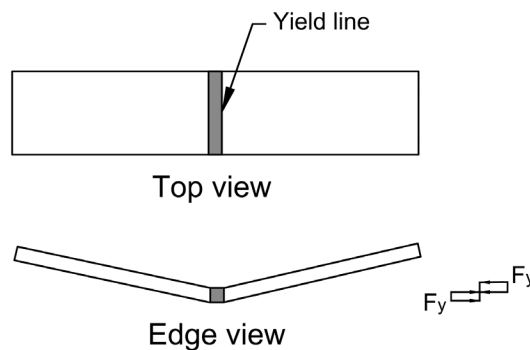
Source: FHWA

Figure 70. Illustration. Weak axis bending resulting in a yield line in a plate element.

122

The heating pattern for repair should be tailored to fit each scenario of the various patterns of inelastic deformation that occur in damaged rolled or built-up shapes. While vee heats are generally used on primary elements of a section bent about their major axes, the stiffening elements may need strip heats, line heat, or no heat at all. Multiple heating patterns introduce additional variability, so the time to complete a heat for a rolled shape may be considerably longer than that for a simple plate. Considerable cooling may occur at the initial heating locations before the heating pattern is completed at the last element, hindering the expected movement because of increased internal restraints. To prevent this, it is good practice to use more than one torch for complex patterns to minimize the overall heating time.

Several parameters can affect a member's behavior during heat straightening, including the jacking force. The effect of the jacking force on movement during heat straightening can be captured via the jacking load factor, equation 35, discussed in section 3.1. Further, various combinations of plate elements found in structural steel shapes introduce additional parameters that affect a member's behavior during heat straightening. The first is a shape factor and the second is a stress factor.

When jacking forces are applied prior to heat straightening, the distribution of stress over the heated section from jacking varies according to the shape of the cross section and the restraint conditions. As the torch moves over the section, the steel temperature rises and falls in a manner somewhat analogous to a wave moving across water. This heat variation produces continuous and complex changes in the combined stress distribution. Consequently, stress distributions may be quite different between two members of different configurations.

One measure of this effect is the ratio of plastic moment, M_p, to the moment at initial yield, M_y. For a constant yield stress, this ratio is Z/S, where Z is the plastic section modulus and S is the elastic section modulus. Because the moment due to jacking is usually expressed as a percentage of M_p, the degree of yielding during heating is often a function of this ratio. For example, $Z/S =$ 1.5 for a rectangular plate and is only about 1.12 for typical wide-flange beams. In other words, yielding is initiated at two-thirds of ultimate capacity for a plate but does not occur until 90 percent of capacity for most wide-flange members. For jacking moments in the range of 35 to 50 percent of M_p, some localized yielding may occur during heat straightening. The amount, and consequently the degree of straightening, depends on the stress factor as a function of Z/S.

This section examines the behavior of various common structural shapes subjected to heat straightening using experimental data and analytical methods originally presented by Avent and Mukai (1998). The basic model for predicting movement of rolled structural shapes during heat straightening is a modification of the plate equation, equation 39 discussed in section 3.1. For mild steel, the equation for plastic rotation of a structural shape can be expressed as:

$$\varphi_p = F_\ell F_s F_a \varphi_b \tag{41}$$

where F_ℓ is the factor associated with the external jacking force, F_s is a factor reflecting the shape of the cross section, and F_a is the stress factor. These factors are derived for various structural shapes in the following sections. The basic plastic rotation factor, φ_b, derived for a rectangular plate (section 3.1), is expressed as:

$$\varphi_b = 0.015\sin\frac{\theta}{3} \tag{42}$$

The following sections discuss experimental data obtained by Avent et al. (1992) on the heat straightening of various structural shapes and derive the formulas used to calculate the factors used in equation 41, adapted for use with various structural shapes from these experiments.

3.2.2. Behavior of Channels with Strong Axis Damage (Category S)

When a channel exhibits category S damage, a flexural plastic hinge forms in the web, and axial yield zones form in the flanges (see figure 69). To repair this type of damage, the heating pattern uses a vee heat on the web followed by a strip heat on the flange that was subjected to tension (flange 1) during the damage phase (figure 70). During the heat straightening process, the vee heat is used to reduce the damage curvature. This is accomplished as the vee begins to close during the cooling process (as a result of upsetting, discussed in chapter 1 and chapter 2). If unheated, flange 1 resists this closure, an example of internal restraint resisting straightening. By continuing the vee heat into the flange as a strip heat, the upsetting process that closes the vee will include the flange. This eliminates the restraint caused by the unheated flange and expedites the straightening process. As such, the heating sequence is: (1) web vee heat, and (2) flange 1 strip heat. Flange 2 is not heated.
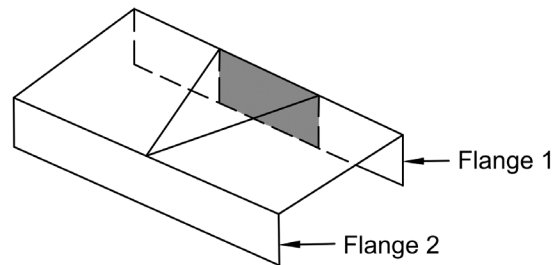
Note: Vee heats not shaded for clarity.
Source: FHWA

Figure 71. Illustration. Heating patterns for channels bent about their strong axis.

One note of caution to consider regarding this and other heating patterns for structural shapes is that the strip heat on the flange may produce minor curvature about the undamaged axis. Typically, this movement is small and can be corrected with a few heats directed toward removing this curvature.

Experiments to capture the behavior of channels during heat-straightening repair of category S damage were conducted by Avent et al. (1992). These experiments involved performing a series of heats on a C6×8.2 channel using the vee and strip pattern (shown in figure 71) to study the plastic rotation achieved as a function of jacking ratio and vee angle. Three heats each were conducted using jacking ratios of 0, 25, and 50 percent, and vee angles of 20 and 45 degrees. Figure 72 shows the average values of plastic rotations. The results from these experiments on channels follow the same trend observed during similar experiments using plates (discussed in section 3.1): the curvature caused by heat straightening is proportional to vee angle and jacking ratio.
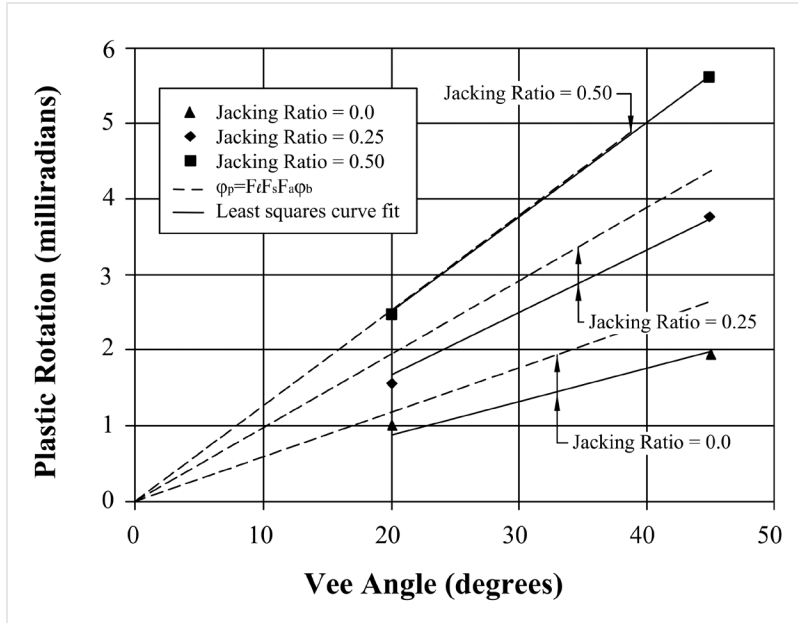
Figure 72. Graph. Experimental and theoretical plastic rotations for a C6×8.2 channel with category S damage.

Using the plate equations discussed in section 3.1 (equation 39), Avent and Mukai (1998) computed the plastic rotation for the web of the channels considered by Avent et al. (1992). The results were significantly lower than the actual channel plastic rotations. Avent and Mukai concluded that the shape of the channel magnifies the movement over that expected from an equivalent sized plate.

An explanation for this behavior by studying the geometry of the section was developed by Avent and Mukai (1998). The channel can be thought of as a folded plate as shown in figure 73. First, consider the section in its unfolded position with the vee plus strip heat applied, beginning with the vee and continuing across the strip. If the vee was extended across the web portion of the unfolded section, the result would be a standard vee heat having a vee depth equal to the channel web depth, d, plus the flange width, b_s. By using a strip heat on the flange portion, the effect is similar, except that the heating pattern is somewhat narrower over the flange. Because most of the plastic deformation occurs over the middle two-thirds of a vee (Roeder, 1985 and 1986), the difference between a vee and strip on the flange portion is small and can be neglected. Assuming the longitudinal strain is small and varies linearly with distance from the vee apex, (figure 73) the relationship between x_1 and x_2 (figure 73) is:

$$x_2 = \left(\frac{d + {}^1/_2 b_s}{d}\right) x_1 \tag{43}$$
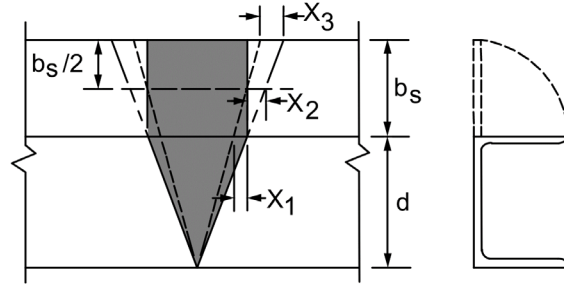
Source: FHWA

Figure 73. Illustration. Unfolded flange for a channel with category S damage.

Applying the same heating pattern to the section in the folded position, Avent and Mukai (1998) proposed that the average longitudinal movement of the folded flange, x_2, will tend toward the same value as in its unfolded position. However, in its folded position, its distance from the apex has been decreased from $d + b_s/2$ to d. If the same movement, x_2, occurs at a shorter distance from the vee apex, the change in curvature is magnified. From equation 43 and the discussion above, Avent and Mukai (1998) developed the magnification factor (or shape factor) as:

$$F_s = \frac{d+ \frac{1}{2}b_s}{d} = 1 + \frac{b_s}{2d} \tag{44}$$

Note, this analysis assumes a full depth vee heat. Because little difference has been noted between a full and three-quarter depth vee, as discussed in section 3.1, the equation is valid in this range.

The stress factor, F_a, was computed by Avent and Mukai (1998) by normalizing the Z/S ratio for the channel bent about the major axis to that of a plate ($Z/S = 1.5$) since the plate equation is used as the basis for developing equations for rolled shapes. The stress factor, they state, should be unity for the zero jacking force case and is assumed to vary linearly to its maximum at the 50 percent jacking ratio case. From this, the stress factor can be written as:

$$F_a = 1 - 2[1 - \left(\frac{2}{3}\right)\left(\frac{Z}{S}\right)]\frac{M_j}{M_p} \tag{45}$$

where Z/S is the ratio of plastic to elastic section modulus for bending about the major axis, i.e., Z_x/S_x in this case. Because channels typically have a Z_x/S_x ratio of about 1.2, the stress factor for channels can be approximated as:

$$F_a = 1 - 0.4\frac{M_j}{M_p} \tag{46}$$

The jacking load factor is identical to that developed for plates in section 3.1, that is:

$$F_\ell = 0.6 + 2\frac{M_j}{M_p} \tag{47}$$

Using these factors (shape, stress, and jacking load factor), the expected plastic rotation of the section can be obtained from equations 41 and 42.

Figure 72 compares the experimental and theoretical (equation 41) results for the C6×8.2. The figure indicates reasonably good agreement between the experimental (Avent et al., 1992) and

126

theoretical (Avent and Mukai, 1998) values. This exercise indicates that the plastic rotation equation for plates can be used as the basis for other rolled shape behavior.

3.2.3. Behavior of Channels with Weak Axis Damage (Category W)

A channel with category W damage is more complex than one with category S damage because of the lack of symmetry about the weak axis of the section. In addition, the heating pattern used for repair will differ depending on whether the compression zone induced by damage is in the web and flange juncture or flange tips. The heat straightening process is based on the open end of the vee heat lying in the zone stressed in tension during the damage phase. Thus, the apex of the vee heat on the flanges may lie at either the flange tips or the web and flange juncture, depending on the direction of bending moment damage. Figure 74 shows the heating patterns for both cases. A combination of vee heats on the flanges and a strip heat on the web is used for the case shown in figure 74-A, referred to here as negative moment damage, and only vee heats on the flanges are used for the case shown in figure 74-B, referred to as positive moment damage.

(A) Negative moment damage

(B) Positive moment damage
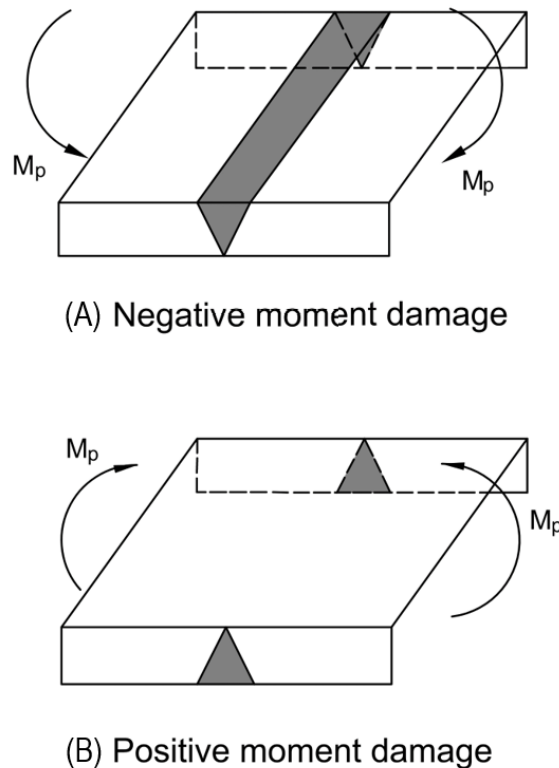
Source: FHWA

Figure 74. Illustration. Heating patterns for channels bent about the weak axis (direction of moment producing damage indicated by M$_p$).

A comprehensive series of tests, conducted by Avent et al. (1992), on C6×8.2 channels that were initially straight, using the heat configurations shown in figure 74-A. To capture the behavior of the section during heating, the plastic rotation of the section was measured after each heat cycle. The results of this testing are plotted in figure 75 along with a linear least squares curve fit. Avent et al. (1992) note that the response of these channels generally corresponded to the typical

127

pattern of behavior observed for heat-straightened plates discussed in section 3.1, although the variations were not as linear. The average values for plastic rotations were higher than expected for 20-degree vee heats and lower than expected for 45-degree vees.
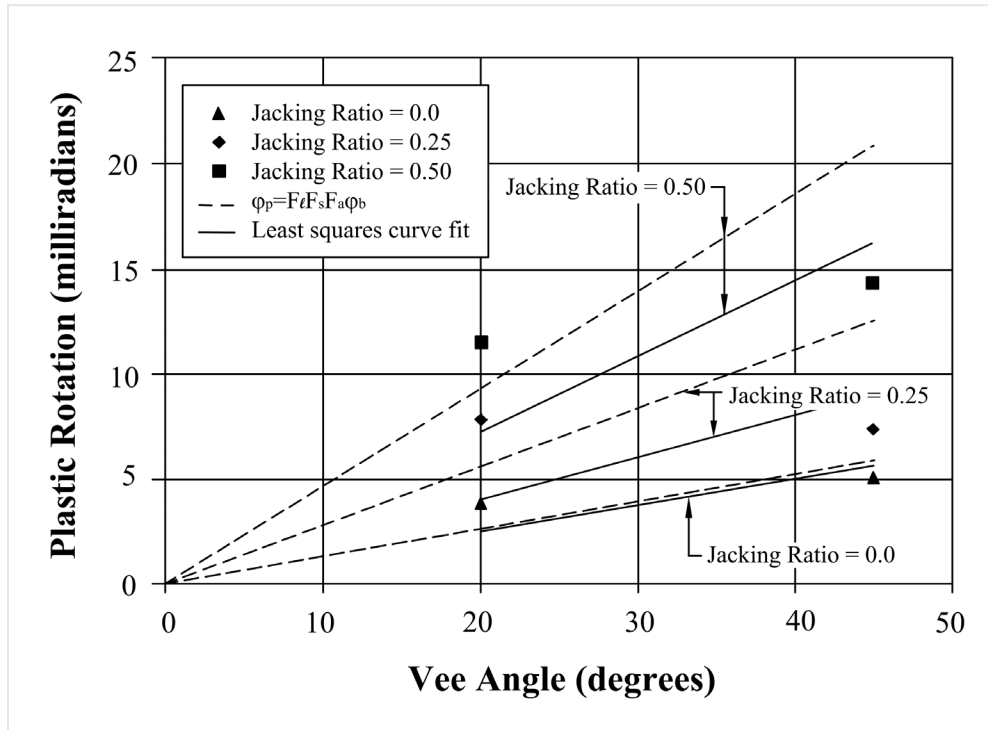
Source: Avent and Mukai (1998)

Figure 75. Graph. Experimental and theoretical plastic rotations for a C6×8.2 channel with category W damage (with the open end of vees at flange-web-juncture).

The behavior observed by Avent et al. (1992) illustrates that even under controlled conditions, consistency in heating is difficult to maintain. Additionally, the amount of plastic rotation observed for a single heat significantly exceeded the expected rotation of a plate with the same dimensions as the flange of the channel. The researchers found that applying the plate equation to the vee-heated flanges of the channel (and neglecting the web) yielded a predicted plastic rotation much smaller than observed in the channel. In fact, the observed plastic rotations of the channel averaged 2.5 times more than an equivalent sized plate.

In addition to conducting testing using the heating pattern shown in figure 74-A, a C6×8.2 was heated with the heating pattern shown in figure 74-B (Avent et al., 1992). Using a jacking ratio (M_j/M_p) of 50 percent and a 45-degree full depth vee, 14 heats produced an average plastic rotation per heating cycle of 5.78 milliradians. For comparison, Avent et al. (1992) calculated the expected rotation using the plate equation for the flange (neglecting the web) and found the equation predicts the nearly identical value of 6.09 milliradians. Thus, no magnification over the plate equation value was needed for the case shown in figure 74-B (Avent et al., 1992).

Avent and Mukai (1998) suggest that the explanation for the seemingly contradictory results from Avent et al. (1992) relate to geometric and stress considerations, with the geometry of the channel section as the most significant aspect. For the case of the vee and strip heat combination shown in figure 74-A, the channel section (figure 76-A) can be viewed in terms of its symmetrical component shown in figure 76-B. This component of the channel section can be considered as a folded plate similar to that used in the discussion of the category S channel. To start, the researchers considered the section in its unfolded position with the heat applied in the standard fashion (i.e., beginning at the apex of the vee, moving across the vee, and then continuing across the strip). If the vee is extended across the web portion of the unfolded section, the result would be a standard vee heat on the flange of depth d plus one-half the web, $d_s/2$. By using the strip heat on the web portion, the effect is similar except the heating pattern is somewhat narrower.
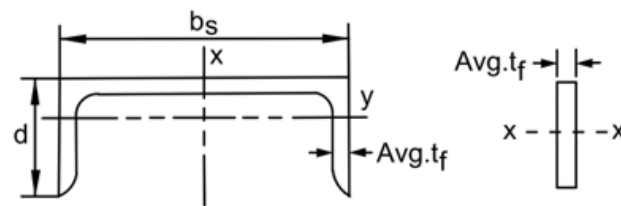
(A) Channel cross section and equivalent plate cross section
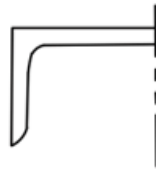
(B) Heating pattern and geometry is symmetrical about the x-x axis
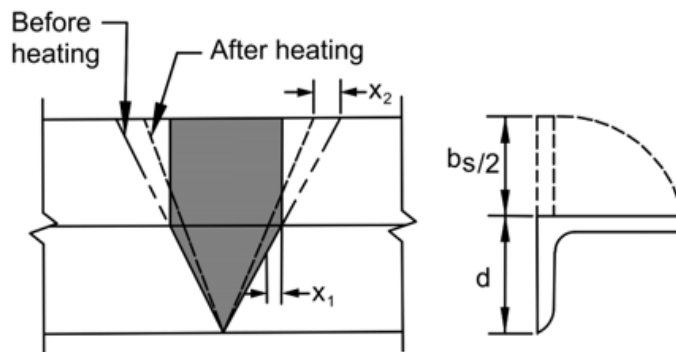
(C) View of heating pattern considering the channel to be unfolded

Source: FHWA

Figure 76. Illustration. Geometric effects on heat straightening a channel with negative curvature damage (as shown in figure 74-A).

129

Referring to figure 76-C, the maximum longitudinal shortening of the web portion of the section occurs at the axis of symmetry of the web, designated by x_2. Because of the linear strain assumption (similar to category S damaged channels), x_1 and x_2 are proportional to the distance from the vee apex such that:

$$x_2 = (d + \frac{b_s}{2}) \frac{x_1}{d} \tag{48}$$

where d is the vee depth (which equals the flange width) and b_s is the width of the stiffening element (web width).

Avent and Mukai (1998) then considered the same heating pattern applied to the section in its folded position. They expected longitudinal movement, x_2, of the folded section to be the same as the unfolded. However, because the channel is folded, this average movement, x_2, acts over the distance d rather than $d + b_s/2$. Hence, the plastic rotation tends to be magnified by the factor F_s, as shown in equation 44.

With that, for the C6×82 channel, $d = 1.92$ inches, $b_s = 6$ inches, and $F_s = 2.56$. Thus, magnification would more than double in comparison to an equivalent plate with the same dimensions as the flange of the channel. From this analysis, Avent and Mukai (1998) conclude that the vee and strip heat combination does indeed magnify the movement for the heating pattern shown in figure 74-A.

Meanwhile, for the case of the vee heat in the opposite direction with no strip heat used, figure 74-B, Avent and Mukai (1998) note that no magnification would be expected since the web is not heated. This conclusion is further reinforced by the experimental results from Avent et al. (1992), which showed no magnification of plastic rotation.

With the above observations in mind, the stress factor, F_a, can be considered in the form previously given by equation 45 where the ratio Z/S is related to weak axis bending, i.e., Z_y/S_y. For typical cases (channels) Z_y/S_y is approximately 2.05 ($Z_y/S_y = 2.02$ for the C6×8.2). Therefore, using $Z_y/S_y = 2.05$ the stress factor can be approximated (for channels with weak axis damage) as:

$$F_a = 1 - 0.7 \frac{M_j}{M_p} \tag{49}$$

The shape factor, F_s, of equation 44 can be written as:

$$F_s = 1 + \frac{b_s d}{2d^2} \tag{50}$$

where d is the vee depth and b_s is the width of the channel web or stiffening element.

The equation can be modified to include both positive and negative moment damage. The term d in the numerator of the second term is replaced by d_s, which is defined as the distance from the apex of the vee to the stiffening element (the web in this case), thus:

$$F_s = 1 + \frac{1}{2} \frac{b_s d_s}{d^2} \tag{51}$$

Consequently, $d_s = d$ for the case in figure 74-A and $d_s = 0$ for the case in figure 74-B. Note that since little difference was noted in plastic rotations for full- and three-quarter-depth vees, d should be taken as unity unless the vee depth ratio is less than 0.75 (Avent and Mukai, 1998). Research data are not available for shallower vee depths.

Applying these factors, the plastic rotation for a channel with flexural damage about the weak axis is given by equations 41 and 42 where F_s is defined by equation 51, F_ℓ by equation 47, and F_a by equation 45 (although F_a can be approximated by equation 49 for most cases). The theoretical equation for plastic rotation (equation 41) is shown for the negative moment damage case in figure 75 for the three jacking ratios. The theoretical results tended to be larger than the least squares curve fit of the experimental data.

3.2.4. Behavior of Wide Flange Beams with Weak Axis Damage (Category W)

For a wide flange beam subjected to weak axis bending, the flanges are the primary elements, bent about their strong axes, and the web is the stiffening element, bent about its weak axis. The heating pattern used to repair this type of damage consists of vee heats on each flange and a strip heat on the web as shown in figure 77. In this case, the stiffening element is located at the neutral axis of bending and introduces additional complexity in behavior. The yield pattern consists of a flexural plastic hinge on the two flanges. Because the web lies at the neutral axis of bending, it does not typically yield. However, a strip heat is used on the web so that the closing of the flange vees is not resisted by the web. This case is one example of when it is appropriate to heat a location where yielding may not have occurred. Care should be taken when performing web heats on sections with slender webs to limit the out of plane distortions of the web that can occur.
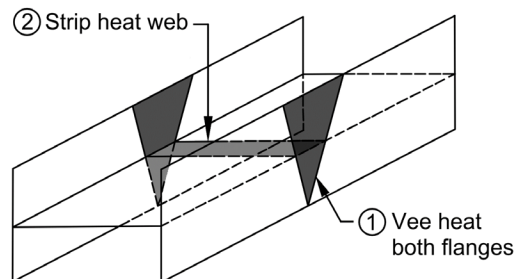
Source: FHWA

Figure 77. Illustration. Heating patterns for weak axis damage to a wide flange beam (category W).

Tests were conducted by Horton (1973) on undamaged wide flange sections subjected to the heating pattern discussed above. The goal of the testing was to capture the behavior of the section during heating. The results of these tests are shown in figure 78. Similar tests were conducted by Avent et al. (1992) on W6×9 beams to capture the relationship between plastic rotation of the section as a function of jacking ratio and vee angle. In some cases, the beams in those tests were undamaged prior to vee heating while others were damaged. The average plastic rotations observed during those experiments are shown in figure 79. The data from Horton's (1973) tests generally followed the pattern of increasing plastic rotation with larger vee angle. The tests by Avent et al.'s (1992) showed the plastic rotation to be proportional to both vee angle

and jacking ratio. The data were linear with respect to vee angle for zero and 25 percent jacking ratios. However, considerable variation was found for the 50 percent jacking ratio.
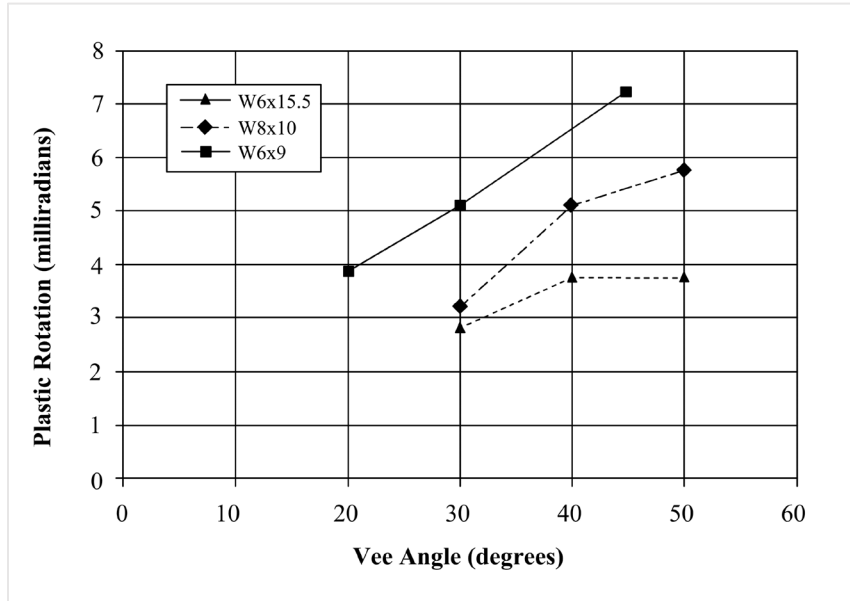
Source: Horton (1973)

Figure 78. Graph. Vee angle versus plastic rotation for the repair of wide flange beams with category W damage.
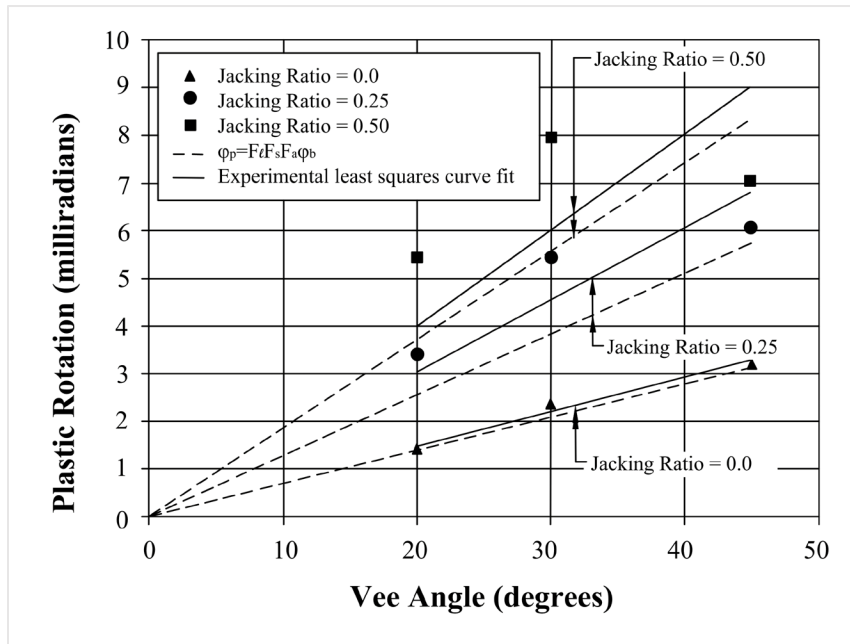
Source: Avent and Mukai (1998)

Figure 79. Graph. Plastic rotation versus vee angle for W6×9 beams with category W damage.

The same theoretical model (equation) used for category W damaged channels is applicable for category W damaged wide flange beams. The plastic rotation is given by equations 41 and 42 where F_ℓ is defined by equation 47, F_s is given by equation 51, and F_a by equation 45. The Z_y/S_y value for typical wide flange beams is around 1.5. Using this value, the stress factor can be approximated by $F_a = 1$. Also note that, in this case, the stiffening element is located at mid-depth, thus d_s equals one-half the flange width ($d_s = 1.97$ inch for the W6×9). This theoretical equation is also plotted in figure 79 and agrees well with the experimental least squares curve fit (Avent and Mukai, 1998).

3.2.5. Repetitive Damage and Straightening for Category W Wide Flange Beams

A comprehensive study, conducted by Avent et al. (1992), on rolled beam sections subjected to multiple cycles of damage and repair. The general procedure used in the study was to damage the beam by bending about the minor axis and then heat straighten the section. After straightening was completed, the beam was re-damaged and again heat straightened. Four beams (W6×9) were used in the study. Each beam was damaged around its weak axis to a degree of about 7 degrees. All beams were repaired using the heating pattern shown in figure 77 and 45-degree vees with a depth ratio of 0.75 and a jacking ratio of 0.5 (50 percent). The number of damage and repair cycles varied for each of the beams. In some cases, up to eight cycles of damage and repair were considered. Each repair cycle consisted of approximately 20 heats, with the average plastic rotation shown for each repair cycle in table 15.

Table 15. Summary of damaged beam repair data for W6×9 beams with category W damage (Avent et al., 1992).

Beam/Repair Cycle No.	Angle of Damage		No. of Heats	Avg. φ_p (millirad)	Coefficient of Variation
	(degree)	(millirad)			
B-1/1	7.34	128.1	20	6.85	0.28
B-2/1	7.67	133.9	20	6.65	0.30
B-2/2	8.22	143.5	23	6.70	0.26
B-3/1	7.15	124.8	18	6.64	0.16
B-3/2	7.21	125.8	22	5.93	0.26
B-3/3	7.14	124.7	19	6.19	0.28
B-3/4	7.17	125.2	21	6.30	0.29
B-4/1	7.06	123.2	18	6.42	0.28
B-4/2	6.56	114.4	17	6.52	0.17
B-4/3	7.50	131.0	21	5.91	0.33
B-4/4	7.20	125.7	20	6.12	0.39
B-4/5	6.87	119.9	21	5.68	0.39
B-4/6	6.42	112.0	13[1]	8.13	—
B-4/7	7.16	125.0	16[1]	8.14	—
B-4/8	7.27	126.9	14[1]	9.47	—

[1] Some heats included two vees due to time constraints.
Note: (—) indicates data not collected or calculated.

For beams subjected to several cycles of damage and repair, a thickening developed in the midspan region of the section as a result of the heat straightening process. This thickening caused a spreading of the yield zone in each subsequent damage cycle, as shown in figure 80 (values shown in table 16). The thickening resulted in a smoother distribution of damage curvature due to thinner portions of the section further from the centerline of the beam yielding earlier than in previous damage cycles, although the total angle of damage was kept as consistent as possible for each damage cycle. Due to the larger yield zone, the vee heats were distributed over a greater length to accommodate the spread and complete the repair (Avent et al., 1992).
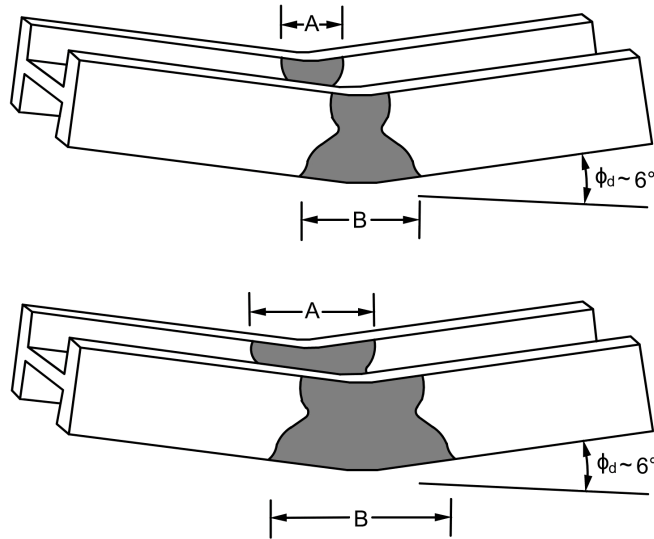
Source: FHWA

Figure 80. Illustration. Spreading of yield zone in subsequent cycles of damage and repair for W6×9 wide flange beam specimens.

Table 16. Increasing yield zone length after each damage and repair cycle for W6×9 with category W damage (Avent et al., 1992).

Beam	Length of yield zone (in) after Bend #: (Top row = A, bottom row = B)							
	1	2	3	4	5	6	7	8
1	—	—	—	—	—	—	—	—
	—	—	—	—	—	—	—	—
2	—	8.20	—	—	—	—	—	—
	—	8.40	—	—	—	—	—	—
3	5.90	8.05	9.75	10.30	—	—	—	—
	6.00	8.65	10.40	11.65	—	—	—	—
4	5.50	8.15	9.50	10.50	10.70	10.70	11.50	11.50
	5.80	8.40	10.20	12.00	13.20	13.30	15.25	15.25
Averages	5.70	8.13	9.63	10.40	10.70	10.70	11.50	11.50
	5.90	8.48	10.30	11.83	13.20	13.20	15.25	15.25

Note: (—) indicates data not collected or calculated.

Because over 200 heats were performed through Avent et al.'s (1992) work, statistical analysis was able to evaluate trends in the data. In prior work, DeBajar et al. (1992) posed two questions: (1) does the response to heat straightening vary if the member is re-damaged and repaired more than once; and (2) is the response during a single repair cycle dependent on the number of heat applications. To investigate these questions, Avent et al. (1992) used an independent sample t-test to evaluate the response from different damage and repair cycles. From this test, the probability was calculated of the average plastic rotation in successive repair cycles being less than the average value of the first repair. The probability was found to range from 71 to 87 percent. This suggested that there may be a small trend toward larger plastic rotations in the first repair cycle.

To look definitively at whether the amount of movement between heat applications within a single repair cycle and confirm the results of the independent sample t-test, Avent and Mukai (1998) used a dependent sample t-test to evaluate the same data. The probability values resulting from that test were high enough for the researchers to conclude that the first heat application does produce greater movement than successive heats. However, there was no trend indicating that another heat (besides the first) had preeminence over others. This conclusion confirmed observations in the field that the first heat produces more movement than successive heats.

The likely cause of this phenomenon is that residual stresses can be created during the damage process. These stresses can act in a direction tending to reduce the damage, thus magnifying the jacking force. The initial heat tends to relax these residual stresses, as such the movements from successive heats are not affected. As a result of this behavior, limiting the jacking force during the first two heats be limited to approximately 25 percent of the member capacity can avoid over-stressing the member.

The results of the dependent sample-t test and associated conclusions were corroborated by the plastic rotations measured by Avent et al. (1992). The average value of plastic rotation for all damage and repair cycles (240 heat cycles) was approximately 5 percent lower than that observed for the first damage and repair cycles only (75 heat cycles). These measured plastic rotation values were within 20 percent of the value predicted by the theoretical model (equation 41).

3.2.6. Behavior of Wide Flange Beams with Strong Axis Damage (Category S)

The heating pattern and yield zone for a wide flange beam with category S damage is shown in figure 81. To capture the behavior of such beams during heat straightening, several researchers (Avent et al., 1992; Moberg, 1979; Boudreaux, 1987) conducted tests on both damaged and undamaged wide flange sections. This work was originally summarized by Avent and Mukai (1998). The discussion, figures, and tables presented below are based on that work.
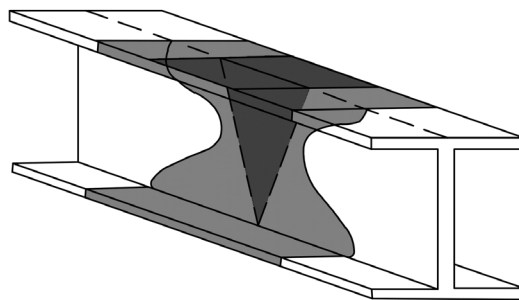
Source: FHWA

Figure 81. Illustration. Yield zone and heating pattern for category S damage to wide flange beams.

The average plastic rotation for each experimental case (section) considered is summarized in table 17. The results shown in the table follow the trend that plastic rotation is proportional to vee angle. However, results are inconsistent. It was suggested by Avent and Mukai (1998) that the W10×33 values are far too low and indicate the use of an improper heating procedure.

Similarly, the values for the shapes heated with a 50-degree vee angle also appear low, again suggesting that the steel temperature was not adequate. The values for the W6×9 with 20- and 30-degree vee angles appear too high, which Avent and Mukai (1998) suggest may have been a result of either excessive temperature or lack of lateral restraint. The only values that appear consistent with other categories of damage (for similar sections) are those with a jacking ratio of 50 percent.

Table 17. Plastic rotations measured during the repair of a wide flange beam with category S damage (Avent and Mukai, 1998).

Section Type	Number of heats	M_j/M_p (%)	Plastic Rotations				
			Vee Angle (degrees)				
			20	30	40	45	50
W6×15.5	2	22	—	2.75	2.93	—	2.71
W6×15.5	2	22	—	2.80	3.10	—	3.01
W8×10	2	22	—	2.14	2.88	—	3.01
W10×33	2	22	—	1.14	0.26	—	1.01
W6×9	4	0	1.74	4.19	—	5.35	—
W6×9	3	0	3.04	2.37	—	5.47	—
W6×9	4	25	2.58	—	—	7.31	—
W6×9	3	25	—	5.41	—	6.21	—
W6×9	3	50	4.23	7.97	—	7.36	—
W6×9	4	50	—	—	—	7.17	—
W6×9	15	50	—	—	—	7.57	—

Note: (—) indicates data not collected or calculated.

To evaluate these inconsistencies, better control the variables, and capture the behavior of a similar section during heat straightening, Avent and Mukai (1998) tested a W12×14 section using similar methodology. A vee heat was applied to the web, and the temperature and jacking force were carefully controlled. The results of this testing are shown in figure 82.
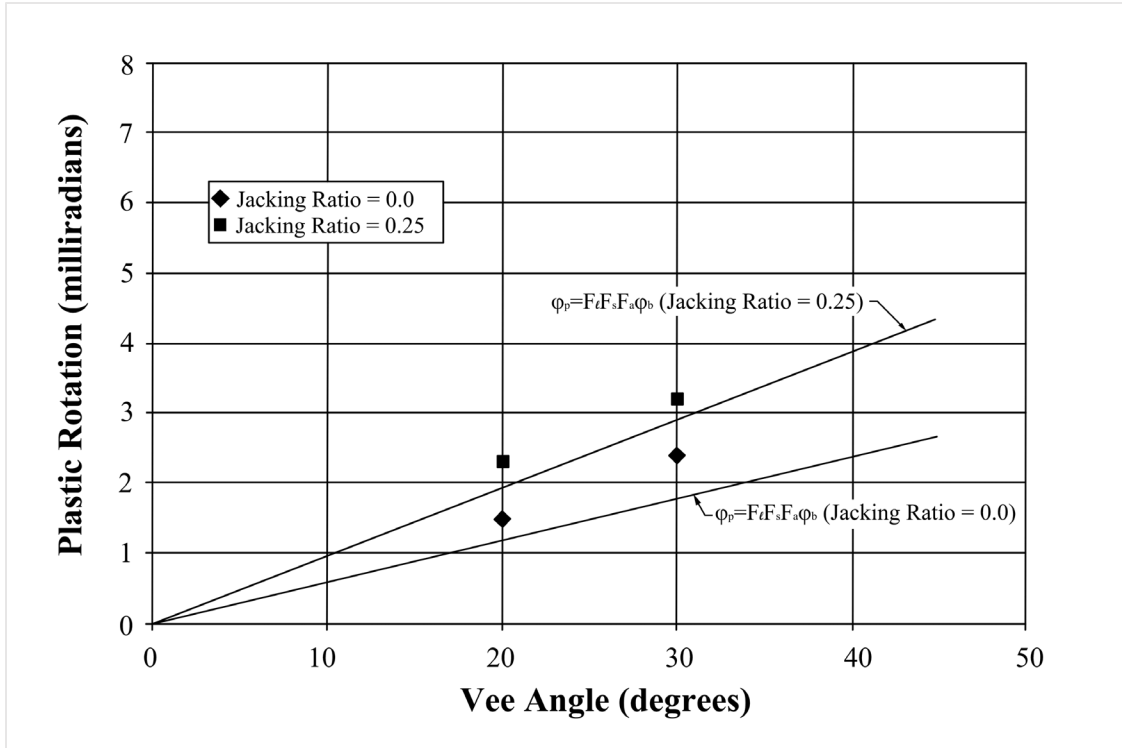
Source: Avent and Mukai (1998)

Figure 82. Graph. Influence of vee angle and jacking ratio on plastic rotation for W12×14 beam with category S damage.

A model to predict this observed behavior was then developed in a similar manner to that of the channel subjected to category S damage (Avent et al., 1992). For the category S damage (and subsequent repair), the web of the beam is the primary element, and the flanges are the stiffening elements. The flange at the open end of the vee provides a magnification effect similar to that of the channel. Using a folded/unfolded flange concept (figure 83) similar to that used for the channel, along with the same assumptions, a shape factor was derived. The shape factor derived for the wide flange beam with category S damage is identical to that of the channel (equation 44 or 51). However, for the wide flange beam, d_s is the beam depth, b_s is the flange width, and d is the beam depth.
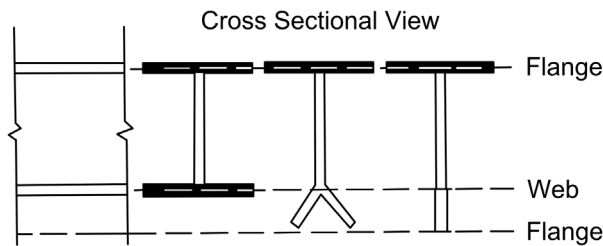
Source: FHWA

Figure 83. Illustration. Geometric relationship between a category S damaged wide flange section and plate.

138

The equation for plastic rotation, φ_p, is given by equations 41 and 42, F_ℓ is given by equation 47, F_s is given by equation 51, and F_a by equation 45. Note that Z_x/S_x is typically around 1.12 for wide flange beams. Using this value in equation 45, the stress factor can be approximated as:

$$F_a = 1 - 0.5 \frac{M_j}{M_p} \tag{52}$$

The theoretical model (equation 41) for the W12×14 is plotted in figure 82 along with Avent and Mukai's (1998) experimental data. As shown in the figure, the theoretical model agrees reasonably well with the experimental data.

3.2.7. Angles

Angles differ from other rolled shapes in that the plate elements of the cross section (legs of the angle) are not orthogonal to the principal axes. As a result, the damage to angles and applied jacking force during repair often induce flexure about a non-principal axis. However, the angle is the simplest of rolled shapes because it can be considered as a plate with a single fold. The heating pattern used for repair consists of a vee on one plate element and a strip on the other (figure 84-A), or simply a vee heat if the apex of the vee is located at the stiffening element (figure 84-B).
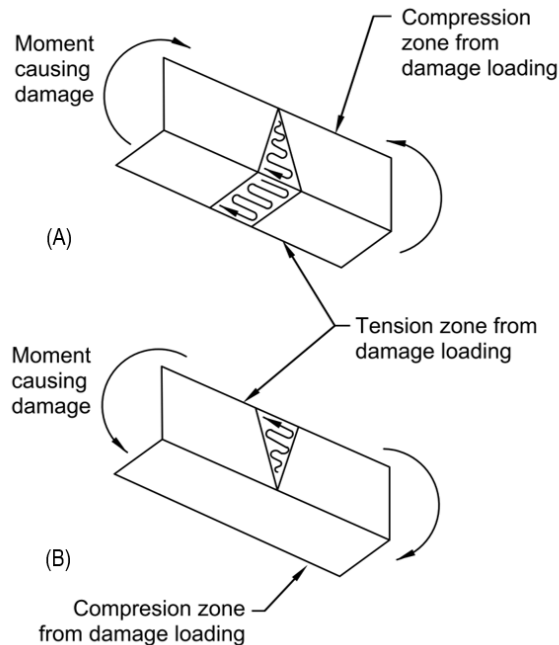
Source: FHWA

Figure 84. Illustration. Yield zone and heating patterns for flexural damage of a typical angle.

As they did for other rolled shapes, Avent et al. (1992) conducted a series of tests on originally straight angles to capture their behavior during heat straightening and develop a model to predict such behavior. To begin, the case using the heating pattern shown in figure 84-A was considered. Additional parameters including jacking ratios, M_j/M_p, of 0, 25 and 50 percent, vee angles of 20

and 45 degrees, a vee depth ratio = 1.0, and a heating temperature of 1,200°F were used. The results of this testing are shown in figure 85. In general, the plastic rotations observed for the angles were significantly larger than expected for a plate of equivalent size. Like the channel and wide flange sections previously discussed, the reasons for this behavior involve both geometric and stress considerations.
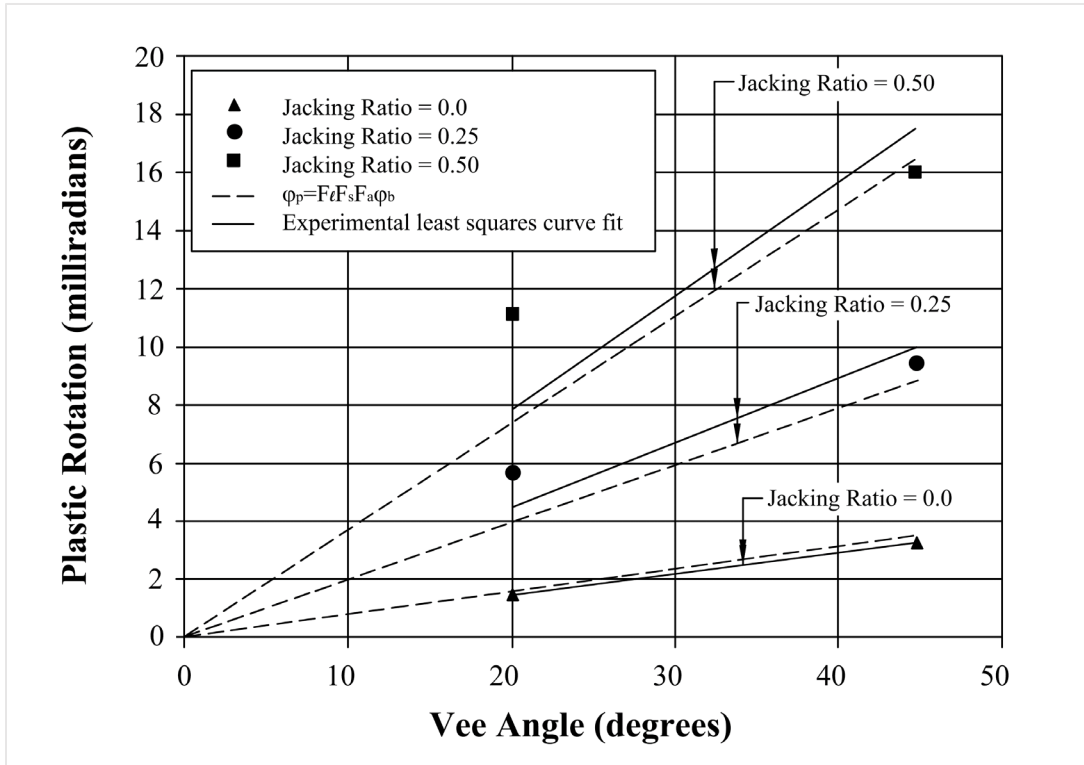
Source: Avent and Mukai (1998)

Figure 85. Graph. Influence of vee angle and jacking ratio on plastic rotation for L4×4×1/4 angles using the heating pattern shown in figure 84-A.

The geometric amplification for the angle (with the apex of the vee heat at the toe of the angle per figure 84-A) is the same as that of the category S channel. Using the same assumptions as for the channel (figure 73), the shape factor, F_s, is the same as that given by equation 51 where d_s is equal to d (the leg length being vee-heated) and b_s is equal to the width of the other leg (Avent and Mukai, 1998).

If a jacking force is applied during the heating process, the stress distribution throughout the vee heat zone differs for an angle compared to a plate. As such, the stress factor differs. First, the ratio of plastic to elastic section modulus is lower. Second, since the cross-section is not symmetrical, bending about the primary element is biaxial unless some type of lateral restraint is used. If no lateral restraint is provided, the simple bending stress formula, M/S, cannot be used to calculate stresses in the vee-heated area due to the jacking force. Instead, the biaxial bending formula must be used. For example, an L4×4×¼ angle bent about the axis of one leg and having no lateral restraint has a maximum stress at the heel of 2.5 times that for the laterally restrained case.

140

To incorporate this behavior into the stress factor, the ratio of *Z/S* is modified by the shape factor, F_s. The stress factor is defined by equation 45 in which the ratio of *Z/S* is defined as:

$$Z/_S = F_s(Z'/_{S'})$$ (53)

where *Z'/S'* is the ratio of plastic to elastic section modulus for the angle about the axis of bending. The plastic rotation can therefore be expressed by equations 41 and 42 where F_ℓ is given by equation 47, F_s by equation 51, and F_a by equations 45 and 53. The theoretical curve (equation 41) is plotted in figure 85 and shows relatively good agreement with the experimental data (Avent and Mukai, 1998).

Following this, to capture the behavior of angles heat-straightened with the heating pattern shown in figure 84-B, a series of angles were damaged and repaired (Avent et al., 1992). The results of these experiments are shown in table 18. The magnitudes of plastic rotation observed were not magnified to the extent of the previous case (figure 84-A). Since the apex of the vee is located at the heel for this heating pattern, the shape factor is equal to one, and only the stress amplification factor is needed (Avent and Mukai, 1998). The stress amplification factor for this heating pattern is the same as that for the heating pattern shown in figure 84-A (due to biaxial bending). Thus, the plastic rotation is given by equations 41 and 42 where $F_s = 1.0$ from equation 51, F_ℓ is given by equation 47, and F_a by equations 45 and 53. The theoretical values from Avent and Mukai (1998) are shown in table 18 and compare reasonably well with most of the experimental values from Avent et al. (1992).

Table 18. Summary of repair data for damaged angle specimens repaired using the heating pattern shown in figure 84-B (Avent and Mukai, 1998).

Specimen/Damage Category	M_j/M_p	Depth Ratio	No. of Heats	Avg. Plastic Rotations (milliradians)	Theoretical Plastic Rotations (milliradians)
L6×4×5/16 (S)*	0.22	1.00	3	4.66	4.31
L6×4×5/16 (S)	0.50	1.00	16	9.10	7.31
L6×4×5/16 (W)	0.50	1.00	3	11.11	7.19
L4×4×1/4	0.33	0.75	2	5.57	7.28
L4×4×1/4	0.33	1.00	5	6.75	7.28

Note: S and W denote bending about the long and short legs respectively. All vee heats were 45 degrees, with the apex located at the stiffening element and heating temperatures = 1,200°F.

3.2.7.1 Out-of-Plane Movement

Based on the geometric configuration of angles, an out-of-plane movement, in the direction perpendicular to the desired direction of movement, is expected to occur. Due to the linear continuous strain concept for folded plates, even though the stiffening element is heated with a rectangle, its strain behavior resembles that of a vee heat. As such, the stiffening element tends to shorten more on one edge than the other (at the free edge away from the vee-heated leg).

For the angles considered in figure 85, the average out-of-plane plastic rotations were measured by Avent et al. (1992) during their work and compared to the plastic rotations in the desired direction. These values and comparisons are shown in table 19. As can be seen from the table,

the out-of-plane movements are quite large in all cases, and they increase significantly with jacking ratio. However, when compared to the plastic rotations in the desired direction, the zero jacking ratio cases exhibited more relative movement. In fact, the out-of-plane movements were greater than the in-plane ones. The researchers noted that the large out-of-plane movements were likely a result of the vee-heated leg of the angle offering less resistance to rotation due to the applied heat. The researchers attributed the lower ratios of out-of-plane to in-plane movement encountered at larger jacking ratios to an ineffective distribution of stresses in the outstanding leg.

Table 19. Comparison of out-of-plane plastic rotations to in-plane plastic rotations for initially straight L4×4×1/4 angles (in-plane movement shown in figure 85) (Avent and Mukai, 1998).

Vee angle (degree)	M_j/M_p	Out-of-Plane Plastic Rotations (milliradians)	Ratio of Out-of-Plane to In-Plane Movement
20	0	2.93	2.07
20	0.25	4.03	0.72
20	0.50	6.59	0.59
45	0	4.55	1.44
45	0.25	7.85	0.84
45	0.50	10.76	0.67

Depending on whether the out-of-plane movements are beneficial to the overall repair of the given specimen, either bracing against this movement or using alternative heating patterns may be necessary to prevent or reduce them. In instances such as these, Avent et al. (1992) suggested applying the vee heat to the primary element as normal, while also heating the stiffening element to allow rotation in the desired direction. However, instead of using a rectangular heating pattern on the stiffening element, it is suggested that a reverse vee heat, continuing from the open end of the original vee, and tapering down to a point, may encourage the desired rotation while reducing the out-of-plane movement. In its "unfolded" position, the heating pattern would resemble a diamond shape, a pattern often used by pipe welders to straighten pipe distortions (Avent et al., 1992).

3.2.8. Example

Problem: A beam is damaged in flexure producing a 45-degree angle of damage at the impact point. Compute the estimated number of heats to straighten the member for each of the following sections using a jacking ratio of 50 percent and 30-degree vee angle: (a) W36×170 (weak axis bending), (b) C12×20.7 (strong axis bending), (c) L5×3×5/8 (bending about the axis of the short leg with tension damage to short leg).

Solution: To determine the number of heats required, n, the movement per heating cycle, φ_p, must be determined. The first step in computing movement per heat cycle is to compute the basic plastic rotation factor, φ_b, from equation 42:

$$\varphi_b = \varphi_b = 0.015\sin(\tfrac{\theta}{3}) = 0.015\sin\left(\tfrac{30}{3}\right) = 0.0026 \; rad = 2.6 \; millirad$$

Next, F_ℓ is obtained from equation 47:

$$F_\ell = 0.6 + 2\frac{M_j}{M_p} = 0.6 + 2(0.5) = 1.6$$

The other factors are dependent on the cross section and are calculated as follows:

(a) W36×170 (category W damage)

$$d_s = \frac{Flange\ Width}{2} = \frac{12.03\ in}{2} = 6.02\ in$$

$$b_s = Beam\ Depth = 36\ in$$

$$d = Flange\ Width = 12.03\ in$$

$$Z/_S = Z_y/_{S_y} = 83.8\ in^3/_{53.2\ in^3} = 1.58$$

From equation 51:

$$F_s = 1 + \frac{1}{2}\frac{b_s d_s}{d^2} = 1 + \frac{1}{2}[\frac{(36)(6.02)}{12.03^2}] = 1.75$$

From equation 45:

$$F_a = 1 - 2[1 - \left(\frac{2}{3}\right)\left(\frac{Z}{S}\right)]\frac{M_j}{M_p} = 1 - 2[1 - \frac{2}{3}(1.58)](0.5) = 1.05$$

and from equation 41:

$$\varphi_p = F_\ell F_s F_a \varphi_b = (1.6)(1.75)(1.05)(2.60) = 7.6\ millirad$$

(b) C12×20.7 (category S damage)

$$d_s = Channel\ Depth = 12\ in$$

$$b_s = Flange\ Width = 2.94\ in$$

$$d = Channel\ Depth = 12\ in$$

$$Z/_S = Z_y/_{S_y} = 3.47\ in^3/_{1.72\ in^3} = 2.02$$

From equation 51:

$$F_s = 1 + \frac{1}{2}\frac{b_s d_s}{d^2} = 1 + \frac{1}{2}[\frac{(2.94)(12)}{12^2}] = 1.12$$

From equation 45:

$$F_a = 1 - 2[1 - \left(\frac{2}{3}\right)\left(\frac{Z}{S}\right)]\frac{M_j}{M_p} = 1 - 2\left[1 - \frac{2}{3}(2.02)\right](0.5) = 1.35\ in$$

and from equation 41:

$$\varphi_p = F_\ell F_s F_a \varphi_b = (1.6)(1.12)(1.35)(2.55) = 6.17 \ millirad$$

(c) L5×3×5/8 (bending about axis of short leg with tension damage to short leg). The vee heat should be located on the long leg with the apex at the toe.

$$d_s = Angle \ Depth = 5 \ in$$

$$b_s = Angle \ Width = 3 \ in$$

$$d = Angle \ Depth = 5 \ in$$

$$Z/_S = Z_x/_{S_x} = 6.27 \ in^3/_{3.55 \ in^3} = 1.77$$

From equation 51:

$$F_s = 1 + \frac{1}{2}\frac{b_s d_s}{d^2} = 1 + \frac{1}{2}[\frac{(3)(5)}{5^2}] = 1.3$$

From equations 45 and 53:

$$F_a = 1 - 2[1 - \left(\frac{2}{3}\right)\left(\frac{Z}{S}\right)]\frac{M_j}{M_p} = 1 - 2\left[1 - \frac{2}{3}(1.3)(1.77)\right](0.5) = 1.53 \ in$$

and from equation 41:

$$\varphi_p = F_\ell F_s F_a \varphi_b = (1.6)(1.3)(1.53)(2.55) = 8.12 \ millirad$$

The number of heats can be determined from equation 19 where the degree of damage $\varphi_d = 78.5$ milliradians as follows:

For the W36×170:

$$n = \frac{\varphi_d}{\varphi_p} = 78.5/_{7.5} = 10.5 \ or \ 11$$

For the C12×20.7:

$$n = \frac{\varphi_d}{\varphi_p} = 78.5/_{6.17} = 12.7 \ or \ 13$$

For the L5×3×5/8:

$$n = \frac{\varphi_d}{\varphi_p} = 78.5/_{8.12} = 9.7 \ or \ 10$$

144

3.2.9. Summary

This section summarizes the response of rolled shapes to heat straightening, focusing on the two fundamental damage conditions: weak axis bending (category W) and strong axis bending (category S). The basis of the equations and experimental data discussed in this section was the experimental research conducted by Avent et al. (1992) and analytical model development by Avent and Mukai (1998). The behavior of channels, wide flange sections, and angles during heat straightening was studied by these researchers to form the basis of simple analytical formulas. These formulas, discussed above, can be used to predict the response of rolled shapes to heat straightening and design heat straightening repairs.

3.2.10. Important Considerations

- There are four fundamental damage categories for rolled shapes:
  - Category S: Bending about the strong axis.
  - Category W: Bending about the weak axis.
  - Category T: Twisting.
  - Category L: Local bulges, dishes, and crimps.
- The heating pattern for rolled shapes typically consists of vee heats on the primary elements and strip heats on the stiffening elements.
- If a stiffening element lies at the apex of the vee heat on a primary element, a strip heat is not applied.
- The amount of movement when heat straightening a rolled shape is a function of the vee angle, heating temperature, magnitude of the externally applied jacking force, the shape of the cross section, and the distribution of stresses due to jacking.
- Typically, the factors listed above tend to magnify the movement of the section compared to that expected from a vee-heated plate of the same size as the primary element (or elements) of the rolled shape.
- Heat straightening of angles produces components of movement in directions parallel to both legs even when movement in only one direction may be desired.
- Rolled shapes can be damaged and repaired multiple times with similar movement response although it is suggested that the same area not be repaired more than twice (see section 2.1.9).
- The first heat cycle often produces larger movements than successive cycles due to residual stresses.
- Analytical formulas were derived to predict movement during heat straightening of rolled shapes subjected to category S and W damage.

The analytical formula was based on the plastic rotation equation for plates (equation 39 from section 3.1) modified by the addition of a shape factor, F_s, and a stress factor, F_a. The plastic rotation formula can be generalized for rolled shapes as shown in equation 41, where the basic plastic rotation factor, φ_b, is given in equation 42 and the modification factors F_a, F_ℓ, and F_s are given in equations 45, 47 and 51.

3.3. HEAT STRAIGHTENING REPAIR FOR COMPOSITE DECK-GIRDER BRIDGES

3.3.1. Introduction

The basics of heat straightening repair and the effects of the heat straightening process on structural steel shapes have been discussed in detail in previous sections. The insights provided and fundamentals discussed in those chapters are useful when considering heat straightening of ordinary steel sections. However, one of the most common heat straightening repairs encountered is repairing damaged composite deck-girder bridges following impact from vehicles. The concepts discussed previously—including material properties following heat straightening repairs, and fundamentals of the heat straightening process—are useful when considering repairs to composite beams. However, there are further complexities associated with heat straightening these types of sections.

To understand the behavior of composite beams during heat straightening and factors affecting the heat straightening of these types of sections, large-scale experiments in which composite beams were damaged and heat-straightened were conducted by Avent and Fadous (1989) and Avent et al. (1993). The results of these studies are discussed in following sections. From the results, the factors affecting heat straightening of composite sections are evaluated and suggestions for conducting such repairs are discussed.

3.3.2. Heat Straightening Repair of Wide Flange Composite Beams

The primary parameters affecting heat straightening—vee heat angle, heating temperature, and depth ratio of vee heat to plate element—have been discussed in previous chapters and in other literature (Avent, 1987; Boudreaux, 1987; Nicholls and Weerth, 1972; and Roeder, 1985 and 1986). However, the influence of restraining forces, the heating patterns used, and pattern of damage experienced also play a central role in the heat straightening process. To investigate the effect of these parameters on the behavior of composite girders being heat-straightened, large-scale experiments in which composite beams were damaged and heat-straightened were conducted and are discussed below.

Investigations were performed by Avent and Fadous (1989) and Avent et al. (1993) on the behavior of damaged composite beams during heat straightening and the effect of heat straightening on composite sections in two related studies. Their work involved testing two full-scale wide flange composite sections, each damaged and subsequently heat-straightened a number of times. The goal of the two studies was to evaluate the behavior of composite beams during heat straightening and assess the results of the heat straightening process. Five specific aspects of heat straightening were evaluated: (1) the degree to which restraining forces affect behavior during heat straightening, (2) the effect of various heating patterns on movement, (3) the effect of successive heating cycles on damage restoration, (4) the effect of repetitive damage and straightening on material properties of the steel, and (5) an evaluation of whether dynamic (as opposed to static) damage influences the heat straightening process. From the results of this study, Avent and Mukai (1998) developed theoretical models for simple span and statically indeterminate composite beams to describe the behavior of composite beams during heat straightening.

146

The experimental procedures and results of the experiments by Avent and Fadous (1989) and Avent et al. (1993) are discussed in sections 3.3.2.1 and 3.3.2.2. Further discussion and interpretation of the results of this study, and the development of the theoretical models by Avent and Mukai (1998) are discussed in sections 3.3.3 and 3.3.4, respectively. Additionally, research by Varma and Sohn (2013) has also been conducted and is discussed in detail throughout chapter 2. The methods presented by Varma and Sohn (2013), as they pertain to this section, follow those presented by Avent and Fadous (1989) and Avent et al. (1993).

3.3.2.1 Heat Straightening Repair of a W10×39 Composite Beam

General Methodology

In the study completed by Avent and Fadous (1989), a W10×39 composite girder composed of A36 steel and a concrete deck was considered. To study the behavior of the beam during and following heat straightening repair, the specimen was subjected to two damage and repair cycles. Damage was induced on the specimen via static force with a jack at the midspan of the simply supported section.

During heat straightening repair, typically a lateral jacking force is applied to the lower flange. However, the determination of an adequate jacking force for composite girders is complicated for several reasons. First, when a lateral jacking force is applied to the lower flange, only a portion of that force produces a moment in the flange. The remaining portion of the force follows a load path through the web into the upper composite flange and is resisted by the concrete deck. The determination of the actual moment in the lower damaged flange is needed to prevent overstress during jacking and to predict the expected movement during heat straightening. Second, the plastic moment capacity, M_p, of the composite section subjected to a laterally applied load is difficult to compute.

To resolve these complexities, Avent and Fadous (1989) adopted the following procedure. The apparent moment due to jacking, M_j, was defined as the moment carried by the lower flange assuming all the jacking force was transferred to the lower flange alone. Likewise, the lateral capacity of the beam, M_p, was defined as the plastic moment of the lower flange alone about its strong axis. The ratio of M_j to M_p for the lower flange was defined as the apparent jacking ratio. The actual moment in the lower flange due to the jacking force was defined as M_f and expressed as a percentage of M_j. This procedure is used in the testing discussed in the following sections, and again in section 3.3.2.2 during testing of a W24×76 composite specimen.

Damage and Repair Cycle 1

The initially straight composite beam was statically loaded with a force of 28,000 pounds to produce a plastic lateral deformation of 2.75 inches at mid-span of the bottom flange. The pattern of the damage induced by Avent and Fadous (1989) is shown in figure 86. This damage pattern is typical for bridge girders (typical damage to fascia girder associated with vehicle impact) and was classified as light to moderate damage. As a result of the load application, two yield zones were formed. The lower flange yielded in flexure (about the strong axis of the flange plate) over a short length and a local bulge formed in this region. Additionally, a yield line formed in the web

approximately 2.25 inches below the top flange, extending over the middle two-thirds of its length.
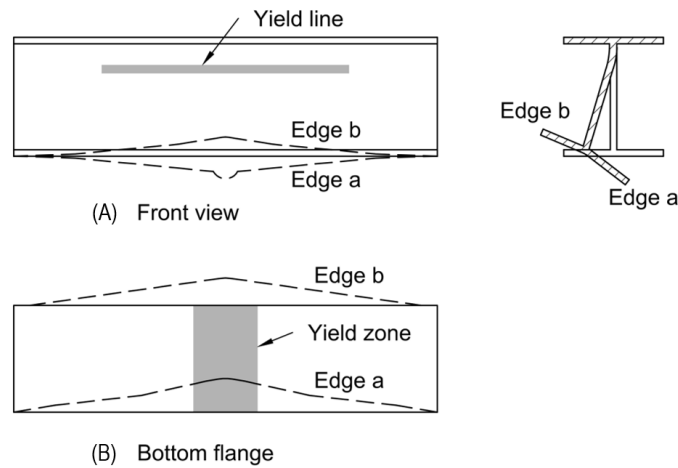
Source: FHWA

Figure 86. Illustration. Typical deformed shape and yield zones in damaged composite girders.

During the first heat straightening repair, Avent and Fadous (1989) used four primary heating patterns/jacking combinations. The basic heating patterns used by the researchers are shown in figure 87. In two cases, a single vee heat on the bottom flange was used in conjunction with an applied lateral restraining force producing an apparent jacking ratio (M_j/M_p) of either 56 percent or 112 percent. The other two cases were identical, except that an additional line heat was applied to the web of the girder along the center two-thirds of the span length at the damage-induced yield line. In all four cases, the vee heats were identical: a vee depth of three-quarters of the flange width, a 30-degree vee angle, and a constant heating temperature in the range of 1,200°F (monitored with contact pyrometer and temperature sensing crayons). The vee heats were always applied within the yield zone of the flange at the point of maximum curvature.
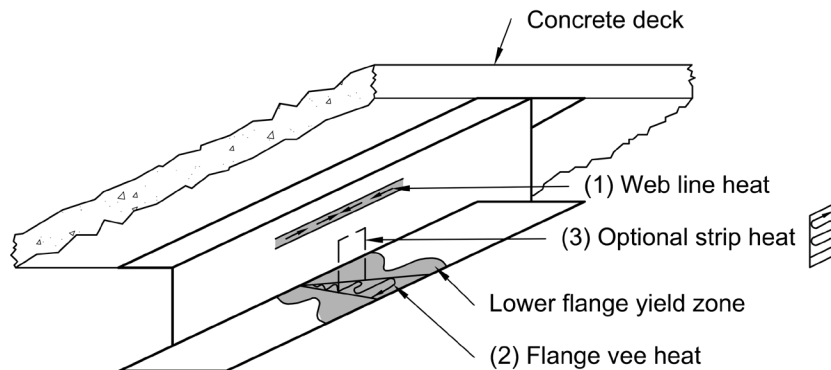
Source: FHWA

Figure 87. Illustration. Heating patterns for composite girder.

148

During the heat straightening process, Avent and Fadous (1989) measured the curvature of the web and computed the length of the yield line after each heating cycle. It was observed that, at the beginning of the 5th sequence, the central 24-inch portion of the web yield line had been completely straightened. This portion corresponded, in length, to the yield zone of the flange where the inelastic deformation occurred. The researchers concluded that, had a line heat been further applied in this region, reverse curvature along the web yield line would have been produced. Thus, in sequence 5 and beyond, the center 2 feet of the web was not heated. Rather, the line heat was only applied to portions of the web still exhibiting plastic curvature.

Following the heat straightening process described above, Avent and Fadous (1989) observed two localized bulges in the flange. To achieve a complete restoration to the original undeformed shape of the girder, the bulges were removed by applying both spot heats and circumferential line heats. As a result of removing the bulges, the lower flange deflected laterally 0.28 inch in a direction opposite to the earlier movements. That movement was expected since the spot heats were acting similarly to small vee heats placed in the wrong location (a detailed discussion of straightening local bulges is given in section 3.5). This movement, caused by correcting the local bulges, was repaired by the researchers through three additional heating cycles, resulting in a complete restoration of the section to the undeformed shape.

Damage and Repair Cycle 2

Following the completion of the first repair process, the researchers re-damaged the same W10×39 composite girder by applying a static load of 32,000 pounds laterally at midspan. The static force induced a permanent deflection in the bottom flange of 2.23 inches. The level of damage induced during the re-damage process was similar to that of the first damage cycle. Based on a load-deflection curve obtained during the re-damage process, the force associated with yield for the section was estimated to be about 16,000 pounds. From this, Avent and Fadous (1989) limited the external jacking force to 35 percent of this yield load. Since a 1,200°F temperature can reduce the yield stress to approximately one-half to one-third its original value, a limit of 35 percent of yield was used to ensure that hot mechanical straightening did not occur. This external jacking force corresponds to a force that would produce approximately 100 percent of the plastic moment in the bottom flange acting alone.

To repair the curvature induced by the second damage cycle, the researchers used a heating pattern similar to that shown in figure 87, except that two simultaneous vee heats were used on the lower flange. The first heating cycle was performed using one vee heat. Subsequent cycles were applied using two vee heats simultaneously. The decision to apply two vee heats in the same heating cycle was made because researchers found that the middle portion of the bottom flange contained two sharp regions of curvature. In addition to the vee heats, each heating cycle involved a line heat along the yield line in the web.

A total of 13 heat cycles were used by Avent and Fadous (1989) to repair the lateral displacement of the girder. Following this, the researchers used one additional heating cycle, a final sequence of line and spot heats, to remove the dish-like distortion in the bottom flange. This process also produced a reverse lateral deflection of 0.18 inch. As a result, two additional heat cycles were applied to remove the slight out-of-plane curvature that developed in the bottom flange, and remove additional lateral deflection developed due to the removal of the bulges.

General Observations Following Two Damage and Repair Cycles

To repair the second damage cycle, Avent and Fadous (1989) used combinations of vee heats and line heats found to be most effective during the first repair cycle. A summary of the heating patterns used during the heating sequences, compiled by Avent and Mukai (1998) during their development of the theoretical heat straightening models based on this research, is shown in table 20. Additionally, a comparison of average plastic rotation obtained to apparent jacking ratio for seven heating sequences, again compiled by Avent and Mukai (1998), is shown in figure 88. From these data, it was observed that certain heating patterns appear to be more effective than others. To account for these differences, Avent and Fadous (1989) point to two parameters: (1) the magnitude of the restraining force, and (2) the inclusion of the line heat on the web in addition to the vee heat on the lower flange.

Table 20. Summary of plastic rotations for a damaged composite W10×39 beam after heat straightening with various heat patterns (Avent and Mukai, 1998).

Damage Cycle	Heating Sequence	Number of Cycles	Number of Simultaneous Vee Heats	Number of Web Line Heats	Apparent Jacking Ratio	Average Plastic Rotation per Vee Heat (milliradians)
1	1	7	1	0	0.56	0.27[4]
1	2	8	1	0	1.12	0.93
1	3	8	1	1	1.12	3.53
1	4	4	1	1	0.56	0.96
1	5	5	1 or 2[1]	1[2]	1.12	1.76
2	6	13	2[3]	1	1	1.32[4]

[1] Two simultaneous vees were used in two cycles while only one vee was used in the other three.
[2] Only a partial line heat was used omitting the center one-third of the web yield line since this portion was essentially straight.
[3] The first heating cycle had only a single vee heat.
[4] The movement from the first heat of each sequence after damage inducement was not included in the average.
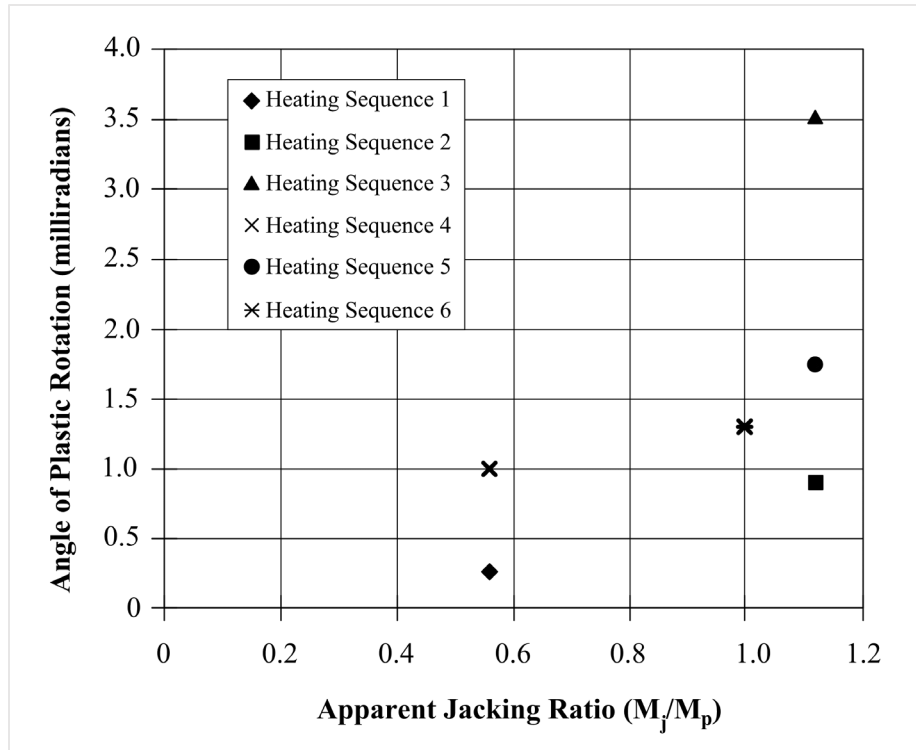
Source: Avent and Mukai (1998)

Figure 88. Graph. Comparison of average plastic rotation for various patterns and jacking ratios.

For the case presented by Avent and Fadous (1989), it was concluded that the wide flange should be analyzed with its web and bottom flange plate components as interacting elements. Each has plastically deformed, so attempting to straighten the first component independently of the second leads to the second component acting as a negative constraining force rather than a positive one (i.e., hindering the heat straightening process). As a result, the researchers concluded that heat should be applied in the vicinity of every zone in which plastic deformation has occurred to reduce this negative restraint. Further, the heating pattern used should correspond to the specific type of damage.

This principle is illustrated in table 20 when comparing the first pair of heating patterns (sequences 1 and 2) to the second pair (sequences 3 and 4). In sequences 1 and 2, the vee heat was applied to the plastic zone of the bottom flange without a web line heat. Since the web was unheated, it tended to resist the straightening effect of the flange. Even with a positive external force applied to the flange, researchers found the restoring effect was relatively small. In sequences 3 and 4, however, the yield line in the web was heated in addition to the vee heat in the flange. As a result, it was observed that the restoring effect had more than doubled during each sequence.

In a similar fashion, Avent and Fadous (1989) observed that the application of an external restraining force acting in the direction of desired movement enhanced the process. Researchers found that doubling the external force more than doubled the restoring movement for both

151

heating patterns. However, suggested limitations to the magnitude of external jacking force are discussed in a later section.

Finally, in addition to the above behavior, Avent and Fadous (1989) observed that, when comparing the heat straightening effect cycle by cycle, a significantly larger amount of movement occurred from the first heat cycle of a given sequence than after successive heat cycles of the sequence. The researchers concluded that residual moments caused by the induced damage, were likely the primary cause of this behavior. Avent and Fadous (1989) proposed that after damage there is a residual moment tending to straighten the beam in addition to the external jacking force. The combination of forces results in larger movement than expected during the first heat sequence. Since most of the residual moment is relieved after the first heat sequence, subsequent heats do not exhibit this behavior. This concept was further reinforced by Avent and Mukai (1998) when compiling the research of Avent and Fadous (1989), among other studies, to develop theoretical heat straightening models for composite beams.

3.3.2.2 Heat Straightening Repair of a W24×76 Composite Beam

General Methodology

Similar to the testing discussed in section 3.3.2.1, Avent and Fadous (1989) completed additional testing on a W24x76 composite beam. This work comprised subjecting a W24×76 composite beam specimen to two damage and repair cycles. The goal of this work was to capture the difference between damage due to dynamic and static loading, and difference in heat straightening response of a deeper section compared to that of a shallower section. To that end, the first cycle of damage was induced dynamically, rather than by static loading. The specimen was damaged by swinging a 3,400 pound ram in pendulum fashion such that the bearing plate impacted the lower flange of the beam. In contrast, the second cycle of damage was induced statically, in a similar fashion used for the W10×39 specimen. The W24×76 specimen had the following configuration: composite connection to the slab, simply supported ends for resistance to gravity loads, and diaphragms at the ends for resistance to lateral loads.

This work was continued by Avent et al. (1993), with further testing on the composite beam specimen originally tested by Avent and Fadous (1989). The continued testing comprised subjecting the same W24×76 composite beam specimen to a third and fourth damage/repair cycle in addition to subjecting a new (not previously damaged) W24×76 composite beam specimen to a single damage and repair cycle for comparison. The goal of this continued work was to investigate the role of constraining forces, both internal and external restraints, during heat straightening repair. All damage to specimens studied in this continued research was induced statically. The configuration of the specimens was similar to that used in the study completed by Avent and Fadous (1989).

Damage and Repair Cycle 1

Following the first cycle of damage, the W24×76 composite specimen was repaired via heat straightening. The repair process used by Avent and Fadous (1989) was similar to the most efficient process found during the repair of the W10×39 specimen discussed in section 3.3.2.1. The horizontal component of the applied jacking force selected by the researchers produced an

apparent jacking ratio, M_j/M_P, of 33 percent. For each heating cycle, a single 1,200°F, three-quarter-depth, 30-degree vee heat was used to repair the damage. The location of the flange vee heat varied from cycle-to-cycle over the 2-ft yield zone. In addition, a line heat was applied along the yield line of the web.

Researchers found that 28 heat cycles were needed to fully straighten the specimen. The average value of the plastic rotation achieved during each heating sequence is presented in table 21. However, it should be noted that only one heating sequence was used to repair the specimen following the first damage cycle. Like the W10×39 specimen, significantly larger plastic rotation angles were observed during the first heating cycle.

Table 21. Summary of plastic rotations for a damaged W24×76 beams after heat straightening with various patterns (Avent and Mukai, 1998).

Damage Cycle	Heating Sequence	Number Cycles	Number Simultaneous Vee Heats	Number Web Line Heats	Apparent Jacking Ratio	Average Plastic Rotation per Vee Heat (milliradians)
1	7	28	1	1	0.33	2.22[2]
2	8	12	2	1	0.33	2.48[2]
3	9	11	1	1	0	2.99[2]
3	10	9	1	1	0.5	3.89
3	11[1]	10	1	1	0.5	3.75
4	12	8	1	1	0.33	4.33[2]
1	13	7	1	1	0.75	9.99[2]

[1] A half depth web strip heat was also used in this sequence.
[2] The movement from the first heat of each sequence was not included in the average.

Damage and Repair Cycle 2

Following the completion of the first repair process, the same W24×76 composite beam specimen was subjected to a second damage and repair cycle. As mentioned previously, a gradually applied static load was used to induce the damage to this specimen. Avent and Fadous (1989) used a sequence similar to that used to repair the first damage cycle, except two vee heats were used simultaneously during this repair. The average plastic rotation achieved during each heating sequence is, again, presented in table 21. The results from the second repair cycle were found to be similar to those following the first repair cycle.

Additional Damage and Repair Cycles

Avent et al. (1993) subjected the same W24×76 composite specimen discussed in the previous sections to a third damage cycle. To repair the specimen, three heating sequences with 30 total heating cycles were conducted with three jacking ratio and heating pattern variations. A 30-degree vee angle, three-quarter-depth vee, and heating temperature of 1,200°F were maintained throughout all 30 sequences. The heat patterns consisted of a vee heat in the deformed portion of the bottom flange, and a line heat applied to the yield line in the web.

The heat straightening parameters used by the researchers and the plastic rotations achieved during each heating sequence are summarized in table 21. As shown in the table, sequence 9 was

conducted without a jacking force, and sequences 10 and 11 were conducted with an apparent jacking ratio of 50 percent. At the completion of sequence 10, the web had developed considerable bulging about the minor axis in the lower half of its depth, extending over the center 18 inches of the span. Researchers concluded that the longitudinal contraction in the heated bottom flange had created enough longitudinal residual stresses in the lower web section to cause buckling. This was likely because the beam had been damaged and straightened several times and the flange shortening had become significant. To help alleviate this issue, researchers opted to apply half-depth strip heats on the web at the location of the vee heat. The width of the strip heat was equal to the width of the vee at the flange fillet. For sequence 11, researchers used this modified heating pattern (vee heat, line heat, strip heat) and an apparent jacking ratio of 50 percent. Following 10 heating cycles using heating sequence 11, it was found that the application of the strip heats did not significantly affect the plastic rotations but effectively relieved the buckling in the web. Additionally, the plastic curvature in the web and lower flange were both corrected.

Following the third damage and repair cycle, the same W24×76 composite beam specimen girder was re-damaged a fourth time. The heating patterns and repair procedures used by Avent et al. (1993) during the fourth repair cycle were identical to those shown in figure 87. The strip heats used to repair the third damage cycle were not included in this repair procedure because web buckling was not an issue following the fourth cycle of damage. For the repair, the researchers used an apparent jacking ratio of 33 percent and only one heating sequence. Nine heating cycles were performed using this sequence. During the ninth heating cycle, a crack was formed on the convex side of the web yield line (where the line heat had not yet been applied), extending over a length of 5 inches. Due to this, the results from the ninth heating cycle were discarded. However, researchers had concluded that enough heating cycles had been completed to fully evaluate the behavior of the specimen during the straightening process. As such, the plastic rotation obtained as a result of the first eight heating cycles is presented in table 21.

Finally, to conclude their testing series, Avent et al. (1993) damaged a newly installed W24×76 composite beam (identical to the first W24×76 specimen) using a midspan static load to obtain the characteristic damage pattern shown in figure 86. The repair was conducted using the basic heating patterns shown in figure 87, similar to the repair procedures used on the previous specimen. However, in this case, researchers increased the apparent jacking ratio to 75 percent. As shown in table 21 this jacking ratio was substantially higher than that used during previous repairs of the W24×76 composite specimen. The researchers' goal was to use a jacking ratio that would replicate the hot mechanical straightening encountered during the repairs of the W10×39 specimens discussed in section 3.3.2.1. Eight heating cycles were performed using one heating sequence. The average plastic rotations obtained as a result of the eight heating cycles are given in table 21.

As expected, the plastic rotations observed by the researchers during the repair process were abnormally high. Compared to the tests where a jacking ratio of 50 percent was used, the average plastic rotation obtained during this repair was 124 percent larger. Additionally, cracking occurred in this specimen during the eighth heating cycle. The cracking initiated on the convex longitudinal edge of the bottom flange at the point of application of the vee heat and continued over a length of 1 inch to the apex of the vee. The cause of cracking during heat straightening is discussed further in section 3.3.3.6.

3.3.3. Evaluation of Factors Affecting Heat Straightening Behavior of Composite Girders

In the studies completed by Avent and Fadous (1989) and Avent et al. (1993), researchers investigated the behavior of composite beam specimens during heat straightening and effectiveness of the heat straightening procedures used. The goal of that work, discussed in sections 3.3.2.1 and 3.3.2.2, was to study the behavior of composite beam specimens during heat straightening and evaluate the effect of several parameters on the effectiveness of heat straightening. It was found that behavior of specimens and results of heat straightening are largely a function of several factors: heating patterns, residual stresses, restraining forces, stiffness of the section (particularly the web of the wide flange section), hot mechanical straightening, and cracking.

The observations made by Avent and Fadous (1989) as well as Avent et al. (1993) are discussed below. While using these works to develop theoretical models of heat straightening, Avent and Mukai (1998) developed their own observations, which are also discussed below.

3.3.3.1 Heating Patterns

The term "heat patterns" refers to the combination and layout of vee heats, line heats, and strip heats used to conduct a heat straightening repair. In general, vee heats are used to repair plate elements with plastic bending about the major axis, while line heats are applied to repair plate elements with flexural damage about the minor axis. Hence, when straightening a wide flange section, vee heats are used on the bottom flange in conjunction with a line heat on the web (as shown in figure 87).

As illustrated by the work completed by Avent and Fadous (1989), when applying line heats to the web of a wide flange composite section, care should be taken to iteratively adjust the length of the line heats, so only portions of the web that show plastic curvature are heated. This was illustrated in section 3.3.2.2, where line heats applied to the W10×39 composite specimen were adjusted by the researchers once the plastic curvature in the web was fully corrected. Similarly, the application of vee heats should be confined to the portion of the bottom flange with plastic deformations.

In addition to the vee and line heats typically used to straighten wide flange sections, some cases may benefit from the application of a half-depth web strip heat. The purpose of this heat pattern is to reduce the differential shortening between the web and flange and relieve the associated residual stresses. Additionally, the strip heat tends to reduce the buckling of the web near the center of damage. This concept was illustrated in the work completed by Avent et al. (1993), discussed earlier in section 3.3.2.2, where researchers effectively corrected web buckling by using a half-depth strip heat in the heating sequence.

3.3.3.2 Residual Moments

Residual moments are a common characteristic of any damaged wide flange section, both simply supported and statically indeterminate. When damage is induced, dynamic or static, the web of the section acts as a spring resisting the movement. While a yield line typically develops near the top of the web, as observed by Avent and Fadous (1989), there is also an elastic component of stored energy, either in the form of internal redundancy or residual moment, that remains in the

web (Avent and Mukai, 1998). During the first heat cycle, this residual moment or restoring force acts as an additional jacking force tending to straighten the girder. This phenomenon was observed by both Avent and Fadous (1989) and Avent et al. (1993), where both sets of researchers found that the plastic rotation due to heat straightening was largest in the first heating cycle. However, since the initial plastic rotation relieves a majority of this residual moment, the plastic rotation obtained during successive heat cycles is typically smaller. This, again, was confirmed by the behavior of the specimens in both studies. Since this behavior is typical, it should be considered when developing a constraint plan for heat straightening. It is suggested that a reduced external restraint, or jacking force, be used during the first two heating cycles to minimize internal force effects and the possibility of cracking. This is discussed further in section 3.3.4.

3.3.3.3 Restraining Forces

The importance of restraining forces in the heat straightening process has been recognized for many years. As a result, jacking forces have often been used to facilitate the heat straightening repair of a wide range of damaged structural steel members. The tests discussed in previous sections 3.3.2.1 and 3.3.2.2 were designed by the researchers (Avent and Fadous, 1998; Avent et al., 1993) to specifically evaluate the effect of external restraining forces on the heat straightening behavior of damaged composite bridge girders.

One method for providing restraining forces during heat straightening is to allow the unheated portion of the member to restrict thermal expansion of the heated portion. This is done by using suitable heat patterns applied in appropriate locations and is a form of an internal constraint. In addition to proper heat pattern selection and application, internal constraints may also be imposed by the self-weight, axial loading, or static indeterminacy of the member. To complement the internal constraints present in a section, external restraining forces are often used. These external restraining forces are applied to enhance the results by either magnifying the effect of internal constraints that facilitate the heat straightening process or negating the effect of internal constraints that hinder it.

As discussed in sections 3.3.2.1 and 3.3.2.2, Avent and Fadous (1989) and Avent et al. (1993) studied the effect of applied external restraints on the plastic rotations obtained during heat straightening. The results of that work and corresponding observations were compiled by Avent and Mukai (1998) and are presented in figure 89. As shown, the jacking ratio-versus-plastic rotation curves exhibit a sharp discontinuity at higher loads for the W24×76 composite beam. This behavior is associated with hot mechanical straightening and is discussed in section 3.3.3.5.
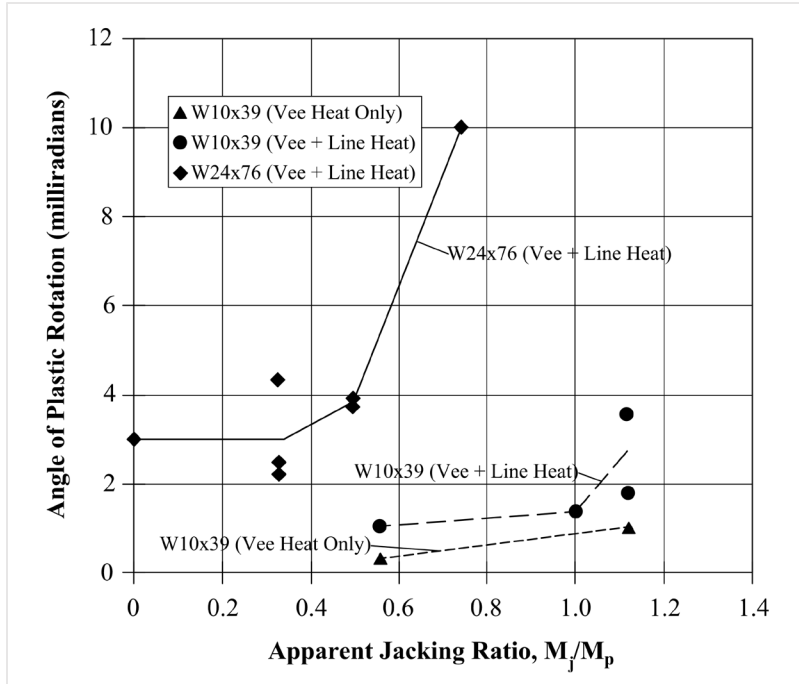
Source: Avent and Mukai (1998)

Figure 89. Graph. Apparent jacking ratio versus plastic rotation for composite girders.

As mentioned previously, internal redundancy and the interaction between internal and external constraints affects the heat straightening response of a composite girder. Consider, for example, the intersection of the bottom flange and the web. At this location, the interaction between the web and flange produces redundant forces that impede the plastic rotations. These forces restrict movement by acting as a negative internal constraint, hindering movement in the bottom flange created by the vee heat. Comparing the plastic rotations obtained by Avent and Fadous (1989) and Avent et al. (1993) for both W10×39 and W24×76 specimens, it is clear that plastic rotations are directly related to the jacking ratio. However, the relationship is not necessarily linear. Comparing the plastic rotations of the W10×39 to that of the W24×76, it is evident that the movement of the W24×76 was consistently larger than that of the W10×39, even when similar jacking ratios were used. From this, it can be concluded that the redundant forces produced by the web-flange interaction in composite members inhibit the straightening effect more for a shallow beam than for a deep beam (Avent et al., 1993).

Similarly, the damage to the composite members produces a plastic deformation in the web along the yield line. This plastic deformation resists any elastic bending of the web about its minor axis during the straightening of the bottom flange. Hence, the presence of the yield line in the web tends to magnify the counterproductive redundant forces and further inhibits the straightening effect produced by the bottom flange vee heat. By using a line heat on the web in addition to the vee heat in the bottom flange, these inhibiting forces are mitigated. This conclusion, observed by Avent et al. (1993), was verified by comparing the results obtained by Avent and Fadous (1989) for the W10×39 specimen heat-straightened with and without web line heats. These results can be seen in table 20, where the plastic rotations obtained during the first

two heating sequences (without web line heats) result in very small plastic rotations in comparison to latter two sequences (with web line heats).

Finally, when considering the lateral load applied to the bottom flange of the composite girder at midspan, the moment produced is transferred to the supports via two mechanisms: (1) the bottom flange bending in strong axis flexure, and (2) the web acting as a flexural plate (and, at large deformations, a membrane plate) supported by the deck and end diaphragms. As such, a shallower girder would be expected to have greater stiffness and thus a smaller lower flange moment than that of the deeper girder subjected to the same lateral load (Avent et al.,1993).

The data obtained by both Avent and Fadous (1989) and Avent et al. (1993) tends to verify this hypothesis. As noted in figure 89, jacking ratio has a smaller effect on shallow girders in comparison to deeper girders. Thus, using a jacking ratio defined as the applied jacking moment over the plastic moment capacity of the bottom flange only assumes that most of the applied jacking force is transferred through the lower flange–which was not the case, especially for shallower girders. As a result, determining the distribution of jacking force between the bottom flange and web is a key aspect of developing a constraint plan. This concept was developed by Avent and Mukai (1998) and is discussed further in section 3.3.4.

Further research by Varma and Sohn (2013) investigated the application of larger jacking ratios with reduced heating temperatures as well as overheating. The findings from their investigations are further discussed throughout chapter 2.

3.3.3.4 Stiffening Effect of Web

As mentioned previously, when an external lateral restraining force is applied to the lower flange of a composite girder, the goal is to generate a restraining moment in the lower flange that facilitates the heat straightening process. However, correlating the jacking ratio to the plastic moment capacity of the bottom flange only is misleading if the web interaction effects are significant. This was discussed briefly in section 3.3.3.3 when comparing the effect of jacking ratios on the amount of plastic rotation obtained during heat straightening. For the same jacking ratio, the plastic rotation obtained in the deeper section was substantially larger than that obtained in the shallower section. This was attributed to the web (and subsequently top flange and composite deck) of the shallower girders contributing significantly to the lateral stiffness of the member (Avent and Mukai, 1998).

Due to the web interaction between the lower flange and the completely restrained upper flange, some of the applied force is transferred through the web into the deck rather than into the lower flange. For deep beams, most of the applied lateral force is carried by the lower flange. However, for more shallow depth beams, an increasing amount of the force is transferred into the deck. In both cases, however, only the fraction of the total force applied to the lower flange provides external restraint to the flange vee heat. Hence, a jacking ratio which considers the applied jacking force and the moment capacity of the lower flange only is not an accurate representation. This is considered the apparent jacking ratio. A more accurate method of calculating the jacking ratio is to consider the actual moment transferred to the bottom flange and plastic moment capacity of the bottom flange. This is considered the effective jacking ratio. These parameters, developed by Avent and Mukai (1998), are discussed in further detail in section 3.3.4.

3.3.3.5 Hot Mechanical Straightening

In the testing completed by Avent et al. (1993), the researchers damaged and repaired a new (undamaged) W24×76 composite specimen. During the repair of this specimen, an apparent jacking ratio of 75 percent was used to study the effect of a high jacking ratio on the behavior of the specimen during straightening. The details of this were discussed in section 3.3.2.2.

The behavior of this specimen compared to the other specimens studied by Avent and Fadous (1989) and Avent et al. (1993) is illustrated in figure 89. As shown in this figure, a large increase in plastic rotation was observed during the straightening of the W24×76 specimen when an apparent jacking ratio of 75 percent was used. The average plastic rotation obtained for this jacking ratio was almost three times the values associated with the lower jacking ratios.

In previous chapters, the effect of temperature on the yield stress of steel has been discussed in detail. From this, it is known that the yield strength of steel decreases with increasing temperature. Further, at 1,200°F the yield strength of ASTM A-36 steel decreases to about half of its original value. Thus, at the elevated temperatures associated with heat straightening, steel can yield at relatively low stresses. Considering the magnitude of the jacking force used during the heat straightening of the W24×76 from Avent et al. (1993), it can be concluded that the applied jacking ratio of 75 percent exerted a load exceeding the yield stress of the hot steel, causing some amount of hot mechanical straightening to occur. In effect, during hot mechanical straightening of a steel member, the jacking forces are merely pushing the member mechanically due to the reduced yield stress. As a result of this, large movements or plastic rotations can occur, especially when compared to the relatively small movements typically associated with heat straightening (Avent and Mukai, 1998).

Hot mechanical straightening is an entirely different procedure from heat straightening and should be avoided when attempting to heat straighten a member. As such, there are suggested limits to the applied jacking force to prevent this type of behavior. These are discussed in detail in section 3.3.4.

3.3.3.6 Cracking

During the experiments completed by Avent and Fadous (1989) and Avent et al. (1993), cracking was observed twice, in two separate specimens, during the heat straightening process. The first crack observed occurred during the fourth damage and repair cycle of the W24×76 composite specimen at the end of the ninth heat cycle. The crack initiated in the web parallel and adjacent to the line heat on the tension side of the web (relative to the jacking force). As discussed in section 2.1, researchers have found that generally after more than two damage and repair cycles, there is a substantial increase in yield stress and decrease in ductility. This is the case when specifically compared to the change in yield stress and ductility after one and two damage and repair cycles. As a result, the material becomes increasingly brittle. Further, it has also been found that areas of concentrated heat, such as the apex of the vee heat, have been particularly sensitive to these material property changes and are subject to higher residual stresses. Since both the apex of the vee heat and the line heats are similar when considering concentration of heat, it was concluded by the researchers that repetitive damage combined with increased residual stresses led to the brittle failure in the web (Avent et al., 1993).

The second crack observed occurred in the new, previously undamaged, W24×76 composite specimen that was subjected to only one cycle of damage. The crack occurred during the eighth cycle of the first heat straightening repair and initiated in the tension side of the bottom flange (relative to the jacking force). During this repair, an unusually high apparent jacking ratio of 75 percent was used. Similar fractures have been reported during field repairs. As such, the researchers concluded that the crack likely occurred as a result of (1) the high jacking force combined with the somewhat reduced ductility due to heating, and (2) the residual stresses within the section, which may have increased the stress in the section above ultimate stress (Avent et al., 1993).

This observed behavior reinforces the concept that the jacking forces should be evaluated analytically and never applied without a gauge to control the magnitude. Suggestions for maximum jacking force are provided in section 3.3.4. Use of these suggestions values reduces the potential of brittle failure or cracking in the section. However, should such cracking occur, the heat straightening procedure should be stopped immediately to allow for evaluation. It may be possible to complete the heat straightening process with the crack present and repair the crack with a splice plate or welding once the section is corrected. However, the exact details of the situation should be evaluated, and engineering judgment applied before proceeding.

The phenomenon of cracking was also encountered by Connor et al. (2008). In some cases, cracking during heat straightening or after repetitive damage was concluded to be a result of cold working of the steel due to impact. This cold working of the steel, in localized areas, reduces the ductility of the steel which, upon further stressing by additional damage cycles or jacking, resulted in cracking. Additionally, undetected cracking was found to further increase in size during the heat straightening process, particularly in fatigue-sensitive details. The importance of testing and removing such cracks and flaws prior to heat straightening is further discussed in section 2.3.

3.3.4. Theoretical Model for Heat Straightening Response

Based on the research discussed above, completed by Avent and Fadous (1989) and Avent et al. (1993), Avent and Mukai (1998) developed a theoretical model to capture the behavior of composite girders during the heat straightening process, and predict the plastic rotation that should result. The following sections detail the development of the theoretical model for both simple span girders and statically indeterminate girders and provide a worked example.

3.3.4.1 Modeling of Simple Span Composite Girders

Avent and Mukai (1998) developed a model to describe the behavior of composite beams during heat straightening, beginning with the simplest case: a simply supported composite beam without diaphragms. The development of this model is discussed below.

Previous sections discussed web interaction between the lower and upper flange and its effect on the applied external restraint. For shallow girders, the effect of web interaction was found to be significantly larger than for deeper girders. This was attributed to the increased lateral stiffness of shallow composite sections compared to that of deeper composite sections. Moreover, due to web interaction, only a portion of the applied jacking force is carried by the lower flange and

restraints are applied to the flange. Therefore, to begin to accurately capture the transfer of load and behavior of the section during heat straightening, it is important to determine the amount of the applied lateral jacking force that is actually distributed to the lower flange as opposed to that which is transferred through the web to the composite deck. This portion of the jacking force that is carried by the lower flange is called the effective jacking force. To further develop the model, the effective jacking force, and subsequently the jacking moment in the lower flange need to be determined. This was captured by Avent and Mukai (1998) as follows.

The apparent moment, M_j, is defined as the moment induced in the lower flange by the jacking force, P_j, assuming the lower flange alone supports the lateral force (i.e., the web and upper composite flange are neglected). If P_j is applied at the center of the span, the apparent moment is:

$$M_j = \frac{P_j \ell}{4} \tag{54}$$

where ℓ is the span length.

The stiffness of the system can be expressed as:

$$K_j = \frac{4EI_j}{\ell} \tag{55}$$

Where E is the elastic modulus of steel and I_j is the equivalent moment of inertia that includes the bottom flange and the web stiffening effect. From this, the deflection of a simply supported beam with a concentrated load at the center is:

$$\Delta = \frac{P_j \ell^3}{48EI_j} \tag{56}$$

or in terms of K_j;

$$\Delta = \frac{P_j \ell^2}{12K_j} \tag{57}$$

Solving for K_j:

$$K_j = \frac{P_j \ell^2}{12\Delta} \tag{58}$$

In the elastic range, K_j can be determined experimentally by measuring Δ for a specified applied load P_j.

The stiffness of the composite beam system includes both the effect of the lower flange and the web stiffening effect due to connectivity with the upper composite flange. Thus, only a portion of the moment generated by the jacking force, P_j, is distributed to the lower flange. An estimate of the actual moment can be obtained by assuming that the moment in the flange, M_f, is equivalent to that produced by the application of a portion of the jacking force to the lower flange with the web effect neglected. The moment in the flange can be written as:

$$M_f = \frac{P_f \ell}{4} \tag{59}$$

where P_f is the portion of the jacking load transferred to the lower flange. The lateral deflection of the flange can be written as:

$$\Delta = \frac{P_f \ell^3}{48EI_f} = \frac{P_f \ell^2}{12K_f}$$

(60)

where I_f is the flange moment of inertia about the axis of bending and K_f is the flange stiffness, $4EI_f/\ell$. Since the deflections from equations 57 and 60 are identical, the two equations can be set equal to each other:

$$\frac{P_f \ell^2}{12K_f} = \frac{P_j \ell^2}{12K_j}$$

(61)

or simplified to:

$$\frac{P_f}{K_f} = \frac{P_j}{K_j}$$

(62)

Using equations 54 and 59 to eliminate the forces P_f and P_j, equation 62 can be written as:

$$\frac{M_f}{M_j} = \frac{K_f}{K_j}$$

(63)

or

$$M_f = \overline{\gamma} M_j$$

(64)

where the distribution factor, $\overline{\gamma}$, is defined as:

$$\overline{\gamma} = \frac{K_f}{K_j}$$

(65)

Since K_f can be calculated for a given lower flange and K_j obtained from experimental measurements, the value for $\overline{\gamma}$ can be directly calculated using equation 65.

For the W10×39 originally tested by Avent and Fadous (1989), using the methodology described above, the distribution factor $\overline{\gamma}$ was determined to be 0.183. Similarly, for the W24×76 originally tested by Avent and Fadous (1989) and Avent et al. (1993), $\overline{\gamma}$ was calculated to be 0.427. These factors were found to be accurate when the effect of the web line heat on bottom flange stiffness was neglected (Avent and Mukai, 1998). However, as mentioned previously, when the researchers compared the results for heating sequences with and without web line heats, it was concluded that the line heat significantly reduces the web's restraining stiffness. As a result, more jacking force is carried by the bottom flange when the web line heat is considered (Avent et al., 1993).

To capture this effect, Avent and Mukai (1998) compared the plastic rotation values for identical cases without the web line heat and with the web line heat. From this, the researchers concluded that the web stiffness reduction effect, as a result of the web line heat, produces a load magnification in the lower flange of about 160 to 190 percent. Specifically, the distribution factor, $\overline{\gamma}$, is increased by an average value of 175 percent when a web line heat is used.

Consequently, the modified factor, γ (where γ is the distribution factor including the line heat effect), was adjusted to 0.320 and 0.747 for the W10×39 and the W24×76, respectively.

Thus, the relationship between the apparent moment, M_j, associated with the jacking force and the actual moment in the bottom flange, M_f, after the line heat to the web is applied is:

$$M_f = \gamma M_j \tag{66}$$

To illustrate the effective load ratio, M_f/M_p, Avent and Mukai (1998) applied this distribution factor to the data shown in figure 89. The data was then replotted to illustrate plastic rotation versus effective load ratio and is presented in figure 90. The plate equation discussed in section 3.2 was also plotted in figure 90 for comparison purposes. As shown, it falls between a curve fit of data for the W10×39 and the W24×76 composite sections. Through comparison to the plate equation, Avent and Mukai (1998) concluded that the web stiffening effect significantly reduces plastic rotations for shallow beams. Further, as the stiffening effect is lessened for deeper beams, with application of a web line heat, the plastic rotations tend to be magnified in a pattern similar to that of damage category W in wide flange beams (discussed in section 3.2). Consequently, the researchers concluded that the stiffness factor would be expected to be a function of the square of d/t_w where d is the beam depth and t_w is the web thickness. Under the assumption that the plate equation is a reasonable model for the composite girder, Avent and Mukai (1998) developed the following to incorporate the web stiffening effect and express the stress factor, F_a, as:

$$F_a = \left(\frac{d/t_w}{46}\right)^2 \tag{67}$$
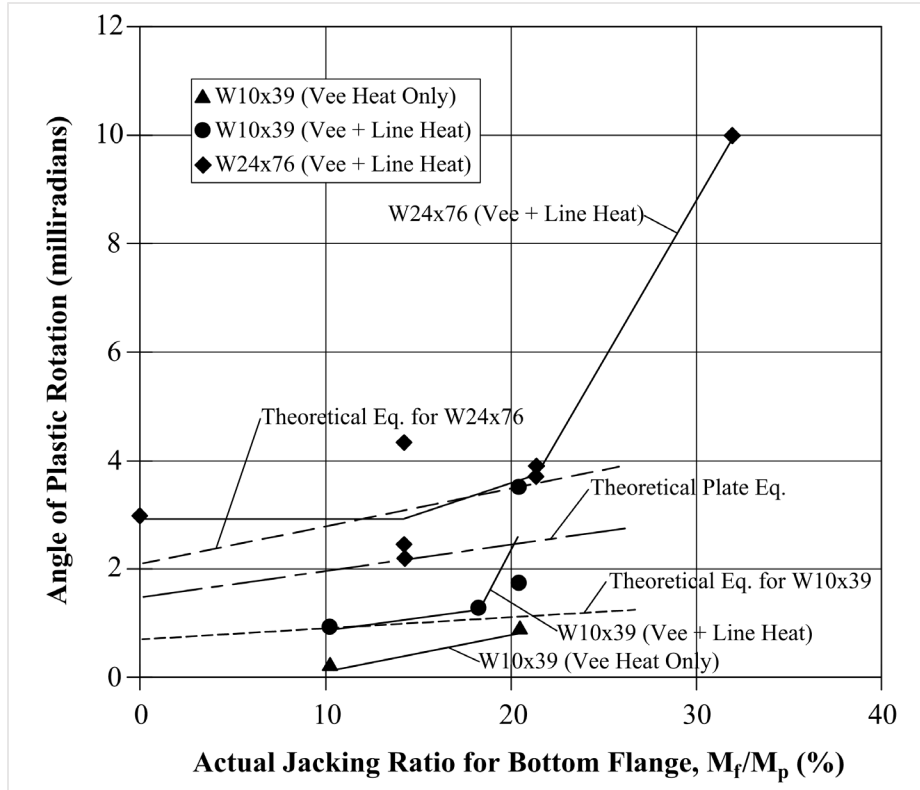
Source: Avent and Mukai (1998)

Figure 90. Graph. Actual jacking ratio versus plastic rotation for composite girders.

Following this, the researchers used the experimental data from Avent and Fadous (1989) and Avent et al. (1993) to translate values of $\bar{\gamma}$ (prior to web line heat) to values of γ (after web line heat) using the following relationship:

$$\gamma = 1.75\,(\bar{\gamma}) \tag{68}$$

Using the experimental data for the W10x39 and W24x76 obtained by Avent and Fadous (1989) and Avent et al. (1993), Avent and Mukai (1998) plotted γ versus d/t_w, as shown in figure 91. Included in the same figure is similar data for a W36x170 obtained from Avent and Brakke (1996). From the relationships and the experimental data discussed above, an equation was obtained for the stiffness reduction factor, γ by assuming a second order curve fit between the known data points. This equation is defined as:

$$\gamma = \frac{d/t_w}{10,000}\,(15 + 2.75\,d/t_w) \tag{69}$$

164
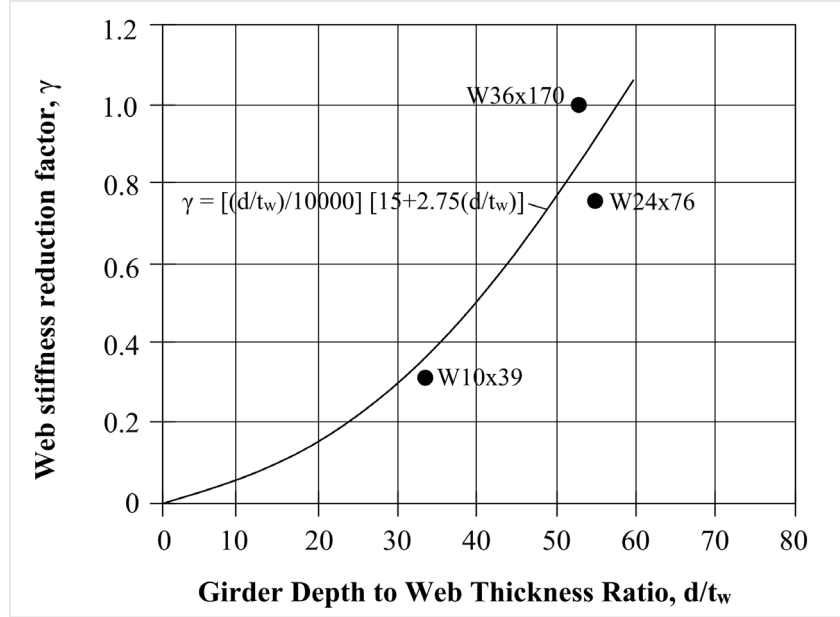
Source: Avent and Mukai (1998)

Figure 91. Graph. Web stiffness reduction factor versus girder depth to web thickness ratio.

Equation 69 was also plotted by Avent and Mukai (1998) in figure 91 for comparison to the measured data.

Utilizing these factors, Avent and Mukai (1998) developed an equation for plastic rotation of composite girders (including web line heats). This equation, written in a form similar to that of rolled shapes in section 3.2, is defined as:

$$\varphi_c = F_a F_\ell \varphi_b \qquad (70)$$

where φ_b is the basic plate plastic rotation factor of the lower flange acting as an independent plate. This parameter, discussed further in section 3.2, is defined as:

$$\varphi_b = 0.015\sin\frac{\theta}{3} \qquad (71)$$

F_a is given by equation 67. The load factor, F_ℓ is defined as:

$$F_\ell = \left(0.6 + 2\frac{M_f}{M_p}\right) \qquad (72)$$

or using equation 66

$$F_\ell = 0.6 + 2\gamma \frac{M_j}{M_p} \qquad (73)$$

where M_p is the plastic moment capacity of the lower flange about its strong axis.

165

Using equation 70, Avent and Mukai (1998) determined the theoretical plastic rotations for the W10×39 and W24×76 composite specimens. These theoretical rotations were then superimposed on the plot of experimental data shown in figure 90. Excluding the high jacking ratio data point (obtained by Avent et al. (1993) for the W24×76 specimen using a 75 percent apparent jacking ratio that induced hot mechanical straightening), Avent and Mukai (1998) concluded that the analytical formulas developed provide a reasonable approximation of behavior during heat straightening.

From the experimental evidence discussed in previous sections and presented in figure 90, Avent and Mukai (1998) concluded that the degree of plastic rotation per heat cycle is proportional to the magnitude of the restraining force up to a certain value. For forces higher than this value, the behavior was found to become nonlinear with increased plastic rotations. This phenomenon was attributed to a combination of (1) the jacking forces creating stresses greater than the reduced yield stress in portions of the flange heated zones (hot mechanical straightening), and (2) the spreading of the yield zone and the associated redistribution of moments. Since little experimental evidence was available to verify the safety of such high jacking forces, the researchers suggest the use of a lower jacking force.

Finally, from the experimental data discussed in previous sections, Avent and Mukai (1998) established suggestions for maximum jacking force. Considering the range of section geometry represented by the W10×39 and W24×76 specimens, the researchers suggest, conservatively, that the actual jacking ratio used for the heat straightening of composite girders be limited to 33 percent, thus:

$$M_f \leq \frac{M_p}{3} \tag{74}$$

The apparent jacking ratio, obtained using equation 66 is then defined as:

$$\frac{M_j}{M_p} \leq \frac{1}{3\gamma} \tag{75}$$

3.3.4.2 Modeling Statically Indeterminate Spans Due to Intermediate Diaphragms

With the case of the simply supported composite girder in mind, Avent and Mukai (1998) developed a similar method to model the behavior of composite girders with intermediate diaphragms. The development of this model is discussed below.

Consider the case of a composite girder with intermediate diaphragms (typical for most steel girders used for highway bridges) subjected to characteristic damage to its lower flange. As a result of the intermediate diaphragms, when the lower flange is damaged, its behavior resembles that of a beam continuous over several supports, with the diaphragms acting as these supports. This behavior is illustrated in figure 92. Due to the damage, a plastic hinge mechanism typically forms as shown in figure 92-B. The development of three plastic hinges results in reverse curvature bending and yield zones at three points: the impact point, and the two adjacent supports. This is illustrated in figure 92-C.

(A) Lower flange of a composite beam modeled as a continuous beam

(B) Plastic hinge mechanism after impact

(C) Plan view of lower flange reverse curvature bending showing yield zone and vee heat patterns (line heats should also be applied to all web yield lines)
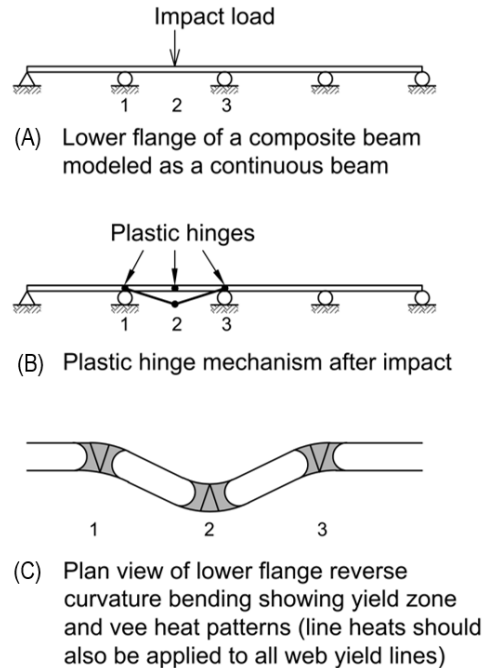
Source: FHWA

Figure 92. Illustration. Lower flange of composite girder modeled as a continuous beam.

Due to the presence of three adjacent yield zones in the flange, it is suggested that these regions be heated either simultaneously or in quick succession, so rotation occurs at all three locations with reduced restraint from adjacent plastic hinges (Avent and Mukai, 1998). The vee heat patterns typically applied to the yield zones of the flange during heat straightening are shown in figure 92-C. Since this more complex damage configuration is repaired using simultaneous heats at all yield zones, this simplifies the behavior of the section. As such, the model for the simply supported composite girder, developed by Avent and Mukai (1998), should provide a reasonable approximation of this more complex situation.

To utilize the model presented in section 3.3.4.1 and approximate the behavior of the composite girder with diaphragms, recall the importance of residual stresses in heat straightening. As discussed in previous sections, an important consideration for composite girder repair is the residual stress induced during both the damage and repair process. For diaphragm-braced composite girders, the residual moments produced during the damage process should be considered to accurately capture the behavior of the girders during heat straightening repair. These moments can be computed by the following process developed by Avent and Mukai (1998).

First a plastic analysis of the continuous beam should be performed to determine the ultimate load (impact force), P_u, and the corresponding plastic moment distribution, M_u. A modified stiffness can be used for these computations. This modified stiffness factor is defined as:

$$K_j = \frac{1}{\gamma} K_f \tag{76}$$

167

where K_j, K_f, and $\bar{\gamma}$ are as defined in section 3.3.4.1.

The second step is to take the computed ultimate load, P_u, apply it in the opposite direction (relative to the original impact force), and compute an elastic moment diagram, M_e (even if the stresses exceed F_y). Finally, the superposition of these two moment diagrams yields the residual moment distribution, M_r, due to the impact loading. These residual moments can either aid or hinder heat straightening depending on their directions.

The moment in the flange is defined as $M_f + M_r$ where M_r is positive when the residual moment has the same sign as the moment due to jacking force. Using the jacking force limit of $M_p/3$, discussed in section 3.3.4.1, the following relationship is obtained:

$$M_f + M_r \leq \frac{M_p}{3} \tag{77}$$

Or

$$M_f \leq \frac{M_p}{3} - M_r \tag{78}$$

The apparent jacking moment is found by substituting equation 78 into equation 66 and solving for M_j:

$$M_j \leq \frac{1}{\gamma}(\frac{M_p}{3} - M_r) \tag{79}$$

Finally, the apparent jacking force, P_j, can be determined from equation 54. It should be noted that although residual moments are initially present, the movement resulting from the first few heat cycles should eliminate them. Therefore, the jacking force should be adjusted following the first few heats.

Due to the presence of residual moments, care should be taken during the first few heats not to over-jack the composite girder. If the residual moments are not computed prior to heat straightening, then the maximum jacking ratio should be reduced during the first two heats to prevent over-jacking. In this case, the jacking ratio limit suggested by Avent and Mukai (1998) for the first two heats is 16 percent (half of the 33 percent limit suggested for the simply supported composite girder). After two heats, following the release of the residual moments, the jacking force can be increased. The suggested limit following the first two heats is 33 percent, as discussed in section 3.3.4.1.

Example of a Statically Indeterminate Composite Girder

The example problem included below was originally presented by Avent and Mukai (1998). This example helps illustrate the methodology discussed in section 3.3.4.2 for modeling the behavior of statically indeterminate composite girders.

Problem Statement: The lower flange of a composite steel beam (W36×170, ASTM A36 steel) was impacted by a crane boom as the truck carrying it passed under the bridge. The deflected shape of the lower flange is shown in figure 93 after the degree of damage at the three plastic hinges had been calculated. Compute the maximum jacking force that should be used in the heat

straightening repair assuming that the diaphragm at joint 5 is removed prior to repair. Shown in figure 93 are the results of the plastic analysis, (a), the elastic analysis, (b), and the residual moments, (c).
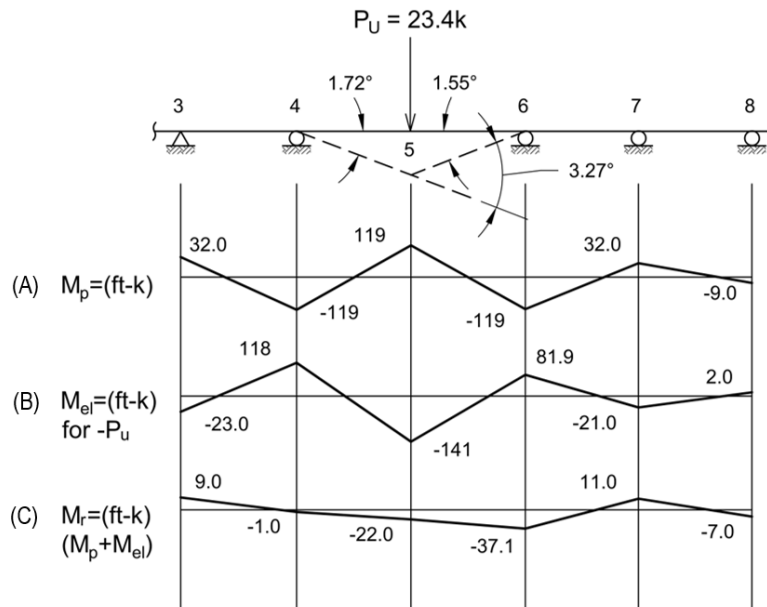
Source: FHWA

Figure 93. Illustration. Deflected shape and structural analysis of damaged beam.

Solution: For a W36×170, the *d/tw* ratio is 53.2. From equation 69:

$$\gamma = \frac{d/t_w}{10,000}(15 + 2.75\, d/t_w) = \frac{53.2}{10,000}[15 + 2.75(53.2)] = 0.858$$

The limiting moment in the flange during heat straightening, from equation 74, is:

$$M_f \le \frac{M_p}{3} = \frac{119}{3}\, ft - k = 39.7\, ft - k$$

The apparent jacking moment can be found from equation 79, if residual moments are included, as:

$$M_j \le \frac{1}{\gamma}\left(\frac{M_p}{3} - M_r\right) = \frac{1}{0.858}\left(\frac{119}{3} - 22\right) = 20.6\, ft - k$$

and the apparent jacking moment, if residual moments are neglected, is:

$$M_j = \frac{1}{\gamma}\left(\frac{M_p}{3}\right) = \frac{1}{0.858}\left(\frac{119}{3}\right) = 46.2\, ft - k$$

Based on the elastic analysis, equation 54, these moments translate to jacking forces, P_j, as follows:

For residual moments included:

169

$$P_j = \frac{4\,M_j}{l} = \frac{4(20.6)}{24} = 3.43\ k$$

For residual moments neglected:

$$P_j = \frac{4\,M_j}{l} = \frac{4(46.2)}{24} = 7.70\ k$$

3.3.5. Important Considerations

- Laterally deformed composite girders are complex, internally indeterminate structures.
- The primary damage mechanism following an impact is a plastic hinge at the impact point on the lower flange and a yield line on the web near the upper fillet.
- Secondary damage frequently occurs in the form of flange bulges at the impact zone, web bulges in the vicinity of diaphragms, and crushed or buckled diaphragms.
- The movement per repair heat is proportional to the magnitude of the jacking forces applied.
- The suggested heating pattern primarily consists of vee heats in the flange and line heats in the web. Strip heats in the web may be needed in special cases.
- Larger movements often occur as a result of the first heat, as opposed to successive heats, due to relieving residual moments in the girder.
- Over-jacking may produce hot mechanical straightening and lead to brittle fracture.
- Repetitive damage and repair cycles may lead to brittle fracture if impact results in high stress damage to the same local region, within 12 inches. Therefore, it is suggested that a composite girder with large strain ratios not be repaired more than twice. This point is discussed further in section 2.1.
- The moment induced in the lower flange by jacking forces can be computed using a distribution factor, γ, (equation 69).
- The plastic rotation per heat (equation 70) can be estimated by modifying the plate equation with a jacking ratio factor (equation 73) and a stiffness modification factor (equation 67).
- Calculation of the actual jacking force should include the web stiffening effect.
- For composite girders with intermediate diaphragms, unless residual moments are directly computed, the first two heats jacking force should be limited to a value that produces an actual flange moment, M_f, of 16 percent of the plastic moment, M_p.
- For composite girders with intermediate diaphragms, after the first two heats, jacking forces should be limited to values that produce an actual flange moment, M_f, of 33 percent of the plastic moment, M_p.

3.4. HEAT STRAIGHTENING TRUSS COMPONENTS AND OTHER AXIALLY LOADED MEMBERS

3.4.1. Introduction

The stress condition of a member plays a major role in its behavior during heat straightening. In some cases, the applied loads on a structure can be reduced such that member stresses are minor. However, for other cases, even after the removal of live loads, the dead loads carried by the member produce significant stresses. An example of such a case is a truss bridge, where dead load stresses in some members can range from 25 to 50 percent of the maximum service load stress. As such, the distribution of stress in a member should be examined prior to initiating heat straightening.

The dead load can have a neutral, positive or negative effect on heat straightening repairs depending on the type of damage, type of member being repaired, and orientation of the section. Consider the simply supported wide flange beam shown in figure 94, where dead loads produce weak axis bending in the section. If the section shown in the figure is damaged about its strong axis, but dead loads produce moments about the weak axis, the dead load stress has little effect on the movement of the section during heat straightening. However, if the damage results in weak axis bending in the section in the direction of the dead loads, then the applied heating pattern works against the dead loads. In this case, without the use of jacking forces to overcome the dead load moments, the straightening effect can be reduced or potentially eliminated. If the weak axis damage to the section, however, occurs in the direction opposite of the dead load, the movement during heat straightening is enhanced by the dead load.
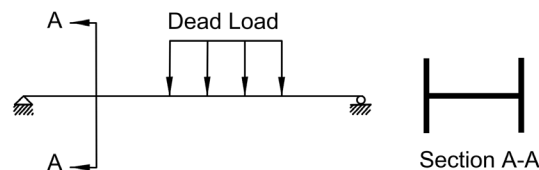
Source: FHWA

Figure 94. Illustration. Dead load conditions on a simply supported beam.

For columns and other axially loaded members, the P-Δ effect should be considered. Take for example the axially loaded member shown in figure 95. If the axially compressed member is damaged by lateral loads as shown in the figure, a moment is generated which is equal to P (axial load) multiplied by Δ (lateral deflection). This P-Δ moment is in the opposite direction to the moment generated by the applied jacking force during the heat straightening process. As such, if the lateral deflection is large, the moment due to the P-Δ effect could slow or completely restrain the restoration movement during heat straightening. In addition, the P-Δ moment can create an instability when the applied heat reduces the strength of the steel in the heated regions.

171
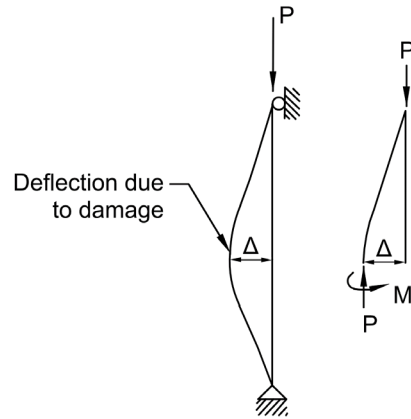
Source: FHWA

Figure 95. Illustration. P-Δ effect on an axially loaded column.

For truss members, the internal stresses in the section are typically axial tension or axial compression. Compressive stresses act as a positive constraint during heat straightening and can be expected to generate larger plastic rotations than if no compression was present. In contrast, tension would be expected to inhibit movement.

To investigate the behavior of axially loaded members during heat straightening repair, a series of tests were conducted by Avent et al. (1992). The purpose was to evaluate the P-Δ effect and magnitude of jacking force on the plastic rotations achieved during heat straightening of compression members. The configurations considered during testing were axial loaded members (compression members) subjected to damage about either the strong axis (category S) or weak axis (category W) of the section. Similar to the methodology used by Avent et al. (1992) for flexural members (discussed in section 3.2), the tests discussed below informed the development of equations that can be used to predict plastic rotations due to heat straightening and design heat straightening repairs for compression members.

Also discussed below is research by Morovat et al. (2014) on the topic of thermal creep and creep buckling of steel compression members at elevated temperatures. The role of creep and creep buckling for steel compression members, specifically members with high magnitude loading (relative to capacity), should be considered when approaching a heat-straightening repair.

3.4.2. Response of Axially Loaded Sections to Heat Straightening

Avent et al. (1992) conducted a study to investigate the response of two steel girders subjected to both axial load and heat straightening repair following damage. The two sections considered were an HP12×53 subjected to weak axis damage (category W) and a W10×39 subjected to strong axis damage (category S). During the repair, axial compression was applied to each section with a magnitude equal to 35 percent of the allowable axial load (per the nonregulatory AISC Steel Construction Manual, 1989). A total of 70 heating cycles were performed with jacking ratios ranging from zero to 50 percent. In addition, a zero jacking force sequence with an applied axial load of 17.5 percent of allowable axial load was also conducted in the case of the category W damage.

172

The specimens used by Avent et al. (1992) were 20 ft in length and rolled from A36 steel. In four cases, the members were damaged about the weak axis, while in three cases, the members were damaged about the strong axis. In all cases the damage was statically induced at the center of the member using hydraulic jacks. The test specimens were simply supported with diaphragms placed only at the ends (near the supports). No axial loads were applied during the damage process. Prior to heating, the axial force was applied to each specimen using tension rods attached to end plates on the members. Lateral jacking forces were applied using hydraulic jacks. The heating pattern used to repair the category S damage was a full depth, 30-degree vee heat on the web followed by a strip heat on the flange at the open end of the vee. The heating pattern used to repair the category W damage was a three-quarter depth, 45-degree vee heat on the flanges with a strip heat on the web. Both heating patterns used are typical of those used for category S and category W damage.

3.4.2.1 Heat Straightening Response of Columns with Category W Damage

As discussed above and shown in figure 95, following damage and applied axial load, a moment is generated in the member as a result of the P-Δ effect. A similar result was observed by Avent et al. (1992) following the application of axial compression to the damaged HP12×53 section. Since this P-Δ moment tends to impede the heat straightening process by magnifying the damage, the approach taken by the researchers was to effectively cancel the P-Δ moment with the application of a lateral jacking force. As suggested by Avent et al. (1992), the magnitude of the lateral jacking force should be adjusted to impose the typical specified jacking ratio for straightening flexural damage, plus an additional force to induce a moment to cancel out the P-Δ moment. As the damage curvature is removed, the P-Δ moment is reduced. As such, for each subsequent heating cycle, the jacking force should then be reduced to compensate for the reduced P-Δ moment.

Using this methodology, Avent et al. (1992) set the jacking ratios as the ratio of the moment at the center of the damage due to both the P-Δ effect and the jacking force, M, divided by the plastic moment capacity of the cross-section about the axis of damage, M_p. The HP12×53 with category W damage had an applied axial load, P, of 81.4 kips, producing a compressive stress of 5.25 ksi (35 percent of the maximum allowable compression of 15 ksi). For the first cycle of damage, a maximum deflection of 3.36 inches was obtained. From this, the applied axial load of 81.4 kips produced a P-Δ moment of 22.8 kip-ft at the point of damage, or 23.5 percent of the plastic moment, M_p. This moment is equivalent to the moment produced by a 4.56 kip lateral load at the point of damage. The lateral force used for a jacking ratio of 50 percent is 9.69 kips. Thus, to compensate for the P-Δ moment acting to hinder movement during straightening, the total jacking force used for the first heating cycle was the sum of these two values, or 14.25 kips. For each subsequent heating cycle, the jacking force was reduced to compensate for the reduced P-Δ moment (Avent et al., 1992).

To generalize the above test methodology, consider a simply supported beam-column with damage at an arbitrary location. For this scenario the applied jacking force, P_a, is:

$$P_a = P_j + P_{ec} \tag{80}$$

where P_j is the jacking force used to create a specified moment at the damage location as a percentage of M_p, or:

$$P_j = \frac{R_\ell L M_p}{ab} \tag{81}$$

where L is equal to the member length, a and b are equal to the distances between the left and right end supports and the applied jacking load, and R_ℓ is equal to the jacking ratio, M_j/M_p.

P_{ec} is the additional jacking force needed to cancel the P-Δ moment due to the axial load, P:

$$P_{ec} = \frac{LP\Delta}{ab} \tag{82}$$

The concept discussed above is illustrated in figure 96 where the stress distribution at the damaged cross section is shown before (figure 96-A) and after (figure 96-B) the jacking force is applied. Recall that the purpose of the jacking force is to create compressive stresses on the material at the open end of the vee. The P-Δ moment produces stresses that tend to reduce this compressive stress. In contrast, the application of the jacking force cancels the P-Δ effect and increases the compressive force at the open end of the vee.
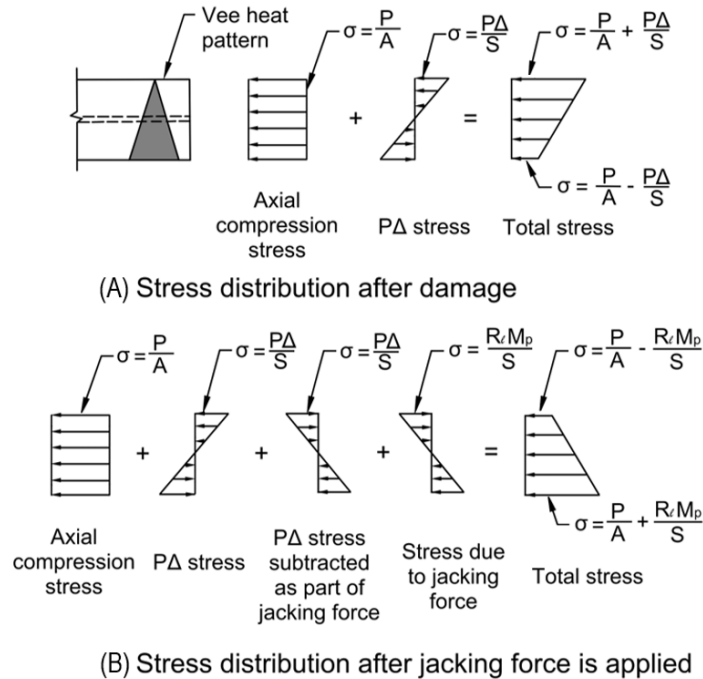
Source: FHWA

Figure 96. Illustration. Stress distribution in axially loaded section (A = cross section area and S = section modulus).

A series of heat straightening repairs were conducted by Avent et al. (1992) on HP12×53 sections with category W damage using a variety of jacking ratios. In all cases, including the zero load ratio cases, the total jacking force was a combination of a specified jacking force (a portion of the plastic moment capacity) and an additional load to cancel out the P-Δ effect. This additional load was recomputed after each cycle to reflect the reduced deflection as the girder

straightened. For each heating cycle, both flanges were heated simultaneously using 45-degree vees, followed by a strip heat on the web. For all cases, the magnitude of the applied axial load was 35 percent of the allowable (as mentioned previously) with the exception of case 4, in which the applied axial load was reduced to 17.5 percent of the allowable.

A summary of the experimental variables used and testing results obtained by Avent et al. (1992) are shown in table 22. For all reported values, both flanges were measured with average values presented in the table. In general, the plastic rotations of both flanges were similar. The response of section no. 1 to heat straightening is shown in figure 97 and was typical in form to all specimens tested with category W damage. For the case of zero jacking force in which the only jacking force used was that to cancel the P-Δ moment), there were several heats in which the resulting movement was in the opposite direction of that expected. However, successive heats produced more favorable movement tending to straighten the damage. This observed behavior illustrates a common phenomenon: small magnitude or reverse movements sometimes occur when small magnitude or zero jacking forces are used. It was suggested by Avent et al. (1992) that the probable cause of this behavior is the build-up of unfavorable residual stresses, which are relieved in successive heats. The researchers noted similar behavior in the category S damaged, axially loaded specimens when zero jacking force was used. This testing is discussed in the next section (section 3.4.2.2). In addition, similar behavior has been observed in other large-scale experiments and field repairs and is discussed further in chapter 2 and section 3.2.

Table 22. Summary of repair data for HP12×53 sections with category W damage and compression axial loads (Avent and Mukai, 1998).

Specimen	Number of Heats	Jacking Ratio	Axial Stress/ Allowable Stress	Maximum Stress[1] (ksi)	Minimum Stress[1] (ksi)	Average Plastic Rotation (milliard)
1	10	0.50	0.35	-32.8	22.4	5.54 (4.94)[2]
2	10	0.25	0.35	-19.0	8.58	3.85 (3.32)[2]
3	10	0	0.35	-5.22	-5.22	1.48 (1.27)[2]
4	10	0	0.175	-2.62	-2.62	0.64

[1] Tension is positive.
[2] Number in parentheses is average plastic rotation neglecting the first heat.
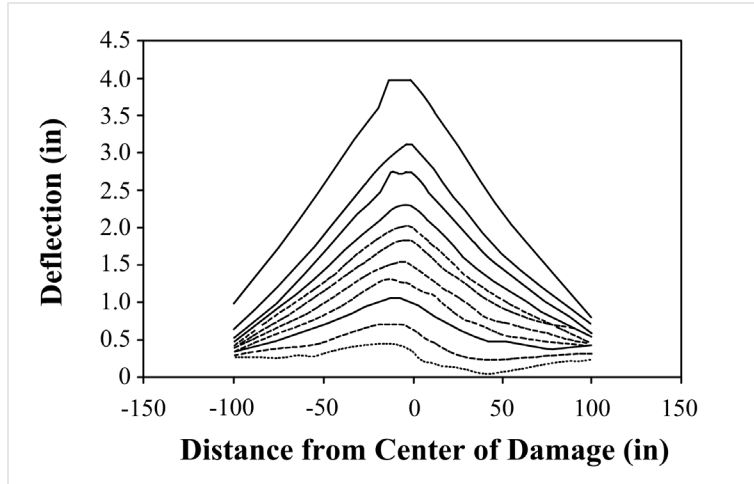
Figure 97. Graph. Deflection of one flange of HP12×53 over 10 heating cycles, section no. 1, 45° vee heat, 1,200°F heating temperature, and modified jacking ratio of 50 percent.

From these results, it was noted that the plastic rotations obtained during the first heat were exceptionally large. It was suggested by the researchers that the cause of this large movement was residual moments (stress) resulting from the induced damage. To compare the measured plastic rotations to the theoretical values discussed below (equation 84), the average plastic rotation was also computed excluding the first heat. These results are plotted in figure 98.
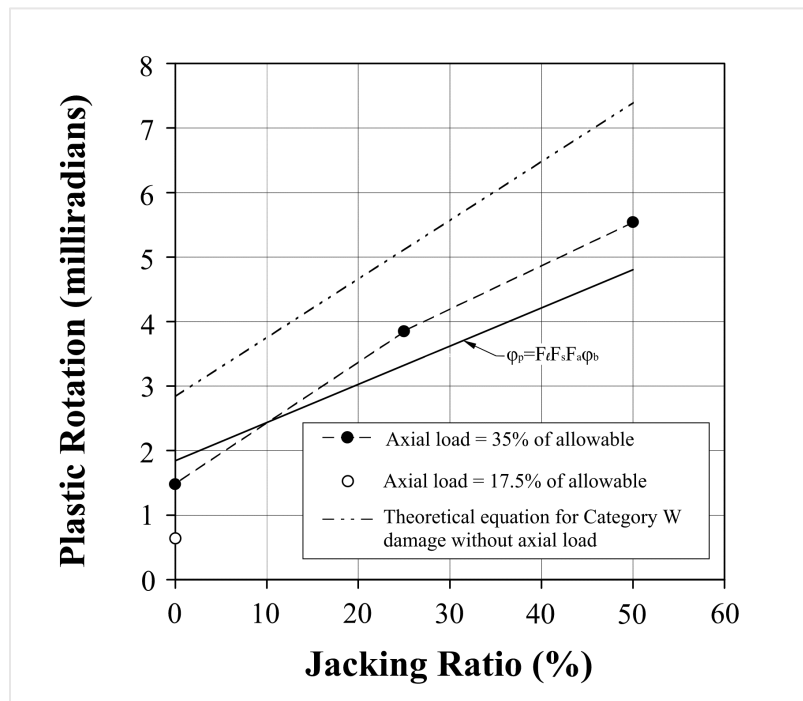
Figure 98. Graph. Plastic rotation versus jacking ratio for axially loaded category W damaged sections, 45° vee angle and 1,200°F heating temperature.

176

Also plotted in figure 98 is the theoretical plastic rotation for a beam without applied axial load based on the same parameters (equation 41). The plastic rotations measured by Avent et al. (1992) varied linearly with the jacking ratio, as shown in the figure. However, they tended to be smaller than those predicted by equation 41, for the same section without axial load. This was thought to be caused by the applied axial force, which tends to reduce the expected plastic rotation during heat straightening compared to sections without axial load. To compensate for this, Avent et al. (1992) and Avent and Mukai (1998) adjusted the equation for plastic rotation developed in section 3.2 using a modification factor. If the plastic rotation is proportionally reduced with higher axial loads, the stress factor, F_a, of equation 45 can be modified as:

$$F_a = [1 - 2\left(1 - \frac{2}{3}\frac{Z}{S}\right)\frac{M_j}{M_p}](1 - \frac{f_a}{F_{allow}}) \tag{83}$$

where f_a equals the axial compression stress in the member and F_{allow} equals the allowable axial stress.

The equation for plastic rotation is then:

$$\varphi_p = F_\ell F_s F_a \varphi_b \tag{84}$$

where F_ℓ is given by equation 47, F_s is given by equation 51, F_a by equation 83 and φ_b by equation 42. A plot of the theoretical plastic rotation for the HP12×53 is also shown in figure 98 and shows good agreement with the measured data.

3.4.2.2 Heat Straightening Response of Columns with Category S Damage

To study the behavior of beam-columns with category S damage during heat straightening repair, Avent et al. (1992) conducted a series of heat straightening repairs on W10×39 sections. The sections were subjected to category S damage and an applied axial load, and heat straightening using a variety of jacking ratios. The researchers found there was a tendency for lateral torsional buckling to occur during the damage phase due to the large load needed to induce strong axis damage to the full-scale specimen. As such, to prevent lateral torsional buckling of the section during the damage phase, the section was laterally braced at the one-third points. The bracing was removed during the repair sequence so as not to influence plastic rotation during heat straightening. A lateral load of 29 kips was used to induce a deflection of 1.70 inches on the initially straight section.

For the heat straightening repair, a vee angle of 30 degrees was used for all cases. The standard category S heating pattern was used, consisting of a web vee heat followed by a flange strip heat at the open end of the vee (see section 2.2 for further discussion). The damaged sections were not completely straightened in each test series, rather a series of heating cycles were conducted simply to capture the response of the section. A summary of the experimental data and average plastic rotations are shown in table 23 and plotted in figure 99. As mentioned previously, because the first heat after damage often results in larger than usual plastic rotations, this heat was not included in the average values shown (Avent et al., 1992).

Table 23. Summary of repair data for W10×39 sections with category S damage and compression axial loads (Avent and Mukai, 1998).

Specimen	Number of Heats	Jacking Ratio	Axial Stress/ Allowable Stress	Maximum Stress[1] (ksi)	Minimum Stress[1] (ksi)	Average Plastic Rotation (milliard)
5	10	0	0.35	-6.23	-6.23	1.15
6	9	0.25	0.35	-20.2	7.77	2.74
7	9	0.5	0.35	-29.9	17.5	4.93

[1] Tension is positive.
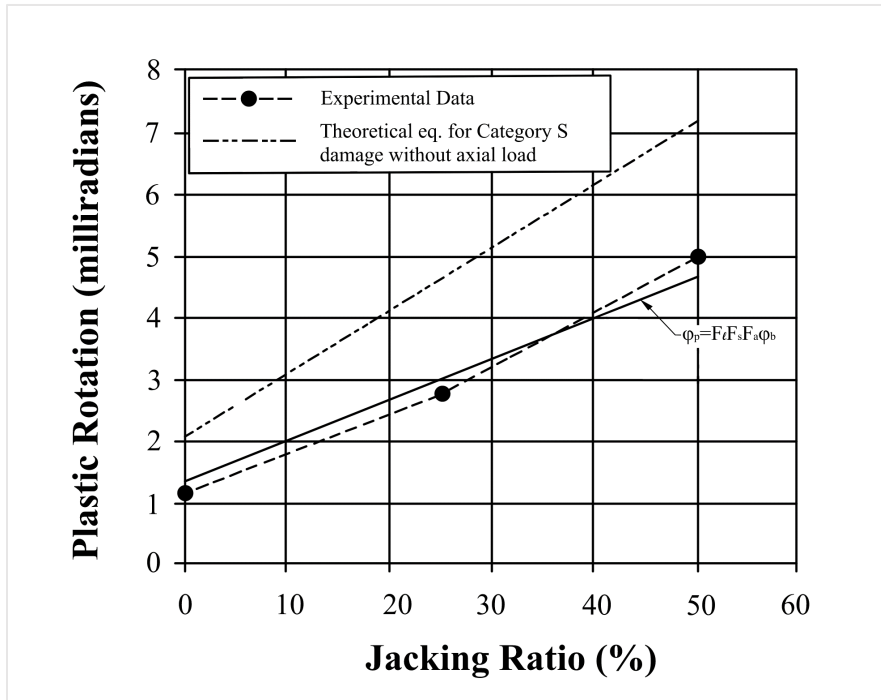
Source: Avent and Mukai (1998)

Figure 99. Graph. Plastic rotation versus jacking ratio for axially loaded category S damaged sections, 30° vee angle, 1,200°F heating temperature (Avent and Mukai, 1998).

Similar to the axially loaded sections with category W damage, plastic rotations for the sections with axial load and category S damage fell well below those predicted by the theoretical equation without axial load. As such, Avent et al. (1992) and Avent and Mukai (1998) used the same modification factor derived in section 3.4.2.1 (equation 83) for compression members with the category W damage to modify the plastic rotation equation (equation 84). The modified plastic rotation equation is plotted in figure 99 and agrees well with the experimental data. Based on this, both Avent et al. (1992) and Avent and Mukai (1998) suggest that equation 84 can be used to predict plastic rotations for repair of category S damaged, axially loaded compression members where F_ℓ is given by equation 47, F_s is given by equation 51, F_a by equation 83 and φ_b by equation 42.

3.4.3. Creep Effects on Axially Loaded Members

While the effects of creep in steel can be neglected in most cases of design, creep becomes an important factor when considering the performance-based design of steel elements exposed to elevated temperatures. Research on the topic of creep (i.e., thermal creep) in steel typically focuses on steel exposed to fire (Morovat et al. 2014). However, as discussed throughout this manual, the process of heat straightening involves the heating of steel to temperatures between 800°F and 1,200°F. These temperatures are captured within the temperature range considered in the research by Morovat et al. (2014) discussed below.

Creep buckling is the phenomenon in which the critical buckling load for a steel member is a function of load duration in addition to steel temperature and member slenderness. The effect of thermal creep (and the resulting creep buckling) on column capacity at elevated temperatures was studied by Morovat et al. (2014). In this study, the effect of creep on steel columns was investigated using two parallel experiments on W4×13 sections. The first experiment, which was referred to as the "Short-Time Buckling" test, studied columns with gradually increasing loads, producing constant displacement deformations, to determine the buckling load of columns heated to a specific temperature (1,112°F/600°C). This experiment illustrates the axial capacity of columns with reduced yield strength due to temperature, in addition to the effect of loading rate on maximum buckling load. The second experiment involved loading heated columns with a constant load, smaller in magnitude than the "Short-Time Buckling" test load, to determine the duration in which the load could be sustained by the heated column. This second experiment they referred to as the "Creep Buckling" test. The results from these two tests are shown in table 24.

Table 24. Experimental results for "Short-Time Buckling" and "Creep Buckling" on W4×13 Columns (Morovat et al., 2014).

Test Performed	Rate of Displacement (inch/minute)	Time-to-Buckling (min)	Buckling Load (kip)
Short-Time Buckling	0.01	—	63.0
Short-Time Buckling	0.05	—	67.8
Creep Buckling	—	5	61.0
Creep Buckling	—	9	58.0
Creep Buckling	—	12	56.0
Creep Buckling	—	53	55.0
Creep Buckling	—	85	54.0

Note: (—) indicates data not collected or calculated.

With these results, Morovat et al. (2014) note that buckling of a column is heavily dependent on not only the magnitude of the load but also the duration over which the load is applied and the rate of load application. The larger the load, the shorter the period in which that load can be sustained at an elevated temperature. While Morovat et al. (2014), note that further research is required and that their findings are preliminary and limited, the concepts of thermal creep and creep buckling are worth consideration when approaching heat straightening of axially loaded members. For members with light loading that are exposed to elevated temperatures for a short period of time, creep buckling is less of a concern than heavily loaded members exposed to elevated temperatures for long durations.

3.4.4. Summary

A series of full-scale tests were conducted by Avent et al. (1992) on both category W and category S damaged axially loaded members. Seven straightening procedures were conducted with at least 10 heat cycles used for each set of parameters. The axial load imposed during the straightening process was typically 35 percent of the allowable value. The jacking force was modified to cancel the P-Δ moment effect in addition to providing the specified jacking ratio. The plastic rotations measured during heat straightening for both cases were significantly less than that predicted for a wide flange beam without axial load. To accommodate this, a modified plastic rotation equation was developed to better capture the behavior of the axially loaded test specimens. The newly developed theoretical model (equations 83 and 84) agreed well with the experimental data (Avent et al., 1992; Avent and Mukai, 1998). The test results, plotted in figure 98 and 99, indicate that heat straightening can be successfully applied to axially loaded compression members. As shown in the figures, the plastic rotations observed varied linearly with the jacking ratio but tended to be smaller than those predicted for the same section without axial compression. From this observed behavior, Avent et al. (1992) concluded that axial force reduces the expected plastic rotation during heat straightening compared to scenarios without axial load.

Based on research by Morovat et al. (2014), the phenomenon of thermal creep can result in a reduced critical buckling load (creep buckling) for a column exposed to elevated temperatures as a function of load magnitude, load duration and loading rate. When approaching heat straightening of axially loaded sections, the concept of thermal creep and creep buckling should be understood. The magnitude of the applied axial load in the section being straightened combined with load duration and heating temperature should be carefully considered. For heavily loaded sections exposed to elevated temperatures for long durations, creep buckling is of more concern than lightly loaded sections heated for only a short period of time.

In summary, heat straightening can be effective for axially loaded sections using the same heating patterns as used for cases without axial loads. The movements during heat straightening tend to be smaller than cases with zero axial loads on the member. To improve the behavior of axially loaded sections during straightening, when designing the repair, the specified jacking forces used should include, at a minimum, a component producing a moment to cancel the P-Δ moment created by the axial load on the damaged section. Once the jacking force is calculated, the expected plastic rotation can be calculated prior to heating using equations 83 and 84.

3.4.5. Important Considerations

- Heat straightening can be effective for axially loaded members using the same heating patterns used for members without axial loads.
- The movements during heat straightening of an axially loaded section tend to be smaller than for the same section without axial load.
- The jacking forces used should include, at a minimum, a component producing a moment at the damaged section equal and opposite to the moment produced by the axial force acting on the damaged section (P-Δ effect). As straightening progresses, the Δ becomes smaller and the jacking force to compensate for the P-Δ is reduced.

3.5. HEAT STRAIGHTENING REPAIR OF LOCALIZED DAMAGE

3.5.1. Introduction

Damage in steel members, typically caused by an impact, can be broadly classified as either global or local damage. Global damage is characterized by the deformation of both the primary and stiffening elements of a section within and extending beyond the impact region. In contrast, local damage is characterized by deformations occurring only in the region of impact, deforming either the stiffened or unstiffened elements of a section. Examples of local damage include small bulges, bends, or crimps in single elements of a cross section.

Two frequently encountered patterns of local damage are flange and web bulges (figure 100). Flange bulges are associated with local damage to unstiffened cross section elements such as the flange of a girder. Web bulges are associated with local damage to stiffened cross section elements such as the web of a girder. Both flange and web bulges are categorized as category L damage, but two sub-classifications are used to distinguish between the two types: category L/U for local damage to unstiffened elements, and category L/S for local damage to stiffened elements. For the heat straightening repair of these types of damage, different methodologies are used.
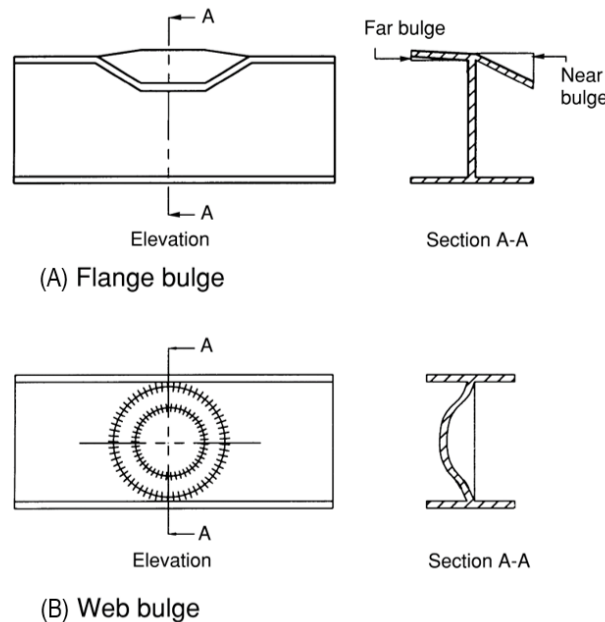
Source: FHWA

Figure 100. Illustration. Typical localized damage classified as category L.

In general, heat straightening studies have focused on global categories of damage and repair such as strong and weak axis damage and twisting. The repair of localized damage is often ignored. As a result, localized damage is often repaired improperly by various combinations of cold mechanical straightening, hot mechanical straightening, and heat straightening.

In cold mechanical straightening, the steel is restored to its original shape by applying external loads in excess of the plastic capacity of the section while the steel is still at ambient temperature. In forging, the steel is heated to very high temperatures, often greater than 1,600°F, causing a severe reduction in yield strength and plastic capacity. External forces are then used to straighten the steel. The forces used are smaller than those used in cold mechanical straightening but are still in excess of the yield capacity of the heated steel. Both methods involve straightening steel by mechanical means. As a result, these techniques may involve strain hardening, which results in a loss of ductility and increased brittleness in the steel. An alternative to this is repair via heat straightening, which does not involve external forces in excess of the yield capacity of the section. This chapter discusses the repair of local damage using heat straightening and provides general repair methodologies.

Local damage patterns display common characteristics: large plastic strains (usually tensile) in the damaged zone and bending of plate elements about their weak axes. To repair the local damage, shortening should be induced in the damaged area equal to the elongation caused when the element was damaged. In addition, the distortion along the yield lines must be removed. Studies on global damage repair have shown that vee-heated regions shorten significantly during cooling and that line heats can be used to induce bending about the yield lines. Thus, a combination of line and vee heats can be used to repair localized damage.

This section describes the basic procedures for heat straightening repair of localized damage in structural sections using results from experiments conducted by Avent and Mukai (1998). In that work, stiffened and unstiffened elements were subjected to damage in a laboratory setting. Although the resulting damage tended to be more symmetrical and less severe than sometimes encountered in practice, the repair procedures used and discussed illustrate the general principles for the repair of localized damage. The heating patterns suggested can be adapted to the more complex and irregular damage patterns often found in practice.

3.5.2. Category L/U – Experimental Damage and Repair

3.5.2.1 Category L/U Damage Behavior

As discussed above, category L/U damage is characterized by deformations in unstiffened elements of a section (such as a flange bulge). The damage shown in figure 101 was observed during a heat straightening project executed in New York State.

Source: Nathan Hackmeister, 2021

Figure 101. Photo. Typical category L/U damage.

Category L/U damage is typical in cases where the impact takes place on a plate element with one free edge, such as the flange of a beam. Figure 102 shows the typical flange bulge pattern characteristic of category L/U damage. Often, with this type of damage, distinct yield lines are formed as well as some zones of flexural yielding where curvature is the highest.
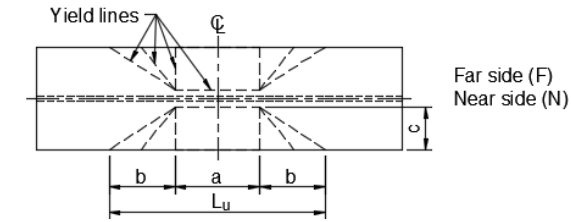
(A) Top view of damaged flange
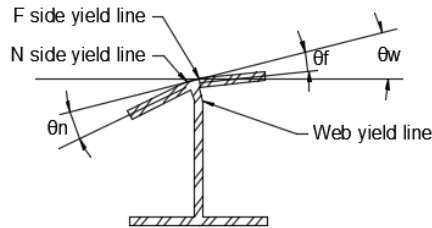
(B) Section through damaged zone
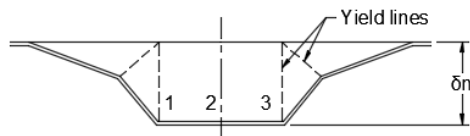
(C) Edge view of flange on side N
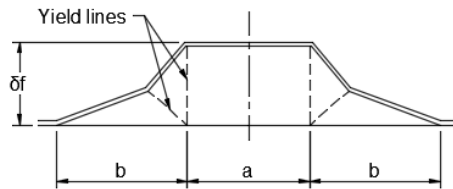
(B) Edge view of flange on side F

Source: FHWA

Figure 102. Illustration. Heat straightening local flange damage (category L/U).

Considering figure 102 above, the impacted side of the damaged flange is referred to as the near side (N). The non-impacted side of the same flange, referred to as the far side (F) of the flange, will also typically incur damage. This damage has a geometry similar to that of side N, but usually of lower magnitude.

The damaged flange typically undergoes rotation about a clearly defined yield-line near the rolled fillet of the web ("k" region in AISC diagrams). Side N of the flange usually deforms in a folded plate pattern, as shown in figure 102-B, where the flange has deformed toward the web. The deformation usually results in yield lines which define the edges of the folded plate (figure 102-C). In some cases, particularly in regions of high curvature, the deformation pattern may be more akin to a flexural yield surface than a series of yield lines. Yield surfaces result from plate element flexure and tend to spread over the surface of the element (e.g., flange) as the degree of

damage increases. The other half of the same flange, side F, usually deforms in a similar pattern in the opposite direction. The damage pattern on side F, shown in figure 102-D, tends to be of a smaller magnitude. As such, δ_n is larger than δ_f (where "n" subscript denotes near side or impacted side and "f" subscript denotes far side or non-impacted side, typical throughout section 3.5.2).

Because the web is often thinner than the flange, a yield line forms in the web near the fillet. The section shown in figure 102-B illustrates this behavior. The tee section at the flange and web juncture remains close to a right angle. The yield line forming in the web fillet allows this tee to rotate through an angle θ_w. The yield line at the flange fillet on the impacted side of side N results from the additional rotation, θ_n, thus the total rotation of side N is θ_w plus θ_n. The other half of the flange, side F, tends to resist rotation; thus, a second flange yield line may form at the F side fillet. The angle formed by this yield line is θ_f, and the rotation of the non-impacted side of the side F flange is θ_w minus θ_f.

3.5.2.2 Category L/U Damage Assessment

Local damage to a member is often minor, typically characterized by small bulges and deformations in the section. However, if severe, local damage can cause a reduction in a structure's load carrying capacity. The reduction in load capacity can be caused by either a local reduction in section properties (moment of inertia, section modulus, etc.), resulting in reduced bending strength, or by local buckling, resulting in instability under a compressive load.

In general, four values can be used to define flange bulge geometry as shown in figure 102. The values are: (1) maximum out-of-plane deflection of the bulge, δ, (2) original length of the free edge of the bulge, L_u, (3) width of the bulge, c, and (4) length of the free edge after damage, L_d, which can be approximated by:

$$L_d = [a + 2(\delta^2 + b^2)^{1/2}] \tag{85}$$

It should be noted that this is not the exact length of the damaged free edge since the small curvatures are neglected.

From this, two parameters can be used to classify the degree of damage based on the geometry. The parameters are: (1) span/deflection ratio, and (2) flange edge elongation. Span/deflection ratio is defined as the ratio of the length over which damage occurs, L_u, to the out of plane deflection of the bulge, δ, where:

$$L_u = a + 2b \tag{86}$$

The severity of damage varies inversely with the span/deflection ratio. Flange edge elongation ($L_d - L_u$), as a result of damage, is defined as the shortening required at the free edge of the bulge to restore the flange to its undamaged shape. The average plastic strain at the free edge, a function of flange elongation, is given by:

$$\varepsilon_d = \frac{(L_d - L_u)}{L_u} \tag{87}$$

A large average plastic strain indicates extensive local damage.

3.5.2.3 Experimental Methods and Results

The repair of local damage, category L/U, was investigated by Avent and Mukai (1998) through a series of experiments on damaged wide flange sections. The goal of their work was to evaluate heating patterns for repair of category L/U damage through experimental damage and repair of W8×13 beams.

To induce local damage in the flange of the beams, Avent and Mukai (1998) applied load to the section through a spreader plate as shown in figure 103-A. Stiffeners were placed 15 inches apart in order to limit the damage to the immediate vicinity of the load application. Four beams were damaged using this method with a maximum deflection in the flange of approximately 1 inch. During load application and damage, a series of yield lines formed in the damaged flanges of the beams, as shown in figure 103-B, typical for category L/U damage. For all four beams, the load producing the yield pattern shown in figure 103 was approximately 30 kips.
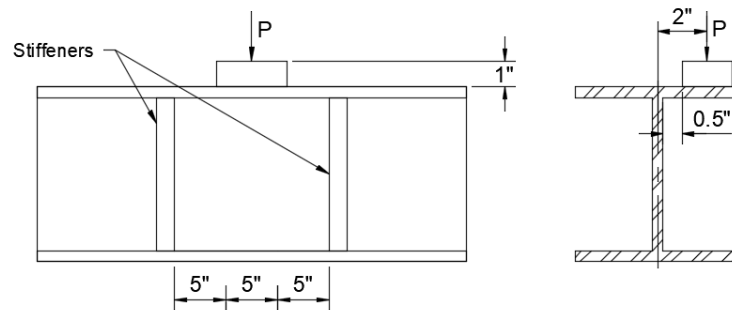
(A) Setup for inducing flange damage
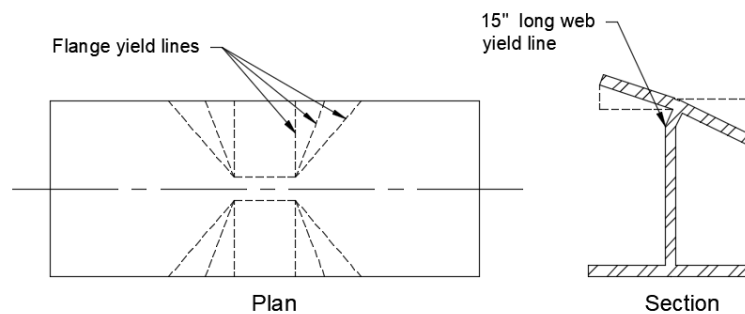
(B) Yield zones for typical flange bulge

Source: FHWA

Figure 103. Illustration. Damage induced by Avent and Mukai (1998) to produce a bulge in the flange of a W8×13 beam specimen.

During repair, to measure the effect of the heat straightening, the researchers utilized the portion of the flange edge at which the maximum deflection occurs, δ_n or δ_f, illustrated in figure 102.

Rather than considering deflection at a single point, however, deflections at three locations (points 1, 2, and 3 in figure 102-B) were averaged. These average deflections were designated as Δ_n and Δ_f. A summary of the flange damage from these experiments is compiled in table 25 (Avent and Mukai, 1998).

Table 25. Configuration of flange damage for category L/U repairs in W8×13 beams (Avent and Mukai, 1998).

Beam	Max. Load (kips)	Max. Deflection (in)		Near Side (Side N)		Span/ Deflection Ratio, L_u/Δ_u	Elongation at Flange Edge			
		Δ_n	Δ_f	a (in)	b (in)		Side N		Side F	
							Length (in)	Multiple of ε_y	Length (in)	Multiple of ε_y
1	32	0.78	0.66	5	5	19.2	0.121	6.5	0.087	4.7
2	29	1.07	0.73	5	5	14.0	0.226	12.2	0.106	5.7
3	27	0.96	0.73	5	5	15.6	0.183	9.8	0.106	5.7
4	32	0.85	0.65	5	5	17.6	0.142	7.7	0.084	4.5

To evaluate the performance of various repair methodologies, Avent and Mukai (1998) conducted repairs to the local damage induced in the beam specimens using a variety of jacking forces and heating patterns. As discussed in previous sections of this manual, one of the fundamental concepts of heat straightening is to heat only the yielded regions of a damaged section. In the case of local flange damage, these zones can include a series of yield lines and some yield surfaces on the flange. Yield lines are often distinct and easy to identify. However, sometimes yield lines merge and form a surface of continuous plastic flexural curvature. This behavior was observed by Avent and Mukai (1998) where yield lines in the flange were difficult to distinguish and flange elongation was substantial. Strain at initial yield for A36 steel, ε_y, is 0.00124. The average plastic strain observed by the researchers over the 15-inch damaged length, shown in table 25 as multiples of ε_y, ranged from 5 to 12 times ε_y. This magnitude of plastic strain indicates significant plastic behavior in the damaged region. Thus, as a result of the extensive damage observed (significant plastic behavior and flange elongation) it was concluded that most heats applied to the outer portion of the flange would fall within the yield zone and application of heat during straightening could be focused in this area.

Based on the type of yield surface observed, Avent and Mukai (1998) concluded that a variety of heating patterns could be applicable. However, two key observations were made: (1) the sharp curvatures at yield lines required straightening, and (2) flange shortening must occur to allow the longitudinal plastic strain to be removed. From this, the researchers concluded that line heats should be placed at all yield lines. For the yield surfaces, the longitudinal contraction may be accomplished using half-depth vee heats on the flange with the apex located at the yield line near the web-flange juncture, and/or additional line heats in these regions as needed.

After preliminary experimentation, Avent and Mukai (1998) found that four key variables play a significant role in heat straightening local damage. The first is the external restraining force. Consideration was given to the magnitude of the restraining force and whether jacking on just the near side of the flange or both sides is most effective. The second variable is vee heats on the flange. Three cases were considered: (1) no vee heats, (2) vee heats on the near side only, and (3) vee heats on both the near and far sides. The effect of vee angle was also investigated with both

20- and 45-degree vees evaluated. The third variable is flange line heats. Again, three cases were considered: (1) no line heats, (2) line heats on the near side, and (3) line heats on both sides. The fourth variable is a web line heat. The web yield line resulting from typical damage is usually distinct and is located near the web fillet. The web line heat was applied to this yield line.

These four parameters were varied by Avent and Mukai (1998) during the heat straightening of the four damaged W8×13 beams described in table 25. Plots of the near and far flange deflections after each heating cycle are shown in figures 104-107 with the specific heat straightening parameters used for each cycle noted at the top of the figures. From these results, Avent and Mukai (1998) concluded that specific combinations of these four heat straightening parameters are much more effective than others. The effectiveness of these combinations was ranked by the researchers. This is illustrated in figure 108. Of these, the three most effective combinations had the following in common:

- A restraining force was applied to both the near and far sides of the flange.
- Flange line heats were applied to both the near and far sides of the flange on the convex surface.
- A line heat was applied to the web on the convex surface.

Heat Number	0-8	8-11	11-13	13-14	14-17	17-18	18-25	25-28
Jacking Location	N	B	B	N	N	B	N	N
Vee Location	N	B	B	N	N	B	N	N
Flange Line Heat Location	N	B	B	N	N	B	N	N
Web Line Heat	n	y	y	n	y	y	y	n
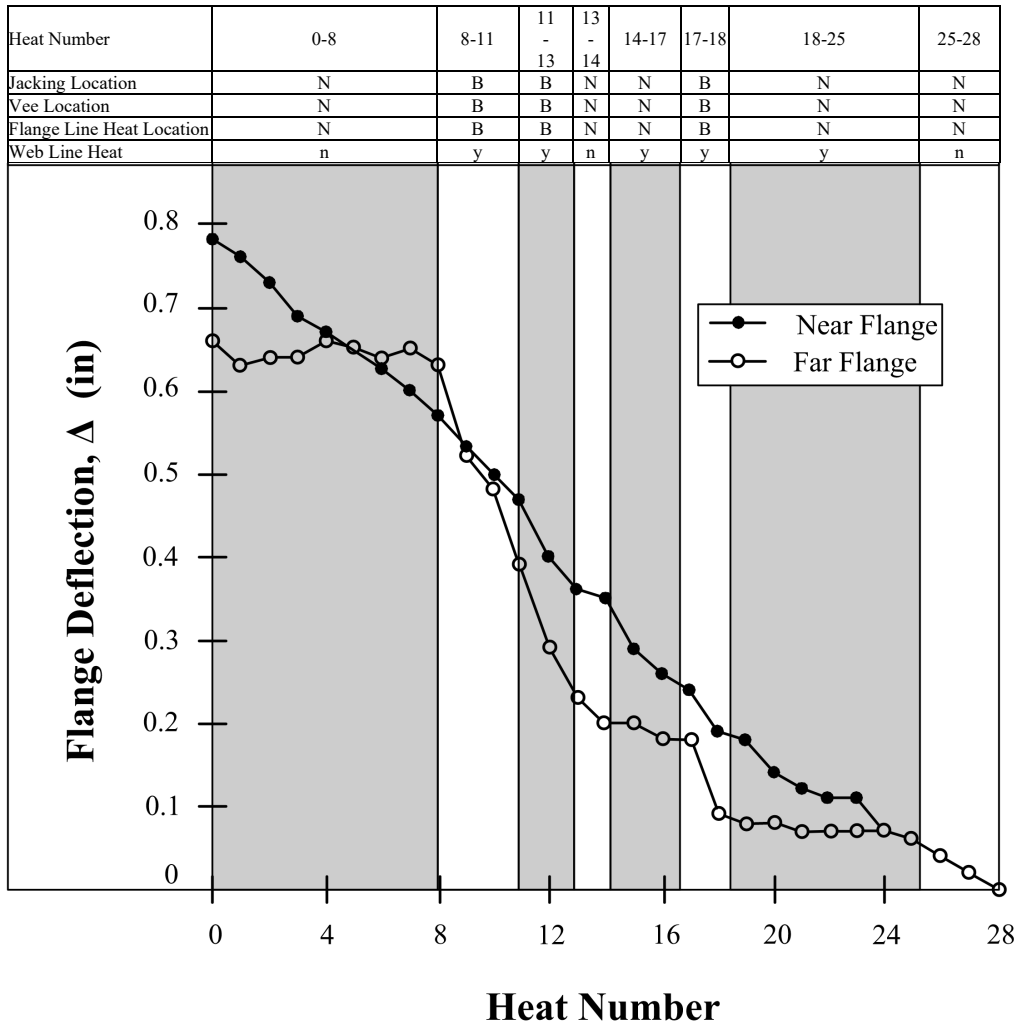
Source: Avent and Mukai (1998)

Figure 104. Graph. Flange movements for various heating patterns, beam no. 1 with category L/U damage (N and B refer to near and both sides of the flange, respectively; y and n refer to yes and no, respectively).

Heat Number	0-2	2-3	3-4	4-5	5-6	6-13	13-14	14-17	17-18	18-20	20-21	21-22
Jacking Location	N	B	B	N	B	N	B	N	B	N	N	B
Vee Location	N	N	B	N	B	N	B	N	B	N	B	B
Flange Line Heat Location	N	N	B	N	B	N	B	N	B	N	B	B
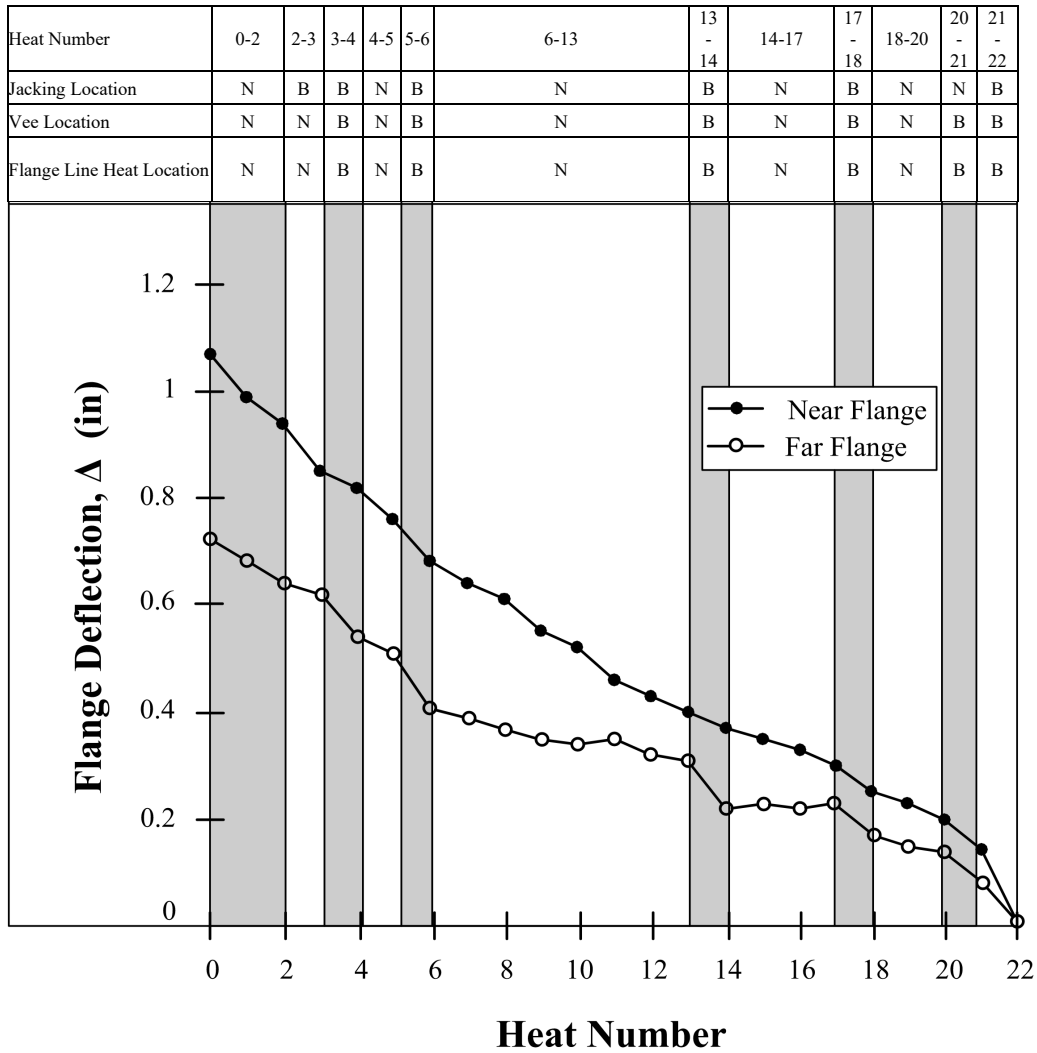
Source: Avent and Mukai (1998)

Figure 105. Graph. Flange movements for various heating patterns, beam no. 2 with category L/U damage (N and B refer to near and both sides of the flange, respectively).

Heat Number	0-3	3-4	4-5	5-8	8-9	9-10	10-11	11-12	12-13	13-15	15-16	16-17
Jacking Location	N	N	N	B	N	N	B	B	B	N	B	N
Vee Location	N	N	N	B	–	–	B	–	B	–	B	N
Lines	–	N	N	B	N	N	B	N	B	N	B	N
Web Line Heat	n	y	n	y	n	y	y	y	y	n	y	y

Source: Avent and Mukai (1998)

Figure 106. Graph. Flange movements for various heating patterns, beam no. 3 with category L/U damage (N and B refer to near and both sides of the flange, respectively; y and n refer to yes and no, respectively).

191

Heat Number	0-1	1-2	2-3	3-4	4-6	6-7	7-8	8-9	9-10	10-11	11-12	12-13	13-14
Jacking	N	B	N	B	N	N	N	B	N	N	N	N	N
Flange Heat	N	B	N	B	N	–	–	B	N	B	N	N	N
Web Line Heat	n	y	y	y	y	y	y	y	n	n	y	y	y
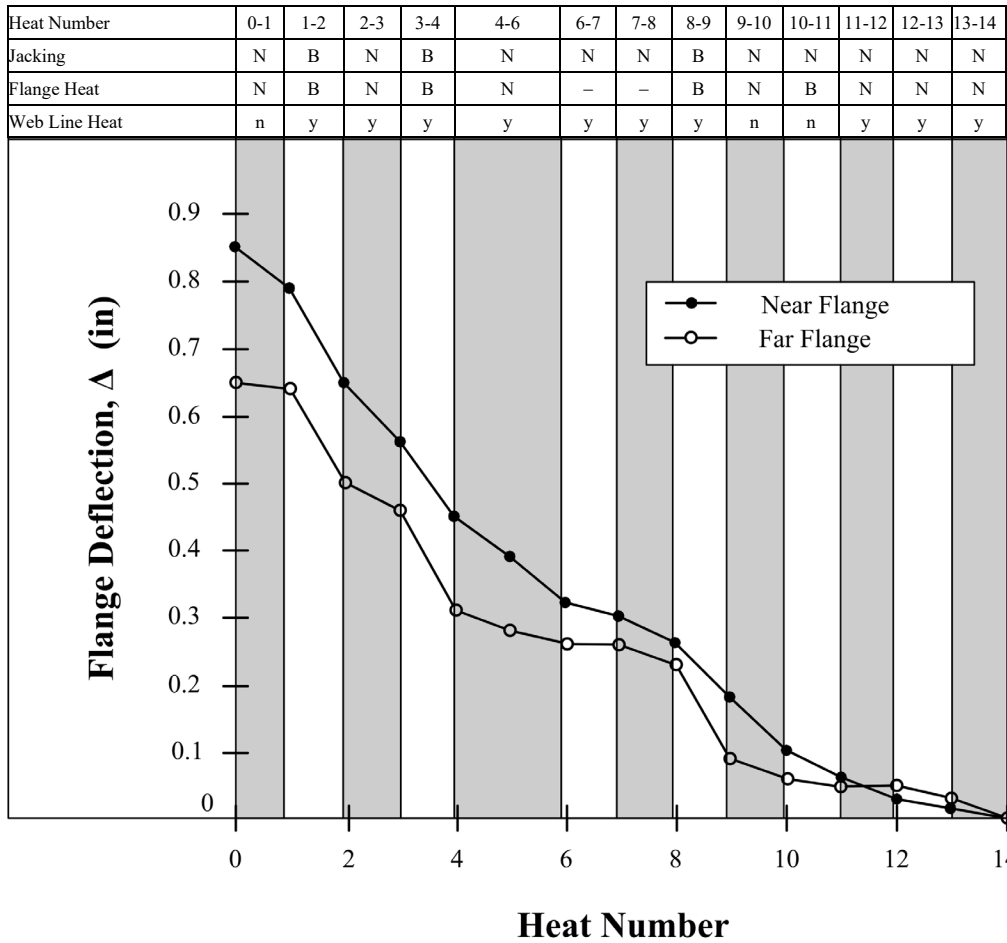
Source: Avent and Mukai (1998)

Figure 107. Graph. Flange movements for various heating patterns, beam no. 4 with category L/U damage (N and B refer to near and both sides of the flange, respectively; y and n refer to yes and no, respectively).

Heating Configuration		1	2	3	4	5	6	7
Jacking Location and Magnitude per Side (kips)	Damaged Side	–	–	–	3.5	3.5	3.5	3.5
	Both Sides	3.5	3.5	3.5	–	–	–	–
Vee Heat and Angle (degrees)	Damaged Side	–	–	–	–	45	45	20
	Both Sides	–	20	45	–	–	–	–
Flange Line Heat	Damaged Side	–	–	–	Yes	Yes	Yes	–
	Both Sides	Yes	Yes	Yes	–	–	–	–
Web Line Heat		Yes	Yes	Yes	Yes	Yes	–	–
Number of Heat Cycles		3	7	11	7	25	12	3
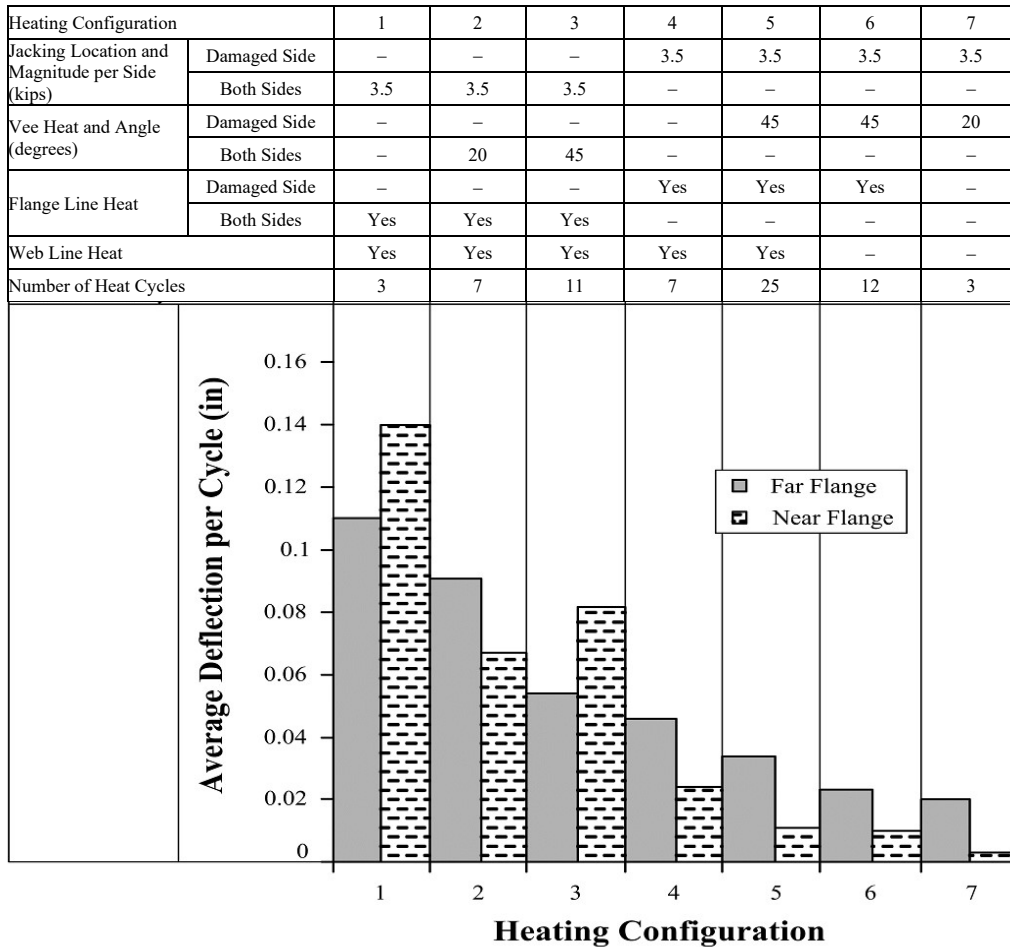
Figure 108. Graph. Average flange deflection (movement) per heating cycle for the most effective repair patterns (3 cycles minimum), category L/U damage.

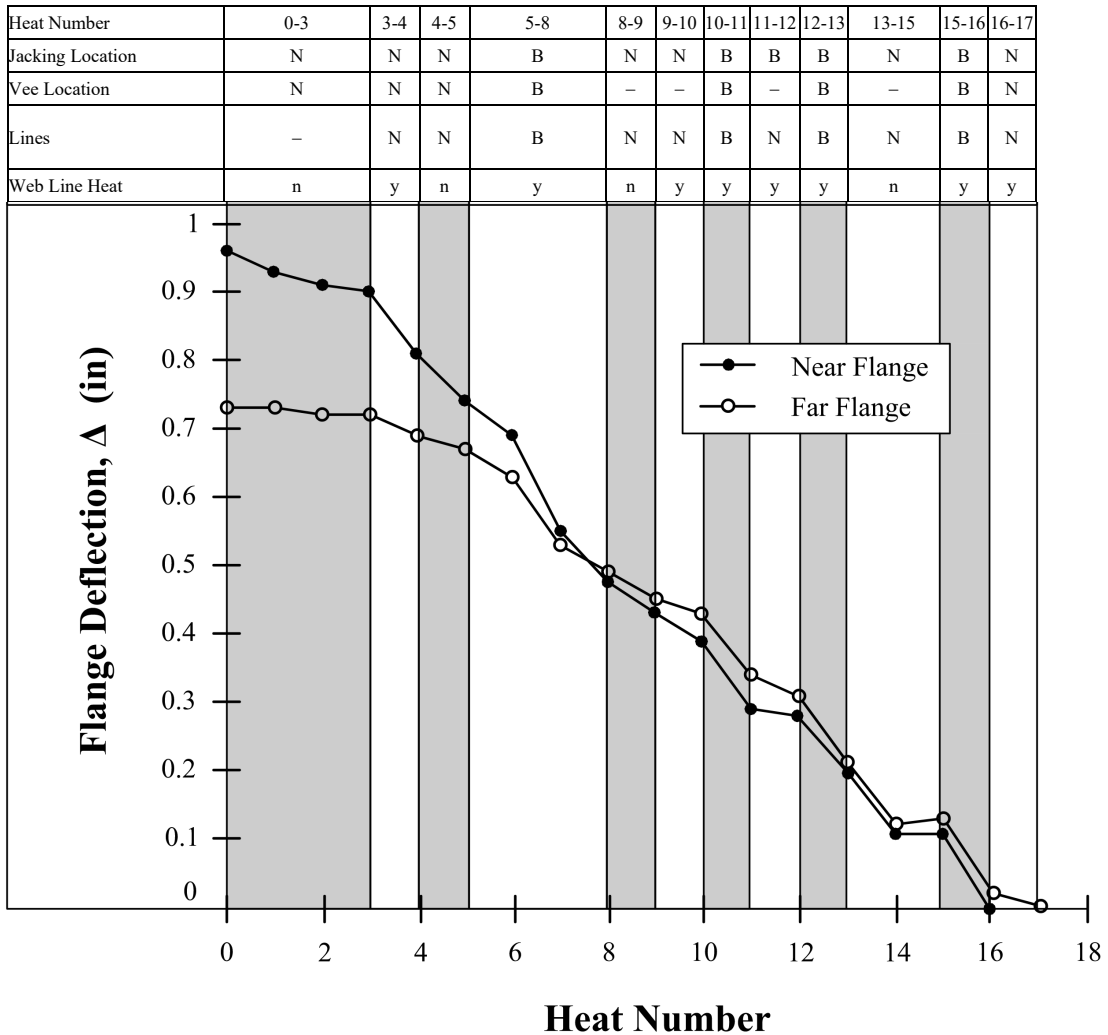An observation of note, illustrated in figures 104-108, was the response of the beams to flange vee heats. Avent and Mukai (1998) found that the "near side movements were inversely proportional to the size of the vees with the most effective pattern being the with line heats only and no vee heats." The use of two 20-degree vees in combination with the line heats on both sides of the flange was 20 percent less effective than the pattern with line heats only. The use of 45-degree vees combined with line heats was 50 percent less effective. The far side flange movements followed a similar pattern, although repairs that used 45-degree vees produced slightly more movement than that with 20-degree vees. This observed behavior illustrates an important heat straightening principal discussed throughout this manual: excess heat can reduce the effectiveness of a heat straightening repair. The heat straightening process depends on heating small areas that are surrounded by cool areas. By superimposing vee heats and several line heats, the internal restraining effect typically provided by the cool steel is reduced. Thus, the most effective patterns are those concentrated on the damaged region of the flange only.

Based on the results from this work, Avent and Mukai (1998) developed a general repair procedure for category L/U damage. This procedure uses the findings from the experiments discussed in this section to capture a general repair methodology applicable for most category L/U damage scenarios. This methodology is discussed in the following section.

3.5.3. Category L/U – Repair Methodology

The specific heating pattern used for repair depends on the details of the damage geometry. A typical cross section subjected to category L/U damage is shown in figure 102-B. There are three components of rotation: (1) the web-flange juncture, which remains at right angles and has a rotation, θ_w, resulting from rotation about the web yield line; (2) the near side flange, N, which has a maximum rotation, θ_n, resulting from additional rotation about the flange yield line; and (3) the far side flange, which has a reduced rotation, θ_w minus θ_f, resulting from the resistance of flange F to rotation caused by forces applied to flange N.

The heating and jacking pattern used to straighten this damage depends on how the section geometry changes as heat straightening progresses. Because there are many possible damage shapes and configurations, specific procedures cannot be established. Rather, this section outlines a typical procedure for the repair of category L/U damage. The repair procedure discussed is based on the findings of the experimental work conducted by Avent and Mukai (1998), detailed in section 3.5.2.

The typical repair procedure is broken into two phases of repair, phase I and phase II. Since the exact repair procedure used is dependent on how the section geometry changes during heat straightening, in some cases only phase I will be needed to complete the repair. Other cases, however, may require additional phases to complete the repair. In these cases, the second repair phase, phase II, is broken down into two paths based on damage geometry and section behavior during phase I. Considering this, the procedure discussed below is intended to capture a general repair procedure that can be applied to a variety of category L/U damage cases. Engineering judgment should be used in applying this methodology to specific cases.

3.5.3.1 Phase I: Initial Heating and Jacking Patterns

The specific parameters to consider for phase I repair are: (1) restraining forces, (2) vee heats, (3) flange line heats, and (4) web line heats. The selection of these parameters, detailed in the following paragraphs, is based on the results from research conducted by Avent and Mukai (1998), discussed in detail in section 3.5.2.

For maximum movement per cycle, restraining (jacking) forces should be placed on both the near (N) and far (F) sides of the damaged flange in the direction tending to restore the flange to its original condition (Avent and Mukai, 1998). As illustrated in figure 109-A, a convenient arrangement on the near side is to place a restraining force, P_n, between the top and bottom flange. The far side restraining force, P_f, requires a clamping type force which is often more difficult to arrange in field applications. If the clamping force cannot be anchored from the opposite flange, a spreader beam arrangement can be used, as shown in figure 109-D, to anchor the clamping force to the straight portions of the far side flange. Another alternative is to only restrain (jack) the near side flange. However, for cases with near side restraining forces only, the

average movement per heat straightening cycle tends to be lower than similar cases with restraining forces on both sides (Avent and Mukai, 1998).

(A) Phase I, initial geometry after damage

(B) Phase II, geometry if $\theta_n = 0$

(C) Phase II, geometry if $\theta_f = \theta_w$

(D) Spreader beam arrangement for applying clamping force to far side bulge
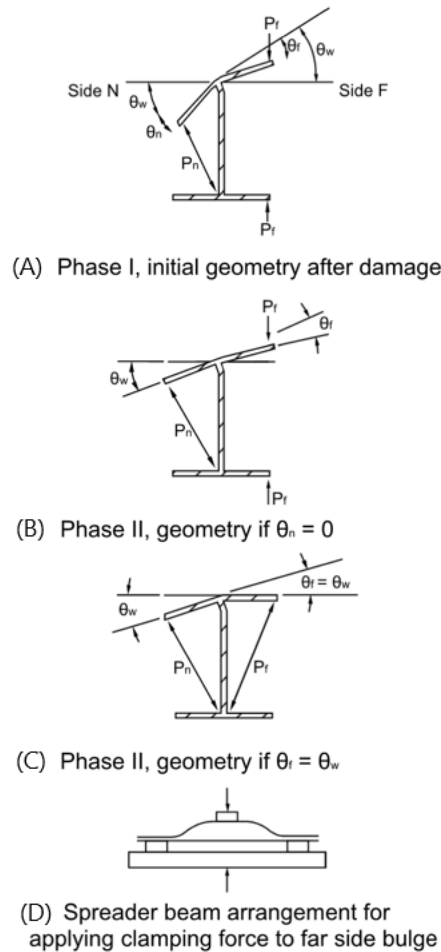
Note: Deflection exaggerated for illustrative purposes
Source: FHWA

Figure 109. Illustration. Arrangement of restraining forces during various stages of repair.

Based on the experiment results discussed in section 3.5.2, Avent and Mukai (1998) concluded that the use of vee heats is not always necessary to repair (straighten) category L/U damage. However, the researchers suggest that a limited number may be used to assist in the flange shortening effort that is required to complete the repair. In these cases, Avent and Mukai (1998) state that vee heats should be approximately half depth and applied to both the near and far sides of the flange to eliminate global curving of the member. The vees should also be narrow with an angle of 20° or less, and oriented such that the open end of the vee is at the flange edge. It is best to place the vee heats in regions where no line heats are required, as mentioned in section 3.5.2, since excessive heat can hinder straightening efforts. In the same context, no more than two vees should be used in one heating cycle (one vee is preferable). Finally, the vee heat location should be shifted with each heating cycle, so the same location is not re-heated for at least three cycles. A typical arrangement of vee heats, as per Avent and Mukai (1998), is shown in figure 110-B.

(A) Typical flange line heat pattern

(B) Vee heat patterns

(C) Web line heat pattern
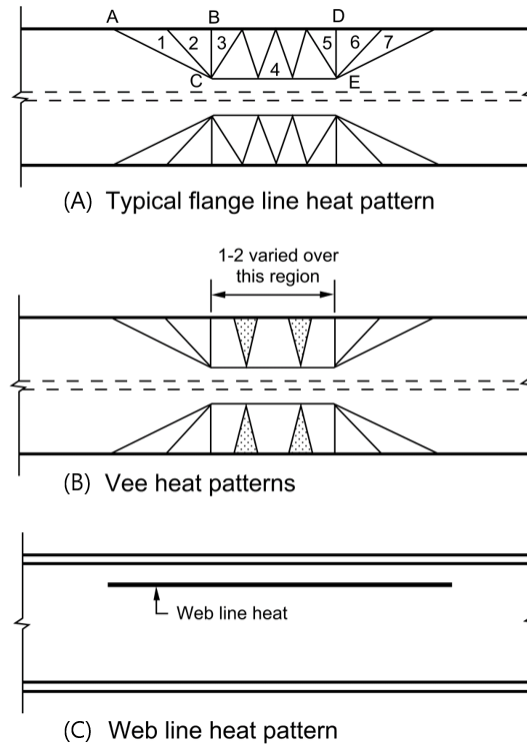
Source: FHWA

Figure 110. Illustration. Arrangement of vee and line heats used to repair local damage.

For the flange yield lines, Avent and Mukai (1998) state that line heats should be applied on the convex surface, if practical, after the application of any vee heats. A typical line heat pattern is shown in figure 110-A. For yield surfaces of continuous plastic strain, often occurring in regions such as ABC in figure 110-A, line heats should be spaced over the section at a spacing of approximately $b_f/4$ where b_f is the flange width. Additionally, line heats may also be used instead of vee heats in section BCDE. The order of the line heat application tends to have only a minor impact on heat straightening results. However, the yield lines at the locations of the most severe damage are typically heated first. Similarly, it is suggested to heat the near side yield lines prior to the far side (Avent and Mukai, 1998).

Lastly, the web yield line should be heated using a line heat. Based on the results from the experiments discussed in section 3.5.2, Avent and Mukai (1998) suggest that the web yield line be heated last, after the vee heats and the flange line heats are completed. The web yield line is typically located at or near the web-flange juncture or fillet as illustrated in figure 110-C.

These four steps, (1) restraining force, (2) vee heat, (3) line heat, and (4) web line heat, complete the phase I repair cycle. In many cases, the phase I procedure can be used to fully repair the section by repeating the cycle until the flange is straightened within the tolerance specified by the engineer. However, depending on the progress of the movement and the geometry of the damage, phase II repairs may be required to correct over-straightening of either the near (N) or far (F) side flanges following the phase I repair cycles. These secondary repairs, as a function of damage geometry, are discussed in the following sections.

196

3.5.3.2 Phase II: Heating and Jacking Patterns if $\theta_n = 0$ or $\theta_f = 0$

During the phase I repair cycles, depending on the movement of the section during straightening, it is possible for over-straightening (or overcorrecting) to occur on the near and far sides of the flange. Should the movement of the damaged flange progress too quickly, then θ_n or θ_f may reach zero degrees prior to θ_w (meaning the flanges are straight while the web is not). This scenario is illustrated in figure 109-B. To prevent further distortion (i.e., overcorrecting the flanges to fully straighten the web), Avent and Mukai (1998) suggest that a modification to the phase I heating pattern be made prior to continuing the straightening procedure. This modified heating pattern for phase II ($\theta_n = 0$ or $\theta_f = 0$) is the same as the phase I procedure, with the exception of the line heat pattern. For phase II ($\theta_n = 0$ or $\theta_f = 0$) yield line 4, illustrated in figure 110-A, should not be heated. However, yield lines 1 through 3, and 5 through 7 may be heated as stated in phase I (Avent and Mukai, 1998).

3.5.3.3 Phase II: Heating and Jacking Patterns if $\theta_f = \theta_w$

Similarly, depending on the movement of the section during phase I repair cycles, it is possible for over-straightening or overcorrecting of the F side flange to occur. Should the movement of the section progress such that $\theta_f = \theta_w$, it is likely that with further phase I repairs, the F side flange would become overcorrected. This behavior is illustrated in figure 109-C. To prevent such movement, Avent and Mukai (1998) suggest that the phase I repair procedure be modified. The phase II ($\theta_f = \theta_w$) repair procedure is the same as phase I, with the exception of the far side restraining force, P_f. To prevent over-straightening of the F side flange, the far side restraining force is reversed while the same phase I heating patterns are used. The reversed restraining force, P_f, will prevent the over-straightening movement in the F side flange without hindering further corrective movement in the N side flange and web (Avent and Mukai, 1998).

3.5.3.4 Flange Damage in Opposite Direction

If the damage to the section is the reverse or opposite of that shown in figure 109-A, i.e., side N is pushed away from the opposite flange instead of toward it, the direction of the applied restraining forces may also need to be reversed. The heating patterns, however, should be used as described in sections 3.5.3.1, 3.5.3.2, and 3.5.3.3. The suggested restraining forces and heating patterns for damage in the opposite direction are shown in figure 111 (Avent and Mukai, 1998).
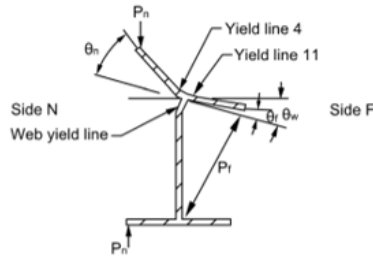
(A) Phase I, initial geometry after damage
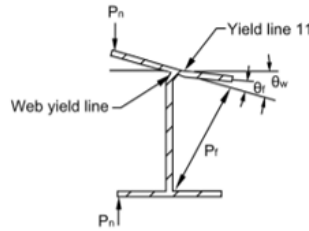
(B) Phase II, geometry if $\theta_n = 0$
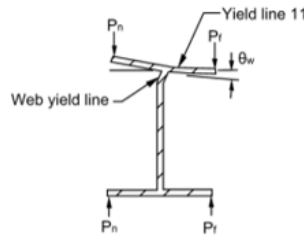
(C) Phase II, geometry if $\theta_r = \theta_w$

Source: FHWA

Figure 111. Illustration. Jacking sequence if damage is reversed from that shown in figure 109.

3.5.3.5 Computation of Restraining Forces

As discussed in section 3.5.2, when a flange is damaged by a concentrated force, the flange initially behaves as a flexural plate and deforms into a series of yield lines. As the deformations increase into the large deflection range, the flange acts as a membrane with large tensile stresses. When the restraining (jacking) force is applied, the reverse behavior occurs. Initially, relatively large axial compression stresses will occur. Then as the plate straightens, the flexural stresses tend to become more dominant. Thus, the restraining force serves two purposes during repair: to create compressive axial stresses which accelerate the flange shortening at both the line and vee heats, and to create bending stresses at yield lines which again accelerate the straightening effort.

When considering the magnitude of restraining force, a conservative approach used by Avent and Mukai (1998) during their experiments discussed in section 3.5.2, is to limit the restraining force to a percentage of the force required to produce a yield line collapse load. A yield line

collapse is defined as the formation of a mechanism in which deformations will continue under a constant load. This load can be computed by a yield line analysis. The restraining force is then limited to a portion of this load. This process, as used by Avent and Mukai (1998), is detailed below.

A generic layout used by Avent and Mukai (1998) to model typical flange bulge geometry is shown in figure 112 where the applied load, W_u, is assumed to be uniformly distributed over one-half of the center region shown in the figure.
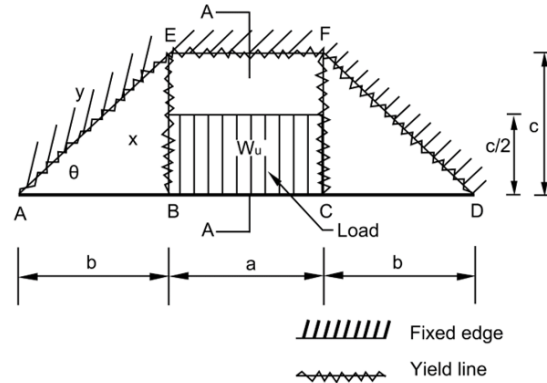
(A) Plan of yield-line layout
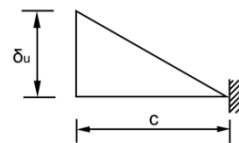
(B) Section AA

Source: FHWA

Figure 112. Illustration. Yield-line analysis for idealized flange bulge geometry.

Using the yield line method to calculate restraining forces is more applicable for small deflections than for large deflections. The simplified assumptions are as follows: (1) the strength of the plate is governed by flexure alone and axial effects are ignored; (2) the plate is assumed to be a thin plate, i.e., the width of the plate is much greater than its thickness; (3) the steel is perfectly plastic and fully yielded at the yield-lines; (4) the plate deforms plastically at failure but is separated into elastic segments by the yield-lines; (5) bending and twisting moments are uniformly distributed along the yield-lines; and (6) elastic deformations are negligible compared to the plastic deformations, i.e., the plate segments rotate as plane segments when a mechanism forms (Avent and Mukai, 1998).

Since the shape of the deformed plate is arched rather than flat, bending stresses induced by the applied load should be lower than that of a flat plate. Assuming the axial component of the load does not exceed the bending component, Avent and Mukai (1998) suggest that the yield-line load will give a conservative approximation of the allowable load. In practice, the aspect ratio of most flange bulge damage is relatively low, and the yield-line analysis is a good approximation.

To develop the equations to calculate restraining force, Avent and Mukai (1998) considered the plate section shown in figure 112. In this configuration, δ_u is the virtual deflection along line BC. The plate is isotropic, so the yield line bending capacity is identical in all directions. The external load, W_u (force/area) is the load producing a mechanism and the moment capacity along a yield line, M_p, is given by:

$$M_p = \frac{F_y t^2}{4}$$ (88)

The work done, W_e, by external loads, W_u, is:

$$W_e = \left(W_u \frac{ac}{2}\right)(0.75\delta_u)$$ (89)

The internal work done, W_I, is computed from the moments along yield-lines AE, EF, FD, EB, and FC.

$$W_I = M_p\left(\frac{a\delta_u}{c} + \frac{2c\delta_u}{b} + \frac{2c\delta_u}{b} + \frac{2b\delta_u}{c}\right)$$ (90)

Equating external and internal work done,

$$W_u = \frac{8}{3}\frac{M_p}{ac}\left(\frac{a}{c} + \frac{4c}{b} + \frac{2b}{c}\right)$$ (91)

If a load ratio of 50 percent is used, then the jacking force on the bulge is:

$$P_j = W_u \frac{ac}{4}$$ (92)

If $c = b_f/2$:

$$P_j = W_u \frac{ab_f}{8}$$ (93)

Using this concept, Avent and Mukai (1998) applied these formulas to calculate restraining force for their test specimens. For these test beams (W8×13), it was assumed that the steel was ASTM A36 (an assumption found to be inaccurate in section 3.5.3.7), $a = b = 5$ in, $c = b_f/2 = 2$ in, $M_p = 0.585$ k-in/in, and the load ratio was 50 percent of the yield line load. From this, the researchers computed the following values for W_u and P_j:

$$W_u = 1.42 \ ksi$$

$$P_j = 3.55 \ kips$$

where P_j, as calculated above, was approximately 50 percent of the yield line load.

3.5.3.6 Experimental Results of Active Heat Straightening

To investigate the effectiveness of active heat straightening on category L/U damage, Avent and Mukai (1998) damaged and repaired an additional beam specimen. The researchers considered a fifth W8×13 beam (beam no. 5) and damaged the specimen in a similar manner to beams no. 1 through no. 4 mentioned in section 3.5.2.3. Following damage, the researchers repaired the specimens using a modified repair procedure based on repair configuration no. 1 (shown in figure 108). The modified repair procedure used the same heating pattern as repair configuration

no. 1, consisting of line heats on both near and far sides of the flange as well as the web, but no vee heats. Similarly, the jacking force of 3.5 kips (as calculated in section 3.5.3.5) was used on both the near and far side. However, this force, unlike that in repair configuration no. 1, was maintained throughout the heating and cooling cycle by continuously adjusting the jacks as the flange straightened. This procedure, characterized by constant restraining force, is referred to as active heat straightening. Caution must be taken when performing active heat straightening as over jacking may occur. For this reason, this method is generally not suggested.

Avent and Mukai (1998) found the procedure to be effective in repairing the damage. Four heat cycles produced average flange deflections of $\Delta_n = 0.16$ inches and $\Delta_f = 0.12$ inches, which was slightly more than those produced with the original repair configuration no. 1 (the results of which are shown in figure 108). This procedure is not applicable for all heat straightening repairs. However, for the repair of shallow bulges, this repair methodology can be beneficial. This is because the placement of the jacks combined with the movement of the section during repair can result in the loosening (and potential dislodging) of the jacks unless adjustments are made. Should this method of repair be utilized to repair category L/U damage, Avent and Mukai (1998) caution that checks be performed to ensure that over-jacking does not occur.

3.5.3.7 Material Properties of Test Specimens

To conclude their research into the repair of category L/U damaged specimens, Avent and Mukai (1998) investigated the effect of heat straightening repair on the steel. Test specimens were taken from an undamaged beam, the heated region of beam no. 3, and the heated region of beam no. 5 (repaired using active heat straightening).

The results of this testing are shown in table 26. As shown, both yield and ultimate strengths were similar across all specimens. However, percent elongation for the heated specimens was lower than that of the undamaged and unheated specimens, a typical finding for heat-straightened steel discussed further in section 2.1.

Table 26. Results of tensile tests on dent specimens (Avent and Mukai, 1998).

Sample	Ultimate Strength (ksi)	Yield Strength (ksi)	Modulus of Elasticity (ksi)	Percent Elongation %
Undamaged	76.1	60.0	32,000	33
Beam No. 3	78.4	60.8	27,000	22
Beam No. 5	80.2	62.4	35,000	23

Following this testing, Avent and Mukai (1998) noted that the measured yield stress of the steel was significantly higher than that assumed for the yield line analysis. As such, the restraining force used in the experiments was 30 percent of the yield line load and not the calculated value of 50 percent.

3.5.4. Category L/S – Experimental Damage and Repair

3.5.4.1 Category L/S – Damage Behavior

Stiffened elements of a beam are defined as those supported on two sides by perpendicular elements. An example of a stiffened element is the web of a wide flange beam, where the flanges provide support on both sides of the web. When stiffened elements are damaged, the pattern formed is usually a dish-shaped bulge.

3.5.4.2 Experimental Method, Heating Patterns and Results

To evaluate methods of straightening category L/S damage, Avent and Mukai (1998) conducted a series of experiments on wide flange sections (beam no. 6 and beam no. 7). Damage was induced in the form of bulges in the webs of the beam specimens. This damage is illustrated in figure 113. Plastic deformations, δ_i, of about 0.5 inch were induced in beam no. 7, resulting in a web bulge with a base diameter, d_b, of 5 inches and a smooth curvature as shown in figure 113-B. For beam no. 6, the loading was continued longer to produce a base diameter, d_b, of 13.5 inches and a maximum deflection, δ_i, of 1.66 inches. The curved surface was relatively smooth as shown in figure 113-A.

To evaluate behavior during repair, Avent and Mukai (1998) measured deflection at the center of the bulge and at the approximate point of contraflexure. These measurements were made on the longitudinal and transverse axes of the beam. Since the response of the beam during repair was generally symmetrical, only the center point and one contraflexure point are shown and discussed in the figures and tables in this section. These points are indicated by δ_i, and δ_c, respectively.
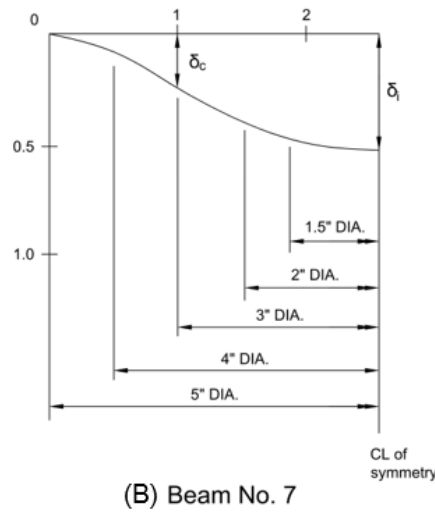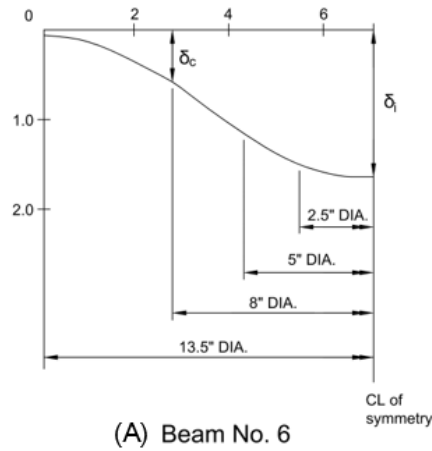
Source: Avent and Mukai (1998)

Figure 113. Illustration. Bulge cross section geometry, beams no. 6 and no. 7.

To restrain the beam sections during repair, Avent and Mukai (1998) applied a restraining force using a jack and spreader plate placed at the center of the bulge. The magnitude of the restraining force was calculated as a function of the bulge geometry. Assuming the shape of the bulge can be approximated as a shallow spherical shell, the constant radius of curvature, R, can be expressed as:

$$R = \left(\frac{\delta_i^2 + r_b^2}{2\delta_i}\right) \tag{94}$$

where r_b is the radius of the sphere at its base. The characteristic length, ℓ_c, is given by:

$$\ell_c = \frac{\sqrt{(Rt)}}{[12(1-v^2)]^{0.25}} \tag{95}$$

where t is the plate thickness and v is Poisson's ratio.

For shallow spherical shells with a concentrated load at the center, the critical stress results from bending about a circumferential line if r/ℓ_c is less than 1.6 (Timoshenko, 1959) where r is the distance from the center to the line in question. The smaller r/ℓ_c, the higher the stress. A practical limit for r could be taken as the radius of the jack used. In these experiments, Avent and Mukai (1998) used a jack with a radius of $r = 0.84$ for beam no. 6 and beam no. 7.

From Timoshenko (1959), the relationship between r/ℓ_c and the shell stress factor, β, is given in table 27 where σ is the maximum shell stress and P_j is the applied restraining (jacking) force at the center of the bulge. The shell stress factor, β, is given by:

$$\beta = \frac{t^2 \sigma}{P_j} \tag{96}$$

Table 27. Relationship between r/ℓc and shell stress factor, β, (Avent and Mukai, 1998).

Parameter	Value					
r/ℓ$_c$	0.4	0.6	0.8	1	1.2	1.4
β	0.80	0.57	0.43	0.33	0.25	0.18

By setting σ equal to the desired percentage of the yield stress (jacking ratio), the appropriate restraining (jacking) force, P_j, can be computed for a given r/ℓ_c ratio. This provides an approximate method of determining the restraining force. As the bulge flattens, δ_i decreases and the restraining force should be reduced to maintain the same stress level. Avent and Mukai (1998) used this procedure to determine restraining force for the repair of their damaged beam specimens (beams no. 6 and 7).

To investigate the effect of heating patterns on the heat straightening repair of category L/S damage, Avent and Mukai (1998) conducted the repairs to their beam specimens using a variety of heating patterns, consisting of one or more of the following basic patterns: (1) ring line heats, (2) radial line heats, and (3) star vee heats. An illustration of these basic heating patterns is shown in figure 114.
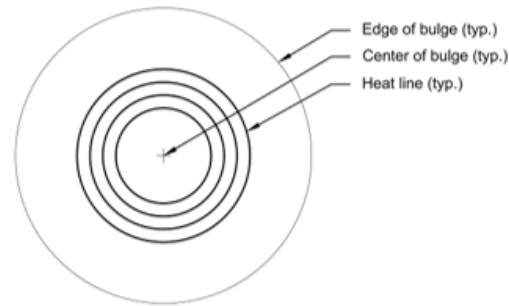
(A) Ring line heats
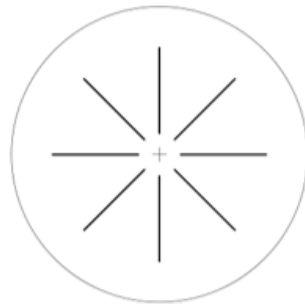
(B) Radial line heat
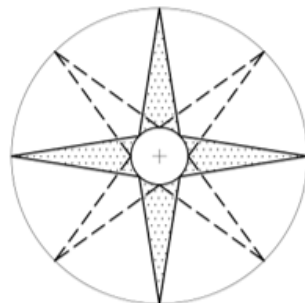
(C) Star vee heat

Source: FHWA

Figure 114. Illustration. Ring line heat, radial line heat, and star vee heat patterns.

Ring line heats are circumferential line heats applied in concentric circles around the center of the bulge. The line heats should be applied at the locations of the largest curvature, on the convex surface of the bulge. In the experimental repairs by Avent and Mukai (1998), each ring was identified by its diameter. A radial line heat pattern is characterized by equally spaced line heats emanating from the center of the bulge. The radial line heat arrangement used by Avent and Mukai (1998) had eight radial lines spaced at 45 degrees. Finally, a star vee heat pattern consists of a series of vees arranged symmetrically around the center of the bulge with the open end of the vees at the center. The star heat arrangement used by Avent and Mukai (1998) consisted of four vee heats spaced at 90 degrees. On alternate heat cycles, the four-point (four vee-heat) pattern was shifted 45 degrees (illustrated by the dashed lines in figure 114-C). The vee angle was limited to 20 degrees. The size of the vees is determined by the diameter of the circle through the tip of the vees.

Beam no. 6 was heated with four-point star vee and ring line heats only. The heating patterns and movements are shown in figure 115. Most of the star vee heats were located near the center portion of the bulge, inscribed in a 5-inch diameter circle. However, a small number of 13.5-inch-diameter star patterns were used at the beginning and end of the repair. In addition to the star vee heats, several ring line heats were used ranging from 2.5 inches to 17.5 inches in diameter. During the first 10 heating cycles, the jacking ratio was kept in the 50 to 60 percent range. For the remaining cycles, it was reduced to the 25 to 30 percent range (Avent and Mukai, 1998).

Avent and Mukai (1998) found that the center point deflection, δ_i, reduced steadily for all heating patterns with an average value per heat cycle of 0.08 inch. Likewise, the outer deflection, δ_c, followed a similar pattern except when both line and vees were concentrated in the central portion of the bulge.

Heat Number	0-4	4-5	5-10	10-15	15-18	18-20
Circumferentail Line Heat Distance from Center	13.5	5	5, 2.5, 8	13.5	2.5, 5	13.5
4 Point Star Vee	13.5	5	5	–	–	13.5
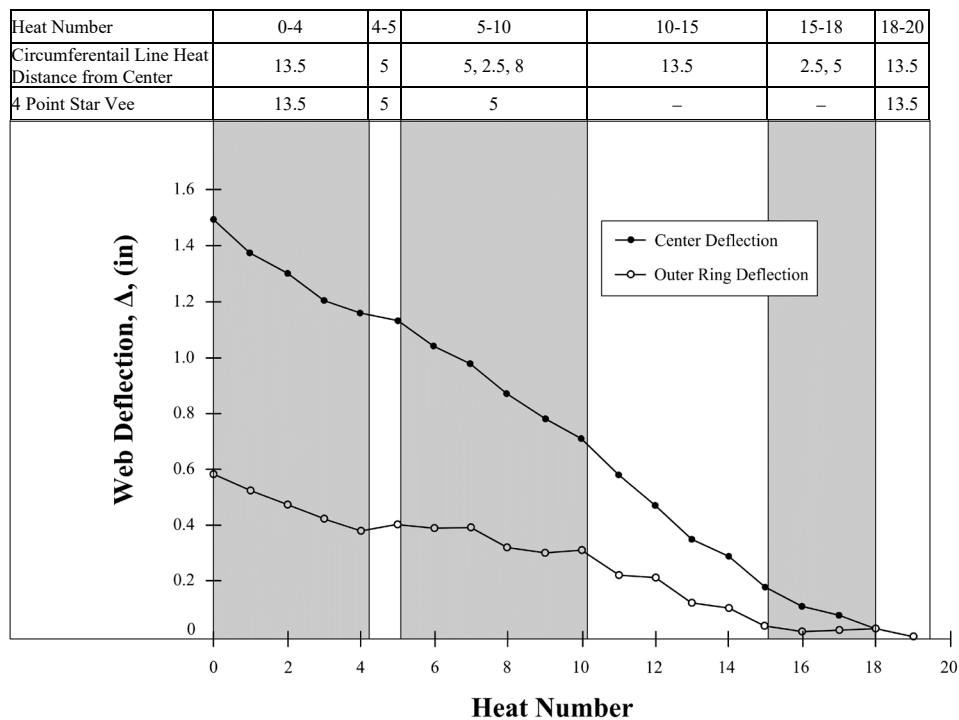
Source: Avent and Mukai (1998)

Figure 115. Graph. Decrease in deflections of stiffened web for beam no. 6 (W16×26) with category L/S damage.

For the repair of beam no. 7, Avent and Mukai (1998) used only radial and ring line heats. The deflections decreased in a regular manner until the last several heat cycles, as figure 116 shows. The average deflection, δ_i, per heat cycle was 0.04 inch. The jacking ratio was initially 41 percent and reduced incrementally to 14 percent by the final heat cycle. Although the average movement per heat cycle for beam no. 7 was less than that of beam no. 6, the damage to beam no. 7 required fewer heat cycles to repair. In terms of bulge-diameter-to-maximum-deflection ratio, d_b/δ_i, the two beam specimens were similar. However, beam no. 6 had a ratio

approximately 10 percent smaller than that of beam no.7, but required more heat cycles to repair (Avent and Mukai, 1998).

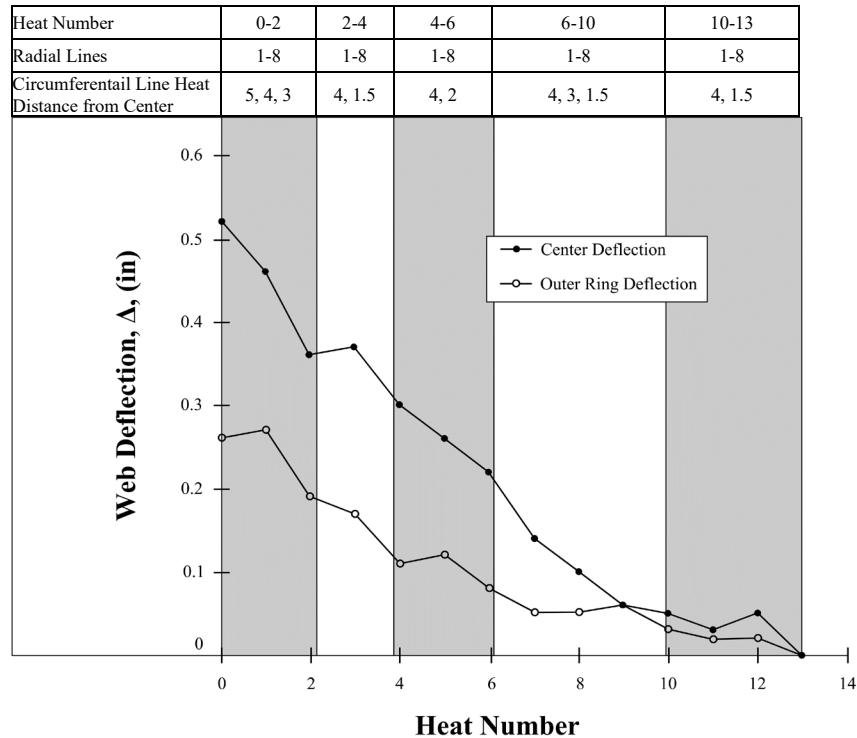| Heat Number	0-2	2-4	4-6	6-10	10-13
Radial Lines	1-8	1-8	1-8	1-8	1-8
Circumferentail Line Heat Distance from Center	5, 4, 3	4, 1.5	4, 2	4, 3, 1.5	4, 1.5

Source: Avent and Mukai (1998)

Figure 116. Graph. Decrease in deflections of stiffened web for beam no. 7 (W16×26) with category L/S damage.

Avent and Mukai (1998) found that the reciprocal of the bulge-diameter-to-deflection ratio is an effective way to compare the rate of straightening for different size bulges. For example, beam no. 6 heating patterns reduced the δ_i/d_b ratio by an average of 0.0065 per heat while the rate for beam no. 7 was 0.0077 per heat. Using this criterion, the researchers concluded that the combination of ring and radial line heats is more effective than the combination of star vee and ring line heats. This conclusion is in agreement with the experimental results for unstiffened elements, discussed in section 3.5.2.3, where line heats were slightly more effective than the line heat and vee heat combination as shown by the required heats to repair beams no. 6 and no. 7.

3.5.5. Category L/S - Repair Methodology

Similar to the repair of local damage to unstiffened elements, engineering judgment is required when selecting the heating patterns to repair damage to stiffened elements. In general, based on the research by Avent and Mukai (1998), heating the regions of sharpest curvature with combinations of lines and/or narrow vees is the most effective approach. Additionally, it is good practice to heat only in the vicinity of regions with plastic curvature. As straightening progresses, this region may become smaller.

The following sections detail a general methodology for the repair of bulges in stiffened elements. Again, similar to unstiffened elements, the exact repair procedure used depends on how section geometry changes during heat straightening. As such, engineering judgment should be used in applying this methodology to specific cases.

3.5.5.1 Computation of Restraining Force

Because there is no direct equivalent to plastic moment for stiffened plate elements, Avent and Mukai (1998) state that the capacity can be taken as the load at initial yielding. With this, jacking forces should be limited such that they do not produce stresses greater than 50 percent of yield. However, it is complex to determine the magnitude of these stresses for category L/S damage analytically. One way to determine the restraining force that produces yield is experimentally. Using this approach, an area of low stress due to live loading would be selected, if available, and a restraining force would then be applied in this area until small permanent deformations are observed. This procedure provides the magnitude of the yield force without inducing significant damage to the member. The maximum restraining force would then be limited to one-half of this value. Otherwise, jacking forces must be estimated and judged by the amount of movement after each cycle. Avent and Mukai (1998) state that movement should not exceed 1/8 inch per cycle using this secondary method.

Based on the results of the experimental repair of damage to stiffened elements, Avent and Mukai (1998) state that the restraining force should be applied at the crown of the bulge using a spreader plate. The restraining force may then be calculated assuming the bulge is a shallow shell. Radius of curvature, R, should be calculated using equation 94 and characteristic length, ℓ_c, calculated using equation 95. A value for the stress factor, β, given by equation 96, can be interpolated from the values given in table 27. For a jacking ratio of 50 percent, σ equals 50 percent of F_y. Thus, the restraining force is calculated as:

$$P_j = \frac{t^2 F_y}{2\beta} \tag{97}$$

where F_y equals the nominal yield stress of the steel.

3.5.5.2 Estimation of the Number of Heats Required and Modification of Restraining Force

As discussed previously, as the web bulge straightens, the jacking force should be reduced to maintain the same magnitude of stress in the section. One approach would be to use the above procedures to compute a new jacking force as δ_i decreases. However, a simpler approach, as proposed by Avent and Mukai (1998), is to estimate the number of heats required to straighten the bulge, then reduce the restraining force proportionally after each heat until it is one-half of its original value at the last heat.

Averaging the results from their two beam specimens, beams no. 6 and 7, Avent and Mukai (1998) suggest that a reasonable estimate of the reduction in the reciprocal of the bulge-diameter-to-deflection ratio per heat cycle is 0.007. Based on this value, the estimated number of heats, n, is calculated as:

$$n = 140\left(\frac{\delta_i}{d_b}\right) \tag{98}$$

208

Reducing the restraining force incrementally, the restraining force for the ith heat, P_i, is calculated as:

$$P_i = (1 - \frac{i}{2n})P_j \qquad (99)$$

Finally, as the heat straightening repair progresses, if the estimate of number of heats is found to be in error, Avent and Mukai (1998) state that the jacking force can be adjusted up or down to compensate.

3.5.5.3 Initial Heating Pattern

A typical flange bulge will have reverse curvature bending as shown in figure 117. Based on Avent and Mukai (1998), the crown region should be heated first with the torch on the convex side. As movement progresses, the heating patterns can be expanded into the reverse curvature region, again, with the torch on the convex side.

The initial heating patterns should consist of radial and ring line heats as illustrated by solid lines in figure 117-B. The exact number of ring heats will depend on the size of this region. The diameter of the smallest ring should be no less than 2 inches with spacing between rings of at least 2 inches. For large bulges, the ring spacing should be larger than 2 inches. For cases where the curvature is relatively uniform, equally spaced rings may be used, but a ring heat should be centered at each location where sharp changes in curvature occur. The outer ring of the crown region (solid lines in figure 117-B) on the convex side should be heated first, working inward. After the rings are heated, the radial lines in the crown region should be heated. Again, heat should be applied from the outside working in. Radial lines should not penetrate inside the interior ring as shown in figure 117-B. This pattern should be continued cyclically until the crown region begins to flatten, allowing the steel to cool completely between heating cycles (Avent and Mukai, 1998).
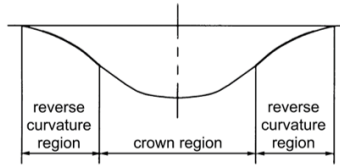
(A) Reverse curvature regions of a bulge
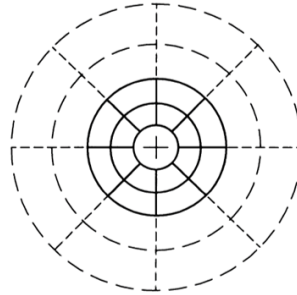
(B) Ring and line heating patterns

Source: FHWA

Figure 117. Illustration. Curvature and line heating patterns for category L/S damage.

To apply the restraining force, it is typical that the jacks are placed at the crown in the direction tending to straighten the bulge. Heating patterns must be adjusted to accommodate jack placement and to avoid heat transfer to the jacks that may damage them (Avent and Mukai, 1998).

3.5.5.4 Final Heating Pattern

As the crown section begins to flatten, the heating pattern should be expanded into the reverse curvature regions. One method of doing so, as stated by Avent and Mukai (1998), is to expand the number of ring heats and extend the radial line heats as described in section 3.5.5.3 and shown by dashed lines in figure 117-B. The second method pointed out by the researchers is to use four-point star vee heats combined with ring line heats instead of radial line heats. The star vee pattern is shown in figure 114-C. Following this second method, the vees should be heated first, working from tip to center, leaving the central portion unheated (the center region where adjacent vees intersect). In addition, vees should be narrow with an angle of 20 degrees or less. After star vee heating, the rings should be heated, starting with the outermost ring. A maximum of three ring line heats should be used at one time with the star vee heats. The star vee pattern should be rotated 30 degrees after each cycle so that the same vees are not repetitively heated. Rings may be repetitively heated or shifted to avoid repetitive heating, depending on the degree of plastic curvature. In all cases, the steel should be allowed to cool completely before beginning the next heating cycle (Avent and Mukai, 1998).

3.5.6. Summary

Avent and Mukai (1998) presented a methodology for the heat-straightening repair of localized damage (category L) for both category L/U damage (unstiffened elements) and category L/S

210

damage (stiffened elements). Experimental data were presented to illustrate the effectiveness of various heating patterns. The basic principles used for the repair of category L damage follow the same principles used for the repair of global damage categories (S, W, and T).

In general, local damage can be heat straightened using a combination of restraining (jacking) forces and a relatively small number of line heats. Repair methods that used line heats rather than vee heats were found to be more efficient for both stiffened and unstiffened elements. From research performed by Avent and Mukai (1998), it is evident that the straightening of local damage is most efficient when completed in stages where both jacking forces and heating patterns are varied in response to the movement of the section during the repair sequence. As a general rule, heat should be applied to the convex side of the damaged element. For shallow configurations without sharp changes in slope, the restraining force may be greatly relieved during the cooling cycle. In contrast, to increase effective movement, the restraining force may be maintained during cooling at the original level established prior to heating by carefully adjusting the jack as the material cools. At no time should the restraining force increase above the original pre-heated value. If jack pressure is maintained, care should be taken to ensure the section is not over-straightened or overcorrected.

Local damage is often highly irregular and may require a variety of heating patterns based on the damage geometry and member configuration. The principles discussed in this chapter provide a general approach for heat straightening repair of local damage, but engineering judgment should be used when applying these concepts to individual cases.

A second area for engineering judgment relates to degree (severity) of local damage that can be repaired using heat straightening. For plate elements bent (damaged) about their weak axis, the strain ratio ($\varepsilon/\varepsilon_y$) may well exceed 150, often considered the upper limit for heat straightening repairs of global damage categories (see section 2.3.3.2). However, local damage often occurs at locations where design live and dead load stresses are smaller, such as secondary bracing members. For such locations, the heat straightening repair of large strain damage, which would be considered too large to repair globally (categories S, W, and T), could be undertaken locally (category L).

3.5.7. Important Considerations

- Local damage to unstiffened elements (category L/U) and stiffened elements (category L/S) can be heat-straightened effectively.
- Local damage, both category L/U and category L/S, typically is most effectively straightened by using line heats rather than vee heats.
- Restraining (jacking) forces are typically used for straightening local damage.
- Restraining (jacking) forces can be calculated prior to heat straightening. For both category L/U and category L/S damage, restraining forces may be adjusted during the straightening process to ensure the most effective movement of the section.
- Straightening of local damage is usually done in stages where both restraining forces and heating patterns are varied in response to the progression of the steel's movements during repair.
- In general, for the repair of local damage, heat should be applied to the convex side of the damaged surface.

- For both category L/U and category L/S damage, heat straightening requires numerous heat cycles to complete the repair.

CHAPTER 4. TECHNICAL GUIDE FOR COLD BENDING

4.1. INTRODUCTION

Cold bending refers broadly to several means of bending structural steel plates and shapes into a desired configuration using only force at ambient temperature (i.e., without the addition of heat). Specific examples of cold bending include folding plate, curving or cambering structural shapes, and straightening plates or shapes.

Steel is well suited to forming by cold bending because of its ductility. This is important because the process of cold bending partially yields the cross section to result in a new, permanent configuration. Since the goal of cold bending is to produce a cross section that can be used in service as a structural member, limits to cold bending are used to preserve the properties of the material.

4.2. USE OF COLD BENDING IN BRIDGES

The use of cold bending in steel bridge construction ranges from forming the main superstructure members to creating connection plates. For steel girder bridges, cold bending is often used to camber W-beams and to create girder haunches by bending flange plates. Connection and bracing members, including bent connection and gusset plates, are also created using cold bending. Further, fabrication of more specialty bridge superstructure types including orthotropic deck panels and press-brake tub girders, often used for accelerated bridge construction, are also created using cold bending. These uses are explored and discussed further in the following sections.

4.2.1. General Mechanism

Several common processes are used for cold bending steel for bridges. Each is adapted to the type of steel section being bent (or cold straightened) and depends on the capability of the equipment used in bending. Regardless of the section type or exact bending process used, cold bending typically involves partially yielding the cross section of the steel (see section 4.3.1). Therefore, a considerable magnitude of force is used. In most cold bending practices, a translating force is applied at a controlled speed on one side of the section and a stationary fixture or fixtures provide a reaction on the opposite side of the section. See figure 118 for an example of a cold bending configuration, which shows three-point loading (note that four-point loading, with two locations of force applied, may also be used).
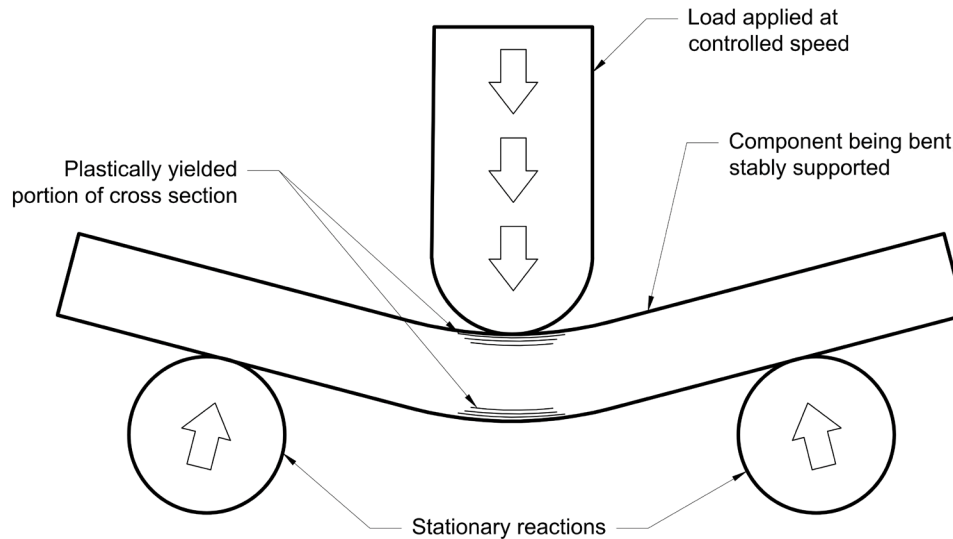
Source: FHWA

Figure 118. Illustration. Basic cold bending diagram.

In cold bending, the bending force is applied until an initial target radius is reached. The initial target radius is chosen to account for spring-back in the bent section after the bending force is removed. When the applied force is withdrawn, and the elastic deformation is recovered, the final product is a component bent to the final desired radius.

Control of the cold bending process is done by displacement rather than force. The equipment should have enough force capacity to partially yield the section of the component being bent, but in bending operations, the amount of force applied is not calculated. Rather, the force is applied at a controlled displacement until the initial target radius is reached.

Given the desired final radius, cross section of the material, and yield strength of the material, it is possible to calculate the initial displacement needed, including the expected spring-back, to achieve the final desired condition. However, in practice, fabricators often base the initial displacement on their experience and, to some extent, trial and error. In high production situations, where the same or similar cross sections are bent repeatedly, fabricators can be precise about the amount of initial displacement needed to obtain the desired final bend. An example of this is the production of high mast lighting towers, where pole producers bend hundreds of poles each year using the same range of material thickness, strength, and desired bend radii. Although some small variations result, primarily due to initial residual stresses, no guess work is involved regarding the displacements needed to produce the desired product.

Initial targets for adding camber to wide-flange bridge beams are another matter. Fabricators who use this process are typically experienced, but there is a much higher degree of variation among the size and shape of members used for bridges than there is among plates used for high mast lighting towers. In table 28, data originally published in Bresch et al. (2016), captures a population of 591 bridge girders cold cambered by a fabricator over a five-year period. The data shown in the table illustrate the wide variation in member length, and consequently section size, and camber desired for bridge girders. In this case, the fabricator used trial and error, typically introducing one inch of displacement at a time until the desired displacement was reached.

214

Table 28. Properties of cold-cambered rolled I-beams (Bresch et al., 2016).

Value	Length (ft)	Max Camber (in)	Δ/L Ratio
Maximum	118.65	9.02	1.11%
Minimum	12.99	0.06	0.01%
Average	66.07	1.79	0.21%
Range	105.65	8.96	1.10%
Median	66.68	1.14	0.15%
Mode	38.99	3.35	0.07%

4.2.2. Roll Forming

In roll forming, a flat strip of plate is drawn through a series of different contour rolls to produce the final desired cross section shape. As the plate is drawn through the rolls, each set of rolls incrementally bends the plate until the desired shape is achieved. The shape of each set of rolls is slightly different from the set preceding it and the set following it. This allows the section to be bent continuously as it is drawn through the machine. The number of rolls used and the number of passes through the rolls affect the uniformity of the final product and are at the discretion of the roll form supplier. Figure 119 illustrates the process of roll forming from flat plate to finished shape.
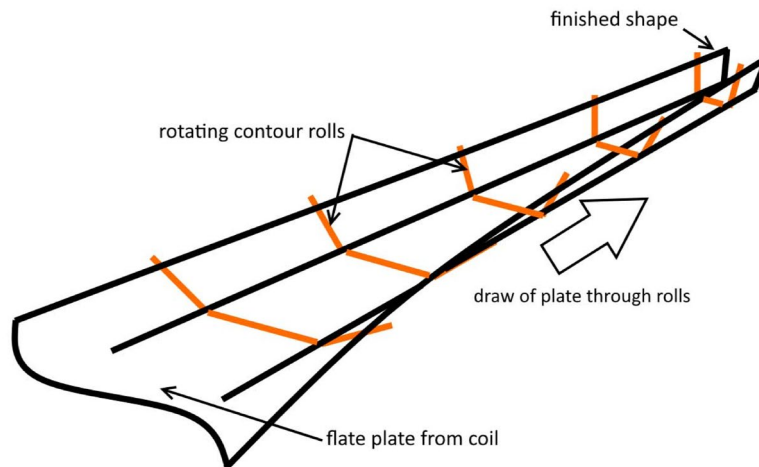
Source: FHWA

Figure 119. Illustration. Roll forming.

Roll forming is a common means of forming long, thin, bent steel components. For example, the metal beam guard fencing used on roadways is produced with this process. Roll forming is also used to form the ribs for orthotropic deck panels (section 4.2.5.3) because the process is suitable for the same thicknesses of plate that can be bent using a press-brake.

In practice, the flat strips of plate used in roll forming are long but are supplied in a coil. The roll form supplier first uncoils the plate, levels it in the mill, and then draws the flattened plate through the contour rolls. The number of rolls used is at the discretion of the fabricator. Increasing the number of rolls improves distortion control but adds cost.

215

Parts are cut to length after forming. Because the flat plate used in roll forming is supplied in a coil, any practical length of component can be produced. After forming, it is common to have some amount of camber, bow, or twist in the final product due to the initial residual stresses in the plate and the stresses introduced during forming. Further cold processing, straightening, or flattening correct this.

4.2.3. Girder Flange Bending

Cold bending is a popular method for bending flanges of girders to a desired radius. Several examples of cold-bent girder flanges are presented in the sections below. There are minimum recommended bend radii in section 11.4.3.3.2 of the AASHTO Construction Specifications (AASHTO 2017a (23 CFR 625.4(d)(1)(iv))) to preserve the mechanical properties of a cold-bent component. These limits and other cold bending practices are discussed further in section 4.3.3.

4.2.3.1 Haunched Girder Flanges

Haunched girders are bridge girders that increase in section depth at support points with the girder profile, specifically the bottom flange, following a curved (often parabolic) shape. The web of a haunched girder is cut to a specific profile, and the flange is shaped such that it follows the profile of the web. Cold bending may be used to form the curved flange or used to form the flange corner at the base of the haunch (see Figure 120).
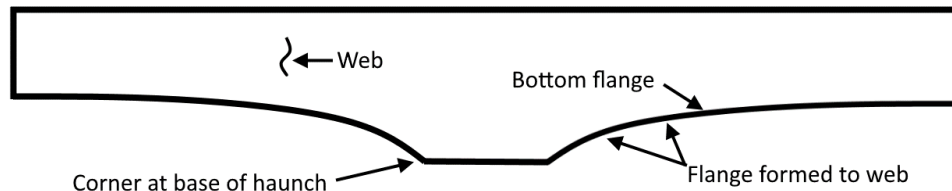
Source: FHWA

Figure 120. Illustration. Haunched girder.

Figure 121 shows an inverted haunched girder with the bottom flange (at the top of the photo – the girder is upside down for fabrication) formed to match the parabolic profile of the girder web. The method used for bending the flange plate to match the haunch profile depends on the thickness of the flange and the severity of the haunch curve. For most cases, the flanges can be cold formed by drawing them down to the web and then attaching them to the web by welding. However, for thicker flange plates or a more severe haunch profile, the flange may be heat curved to the desired shape before being attached to the web.

216

Source: FHWA

Figure 121. Photo. Haunched girder in fabrication (upside down).

Figure 122 shows a flange corner at the base of the haunch that has been formed by cold bending.

Source: FHWA

Figure 122. Photo. Cold-bent flange corner on haunch girder.

4.2.3.2 Bascule Bridge Flanges

Bascule bridges are a type of lift bridge where the span of the bridge is raised by a counterweight that balances the span through its upward rotation. Through its movement, the bridge span typically pivots about a single point (fixed-trunnion). For these types of bascule bridges, the girders are often designed as plate girders that have a radial bottom flange at the trunnion for the gear rack. The bascule girders in these photos also feature an access hole near the trunnion that is stiffened with curved plates. The curved flange plates, and curved stiffener plates around access holes, if present, are fabricated using cold bending. Figure 123 shows examples of these curved plates during fabrication and in-place.

Source: Industrial Steel Construction (ISC), 2007 (top left, top middle),
Oakley Steel Products Co., 2017 (top right), ISC, 2017 (bottom)

Figure 123. Photos. Cold bent bascule bridge components.

4.2.3.3 Turned-Down Top Flanges on Railroad Girders

Top flange turn-downs, where the top flange of a plate girder is curved or sloped down, are common on railroad through-girder bridges as shown in figure 124. Such turn-downs help protect girders from equipment impacts. This is particularly important in areas where snow is deep and the potential for plow impact is high due to limited visibility of the girder ends. Turn-downs are produced by cutting the web of the girder to the desired profile, cold bending the flange to the desired radius, and then attaching the bent flange to the pre-cut web.

Figure 124. Photos. Railroad bridge girders with turned-down flanges.

4.2.4. Beam and Girder Bending and Straightening

Cold bending to introduce camber into rolled beams is common. Cold bending to introduce or correct sweep in both rolled and build-up beams and girders is not as common but can be used effectively. Both practices are discussed in detail in the following sections.

4.2.4.1 Cold Cambering of Rolled Beams and Girders

Rolled beams (W-shapes) are often used as stringers in shorter span bridges. Rolled beams have a natural camber (i.e., out-of-straightness on the strong axis of the shape) that results from production of the shape at the mill. Table 24 of ASTM A6, while not a Federal requirement, provides tolerances for such "natural" camber. This natural camber is often adequate for simpler, short span bridges where beams are simply installed with the natural camber pointing up. However, rolled beams for highway bridges may have a design camber that is greater than this natural camber, so additional camber is introduced in fabrication, and usually this is by cold bending.

Cold bending, or cambering by force at ambient temperature, is the most common method used to introduce camber into rolled beams. Acceptance of this practice has not been universal. In 2010, AASHTO adopted language for the first time to allow this practice into the *LRFD Bridge Construction Specifications* (BCS) (AASHTO 2010), which stays in the 4th Edition LRFD BCS (AASHTO 2017a (CFR 625.4(d)(1)(iv))) in article 11.4.12.2.7.

Since bridge camber is designed to accommodate dead load deflections and the profile grade's vertical curve, the shape of beam camber is typically parabolic along the span length. Rolled shapes can be cold cambered by use of hydraulic rams or by rollers. With this method, beams are incrementally bent by using two fixed anchor points on the far side of the beam and hydraulic cambering rams (one or two) on the near side of the beam between the anchor points, creating a three- or four-point frame. The rams induce small bends at the load points and then the beam is shifted, allowing a series of small deformations to approximate a curve. Roller bending uses two rollers on one side and one roller between them on the other side in a pyramid configuration. The beam moves back and forth through the rollers as the opposing sides are incrementally moved closer together. This can produce a uniform curvature and is preferred for small radius curves or highly visible elements. Fabricators do not routinely have this equipment so members must be shipped to providers, affecting schedule and cost.

Bridge fabricators typically prefer use of rams because this method is easily implemented in a bridge fabrication shop and adaptable to the large sections often used for bridge members. Further, using four-point loading equipment provides better control of the bending process and approximates a parabolic camber profile using smaller bending loads (Gergess and Sen, 2016). Generally, the number of impacts and magnitude of force applied are a matter of experience on the part of the shop.

4.2.4.2 Cold Bending to Introduce or Correct Sweep of Rolled Beams and Built-Up Girders

In fabrication, introducing, modifying, and correcting sweep (i.e., curve or straightness on the weak axis of a member) in rolled beams and plate girders is common. The process of curving members (introducing or modifying sweep) can be done using various methods. In the shop, large radius curves in beams and girders are usually produced via heat curving. However, small radius curved girders can be produced with flanges cut to the desired radius and the web bent to match the curve of the pre-cut flanges. Smaller radius beams may employ a combination of cold and heated methods, depending on the geometry required. Beam and girder straightening can be done via heat or cold straightening.

Gergess and Sen (2008) investigated and demonstrated the suitability of cold bending for curving beams. The study was related to the use of cold bending on the Miami Metromover project completed in the early 1990s. In collaboration with a fabricator, the researchers developed a cold-bending methodology suitable for symmetric and asymmetric sections. The approach, originally developed by the fabricator for use on the project, includes the load and reaction configuration and a method for calculating the load needed for bending based on the section properties. The method "uses a mobile, crane-supported, U-shaped self-straightening frame that can apply horizontal (lateral) loads to the top and bottom flanges of an I-girder at designated intervals along its length" (Gergess and Sen). To cold bend the section, several impacts are used and spread along the length of the member, with no point being hit more than once. Limiting the number of impacts helps to prevent Bauschinger effects (i.e., lower yield strength under reverse loading). For slender and non-compact shapes, special consideration is taken to avoid buckling. For compact sections, Gergess and Sen (2008) provide a means of calculating residual stresses and offset limits to avoid flange buckling.

Gergess and Sen (2008) demonstrated that cold bending for curving girders is achievable in practice. However, as with all fabrication methods, the means used to achieve the desired curve of a member are at the discretion of the fabricator. Because the members, curved or otherwise, can be designed without regard for the fabrication method, whether cold bending is used depends on the fabricator's available equipment and expertise.

4.2.5. Press-Brake Bent Elements

4.2.5.1 Press-Brake Tub Girder

The press-brake tub girder (PBTG) is a beam made by bending a plate into the desired geometry using press brake bending at ambient temperature. The PBTG may be pre-decked for rapid construction. Figure 125 shows a PBTG without the deck. With the first installation in 2004, there are now over 30 bridges in service in the United States. Effective performance of this

system was verified by research conducted by West Virginia University and live load tests on bridges in Buchanan County and Muskingum County, Iowa.

Source: TEG Engineering, LLC (2010)

**Figure 125. Photo. Press-brake bent into beam for deck unit.**

4.2.5.2 Folded Plate Bridge System

The folded plate bridge system is a bridge superstructure unit comprised of a steel beam produced by cold bending a plate using a press-brake. The system is available with the steel beam alone and in modular form with a precast deck system affixed to the top of the steel beam. This system is like the PBFS tub girder system, discussed in section 4.2.5.1, in fabrication process and general beam shape; however, the steel beam used in the folded plate bridge system is an inverted tub girder (i.e., open bottom).

At the time of this publication, 11 bridges of this type are in service in the United States. Non-published research conducted in development of the folded plate bridge system included fatigue testing, with a beam successfully loaded for more than 7.5 million cycles.

4.2.5.3 Orthotropic Deck Ribs

Orthotropic decks are bridge decks using a steel plate as a driving surface, stiffened both longitudinally and transversely by elements attached to the underside of the deck plate. The longitudinal elements run the full length of the deck, typically including bolted field splices at a spacing of 40 to 60 feet. The longitudinal ribs of the first orthotropic decks were open sections, such as W-shapes or tees, but in more recent designs, closed sections have been used. Construction with open sections is more economical, but the use of closed sections improves load distribution among the ribs and buckling resistance. Additionally, the use of closed sections improves design efficiency and results in a superstructure that weighs less. Closed section ribs are rectangular, trapezoidal, or U-shaped sections made from a plate that is shaped by cold bending. Typically, the closed rib sections are made by press-brake bending but roll forming can also be used.
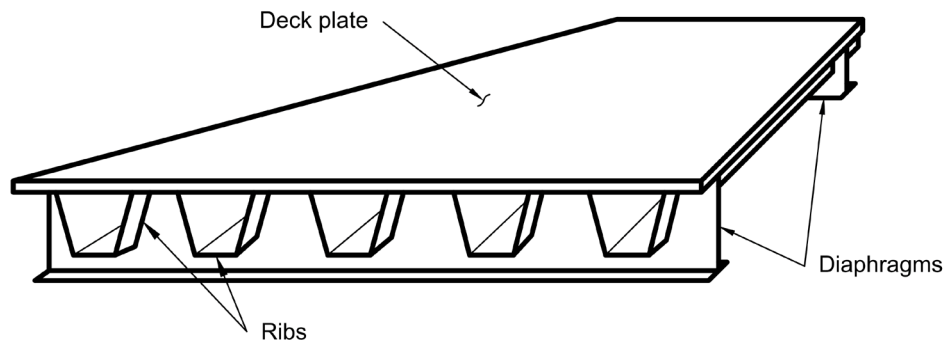
Source: FHWA

Figure 126. Illustration. Orthotropic deck panel with closed ribs.

4.2.6. Miscellaneous Bridge Parts

4.2.6.1 Bent Plate Diaphragms

Bent plate diaphragms can be a cost-effective way to provide intermediate framing for steel girder bridges with shallow beam depths. Examples of bent plate diaphragms are shown in figure 127. The diaphragms are produced from a steel plate using press-brake bending, which creates the top and bottom flanges of the section.

Source: FHWA

Figure 127. Photos. Bent plate diaphragms.

4.2.6.2 Bent Connection Plates

The use of bent plates as connecting elements between transverse diaphragms and bridge girders is common in modern steel bridges. Bent plates are used as connecting elements on skewed bridges where transverse members are parallel to the skew of the bridge, rather than perpendicular to the girder. Examples of bent connection plates are shown in figure 128. Cold bending is typically considered for producing the bends in these types of connection plates.

Source: FHWA

Figure 128. Photos. Cold-bent connection plates.

4.2.6.3 Bent Gusset Plates

Cold bending by press-brake bending is a common way to produce bent gusset plates. As illustrated in the photos in figure 129, precise angles and corners ranging from very subtle (left) to more substantial (right) can be achieved.

Source: FHWA

Figure 129. Photos. Bent gusset plates.

4.2.6.4 Structural Tubes (HSS)

Structural tubes, or hollow structural sections (HSS), can be bent to a desired radius using cold bending. Induction heating is also used for such bending. Kennedy et al. (1986) investigated the distortion that results from using cold bending for a range of tube sizes and bend radii. The primary distortions that resulted from cold bending the HSS sections were bowing in the compression flange and elongation in the top of the web. The equipment used to cold bend the tubes in this investigation was a pyramid-type, three-roller bending machine.

Through the research completed by Kennedy et al. (1986), which included the measured distortion of 108 cold bent tubes with a range of bend radii, the magnitude of distortion for cold bent tubes as a function of bend radius and section properties was established. Kennedy et al. concluded that, generally, distortions increase with decreases in HSS wall thickness or bend radius, and with increases in the depth or width of the HSS cross section.
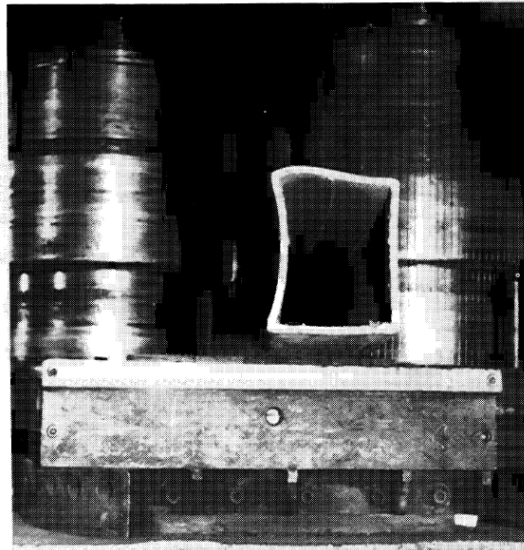
Source: Kennedy et al. (1986)

Figure 130. Photo. Typical distortion associated with cold bending structural tubing.

4.3. EFFECTS OF COLD BENDING ON MATERIAL

Like all methods of bending used for steel, the process of cold bending affects the material properties of a section. In general, the magnitude of the effect on the material properties depends on the magnitude of bending (i.e., the amount of strain on the section being bent).

4.3.1. Material Behavior in Cold Bending

In the process of cold bending, the cross section being bent is permanently deformed to produce the desired shape. As force is applied to bend the section, and part of the section yields under the force to produce a permanent deformation. When the force is removed, the plastically yielded section partially recovers, leaving a permanently deformed, or bent shape. This partial recovery is known as spring-back.

The behavior of a section during cold bending can be understood in the context of the tensile stress-strain relationship of steel. Consider the section being bent in figure 131-A and assume that the stress-strain relationship of this material can be described by the graph in figure 131-B. Before applying the bending force, all points in the cross section are at zero stress, assuming no initial residual stresses are present.
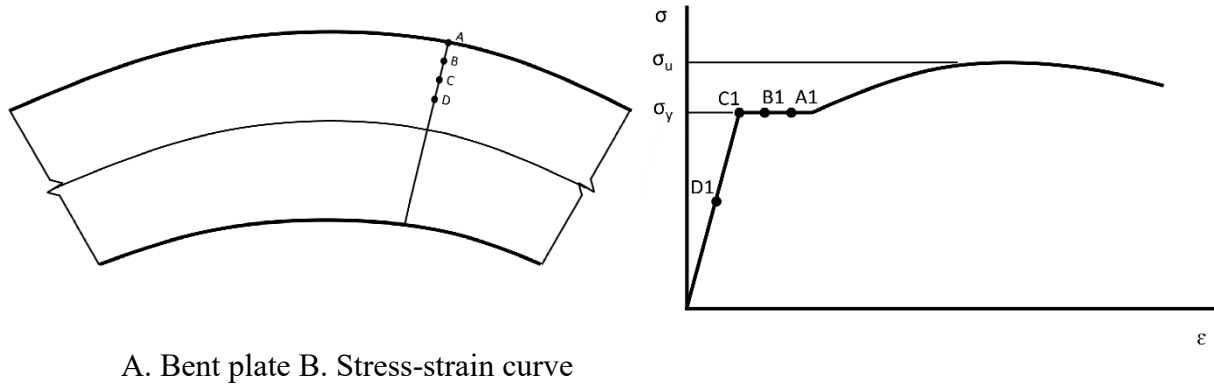

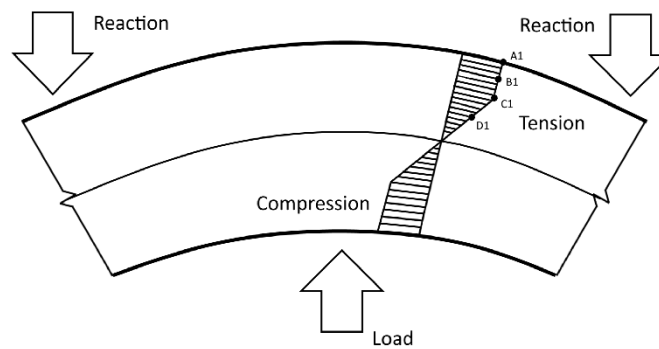| A. Plate to be bent | B. Stress-strain curve of material |
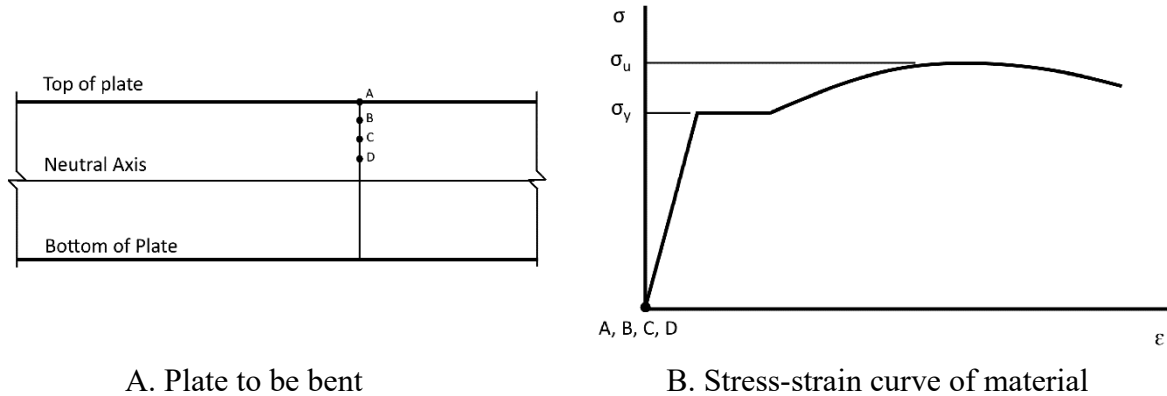
Source: FHWA

Figure 131. Illustration. Plate to be bent with stress-strain curve of material (before bending).

When the bending force is applied to the section shown in figure 132-A, the fibers strain with corresponding stress generated across the section. As illustrated in figure 132-B and figure 132-C, the strain and corresponding stress at each point, A through D, are proportional to the distance from the neutral axis. The section above the neutral axis goes into tension, the section below goes into compression, and the distribution of stress across the section is dependent on the section geometry. Points A and B are strained plastically beyond the yield point of the material; point C is strained such that it is just reaching yield; and point D is strained elastically, with its state of stress remaining below yield. Above the yield stress level of the material, at points A and B, the stress of the material does not increase.

As the section in figure 132-A begins bending, the extreme fiber on the material's surface, point A, yields first. As bending continues, the fiber at point A continues to strain, but because this material has yielded, its stress does not increase. This region of the stress-strain curve where a material's strain increases with no increase in stress is called the yield plateau. The not-yet-yielded portions of the section, points B through D, follow a similar pattern where stress and strain both increase until these fibers yield.

225

A. Bent plate B. Stress-strain curve

C. Stress distribution

Source: FHWA

Figure 132. Illustration. Plate to be bent with stress-strain curve of material, and stress distribution across the section (with bending force applied).

As bending continues, the strain in the section increases, eventually exceeding the strain at the end of the yield plateau. At this instance, stress begins to increase with increased strain. This behavior begins at the extreme fiber, point A, with points B through D following a similar pattern with increased bending. Finally, with increased applied force and further bending, the stress in the section approaches the ultimate stress of the material. With further loading, the material will begin to neck and rupture, or rupture without necking (depending on the material properties).

Figure 133 presents the state of stress and strain in the bent section after the applied load shown in figure 132 is removed. As shown in figure 133-A, the section unloads elastically but retains some amount of residual stress and plastic strain. The stress distribution over the section is shown in figure 133-B. For point A, the strain resulting from the original elastic loading is recovered (spring-back), but the plastic strain, or strain from loading beyond the yield point of the material, is retained. Similarly, points B, C, and D unload elastically, and in the final condition, retain some residual stress and plastic strain. This plastic strain is the deformation in the material that creates the desired bent shape.

A. Stress-strain curve   B. Stress on plate section
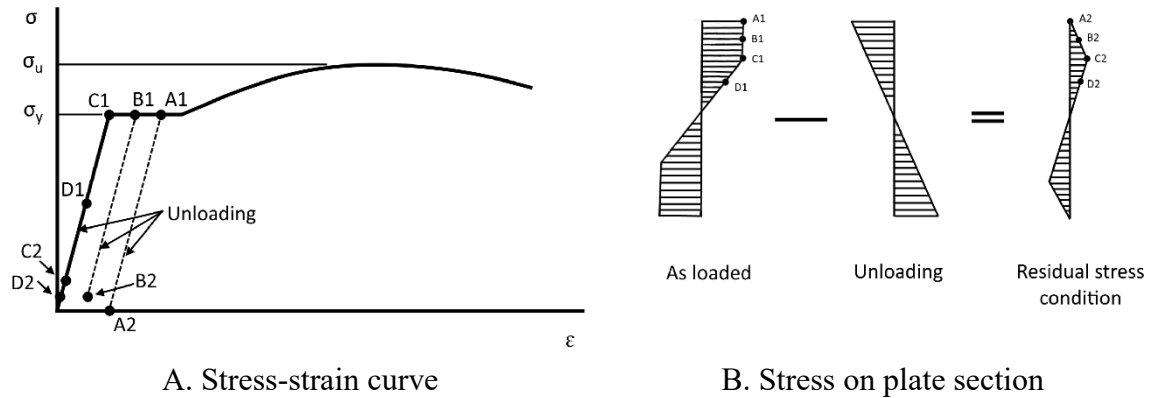
Source: FHWA

Figure 133. Illustration. Section properties of bent plate (after unloading).

The stress-strain curves of different steel types can vary, as shown in figure 134. Specifically, not all steels have a distinct yield plateau. Figure 134-A shows a stress-strain curve with a well-defined yield plateau. This material was grade 50 steel studied by Barth and Michaelson (2018) and was used to produce press-brake bent tub beams. In contrast, the material shown in figure 134-B, which was tested in a gusset plate research study, does not have a distinct yield plateau. Although the presence or lack of a yield plateau does not affect the effectiveness of cold bending, it can affect the amount of overall displacement needed to achieve a specific bent shape and the amount of spring-back observed.

A. Stress-strain curve (with yield plateau)   B. Stress-strain curve (without yield plateau)
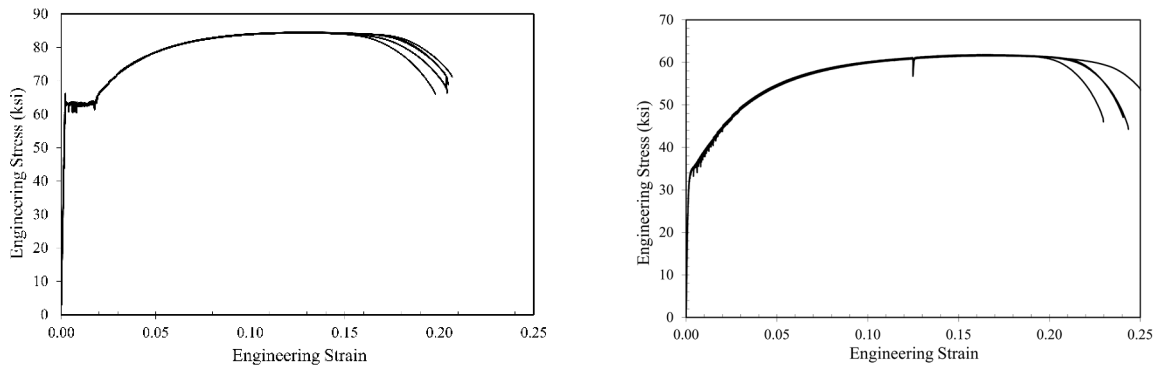
Source: Barth and Michaelson, 2018 (left) and FHWA (right)

Figure 134. Graphs. Stress-strain curve of grade 50 steel.

4.3.2. Effects of Cold Bending on Material Properties

4.3.2.1 Tensile Properties

In the bending configuration described in section 4.3.1, the strain in the material during bending exceeded the yield strain but remained within the yield plateau for all areas of the section. Depending on the amount of strain that results from bending and the actual properties of the material, fibers may be loaded beyond the yield plateau. This is illustrated by point A_1 in figure

135-A. Like the scenario in section 4.3.1, when the bending force is released, the section unloads elastically but retains a plastic strain. In addition, in the case where the section is loaded beyond the yield plateau and unloaded, an increase in yield strength occurs upon reloading. Later, when the section is loaded during service, the stress in the section will increase proportionately with strain until the new yield stress is reached (denoted by point A1 in figure 135). Depending on the amount of strain induced during the original bending of the section, the ultimate strength of the material may or may not change. In these instances, the strain at failure decreases, resulting in a less ductile material. Thus, as described in figure 135-B, portions of the cold-bent section that are bent such that they are strained beyond the yield plateau have been strain-hardened: they have a new, higher yield strength and are now less ductile.
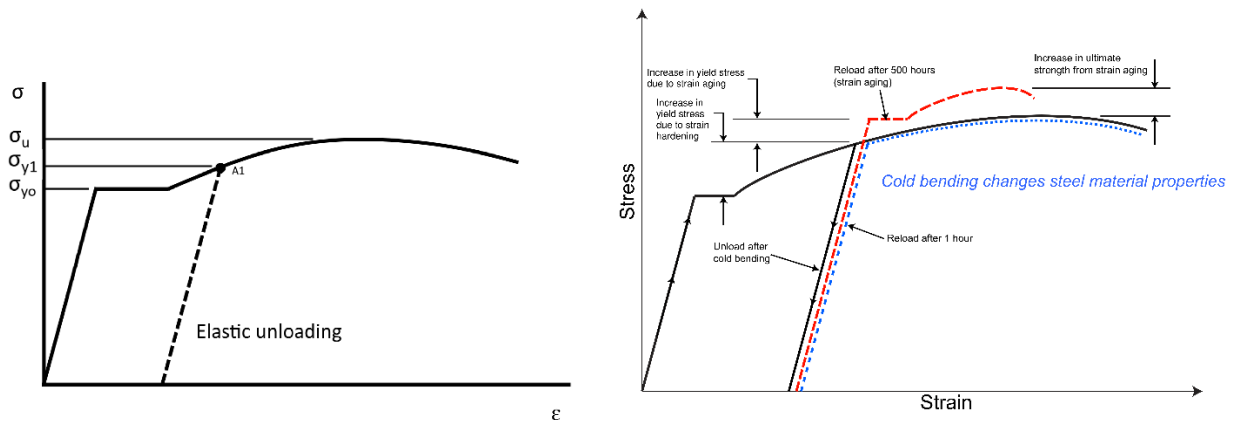
A. Stress-strain curve (load beyond yield plateau)   B. Stress-strain curve (strain-hardening)

Source: FHWA (left) and Moen (2011) (right)

Figure 135. Illustrations. Stress-strain curve and elongation beyond yield plateau.

4.3.2.2 Ductility

Ductility is the ability of a material to strain plastically beyond its yield point without fracture. This property allows for the use of cold bending with steel. As described in section 4.3.1, as the section is loaded and strain increases past the yield strain of the material but within the yield plateau, the material continues to strain without an increase in stress. When unloaded, the section partially recovers elastically, resulting in a recovery of elastic strain (or spring back), and a plastic strain that results in the permanent bend in the section. As described in section 4.3.2.1, when the loading on the section causes a strain in the section beyond the yield plateau, the material strain-hardens, resulting in a higher yield strength but same ultimate strength. Although, as discussed in section 4.3.2.1, depending on material properties, the ultimate strength also can be increased through strain hardening.

It is steel's ductile nature that makes its use appropriate in bridge construction. Thus, it is prudent in fabrication, including cold bending, to avoid compromising ductility. As reflected in the stress-strain curves used in section 4.3.1, the strains observed during cold bending are relatively small compared to the strains needed to reach ultimate strength. Therefore, while cold bending of the elements shown above practices yield portions of cross sections, when practical strain limits

228

are observed, the bending is not enough to have a deleterious effect on the steel and its performance in service.

Keating and Christian (2012) investigated the effects of hot and cold bending on the ductility of steel sections being formed, specifically flange plates for dapped steel girders. They intended to test full-scale, bent flange specimens, but found this was not practical. Instead, flat specimens heated to various temperatures were used and loaded to achieve target strains. The results measured capture the change in material properties (hardness, loss of ductility) at different strain levels and temperatures. This research found that the process of cold bending had less of an impact on ductility than hot mechanical bending. Specifically, Keating and Christian (2012) found that CVN energy decreased as strains increased and saw that bending in conjunction with heat decreased ductility and increased crack susceptibility. Based on these findings, Keating and Christian (2012) recommend the use of cold bending over use of heat while bending and a strain limit of 10 percent. This minimum bend radius was adopted in the *AASHTO LRFD Bridge Construction Specification* (AASHTO 2017a (CFR 625.4(d)(1)(v))), which will be further discussed in section 4.3.3. It should be noted that cold bending on fracture critical members is now permitted under *AASHTO/AWS Bridge Welding Code, D1.5* (AWS 2020), under FHWA April 2022 Memo[1].
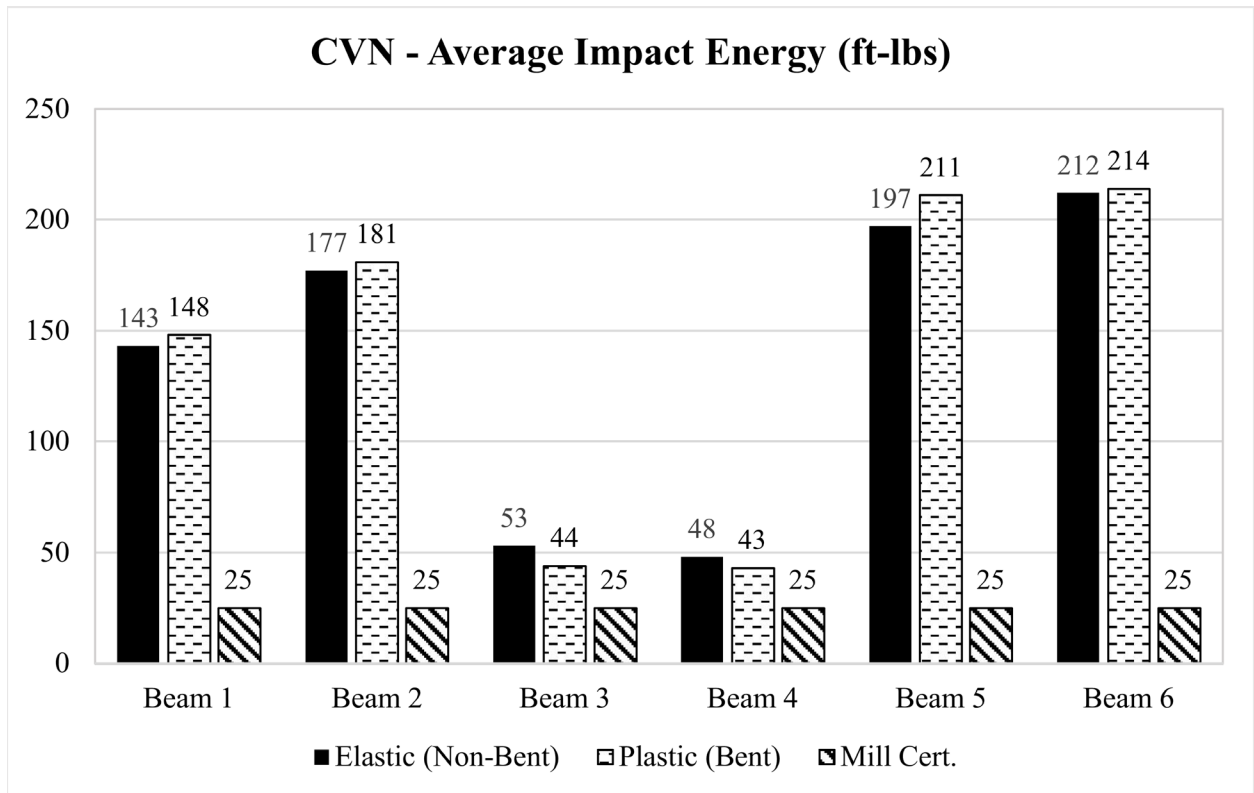
[1] AASHTO/AWS. 2020. *AASHTO/AWS D1.5M/D1.5:2015 Bridge Welding Code (BWC), 8th Ed.,* American Association of State Highway and Transportation Officials and American Welding Society, Washington, DC., is not a federal requirement but is allowed under FHWA April 11, 2022 Memo (citing 23 CFR 625.3(d)): *Approval of the use of structural design standards memorandum*: https://www.fhwa.dot.gov/bridge/structures/04112022.pdf. The standards currently incorporated by reference at 23 CFR 625.4(d) continue to be required

4.3.2.3 CVN Toughness

Studies have shown that CVN energy changes somewhat under cold bending. Pense (2004) provides a helpful synopsis of research related to the effect of cold bending on CVN values. As he reports, research during World War II discovered that steels undergo a temperature-related transition in toughness, and CVN testing can be used to effectively measure this change in toughness. Various studies over the following decades demonstrated that bending steel, particularly at temperatures between 500°F and 800°F (the "blue brittle range"), shifts the CVN transition temperature, although the effect varies among steels depending on their constituent alloys and manufacture processing. Hence, steel should not be subjected to higher strains while it is in the blue brittle range. In summary, Pense averred that strains in bridges are typically 5 percent or less, and within this range, toughness losses are limited. As discussed above, Keating and Christian's (2012) work studying bent flanges for dapped girders also measured changes in CVN energy.

Studies investigating cold bending of wide flange shapes have demonstrated that the process of cold bending has a negligible effect on CVN toughness because of the small strains associated with the amount of bending used on wide flange shapes. Schlim (1987) studied 8.8-inch-deep grade 36 shapes that had been curved to a 44 ft radius, or a strain of about 1 percent, and found no measurable change in fracture toughness based on CVN testing. Bresch et al. (2016) studied the effect of cold cambering on CVN energy for wide-flange shapes and plate girders. In the study, three 30-ft-long specimens were cambered 1½ inches, a strain of approximately 0.05 percent. These specimens included: W14×68 shapes with compact flanges (beams 1 and 2);

W14×90 shapes, with non-compact flanges (beams 3 and 4); and slender plate girders with 5/16-inch × 15-inch flanges and 7/16-inch × 13 3/8-inch webs (beams 5 and 6). In general, for all girders, CVN energy remained relatively unchanged after bending. Slight increases in CVN toughness were noted in the wide flange beams with compact flanges and plate girders, and slight decreases in CVN toughness were noted in the wide flange beams with non-compact flanges.

CVN - Average Impact Energy (ft-lbs)

	Beam 1	Beam 2	Beam 3	Beam 4	Beam 5	Beam 6
Elastic (Non-Bent)	143	177	53	48	197	212
Plastic (Bent)	148	181	44	43	211	214
Mill Cert.	25	25	25	25	25	25

Source: Bresch et al., (2016) with modifications by the authors

Figure 136. Graph. CVN values for cold bent beams.

4.3.2.4 Residual Stress

As described in section 4.3.1, the process of cold bending produces residual stresses in the sections being bent. In cold bending, sections are strained such that a portion of the cross section is stressed plastically, and the remainder of the section is stressed elastically. When the bending force is removed, the entire section unloads elastically. The residual stress, or the stress remaining in the section after unloading, is equal to the stress introduced during the bending process, minus the stress recovered when the section is unloaded.

However, residual stresses are often present in the original section prior to cold bending as a result of fabrication. Steel plates and rolled shapes have residual stresses that are introduced during the raw material manufacturing process as a result of differential cooling, rolling, or other thermal or mechanical processes. Further, fabrication processes such as cutting and welding also affect residual stresses. This means that the actual residual stress condition after cold bending is a

combination of the initial residual stress in the section prior to cold bending and the residual stresses that are produced during cold bending.

Because of this combination, residual stresses increase when compressive residual stresses from bending are introduced into zones that are already in compression and when tensile residual stresses from bending are introduced into zones that are already in tension. Conversely, stresses decrease where compression from bending is added into zones in tension and tension from bending is added into zones in compression.

It is not practical to accurately calculate the residual stresses present after cold bending. In theory, considering the mechanism by which residual stresses are created during cold bending (as described in section 4.3.1), the residual stresses from bending can be calculated given the yield strength of the material and the amount of strain introduced during bending. However, actual yield strengths tend to be higher than nominal and often vary across the section. Mill test reports of grade 50 steel plate used for bridges typically report yield strengths between 60 ksi and 65 ksi. Further, the actual stress-strain curves for steel, namely the presence of a yield plateau, can vary (discussed in section 4.3.1). Finally, it is not practical to determine the initial residual stress condition of the section being bent prior to bending.

Although it is not practical to know or calculate the residual stress condition before or after cold bending, this does not pose an issue for the use of the process. As discussed in section 4.3.3, the practice of cold bending is controlled by displacement, and knowledge of the initial residual stress condition is not needed for determining how much displacement to apply. Variations in the initial stress condition may cause variations in the anticipated spring-back. However, these variations are usually not large enough in magnitude to affect the use of the final bent section. As a result, residual stresses are often neglected in cold bending methods developed by researchers. Gergess and Sen (2004) present a cold bending methodology and corresponding analytical framework in which residual stresses are disregarded.

There are situations where the residual stresses from cold bending are worth considering. The first is the cold bending (or straightening) of large structural shapes. In forming such shapes, the process of rotary straightening, a common method of straightening shapes to meet specific design requirements, increases the yield strength of the material (Bjorhovde, 2006). However, rotary straightening of wide flange shapes can also cause higher shear yield strains at the k-area of large structural shapes. This results in a localized increase in strength and hardness and decrease in toughness and ductility. "The higher material strength and lower toughness have no effect for the overall strength of the member as a column or a beam. However, when detailing certain types of welded connections, that welds should not be terminated in or near the k-area" (Bjorhovde, 2006).

Another discrete residual stress problem from cold bending occurs in the manufacture of poles, such as high mast lighting towers. The bases of these towers have full penetration welds, and the poles themselves are formed using cold bending. Pole manufacturers report that when such poles are galvanized and tin is present in the galvanizing bath, cracks sometimes appear at the toes of the welds in the bend locations. These cracks are attributed to liquid metal embrittlement in conjunction with residual stress effects from the bending and welding that previously occurred in the crack area.

4.3.3. Radius Limits for Cold Bending of Plates

Steel plates can be cold bent via press brake bending or roll forming. Typically, the choice of method depends on the nature of the bend and the equipment available. Roll forming is more prevalent for shapes with long continuous radii, such as sheet pile, and press brake bending is more common for shapes with discrete corners, such as formed girders. Bridge fabricators may have their own equipment to produce the desired bent shapes, or they may send the plate to a subcontractor for bending.

Brockenbrough (2006) developed fabrication suggestions for cold bending of steel plates based on experimental data. Several types of structural steels were studied, including two steels commonly used in bridges: A709 grades 50 and 50W, and hundreds of plates were bent. During testing, the plates were bent to 120 degrees and if they did not crack, they were bent to 180 degrees. The behavior of the plates during bending (cracking versus not cracking) and measured strain in the plates were used to build bending limit diagrams. From these, minimum bend radius recommendations as a function of plate thickness were developed. Based on this work, Brockenbrough (2006) provided bending radius suggestions for several structural steel types that considered plate thickness, yield strength, and material elongation specifications. These recommendations were adopted by ASTM in Specification A6.

Until 2012, AASHTO used minimum bend radius recommendations that were adapted from AISC's *Specification for Structural Steel Buildings* (AISC 2005). The minimum radii varied by thickness and nominal yield strength, with large bend radii required for thicker plates or higher yield strengths. These minimum bend radii values are shown in table 29, which is excerpted from the *AASHTO LRFD BCS* of 2010, section 11.4.3.3.2-1 (AASHTO 2010), which is not a Federal requirement.

**Table 29. AASHTO pre-2012 specified minimum bend radii, (AASHTO 2010).**

Material	Thickness, t (inch)			
AASHTO M 270M/M 270 (ASTM A709/A709M) Grades (ksi)	**≤ 0.75**	**> 0.75 and ≤ 1.0**	**> 1.0 and ≤ 2.0**	**> 2.0**
36	1.5t	1.5t	1.5t	2.0t
50, 50S, 50W, or HPS 50W	1.5t	1.5t	2.0t	2.5t
HPS 70W	1.5t	1.5t	2.5t	3.0t
HPS 100W	1.75t	2.25t	4.5t	5.5t

Source: Modified table 11.4.3.3.2-1 from AASHTO (2010)

The minimum bend radii specifications were updated to include recommendations developed by Keating and Christian (2012). Based on their work, the minimum bend radius included in *AASHTO LRFD BCS* (AASHTO 2017a (23 CFR 625.4(d)(1)(iv))) now use a uniform 5t. These radii are different from before because the earlier were based on work from Brockenbrough, which were cracking limits, whereas the Keating and Christian limits are based on mechanical properties of material after bending.

However, for cross-frame and diaphragm connections, the current minimum bend radius remains at 1.5t for such connections with plates up to ¾ inch thick. For these connections, a minimum

bend radius of 1.5*t* has demonstrated satisfactory behavior in service, and an increase of the limit to 5*t* would have a significant impact on framing geometry. Consider the example shown in figure 137. As shown, increasing the radius of the connection angle from 1.5t to 5.0t significantly increases the connection angle size and bolt spacing, increasing the space needed for the connection angle. Considering other framing that may be present, this space may not be available. Similarly, for bent gusset plates used in skewed bridges, a minimum bend radius limit of 5*t* could cause cross-frame work-points to move significantly along the length of the girders. As a result, the fabricator may have difficulty locating the cross-frame as originally intended in the design. Further, the increased radius could make connections more eccentric, which may necessitate an increase in plate size or an increase in the number of bolts or size of weld. These issues are illustrated in figure 138. Based on these considerations, AASHTO (AASHTO 2017a (23 CFR 625.4(d)(1)(iv))) retained a minimum bend radius of 1.5*t* for connections with plates up to ¾ inch thick.
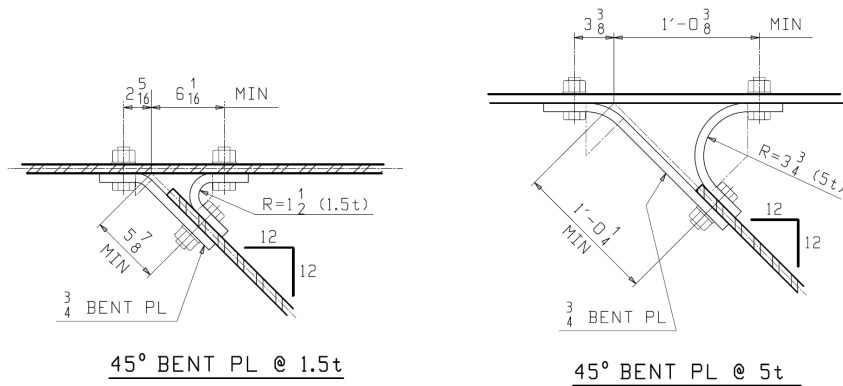
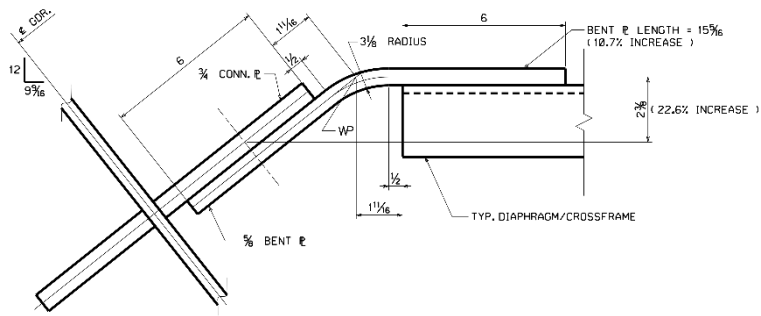Source: Tensor Engineering (2012)

Figure 137. Illustration. Minimum radius effect on connection plate size.
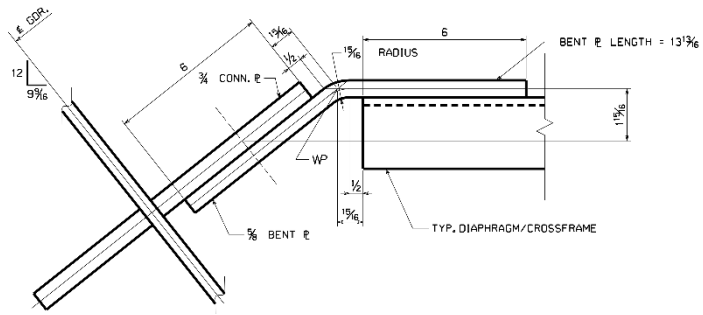
TYPICAL BENT ℄ CONN. @ CROSSFRAMES
PRESENT AASHTO COLD BENDING RADIUS
1½ t COLD BENDING METHOD

TYPICAL BENT ℄ CONN. @ CROSSFRAMES
PROPOSED AASHTO COLD BENDING RADIUS
5 t COLD BENDING METHOD

Source: High Steel (2012)

Figure 138. Illustration. Minimum radius effect on work points.

234

EQUATIONS

$$S = 0.005W\varphi_d \quad 0 < \varphi_d < 24° \tag{1}$$

$$\theta = 2tan^{-1}\frac{V}{2W} \tag{2}$$

$$\varphi_d = tan^{-1}\left(\frac{Y_2-Y_1}{L_1}\right) + tan^{-1}\left(\frac{Y_3-Y_4}{L_2}\right) \tag{3}$$

$$R = \frac{C_d}{2sin(\varphi_d/2)} \tag{4}$$

$$\frac{1}{R} = \frac{Y_{r-1}-2Y_r+Y_{r+1}}{L^2} \tag{5}$$

$$sin\frac{\varphi_d}{2} = \frac{L}{R} \tag{6}$$

$$\varphi_d = 2sin^{-1}\left(\frac{L}{R}\right) \tag{7}$$

$$R_y = \frac{Ey_{max}}{F_y} \tag{8}$$

$$\varepsilon_{max} = \frac{1}{R}y_{max} \tag{9}$$

$$\varepsilon_y = \frac{F_y}{E} \tag{10}$$

$$\mu = \frac{Ey_{max}}{RF_y} \tag{11}$$

$$A.F. = \frac{Y_o}{1-P/P_{euler}} \tag{12}$$

$$M_j \leq \frac{M_p}{2} \tag{13}$$

$$M_j \leq \frac{1}{2}(M_p \pm M_r) \tag{14}$$

$$\delta_{max} = \frac{1}{\gamma_{max}}\left(\frac{\ell}{140}\right)^2 \tag{15}$$

$$\delta_{max} = \frac{1}{\gamma_{max}}\left(\frac{\ell}{200}\right)^2 \tag{16}$$

$$\delta_{max} = \frac{1}{\gamma_{max}}\left(\frac{\ell}{120}\right)^2 \tag{17}$$

$$\delta_{max} = \frac{1}{\gamma_{max}}\left(\frac{\ell}{170}\right)^2 \tag{18}$$

$$n = \frac{\varphi_d}{\varphi_p} \tag{19}$$

$$SAF = \left(\frac{(1.35\ln(H)+4.25)t_f^{-0.06}-1.2}{-\ln(40H^{0.43})}\right)\ln(L) + (1.35\ln(H)+4.25)t_f^{-0.06} + 0.1H(b_f-10) \tag{20}$$

$$\varphi_p = \frac{S_pV}{W} \tag{21}$$

$$\varphi_p = \frac{S_pVd_v}{W^2} \tag{22}$$

$$\delta = 2d_v\left[tan\frac{\theta}{2} - tan\left(\frac{\theta}{2}-\frac{\varphi_p}{2}\right)\right] \tag{23}$$

$$\varepsilon_p'(T) = \frac{\delta}{V} \tag{24}$$

$$\delta = 2d_v\varepsilon_p'(T)\tan\frac{\theta}{2} \tag{25}$$

$$\varepsilon_p'(T)\tan\frac{\theta}{2} = \left[\tan\frac{\theta}{2} - \frac{\tan\frac{\theta}{2}-\tan\frac{\varphi_p}{2}}{1+\tan\frac{\theta}{2}\tan\frac{\varphi_p}{2}}\right] \tag{26}$$

$$\varphi_p = 2\varepsilon_p'(T)\sin\frac{\theta}{2} \tag{27}$$

$$\varphi_p = 2\varepsilon_p'(T)\sin\frac{\theta}{3} \tag{28}$$

$$\varepsilon_p(T) = \varepsilon_t(T) - \varepsilon_e(T) \tag{29}$$

$$\varepsilon_t(T) = \int \alpha(T)dT \tag{30}$$

$$\varepsilon_t(T) = \frac{F_y(T)}{E(T)} \tag{31}$$

$$\varepsilon_t = (0.001T^2 + 6.1T - 415)10^{-6} \tag{32}$$

$$\varepsilon_e = \frac{F_y(-720,000+4,200T-2.75T^2)}{29,000(500,000+1,333T-1.111T^2)} \tag{33}$$

$$\varphi_b = 0.015\sin\frac{\theta}{3} \tag{34}$$

$$F_\ell = 0.6 + 2\frac{M_j}{M_p} \tag{35}$$

$$\varphi_p = 2F_\ell\varepsilon_p(T)\sin\frac{\theta}{3} \tag{36}$$

$$F_t = [0.5 + 0.00125(T - 800)] \tag{37}$$

$$\varphi_p = 2F_tF_\ell\varepsilon_p(T)\sin\frac{\theta}{3} \tag{38}$$

$$\varphi_p = F_\ell\varphi \tag{39}$$

$$\varphi = 0.015\sin\frac{\theta}{3} \tag{40}$$

$$\varphi_p = F_\ell F_s F_a \varphi_b \tag{41}$$

$$\varphi_b = 0.015\sin\frac{\theta}{3} \tag{42}$$

$$x_2 = \left(\frac{d+\frac{1}{2}b_s}{d}\right)x_1 \tag{43}$$

$$F_s = \frac{d+\frac{1}{2}b_s}{d} = 1 + \frac{b_s}{2d} \tag{44}$$

$$F_a = 1 - 2[1 - \left(\frac{2}{3}\right)\left(\frac{Z}{S}\right)]\frac{M_j}{M_p} \tag{45}$$

$$F_a = 1 - 0.4\frac{M_j}{M_p} \tag{46}$$

$$F_\ell = 0.6 + 2\frac{M_j}{M_p} \tag{47}$$

236

$$x_2 = (d + \frac{b_s}{2}) \frac{x_1}{d} \tag{48}$$

$$F_a = 1 - 0.7 \frac{M_j}{M_p} \tag{49}$$

$$F_s = 1 + \frac{b_s d}{2d^2} \tag{50}$$

$$F_s = 1 + \frac{1}{2} \frac{b_s d_s}{d^2} \tag{51}$$

$$F_a = 1 - 0.5 \frac{M_j}{M_p} \tag{52}$$

$$Z/_S = F_s(Z'/_{S'}) \tag{53}$$

$$M_j = \frac{P_j \ell}{4} \tag{54}$$

$$K_j = \frac{4EI_j}{\ell} \tag{55}$$

$$\Delta = \frac{P_j \ell^3}{48EI_j} \tag{56}$$

$$\Delta = \frac{P_j \ell^2}{12K_j} \tag{57}$$

$$K_j = \frac{P_j \ell^2}{12\Delta} \tag{58}$$

$$M_f = \frac{P_f \ell}{4} \tag{59}$$

$$\Delta = \frac{P_f \ell^3}{48EI_f} = \frac{P_f \ell^2}{12K_f} \tag{60}$$

$$\frac{P_f \ell^2}{12K_f} = \frac{P_j \ell^2}{12K_j} \tag{61}$$

$$\frac{P_f}{K_f} = \frac{P_j}{K_j} \tag{62}$$

$$M_f = \overline{\gamma} M_j \tag{64}$$

$$\overline{\gamma} = \frac{K_f}{K_j} \tag{65}$$

$$M_f = \gamma M_j \tag{66}$$

$$F_a = \left(\frac{d/t_w}{46}\right)^2 \tag{67}$$

$$\gamma = 1.75 \, (\overline{\gamma}) \tag{68}$$

$$\gamma = \frac{d/t_w}{10,000} (15 + 2.75 \, d/t_w) \tag{69}$$

$$\varphi_c = F_a F_\ell \varphi_b \tag{70}$$

$$\varphi_b = 0.015\sin\frac{\theta}{3} \tag{71}$$

$$F_\ell = \left(0.6 + 2\frac{M_f}{M_p}\right) \tag{72}$$

$$F_\ell = 0.6 + 2\gamma\frac{M_j}{M_p} \tag{73}$$

$$M_f \leq \frac{M_p}{3} \tag{74}$$

$$\frac{M_j}{M_p} \leq \frac{1}{3\gamma} \tag{75}$$

$$K_j = \frac{1}{\gamma}K_f \tag{76}$$

$$M_f + M_r \leq \frac{M_p}{3} \tag{77}$$

$$M_f \leq \frac{M_p}{3} - M_r \tag{78}$$

$$M_j \leq \frac{1}{\gamma}\left(\frac{M_p}{3} - M_r\right) \tag{79}$$

$$P_a = P_j + P_{ec} \tag{80}$$

$$P_j = \frac{R_\ell L M_p}{ab} \tag{81}$$

$$P_{ec} = \frac{LP\Delta}{ab} \tag{82}$$

$$F_a = \left[1 - 2\left(1 - \frac{2}{3}\frac{Z}{S}\right)\frac{M_j}{M_p}\right]\left(1 - \frac{f_a}{F_{allow}}\right) \tag{83}$$

$$\varphi_p = F_\ell F_s F_a \varphi_b \tag{84}$$

$$L_d = [a + 2(\delta^2 + b^2)^{1/2}] \tag{85}$$

$$L_u = a + 2b \tag{86}$$

$$\varepsilon_d = \frac{(L_d - L_u)}{L_u} \tag{87}$$

$$M_p = \frac{F_y t^2}{4} \tag{88}$$

$$W_e = \left(W_u\frac{ac}{2}\right)(0.75\delta_u) \tag{89}$$

$$W_e = \left(W_u\frac{ac}{2}\right)(0.75\delta_u) \tag{89}$$

$$W_I = M_p\left(\frac{a\delta_u}{c} + \frac{2c\delta_u}{b} + \frac{2c\delta_u}{b} + \frac{2b\delta_u}{c}\right) \tag{90}$$

$$W_u = \frac{8}{3}\frac{M_p}{ac}\left(\frac{a}{c} + \frac{4c}{b} + \frac{2b}{c}\right) \tag{91}$$

$$P_j = W_u\frac{ac}{4} \tag{92}$$

$$P_j = W_u \frac{ab_f}{8} \tag{93}$$

$$R = \left(\frac{\delta_i{}^2 + r_b{}^2}{2\delta_i}\right) \tag{94}$$

$$\ell_c = \frac{\sqrt{(Rt)}}{[12(1-v^2)]^{0.25}} \tag{95}$$

$$\beta = \frac{t^2\sigma}{P_j} \tag{96}$$

$$P_j = \frac{t^2 F_y}{2\beta} \tag{97}$$

$$n = 140\left(\frac{\delta_i}{d_b}\right) \tag{98}$$

$$P_i = \left(1 - \frac{i}{2n}\right)P_j \tag{99}$$

ACKNOWLEDGMENTS

REFERENCES

AASHTO (2010). *AASHTO LRFD Bridge Construction Specifications*, 3rd Edition, LRFDCONS-3, American Association of State Highway and Transportation Officials, Washington, D.C. (not a current Federal requirement)

AASHTO (2017a). *AASHTO LRFD Bridge Construction Specifications*, 4th Edition, LRFDCONS-4, American Association of State Highway and Transportation Officials, Washington, D.C. (23 CFR 625.4(d)(1)(iv)).

AASHTO (2017b). *AASHTO LRFD Bridge Design Specifications*, 8th Edition, LRFD-8. American Association of State Highway Transportation Officials, Washington, DC (23 CFR 625.4(d)(1)(v)).

AASHTO/AWS (2016). *Bridge Welding Code,* AASHTO/AWS D1.5-2015, Miami, Florida. (23 CFR 625.4(d)(2)(i)).

AASHTO/AWS (2020). *Bridge Welding Code,* AASHTO/AWS D1.5-2020, Miami, Florida. (not a current Federal requirement)

AISC (2005). Steel Construction Manual, 13th Edition, American Institute of Steel Construction, Chicago, Illinois.

AISC (2018). *Design Guide 33 Curved Member Design*, American Institute of Steel Construction, Chicago, Illinois.

AREMA (2020). *Manual for Railway Engineering*, Lanham, Maryland.

Avent, R.R. (1987). "Use of Heat Straightening Techniques for Repair of Damaged Steel Structural Elements in Bridges." *Final Report,* Louisiana Transportation Research Center, Louisiana State University, Baton Rouge, Louisiana.

Avent, R.R. (1992). "Designing Heat-Straightening Repairs." *Proceedings, National Steel Construction Conference,* AISC, Las Vegas, Nevada, pp. 21-23.

Avent, R.R. (2008). *Guide for Heat-Straightening of Damaged Steel Bridge Members, Final Draft of the AASHTO Guidelines,* Technical Report No. FHWA-IF-08-999, Federal Highway Administration, Washington, D.C.

Avent, R.R., and Brakke, B.C. (1996). "Anatomy of Steel Bridge Heat Straightening Project." *Transportation Research Record*, Transportation Research Board, Vol. 1561, pp. 26-36.

Avent, R.R., and Fadous, G.M. (1989). "Heat-Straightening Prototype Damaged Bridge Girders." *Journal of Structural Engineering,* ASCE, Vol. 115, No. 7, pp. 1631-1649.

Avent, R.R., and Mukai, D. (1998). *Heat-Straightening Repairs of Damaged Steel Bridges A Technical Guide and Manual of Practice,* Technical Report No. FHWA-IF-99-004, Federal Highway Administration, Washington, D.C.

Avent, R.R., Mukai, D., Robinson, P., Boudreaux, R. (2000). "Heat Straightening Damages Steel Plate Elements." Journal of Structural Engineering, ASCE, Vol. 126, No. 7, pp. 747-754.

Avent, R.R., Madan, A., and Shenoy, S. (1993). "Design and Implementation of Heat-Straightening Repair for Composite Deck-Girder Bridges." *Transportation Research Record,* Transportation Research Board, Vol. 1392, pp. 90-98.

Avent, R.R., Robinson, P.F., Madan, A., and Shenoy, S. (1992). "Development of Engineering Design Procedures for Heat-Straightening Repair of Damaged Structural Steel Bridges." *Louisiana Transportation Research Center,* LTRC 251, Baton Rouge, Louisiana.

Barsom, J.M., and Rolfe, S.T. (1987). *Fracture and Fatigue Control in Structures-Applications of Fracture Mechanics, 2nd Ed.,* Prentice-Hall, Englewood Cliffs, New Jersey.

Barth, K.E., and Michaelson, G.K. (2018). "Development and Experimental Testing of Press-Brake-Formed Steel Tub Girders for Short Span Bridge Applications – Volume I: Development and Feasibility Assessment of Shallow Press-Brake-Formed Steel Tub Girders for Short Span Bridge Applications." *AISI Steel Market Development Institute Short Span Steel Bridge Alliance.*

Blodgett, O.W. (1972). "Distortion: How Metal Properties Affect It." *Welding Engr.*, Vol. 57, No. 2, pp. 40-46.

Boudreaux, R.J. (1987). "Heat Straightening of Steel: Identifying the Important Parameters and Predicting Member Response." Thesis, Louisiana State University at Baton Rouge, Louisiana.

Bresch, M.T., Medlock, R.D., and Chen, Y.F. (2016). "Influence of Cold Cambering on the Toughness of Rolled I-Beams." *Proc. International Bridge Conference*, Washington, DC, June, pp. 169-174.

Brockenbrough, R.L. (2006). "Development of Fabrication Guidelines for Cold Bending of Plates." *Engineering Journal,* American Institute of Steel Construction, Vol. 43, pp. 49-56.

Bjorhovde, R. (2006). "Cold Bending of Wide-Flange Shapes for Construction." *Engineering Journal,* American Institute of Steel Construction, Vol. 43, pp. 271-286.

Connor, R.J., Urban, M.J., and Kaufmann, E.J. (2008). *Heat-Straightening Repair of Damaged Steel Bridge Girders: Fatigue and Fracture Performance,* National Cooperative Highway Research Program Report No. 604, Transportation Research Board, Washington D.C.

DeBajar, L.A., Robinson, P.F., and Avent, R.R. (1992). "Risk Consistent Estimate of Heat-Straightening Applications. I: Plates." *Journal of Structural Engineering*, ASCE, Vol. 118, No. 12, pp. 3394-3409.

DeBajar, L.A., Robinson, P.F., and Avent, R.R. (1992). "Risk Consistent Estimate of Heat-Straightening Applications. II: Beams." *Journal of Structural Engineering*, ASCE, Vol. 118, No. 12, pp. 3440-3426.

Ditman, O. (1961). "Determination of Thermal Shrinkage in Structural Steel." Thesis, University of Washington, Seattle, Washington.

Gergess, A., and Sen, R. (2004). "Fabrication Aids for Cold Straightening I-Girders." *Engineering Journal,* American Institute of Steel Construction, Vol. 41, pp. 74-84.

Gergess, A., and Sen, R. (2008). "Cold Curving Steel Bridge Girders." *Transportation Research Record,* Transportation Research Board, Vol. 2081, no. 1, pp. 165-175.

Gergess, A., and Sen, R. (2016). "Curving Structural Steel Girders by Two-Point Bending." *Journal of Constructional Steel Research*, Vol. 122, pp. 511-519.

Harrison, H.L. (1952). "Straightening Structural Members in Place." *Welding Journal*, Vol. 31, No. 5, Res. Supplement, pp. 257-262.

Holt, J.E. (1965). "Flame Straightening Basics." *Welding Engineer*, Vol. 50, No. 9, pp. 49-53.

Horton, D.L. (1973). "Heat Curved Mild Steel Wide Flange Sections: An Experimental and Theoretical Analysis." Thesis, University of Washington, Seattle, Washington.

Keating, P.B. and Christian, L.C. (2012). *Effects of Bending and Heat on the Ductility and Fracture Toughness of Flange Plate*, Technical Report 0-4624-2, Texas Transportation Institute, College Station, Texas.

Kennedy, J.B., Seddeik, M., and Brady, F. (1986). "Deformations in Cold-Bent HSS Members." *Engineering Journal*, American Institute of Steel Construction, Vol. 23, pp. 117-123.

Kowalkowski, K., and Varma, A.H. (2007). "Effects of Multiple Damage-Heat Straightening Repairs on Steel Beams." *Transportation Research Record,* Transportation Research Board, Vol. 2028, pp. 66-77.

Moberg, K.L. (1979). "Damage Assessment and Contraction Straightening of Steel Structures." Thesis, University of Washington, Seattle, Washington.

Moen, C. "Cold Bending Fabrication – State-of-the-Art, Industry Challenges, Engineering Solutions." Presentation, Transportation Research Board AFH70 Committee Meeting, Fabrication and Inspection of Metal Structures, January 24, 2011.

Morovat, M., Engelhardt, M., Helwig, T., and Taleff, E. (2014). "Experimental Investigation of Time- And Temperature- Dependent Stability of Steel Columns in Fire." *8th Internation Conference on Structures in Fire*, Shanghai, China.

Nicholls, J.I., and Weerth, D. E. (1972). "Investigation of Triangular Heats Applied to Mild Steel Plates." *Engineering Journal,* American Institute of Steel Construction, Vol. 9, pp. 137-141.

Pattee, H.E., Evans, R.M., and Monroe, R.E. (1970). "Effect of Flame and Mechanical Straightening on Material Properties of Weldments." *Summary Report on Ship Structure Committee on Project SR-185, Straightening Distorted Weldments*, Battelle Memorial Inst., Columbus, Ohio.

Pense, A. (2004). "HPS Corrugated Web Girder Fabrication Innovations – Final Report – Part 4: Literature and Experimental Study of Strain Aging in HPS and Other Bridge Steels." *Report,* American Iron and Steel Institute, Washington D.C.

Putherickal, J. (1992). *Effects of Heat Straightening Structural Steel*, Final Report for MLR-91-3, Iowa Department of Transportation, Ames, Iowa.

Roeder, C.W. (1985). *Use of Thermal Stress for Seismic Damage Repair,* Final Report on NSF Grant CEE-82-05260, University of Washington, Seattle, Washington.

Roder, C. W. (1986). "Experimental Study of Heat Induced Deformation." *Journal of Structural Engineering,* ASCE, Vol. 112, No. 10, pp. 2247-2262.

Schlim, R. (1987). "Effect of Bending on Mechanical Properties of Sections." *Technical Report*, Arbed, Centre de Recherches, Esch-sur-Alzette, Luxembourg.

Shanafelt, G.O., and Horn, W.G. (1984). *Guidelines for Evaluation and Repair of Damaged Steel Bridge Members*, National Cooperative Highway Research Program Report No. 271, Transportation Research Board, Washington, D.C.

Sharma, M. (2005). "Behavior of Heat Straightened Plates Bent Along the Minor Axis." Thesis, Louisiana State University, Baton Rouge, Louisiana.

Timoshenko, S. (1959). *Theory of Plates and Shells*. McGraw Hill, New York, New York.

Varma, A.H., and Sohn, Y. (2013). *Effects of Realistic Heat Straightening Repair on the Properties and Serviceability of Damaged Steel Beam Bridges,* Technical Report No. FHWA/IN/JTRP-2013/03, Joint Transportation Research Program, Indiana Department of Transportation and Purdue University, West Lafayette, Indiana.

Weerth, D.E. (1971). "Theoretical and Experimental Analysis of Heat Curved Mild Steel." Thesis, University of Washington, Seattle, Washington.

Wilson, W. (1946). "The Shortening of Eyebars to Equalize the Stress." *Bulletin No. 460,* American Railway Engineering Association, Chicago, Illinois.

Yu, L. (2006). "Behavior of Bolted Connections During and After a Fire." Dissertation, University of Texas at Austin, Austin, Texas.